

**Influence of Openings on the Structural Response of
RC Shear Walls**

THESIS

Submitted in partial fulfilment
of the requirements for the degree of

DOCTOR OF PHILOSOPHY

by

G. MUTHUKUMAR

Under the supervision of
Prof. MANOJ KUMAR



BITS Pilani
Pilani | Dubai | Goa | Hyderabad

**BIRLA INSTITUTE OF TECHNOLOGY & SCIENCE
PILANI – 333 031 (RAJASTHAN) INDIA**

2015

Influence of Openings on the Structural Response of RC Shear Walls

THESIS

Submitted in partial fulfilment
of the requirements for the degree of

DOCTOR OF PHILOSOPHY

by

G. MUTHUKUMAR
(2008PHXF002P)

Under the Supervision of
Prof. MANOJ KUMAR



BITS Pilani
Pilani | Dubai | Goa | Hyderabad

**BIRLA INSTITUTE OF TECHNOLOGY & SCIENCE
PILANI – 333 031 (RAJASTHAN) INDIA**

2015



**BIRLA INSTITUTE OF TECHNOLOGY & SCIENCE
PILANI – 333 031 (RAJASTHAN) INDIA**

CERTIFICATE

This is to certify that the thesis entitled “**Influence of Openings on the Structural Response of RC Shear Walls**” submitted by **G. Muthukumar**, ID.No. **2008PHXF002P** for award of Ph.D. Degree of the Institute embodies the original work done by him under my supervision.

Signature in full of the Supervisor _____

Name : **Prof. Manoj Kumar**
Designation : **Associate Professor, Department of Civil Engineering**
BITS-Pilani, Pilani Campus

Date: _____

Dedicated to

Lord Shri Kunrakkudi

Shanmughanathan

Acknowledgements

At the outset, I wish to express the deep sense of gratitude and sincere thanks to my supervisor Prof. Manoj Kumar, Associate Professor, Department of Civil Engineering for his valuable guidance, encouragement, suggestions, and moral support throughout the period of this research work. It has been a privilege for me to work and learn under his valuable guidance.

I express my deep sense of appreciation to BITS Pilani leadership team for providing all the necessary facilities and support to complete the research work. I convey my honest thanks to Director of BITS-Pilani, Pilani Campus Prof. A. K. Sarkar, Senior Professor Department of Civil Engineering, BITS Pilani for his kind words of encouragement and motivation throughout my stay at BITS-Pilani, Pilani Campus. I am very much indebted to Prof. G. Sundar, Director (Off-Campus Programmes & Industry Engagement) for motivating me throughout my Degree programme. I also thank Prof. G. Raghurama, former Director Pilani Campus for his constant support.

I also express my gratitude to Prof. S.K. Verma, Dean, Academic Research (Ph.D. Programme) Division and Prof. Hemant R Jadhav, Associate Dean, Academic Research (Ph. D. Programme) Division for providing valuable support throughout the programme.

I would like to take this opportunity to express my gratefulness to Prof. S.B. Singh and Prof. Ravi Kant Mittal, who are the members of Doctoral Advisory Committee (DAC), for their kind suggestions, motivation and moral support throughout the programme both technically and personally. I would like to thank Prof. Niranjana Swain, Dean, Practice School and Prof. P. Srinivasan, Associate Dean, Practice School for their motivation during difficult times.

I am also thankful to all my professors notably Prof. Rajiv Gupta, Prof. K.S. Raju, Prof. A.P. Singh, Prof. V.R. Vinayaka Ram, Prof. Anshuman, Prof. A. Vasana, Prof. Srikanta Routroy for their support and motivation throughout my studies at BITS-Pilani, Pilani Campus. I am also thankful to Dr. Shrinivas S. Arkatkar, Dr. Anupam Singhal, Dr. Dipendu Bhunia and Dr. Shuvendu N. Patel for their support and

motivation in completing my thesis. I am also thankful to all Off-Campus faculty members in Practice School centers for their motivation and support.

I also thank all my friends, especially Mr. Parikshit K. Singh, Mr. M.M. Pandey and Mr. P.K. Rajesh, who have helped me during my Ph.D. I also thank Dr. S. Madappa S. Vigneasuva Raja for his support during my Ph.D. Thanks are also due to all faculty and staff members of BITS-Pilani, Pilani Campus, especially Practice School and Civil Engineering for helping me out at various times. I also thank my students for their support and cooperation.

I would also like to thank Mr. Santosh Kumar Saini, Academic Registration & Counselling Division (ARCD), BITS-Pilani for his help in compilation of thesis.

Last but most importantly, I thank my parents for their care and affection shown towards me. My thanks are also extended to my two elder brothers and their families for their affection.

G. Muthukumar

The reinforced concrete buildings are subjected to lateral loads due to wind and earthquake and these forces are predominant especially in tall and slender buildings. In order to resist these lateral loads, shear walls are provided in the building as a lateral load resisting element which inherently possesses sufficient strength and stiffness. The importance of shear wall in mitigating the damage to reinforced concrete structures is well documented in the literature. The shear walls are generally classified into three categories on the basis of aspect ratio of the shear wall (height/width ratio) viz., short, squat and slender shear walls. The short shear wall, though not very common, has the aspect ratio less than unity. The shear walls with aspect ratio between 1 and 3 are generally considered to be of squat type and shear walls with aspect ratio greater than 3 are considered to be of slender type. Due to functional as well as the architectural requirements, sometimes the shear walls are penetrated with openings to accommodate doors and windows. In general, the structural response of shear wall strongly depends on the type of loading, aspect ratio of shear wall, size and location of the openings in the shear wall and ductile detailing (strengthening) around the openings of shear walls.

Although it is implied that the behavior of shear wall is strongly influenced by the severity of loading, it is essential to understand the response characteristics of shear wall under different type of loading conditions, viz. static and dynamic, as well as at different regimes, i.e. linear as well as non-linear. Though the behavior of shear wall remains linearly elastic till certain level of loading, it may not be possible for a shear wall to behave in a same fashion throughout the loading history. As prevention of collapse is the fundamental requirement of any design, it is essential that the buildings comprising shear walls behave in a ductile way, allowing certain safe inelastic deformations. Hence, in order to properly proportion and design the shear wall, it is of paramount importance to understand the behavior of shear wall, in linear as well as in non-linear regimes.

The aspect ratio of the shear wall strongly influences the behavior of the shear wall. The squat shear walls generally fail in shear mode whereas the slender shear walls fail in a flexural mode. Although, the flexural mode of failure is desirable for both slender as well as squat shear wall, however, flexural failure mode has been found to be difficult to achieve in the case of squat shear wall.

The presence of openings in shear walls needs special attention. It has been observed from the literature that the strength and ductility of the shear wall is greatly influenced due to the presence of openings in shear wall. The magnitude of strength reduction depends on the size of the openings and its locations. Inevitably, the openings in shear wall result in severe stress concentration around openings and hence ductile detailing (strengthening) needs to be done around openings. The size as well as the location of openings in shear wall needs to be carefully designed not only to cater the functional requirements, but also to satisfy the overall structural performance of the shear wall.

Though reasonable experimental investigations on shear walls with openings have been reported in the literature, there were only very few analytical investigations pertaining to the assessment of influence of openings on shear wall, primarily due to lack of sophisticated analytical technique, until the last decade. Though many simplified conventional methods evolved over the years to study the behavior of shear wall with openings, but its accuracy was always in doubt in predicting the non-linear behavior. The limit on the opening size has been imparted in certain design codes only to make conventional methods applicable for the analysis, and not from the structural viewpoint. With the advent of computing technology, finite element analysis has overcome these issues and is prominently being used for the analysis of shear wall with openings, even in design and consulting firms. Not many analytical investigations have been found in the literature, focusing exclusively on the correlation between opening size, opening location and ductility. Moreover, the influence of damping on the dynamic structural response of shear wall with openings has also not been thoroughly investigated. The present study aims to analyze the behavior of slender and squat shear wall with different opening sizes and locations for static and dynamic loading conditions using the finite element analysis.

In order to carry out the above analyses, the finite element program has been developed in FORTRAN with state-of-the-art material and geometric modeling. The program is capable of performing static as well as dynamic analyses in linear and non-linear regimes. The modeling of the shear wall geometry has been the subject of great interest over the past few decades and several elements were used in the past such as beam element, plane stress element and plate element. Nevertheless, the performances were not found to be good due to the poor convergence of solution. On the other hand, shell

elements are being used predominantly in modeling the shear wall geometry and resulted in a better performance for both thick and thin shells. Since the formulation based on the classical shell theory has been found to be mathematically complex, the use of degenerated shell element came into picture and was found promising when it was first developed for the analysis of moderately thick plates and shells. Nevertheless the element suffered from locking phenomenon. Though several methods such as reduced integration, selective integration, assumed natural strain concept, and enhanced natural strain concept have been used in the past to alleviate locking phenomena, the present study uses the concept of assumed strain to avoid shear as well as membrane locking. Hence, to geometrically model the shear wall, the nine-noded locking free layered Lagrangian degenerated shell element with assumed strain approach has been adopted. The layered approach has been introduced, thus allowing the different material properties through the thickness direction, especially to facilitate the reinforcement modeling.

The nonlinearities in the shear wall may be due to the large deformation (Geometrical Non-linearity) or due to degradation in material properties (Material Non-linearity). Since the shear wall is inherently very stiff, it is expected that even at the large loads, deformation may not be very large and therefore, in this study, only material non-linearity is considered. The material nonlinearities considered in this study are due to cracking, yielding and crushing of concrete and steel yielding. The modeling of concrete in compression has been formulated using plasticity theory with Willam-Warnke five-parameter failure criterion to define the yield/failure surface. The isotropic hardening with associated flow rule has been adopted in defining the strain-hardening behavior of the concrete. The smeared crack modeling has been adopted in which cracks are assumed to be smeared over the element. To represent the capacity of the intact concrete between neighboring cracks, the linearly descending branch of tension stiffening has been adopted in the present investigation. The modeling of reinforcement has been done assuming steel reinforcement to be smeared in a particular layer. The bilinear stress-strain curve has been adopted in defining the steel in tension as well as in compression.

For the dynamic analysis, the direct method of time integration has been adopted using unconditionally stable implicit Newmark Constant Acceleration Scheme. The formulation of mass matrix has been done using the consistent mass matrix approach and the Rayleigh

damping has been adopted with stiffness proportionality. The finite element program developed has been validated against the benchmark problems to test the sensitivity of the element, aspect ratio, with respect to monotonic static and dynamic analysis.

In order to assess the influence of openings (sizes as well as location) on the squat and slender shear walls, five storeyed (squat) and ten storeyed (slender) shear walls, have been considered. The influence of strengthening (ductile detailing) around the openings has also been investigated. In general, the presence of opening reduces the load carrying capacity significantly as the opening size increases. On the basis of non-linear static analysis, even with strengthening of shear wall around the openings, the 21% opening in shear wall resulted in the degradation in the load carrying capacity as well as in the ductility index and hence need to be avoided. The ultimate displacement of slender shear wall with 21% opening has been considered to be too low as compared to solid shear wall. In the similar lines, when subjected to dynamic ground motion, the slender shear wall with 21% opening has been considered highly undesirable for both 5% damping and 2% damping without strengthening, characterized by the heavy one-sided displacement response history. Also larger opening puts tremendous base shear demand which may be difficult to satisfy practically.

However, upto 18% opening, slender shear wall shows very stable displacement time history response characterized by vibrations of high frequency for both 5% and 2% damping. However, for squat shear wall, the displacements are relatively high with respect to solid squat shear wall especially for 2% damping without strengthening around the opening. Hence, 18% opening has not been considered very safe opening size for squat shear wall. For shear wall upto 14% opening, the response of shear wall is not overly dependent on the strengthening around the openings and hence considered to be safe opening percentage in shear wall. The displacement ductility index has been considered to be better in the case of shear wall with 14% opening. Moreover, for this opening, strengthening results in the increase in the load carrying capacity, ultimate displacement and ductility index. Hence, the optimum size of openings for both slender and squat shear walls have been fixed at 14%.

The opening locations strongly affect the performance of shear wall. The single central opening results in less displacement response and base shear demand for both slender as well as squat shear wall. The shear wall with central opening resulted in the better load

carrying capacity as well as the ductility index in comparison to other opening locations. The aspect ratio of opening plays significant role on the response of shear wall in terms of load carrying capacity, ultimate displacement, and ductility index. The consistent performance of the shear wall with single central opening and four window opening is partly to the square openings. In all cases considered, the influence of damping has also been investigated and found that the damping has significant impact in reducing the displacement responses especially for large openings.

The load carrying capacity gets severely affected for shear wall with openings located in the form of two windows or three windows. The two window staggered opening resulted in the decreased load carrying capacity for both slender as well as squat shear walls when the openings are provided. The strengthening of the walls provided for two windows (regular) and three window openings resulted in brittle failure with reduced ductility index and hence such openings are not recommended. These investigations may lead to the possibility of developing certain guidelines in terms of optimum size of the opening as well as in identifying the potential zones of vulnerability of shear wall when the openings are present in certain precarious locations.

Keywords: *Shear wall, openings, ductility, cracking, yielding, time integration, damping, degenerated, shell, locking, nonlinear, time history, strengthening.*

Table of Contents

CONTENTS	Page No.
Acknowledgements	i-ii
Abstract	iii-vii
Contents	viii-xii
List of Tables	xiii
List of Figures	xiv-xvii
List of Abbreviations	xviii
List of Symbols	xix-xxiii
Chapter 1 Introduction	1-24
1.1 Background	1
1.2 Classification of Shear Walls	4
1.2.1 Based on structural materials	4
1.2.2 Based on aspect ratio	4
1.2.3 Geometry of shear wall	6
1.3 Failure Modes of RC Shear Wall	8
1.3.1 Shear failure mode (diagonal tension failure) - A brittle failure mode	8
1.3.2 Crushing failure mode - A brittle failure mode	9
1.3.3 Flexural failure mode - A ductile failure mode	9
1.3.4 Sliding shear failure mode	11
1.3.5 Rocking failure mode	11
1.4 Methods of Analysis of Shear Wall	11
1.4.1 Linear elastic procedure	12
1.4.2 Linear dynamic procedure	12
1.4.3 Non-linear static procedure	13
1.4.4 Non-linear dynamic procedure	13
1.5 Damping Characteristics in Structures	15
1.6 Ductility in Shear Wall	16
1.7 Shear Wall with Openings	19
1.8 Scope of the Present Study	20
1.9 Organization of the Thesis	20
<i>References</i>	22

CONTENTS	Page No.
Chapter 2 RC Shear Walls: State-of-the-Art	25-62
2.1 Background	25
2.2 Methods of Analysis of Shear Wall	26
2.2.1 Simplified methods	26
2.2.2 Finite element methods	30
2.3 Structural Response of Solid Shear Wall	31
2.4 Structural Response of Shear Wall with Openings	36
2.4.1 Experimental investigation	36
2.4.2 Analytical investigation	44
2.4.3 Shear walls - Codal Provisions	47
2.5 Damping in Structures	49
2.6 Damping Models	50
2.6.1 Viscous damping models	50
2.6.2 Non-viscous damping models	52
2.6.3 Active control damping models	53
2.6.4 Passive control damping models	53
2.7 Gaps in Existing Research	55
2.8 Objectives of the Present Study	54
<i>References</i>	56
Chapter 3 Material Modeling of RC Structures	63-100
3.1 Background	63
3.2 Experimental Behavior of Concrete	64
3.2.1 Uni-axial behavior	65
3.2.2 Bi-axial behavior	65
3.2.3 Tri-axial behavior	66
3.2.4 Cyclic behavior	66
3.3 Characteristics of Failure Surface of Concrete	67
3.4 Modeling of Concrete in Compression	71
3.4.1 Failure models of concrete	72
3.4.2 Willam-Warnke five parameter failure model: mathematical formulation	73

CONTENTS	Page No.
3.4.3 Hardening rule	75
3.4.4 Flow rule	79
3.4.5 Incremental theory of plasticity: Step-by-step procedure	81
3.5 Modeling of Concrete in Tension	87
3.5.1 Discrete crack modeling	88
3.5.2 Smeared crack modeling	88
3.5.3 Tension stiffening in reinforced concrete	91
3.5.4 Shear transfer	92
3.5.5 Constitutive law of concrete	94
3.6 Modeling of Steel Reinforcement	95
3.7 Summary	96
<i>References</i>	97
Chapter 4 Finite Element Analysis of RC Structures: Programming & Validation	101-148
4.1 Background	101
4.2 Finite Element Selection	103
4.3 Evolution of Shell Elements	105
4.3.1 Curved shell elements	105
4.3.2 Flat plate shell elements	105
4.3.3 Three-dimensional solid element for shell analysis	106
4.3.4 Degenerated shell elements	107
4.4 Formulation of Degenerated Shell Element	108
4.4.1 Strain displacement relationship	112
4.4.2 Element locking	115
4.4.3 Assumed natural strain formulation	118
4.5 Dynamic Analysis of RC Structures	119
4.5.1 Formulation of mass matrix	120
4.5.2 Formulation of damping matrix	122
4.6 Formulation of Newmark Method	124

CONTENTS	Page No.
4.7 Solution Algorithms	127
4.7.1 Euler – Cauchy forward integration	127
4.7.2 Newton – Raphson iterative procedure	127
4.8 Development of Computer Program	129
4.9 Program Validation	131
4.9.1 Analysis of structures subjected to static loads	131
4.9.2 Analysis of structures subjected to dynamic loads	136
4.10 Element Sensitivity Analysis	143
4.11 Summary	144
<i>References</i>	145
Chapter 5 Non-Linear Static Response of Shear Wall	149-180
5.1 Background	149
5.2 Influence of Openings on the Static Response of Shear Wall Panel	150
5.3 Influence of Opening Size on Structural Response of Slender and Squat Shear Wall	154
5.3.1 Influence of opening size on the ultimate load carrying capacity	159
5.3.2 Influence of openings on the displacement response of shear wall	161
5.4 Influence of Door Window Openings on the Response of Slender and Squat Shear Walls	167
5.4.1 Influence of door window openings on the load carrying capacity of shear wall	170
5.4.2 Influence of door window openings on the displacement response of shear wall	172
5.5 Summary	178
<i>References</i>	180

CONTENTS		Page No.
Chapter 6	Non-Linear Dynamic Response of Shear Wall	181-218
6.1	Background	181
6.2	Influence of Openings on Dynamic Response of Shear Wall Panel	182
6.3	Influence of Opening Size on Displacement Time History Response of Slender and Squat Shear Wall	187
6.4	Influence of Door Window Openings on Displacement Time History Response of Shear Wall	202
6.5	Summary	216
	<i>References</i>	218
Chapter 7	Summary and Conclusions	219-226
7.1	Summary	219
7.2	Conclusions	224
7.3	Further Scope of the Work	226
Appendix-1		
Appendix-2		
List of Publications		
Brief biography of Candidate		
Brief biography of Supervisor		

List of Tables

Table No.	Title	Page No.
4.1	Step by step Newmark β method of time integration	126
4.2	Displacement of square plate under uniform loading	132
4.3	Normalized vertical displacement at the free-end of cantilever beam	133
4.4	Comparison of displacement response of present study with Jagd (1996)	139
4.5	Material properties of concrete and steel	140
4.6	Displacement responses at different times	142
4.7	Comparison of responses for different mesh sizes	144
5.1	Ductility index and strength ratio of shear wall panel with various opening locations	153
5.2	Material properties used for the analysis	156
5.3	Summary of different opening sizes considered	156
5.4	Response of slender shear wall with different opening sizes	159
5.5	Response of squat shear wall with different opening sizes	159
5.6	Response of slender shear wall with different door window opening combinations	169
5.7	Response of squat shear wall with different door window opening combinations	169
6.1	Dynamic response of RC shear wall panel	186
6.2	Material properties used for the analysis	189
6.3	Dynamic characteristics of squat & slender shear wall	189
6.4	Geometrical details of openings	189
6.5	Max. displacement response and base shear demand - Slender shear wall with different opening sizes	194
6.6	Max. displacement response and base shear demand - Squat shear wall with different opening sizes	197
6.7	Max. displacement response and base shear demand - Slender shear wall with different door window opening combinations	207
6.8	Max. displacement response and base shear demand- Squat shear wall with different door window opening combinations	212

List of Figures

Figure No.	Title	Page No.
1.1	Building plan configuration of shear wall	1
1.2	In-plane deformation of shear wall	2
1.3	Deformation of shear wall	3
1.4	Classification of shear wall on the basis of aspect ratio	5
1.5	Orientation of diagonal cracks in the shear wall	5
1.6	Section of rectangular shear wall without boundary elements	7
1.7	Section of rectangular shear wall with boundary elements	7
1.8	Bar bell shaped shear wall with boundary elements	7
1.9	Flanged shear walls	7
1.10	Failure modes of the short/squat shear wall	10
1.11	Failure modes of the slender shear wall	10
1.12	Dynamics of rigid block	13
1.13	Vibration of a system	15
1.14	Various aerodynamic modifications to corner geometry	16
1.15	Displacements and rotations at yield, plastic and ultimate stage	17
1.16	Ductility models	18
2.1	Simplified methods of analysis of shear wall	27
2.2	Continuous system approach	29
2.3	Shear wall with openings	39
2.4	Shear wall with staggered opening	40
2.5	Shear wall panel with different opening positions	41
2.6	Shear wall panels with openings of various sizes and locations	43
2.7	Effect of diagonal reinforcement on the structural response of shear wall	45
2.8	Viscous damping response	51
2.9	Different types of auxiliary damping system	53

Figure No.	Title	Page No.
3.1	Yield surface in 3-dimensional principal stress space	69
3.2	Characteristics of failure surface	69
3.3	Trace of the deviatoric section of Willam-Warnke five parameter failure surface	74
3.4	Isotropic hardening with expanding yield surfaces and the corresponding uni-axial stress-strain curve	76
3.5	Incremental stress changes in an already yielded point in an elasto-plastic continuum	86
3.6	Incremental stress changes in an already yielded point in an elasto-plastic continuum at initial yield	87
3.7	Refined process for reducing a stress point to the yield surface	87
3.8	Discrete crack approach	89
3.9	Smearred crack approach	89
3.10	Tension stiffening effect of cracked concrete	92
3.11	Stress-strain curve for steel	96
4.1	Isoparametric class of finite elements	104
4.2	Geometry of 9-noded degenerated shell element	108
4.3	Sampling point locations for assumed shear/membrane strains	118
4.4	Variation of damping with circular frequency	124
4.5	Iterative algorithm	128
4.6	Program layout – NLDAS	130
4.7	Clamped square plate under uniform loading	131
4.8	Cantilever beam subjected to point load at the free end	133
4.9	Geometry of solid RC shear wall	135
4.10	Load deformation response of shear wall subjected to monotonically increasing load	136
4.11	Crack and yield patterns	136
4.12	Web side elevation of international standard problem	137
4.13	Flange side elevation of international standard problem	137
4.14	Top view of shear wall	138
4.15	Reinforcement pattern for ISP shear wall	138
4.16	Earthquake ground motion applied at the base of the structure	138

Figure No.	Title	Page No.
4.17	Finite element idealization of rectangular shear wall	140
4.18	Input ground acceleration applied at the base of shear wall	141
4.19(a)	Experimental displacement time history of the shear wall	141
4.19(b)	Analytical displacement time history of the shear wall	142
4.20	Displacement response history response of shear wall subjected to scaled EL Centro earthquake 1940 (Present study)	142
4.21	Load-displacement response of squat shear wall for different mesh sizes	143
5.1	Geometry of solid RC shear wall panel	151
5.2	Shear wall panel with different opening locations	151
5.3	Load-displacement response of RC shear wall panel	152
5.4	Yield pattern of shear wall panel with various opening locations	153
5.5	Ductile detailing (strengthening) around openings for a typical storey	155
5.6	Discretization of slender shear wall with various opening sizes	157
5.7	Discretization of squat shear wall with various opening sizes	157
5.8	Influence of opening size on the response of slender and squat RC shear wall	158
5.9	Ductility based on reduced stiffness equivalent elasto-plastic yield	162
5.10	Normalized ultimate load, ultimate displacement and ductility of slender shear wall with different openings without strengthening	163
5.11	Normalized ultimate load, ultimate displacement, ductility of RC slender shear wall with different openings with strengthening	163
5.12	Normalized ultimate load, ultimate displacement, ductility of RC squat shear wall with different openings without strengthening	165
5.13	Normalized ultimate load, ultimate displacement, ductility of RC squat shear wall with different openings with strengthening	165
5.14	Influence of door window openings on the displacement response of slender and squat shear wall	168
5.15	Normalized ultimate load, ultimate displacement, ductility of RC slender shear wall with different door window opening combinations without strengthening	173

Figure No.	Title	Page No.
5.16	Normalized ultimate load, ultimate displacement, ductility of RC slender shear wall with different door window opening combinations with strengthening	173
5.17	Normalized ultimate load, ultimate displacement, ductility of RC squat shear wall with different door window opening combinations without strengthening	178
5.18	Normalized ultimate load, ultimate displacement, ductility of RC squat shear wall with different door window opening combinations with strengthening	178
6.1	Geometry of solid RC shear wall panel	183
6.2	Input ground acceleration	183
6.3(a)	Displacement time history response of shear wall panel for various opening locations (5% damping)	184
6.3(b)	Displacement time history response of shear wall panel for various opening locations (2% damping)	185
6.4	Discretization of slender shear wall with various opening sizes	190
6.5	Discretization of squat shear wall with various opening sizes	190
6.6	Displacement time history response of RC slender shear wall for different opening sizes for 5% damping	191-192
6.7	Displacement time history response of RC slender shear wall for different opening sizes for 2% damping	192-193
6.8	Displacement time history response of RC squat shear wall for different opening sizes for 5% damping	197-198
6.9	Displacement time history response of RC squat shear wall for different opening sizes for 2% damping	199-200
6.10	Displacement time history response of RC slender shear wall for different door window opening combinations for 5% damping	203-204
6.11	Displacement time history response of RC slender shear wall for different door window opening combinations for 2% damping	205-206
6.12	Displacement time history response of RC squat shear wall for different door window opening combinations for 5% damping	209-210
6.13	Displacement time history response of RC squat shear wall for different door window opening combinations for 2% damping	211-212

List of Abbreviations

Abbreviations	Description
DTREC	Interval at which the earthquake records are available
IFIXD	Indicator for excitation 0 - Horizontal Acceleration 1 - Vertical Acceleration 2 - Both Horizontal & Vertical excitation
IFUNC	Time Function Code 0 - Acceleration Time History 1 - Heaviside function 2 - Harmonic excitation
IPRED	Algorithm type 0 - Standard Algorithm 1 - Modified Algorithm
KSTEP	Number of steps after which the stiffness matrix is updated
MITER	Maximum number of iterations
NACCE	Number of acceleration points
NCONM	Number of concentrated masses
NGAUM	Integration rule for mass matrix
NGAUS	Order of integration rule to be employed
NLAPS	Indicator for type of analysis 0 - Elastic Analysis 1 - Elasto-Plastic small displacement analysis 2 - Elastic-large displacement analysis
NOUTD	Writes displacements and stress histories of required points
NREQD	Number of nodes for selective output of displacement
NREQS	Number of integration points for selective output of stresses
NSTAT	State of the Gaussian Point during the analysis 1 - Concrete in elastic stage 2 - Cracking of concrete in one direction 3 - Cracking of concrete in both directions 4 - Yielding of concrete 5 - Reinforcement in elastic stage 6- Yielding of reinforcement (Hardening) 7 - Crushing of concrete
NSTEP	Number of Time Steps specified for the total solution
POSGP	Sampling Point Positions (Gaussian points)
TOLER	Tolerance for Displacement convergence criteria
WEIGP	Weighting factors for Gaussian Integration

Symbols

\ddot{u}	Acceleration
ν	Accuracy parameter in Newmark method
θ	Angle of similarity
$V_{b,d}$	Base shear demand
K	Bulk modulus
f_{ck}	Characteristic compressive strength of concrete in 28 days
ω	Circular Frequency (in rad/Sec)
α	Coefficient for mass proportional damping
β_d	Coefficient for stiffness proportional damping
$\{ \}$	Column vector
Δt_{cr}	Critical time step
Δt_{cr}	Critical time step
ϕ_u	Curvature at ultimate stage
ϕ_y	Curvature at yield stage
μ_ϕ	Curvature ductility ratio
f_{cy}	Cyclic Frequency (in Hz)
ω_D	Damped circular frequency (in rad/s)
T_D	Damped time period
C_d	Damper coefficient
F_d	Damper force
c	Damping
α_d	Damping exponent
ζ	Damping ratio
C	Dashpot constant
$u_i, v_i, w_i, \theta_x, \theta_y$	Degrees of freedom (3 translation+2 rotations of normal)

$ $	Determinant
r	Deviatoric length
e_{ij}	Deviatoric strain tensor
ρ	Deviatoric stress invariant
S_{ij}	Deviatoric stress tensor
v_{3k}	Direction Cosines of the normal
δ	Displacement
u	Displacement
Δ_p	Displacement at plastic stage
Δ_u	Displacement at ultimate stage
Δ_y	Displacement at yield stage
μ_Δ	Displacement ductility ratio
$\mu_\Delta, \mu_\phi, \mu_s$	Displacement Ductility, Curvature ductility, Strain ductility
u, \dot{u}, \ddot{u}	Displacement, velocity, acceleration
μ	Ductility ratio
M_L	Earthquake magnitude
K^*	Effective stiffness matrix
D	Elastic constitutive matrix
D_{ep}	Elasto-plastic Constitutive Matrix
E	Energy released in Earthquake
γ	Engineering shear strain
f'_{bc}	Equal biaxial compressive strength
$R(t)$	External force varying with time
f	Failure/yield function
I_1, I_2, I_3	First, second, third invariants of stress tensor
\mathbf{a}	Flow vector
f_n	Fundamental natural frequency

T	Fundamental natural time period
κ	Hardening parameter
H	Height of the shear wall
ξ	Hydrostatic length
p_{hs}	Hydrostatic pressure or spherical stress
ξ	Hydrostatic stress invariant
u_0	Initial displacement
\dot{u}_0	Initial velocity
J	Jacobian matrix
ω_{max}	Largest natural frequency of the structure
L_p	Length of plastic hinge
m	mass
ρ_m	Mass density of a material
\mathbf{M}	Mass matrix
m_i	Mass of the i^{th} story
$[\]$	Matrix
u_{max}	Maximum displacement
ε_j	Maximum value reached by the tensile strain at the point considered
σ_m	Mean normal stress
τ_m	Mean shear stress
ω_n	Natural circular frequency (in rad/s)
ξ, η, ζ	Natural coordinates
$\tilde{\xi}, \tilde{\eta}$	Natural coordinates of the sampling points for the interpolation of $\gamma_{\xi\zeta}$
$\bar{\xi}, \bar{\eta}$	Natural coordinates of the sampling points for the interpolation of $\gamma_{\eta\zeta}$
T_n	Natural time period
σ	Normal stress
γ_{oct}	Octahedral engineering shear strain
ε_{oct}	Octahedral normal strain

σ_{oct}	Octahedral normal stress
τ_{oct}	Octahedral shear stress
$a_0, b_0, a_1, b_1, a_2, b_2$	Parameters of Willam-Warnke failure model
g	Plastic potential function
ν_{ij}	Poisson's ratio for transverse strain in the i^{th} direction when stressed in j -direction
β_{rg}	Pre selected constant to take care of aggregate interlock
$\epsilon_1, \epsilon_2, \epsilon_3$	Principal strains, tensile strain positive
S_1, S_2, S_3	Principal stress deviators
$\sigma_1, \sigma_2, \sigma_3$	Principal stresses, tensile stress positive
\dot{u}_d	Relative velocity between the two ends of the damper
θ_p	Rotation at plastic stage
θ_u	Rotation at ultimate stage
θ_y	Rotation at yield stage
$\{ \}^T$	Row vector
J_2	Second invariant of stress deviator tensor
N_i	Shape functions
c_1, c_2	Shear Correction factors in the 1-3 plane and 2-3 plane respectively
G_{12}, G_{13}, G_{23}	Shear Modulus of cracked concrete in 12, 13, 23 planes respectively
τ	Shear stress
β	Stability parameter in Newmark method
k	Stiffness
ϵ_u	Strain at ultimate stage
ϵ_y	Strain at yield stage
μ_s	Strain ductility ratio
ϵ_{ij}	Strain tensor
B	Strain-displacement matrix

σ_{ij}	Stress tensor
α_{ts}	Tension stiffening coefficient, may vary from 0.5 - 0.7, depending on the relative percentage of steel
ε_{ts}	Tension stiffening constant
ξ_{eff}	The composite damping ratio of the structure
h_i	Thickness of shell element at node 'i'
J_3	Third invariant of stress deviator tensor
t	Time
Δt	Time increment
Δt	Time step
\mathbf{T}	Transformation matrix
ε_u	Ultimate strain/Crushing strain
f'_c	Uni-axial compressive cylinder strength
H'	Uni-axial strain hardening parameter
f'_t	Uni-axial tensile strength
\dot{u}	Velocity
ε_v	Volumetric strain
W	Width of the shear wall
E_i	Young's Modulus in i^{th} direction

1.1 Background

In the 21st century, there has been the tremendous growth in the infrastructure development in the developing countries, especially India, in terms of construction of buildings, bridges and industries etc. This infrastructure development is mainly due to the growing population and to fulfill their demands. Since the land is limited, there is a huge scarcity of land in urban cities. To overcome this problem tall and slender multi-storied buildings are constructed. There is a high possibility that such structures are subjected to huge lateral loads. These lateral loads are generated either due to wind blowing against the building or due to inertia forces induced by ground shaking (excitation) which tends to snap the building in shear and push it over in bending. In the framed buildings, the vertical loads are resisted by frames only, however, the lateral resistance is provided by the infill wall panels. For the framed buildings taller than 10-stories, frame action obtained by the interaction of slabs and columns is not adequate to give required lateral stiffness (Taranath, 2010) and hence the framed structures become an uneconomical solution for tall buildings. The lateral forces due to wind and earthquake are generally resisted by the use of shear wall system, which is one of the most efficient methods of maintaining the lateral stability of tall buildings. In practice, shear walls are provided in most of the commercial and residential buildings upto thirty storeys beyond which tubular structures are recommended. Shear walls may be provided in one plane or in both planes. The typical shear wall system with shear walls located in both the planes and subjected to lateral loads is shown in Fig. 1.1(a). In such cases, the columns are primarily designed to resist gravity loads.

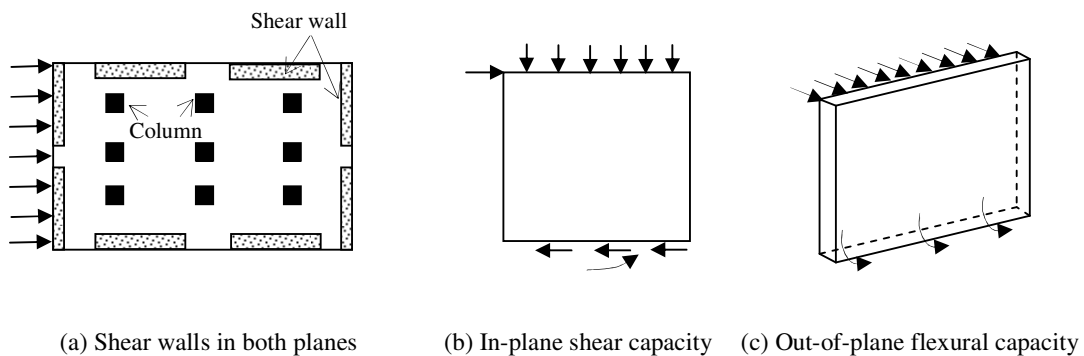


Fig. 1.1: Building plan configuration of shear wall

The shear walls are expected to resist large lateral loads (due to earthquake or wind) that may strike “in-plane” [Fig. 1.1(b)] and “out-of-plane” [Fig. 1.1(c)] to the wall. The in-plane shear resistance of the shear wall can be estimated by subjecting the wall to the lateral loads as shown in Fig. 1.1(b). On the other hand, the flexural capacity can be estimated by subjecting the shear wall to the out-of-plane lateral loads as shown in Fig. 1.1(c). During extreme earthquake ground motions, the response of a structure is dependent upon the amount of seismic energy fed in and how this energy is consumed. Since the elastic capacity of the structure is limited by the material strength, survival generally relies on the ductility of the structure to dissipate energy. At higher loads, inelastic deformation arises which are permanent and imply some damage. The damages generally vary from minor cracks to major deterioration of structure, which may be beyond repair. It has been learnt from past experiences that the shear wall buildings exhibit excellent performance during the severe ground motion due to stiff behavior at service loads and ductile behavior at higher loads thus preventing the major damage to the RC buildings (Fintel, 1977). The behavior of shear wall can be ascertained well by observing the deflected shape. The deflected shape of the tall shear wall is dominated by flexure and that of short shear walls by shear as shown in Fig. 1.2.

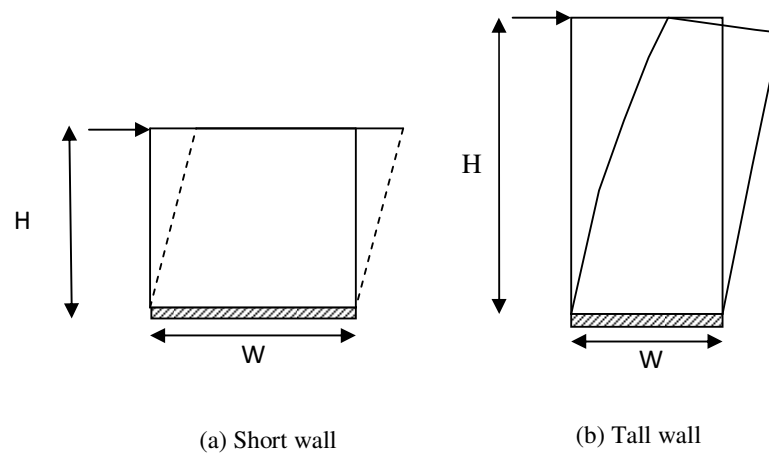


Fig. 1.2: In-plane deformation of shear wall

Thus, in the case of tall shear wall, the deflected shape can be determined using the simple bending theory by ignoring shear deformation. However, it becomes necessary to include shear deformation in the case of short walls. The total deformation of a shear wall is the sum of the (i) flexural deformation, (ii) shear deformation, and (iii) slip deformation as shown in Fig. 1.3.

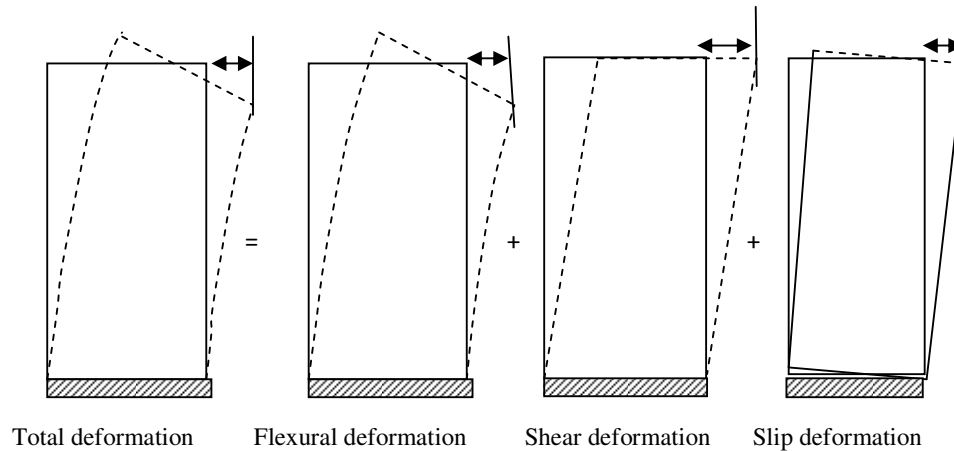


Fig. 1.3: Deformation of shear wall

Though tall shear wall is to be precisely defined as structural walls, however, for simplicity, it is denoted as shear wall only. Several experimental and analytical investigations have been performed in assessing the behavior of the shear walls (Rahimian 2011; Klinger et al. 2012; Paulay and Priestley 1992; Atimtay and Kanit 2006; Elnashai et al. 1990; Taranath 2010; Lefas et al. 1990; Derecho et al. 1979; Mullapudi et al. 2009; Paknahad et al. 2007; Thomsen and Wallace (1995, 2004); Ghorbanirenani et.al. 2012). On the basis of above investigations, it was found that shear walls possess certain inherent characteristics if designed and detailed properly.

The strength, stiffness and ductility are the essential requirements of shear wall and need to be assessed for its structural performance (Derecho et al. 1979; Farvashany et al. 2008; IS 13920 1993; IS 4326 1993). Strength limits the damage and stiffness reduces the deformation in the shear wall. Ductility, defined as ability to sustain inelastic deformations without much strength and stiffness degradation, has been considered very essential requirement, especially under severe dynamic loading conditions. Hence, the basic criteria that the designer has to satisfy while designing shear walls in earthquake resistant structures are as follows:

- To impart adequate stiffness to the building so that during moderate seismic disturbances, complete protection against damage, particularly to non-structural components, is guaranteed.
- To provide adequate strength to building in order to ensure that an elastic seismic response does not result in more than superficial structural damage.

- To provide adequate structural ductility to building in order to dissipate energy for the situation when the largest disturbance to be expected in the region does occur. Even the extensive damage, perhaps beyond the possibility of repair, is accepted under extreme conditions, but prevention of sudden collapse must be ensured under any dire circumstances.

Sometimes, shear walls are pierced with openings to fulfill the functional as well as architectural requirements of buildings. The structural response of shear wall may be influenced by the presence of openings, depending upon their sizes and their positions. The present study aims to accomplish this task by investigating the response of shear walls in the presence of openings.

1.2 Classification of Shear Walls

Based on several experimental and analytical investigations, the shear walls are mainly classified on the basis of (i) structural materials (ii) aspect ratio, and (iii) geometry.

1.2.1 Based on structural materials

Depending on the structural materials, shear walls are usually classified as (i) steel shear wall (ii) timber shear wall (iii) reinforced masonry shear wall, and (iv) RC shear wall. Though steel shear walls are considered to have excellent strength to weight ratio, its use is normally restricted to industrial structures due to high initial cost. The timber shear walls, light weight structure, are very advantageous in the cold region; its use is not advisable for high-rise structures due to its limited strength. Similarly, reinforced masonry shear walls are not permitted beyond four storeys because of inherent instability of tall buildings. The RC shear walls are very prominently used in common residential and commercial complexes and hence been the subject of intense research for many decades.

1.2.2 Based on aspect ratio

The ratio of height (H) to width (W) of the shear wall, generally referred as aspect ratio, is one of the most important parameters influencing the structural behavior of shear wall. The classification of shear walls based on aspect ratio is shown in Fig. 1.4. The shear wall is considered to be short if the aspect ratio is less than unity. The short shear walls

were extensively used in the early 1920's to provide the line of defense in military operations though not with the name 'shear walls'.

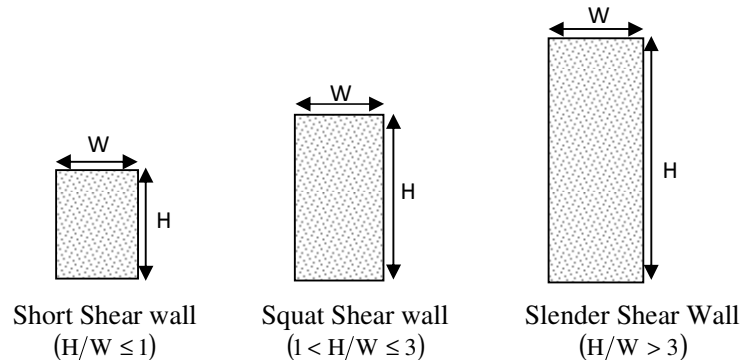


Fig. 1.4: Classification of shear wall on the basis of aspect ratio

The shear walls are considered squat if the aspect ratio lies between one and three. The squat and short shear walls generally fail in shear, which is often undesirable since they result in brittle failure (Paulay and Priestley, 1992). On the other hand, the shear wall with aspect ratio greater than three is considered slender shear wall. In case of slender shear walls, flexure mode predominates and, therefore, the shear deformation is generally neglected in the analysis. The analysis of squat shear walls becomes complex due to heavy coupling of flexural and shear modes. The cracks in the lower portion of the shear wall are common irrespective of their aspect ratio. These cracks usually originate at bottom portion of shear wall at an angle of 45° with respect to horizontal axis and referred as diagonal cracks. For slender and squat shear walls these cracks are extended up to full width of the shear wall, however, for short shear walls these cracks terminate somewhere within the width of the shear wall depending on the aspect ratio.

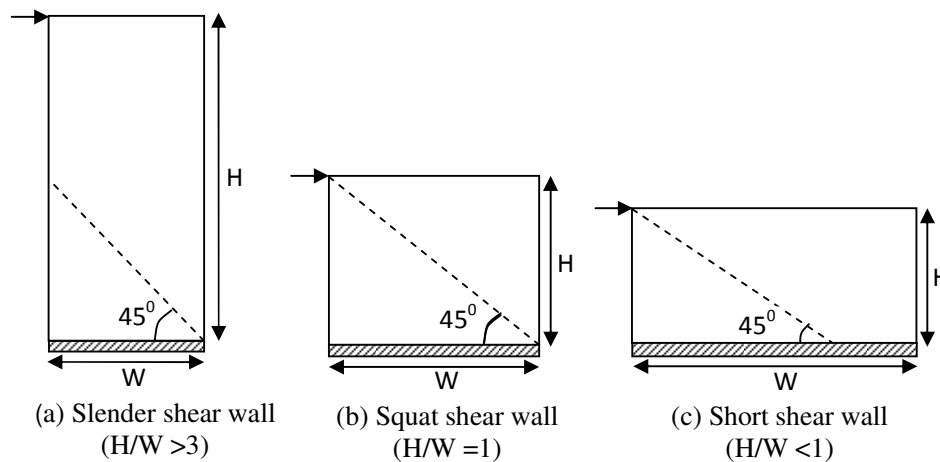


Fig. 1.5: Orientation of diagonal cracks in the shear wall

Moreover, for the slender shear walls the cracks are concentrated near the bottom of the shear wall, however, for short and squat shear walls these cracks are found to be smeared throughout the height of shear wall. The orientation of diagonal cracks in typical slender, squat, and short shear walls is shown in Fig. 1.5.

1.2.3 Geometry of shear wall

Based on the geometry of shear wall, there may be many types of reinforced concrete shear walls such as (a) rectangular shear walls, (b) Bar bell shaped shear walls, (c) flanged shear walls, (d) coupled shear walls, (e) framed shear wall, (f) column supported shear wall, and (g) core shear wall. Out of all shear walls, rectangular shear walls, bar bell shaped shear walls and flanged shear walls are quite common and adopted in practice. Hence, the current section deals with these types of shear wall only.

Rectangular shear wall without boundary elements

The plane rectangular shear wall is the simplest form of shear wall in which only horizontal and vertical reinforcement are provided. The vertical and horizontal reinforcing bars are provided at a uniform spacing throughout the shear wall as shown in Fig. 1.6. The vertical reinforcement not only provides flexural as well as shear resistance, but also controls the shear cracking and improves the ductility. Horizontal reinforcement provides partial shear strength. Nevertheless, the edges experience high compressive and tensile stresses which necessitate the need to strengthen those portions. The strengthening of the edges can be accomplished by any one of the following means.

Rectangular shear wall with boundary elements

In order to strengthen the shear wall as well to prevent the overstressing of the ends, the rectangular shear wall is generally being provided with the extra reinforcement at the ends without any increase in thickness of shear wall. Such type of shear walls are commonly known as rectangular shear wall with boundary elements and these end regions of the walls with increased reinforcement are called boundary elements (Murthy, 2004), which adds confinement to the concrete. To achieve this confinement in the boundary elements, vertical as well as horizontal bars are provided at much closer spacing as shown in Fig. 1.7.

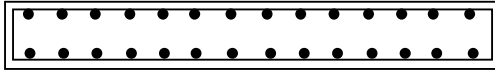


Fig. 1.6: Section of rectangular shear wall without boundary elements

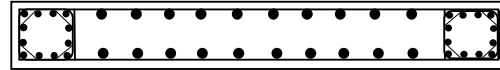


Fig. 1.7: Section of rectangular shear wall with boundary elements

The shear walls with boundary elements, enhances the shear resistance and ductility of the shear wall, however, no significant increase in flexural capacity is observed. Nevertheless, this confinement enables concrete to sustain the load reversals without losing strength. Shear walls with boundary elements are commonly used in shear wall buildings of shorter height (i.e. up to five storeys).

Bar bell shaped shear wall

Sometimes, the steel in boundary elements becomes very large to accommodate within normal thickness. Hence, there is a need to increase the thickness of the shear wall at the ends. Such shear walls are known as bar bell shaped shear walls, as shown in Fig. 1.8.

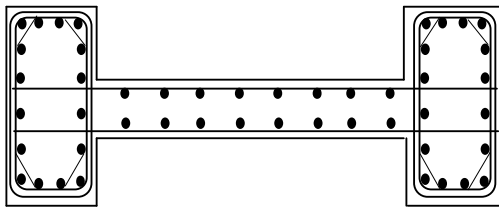


Fig. 1.8: Bar bell shaped shear wall with boundary elements

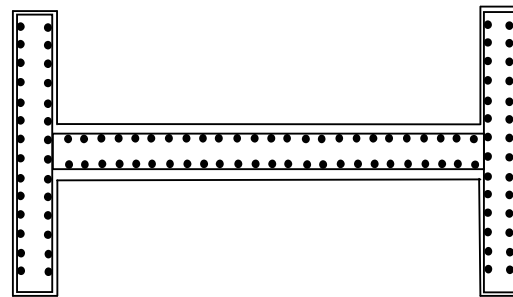


Fig. 1.9: Flanged shear walls

The ends are known as boundary elements. The bar bell shaped shear walls are somewhat stronger and more ductile than the simple rectangular type of uniform section. These walls are generally designed to possess higher shear strength and hence failure is designed to take place by yielding of steel. Nevertheless, bar bell shear walls are very rigid during severe ground motion and hence attracts larger inertia forces and dissipate lot of energy by cracking, which is difficult to repair. Bar bell shaped shear walls are particularly strong in developing moment-capacity. These types of shear walls are frequently used for tall multi-storeyed buildings where both vertical load carrying capacity and lateral resistance are considered essential.

Flanged shear wall

The flanged shear walls are widely used in nuclear power plants as well as in the elevator cores of high-rise buildings. Flanged shear walls are preferred over the rectangular shear walls when the aspect ratio of the shear wall exceeds unity. Though the flanges are out-of-plane to the web as shown in Fig. 1.9, it has been observed that the performance of flanged shear walls has been found to be better in resisting bending stresses as compared to rectangular shear walls. However, flanged shear walls do not enhance shear capacity as much as the moment, because the flange does not increase the gross area as it does the moment of inertia. The flanged shear walls are mostly suitable for tall multi-storey buildings where vertical load carrying capacity as well as lateral load resistance is important.

1.3 Failure Modes of RC Shear Wall

In order to characterize the behavior of RC shear wall, it is essential to understand the failure modes of RC shear wall. The failure modes of the shear wall are greatly influenced by (i) aspect ratio, and (ii) cross-sectional geometry. Slender shear walls, designed for flexural strength, behave like a vertical slender cantilever beam, and therefore, primary mode of deformation of slender shear wall is bending. On the other hand, the design of short/squat shear walls is governed by shear strength and possesses significant amount of shear deformation in addition to bending deformation. In the short/squat shear walls, shear transfer takes place by the truss action which provides a stiffer system than that for slender walls. Unlike slender shear walls, squat shear walls do not show any significant difference in behavior under monotonic and reversed cyclic loading. Several experimental investigations have been conducted over the period of last five decades in order to assess the failure modes of the shear wall (Thomsen and Wallace 1995, 2004). The different failure modes namely, flexure, shear, crushing, sliding and rocking are discussed in the current section.

1.3.1 Shear failure mode (diagonal tension failure) - A brittle failure mode

Shear failure mode is generally not the desired failure mechanism and is considered unsafe. This type of failure is mainly due to the diagonal tension and hence shear failure is also known as diagonal tension failure. Due to shear failure, the vertical load carrying

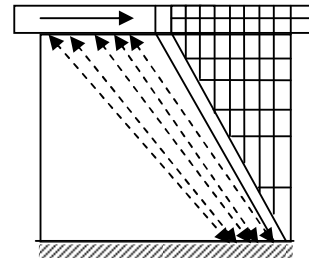
capacity of the shear wall is lost even at relatively low strains. Shear failure is the common mode of failure of squat shear walls as shown in Fig. 1.10(a), where achieving ductility is a herculean task. Due to high shear stresses and relatively low flexural stresses, shear walls develop principal tensile stresses with approximately 45° inclinations. Since the tensile strength of concrete is considered very low in comparison to compressive strength, the cracks are formed during the early stages of loading itself. The diagonal cracks are effectively restrained by providing horizontal reinforcement. Nevertheless, if the horizontal reinforcement provided is less or insufficient to sustain diagonal tensile stresses then the diagonal tension failure occurs. The horizontal reinforcement improves the inelastic response of shear walls subjected to high nominal shear stress by reducing shear deformation. However, the horizontal reinforcement is ineffective in resisting sliding shear.

1.3.2 Crushing failure mode - A brittle failure mode

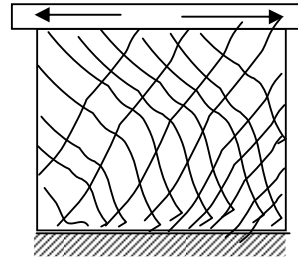
Crushing failure mode occurs due to the diagonal compression because of inadequate confinement of the compression zone. This mode of failure is the most unsafe of all mechanisms and such failures are considered very brittle as crushing of concrete takes place prior to yielding of steel. The diagonal compression failure becomes more severe under reversed cyclic loading conditions. The crack pattern due to diagonal compression failure mode is shown in Fig. 1.10(b).

1.3.3 Flexural failure mode - A ductile failure mode

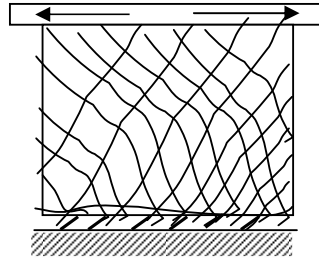
Flexural failure mode, a ductile failure mode, is a very safe mechanism and is considered an ideal choice of failure modes. Flexural failure is generally observed in the case of slender shear walls as shown in Fig. 1.11(a), and such mode of failure is very difficult to attain in the case of squat and short shear walls. They develop a predominantly horizontal crack pattern in the lower hinging region after a few cycles of inelastic deformation. Nevertheless, under reversed cyclic loading, slender shear walls show less flexural strength and deformation in comparison to monotonic loading. Moreover, the actual flexural capacity of the wall is generally found to be significantly higher than the design flexural capacity, due to strain hardening of the vertical reinforcement. It has been observed that for the same amount of vertical reinforcement, shear walls having reinforcement concentrated in the boundary elements possess higher flexural capacity and higher ultimate curvature than the walls having uniformly distributed reinforcement (Paulay and Priestley, 1992).



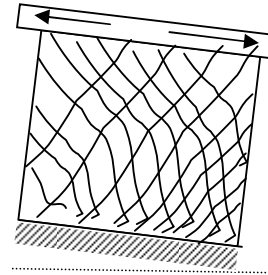
(a) Diagonal tension failure



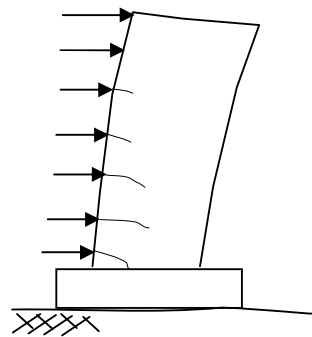
(b) Diagonal compression failure



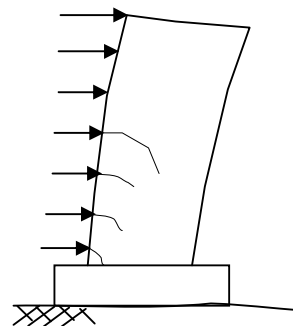
(c) Sliding shear failure



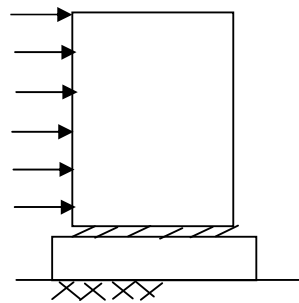
(d) Rocking failure

Fig. 1.10: Failure modes of the short/squat shear wall

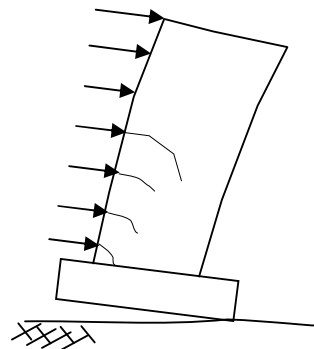
(a) Flexural failure



(b) Flexural shear failure



(c) Sliding failure



(d) Rocking failure

Fig. 1.11: Failure modes of the slender shear wall

1.3.4 Sliding shear failure mode

Sliding shear failure mode is caused primarily because of horizontal crack formation at the interface of wall and foundation. This mode of failure is responsible for significant degradation of stiffness and pinching of hysteresis loops. Sliding shear failure mode can be recognized by sliding of the wall along the construction joint at the base. The sliding shear failure for short/squat and slender shear walls are shown in Fig. 1.10(c) and Fig. 1.11(c) respectively. Sliding shear failure is especially more common in walls having considerably low aspect ratio. The sliding shear failure can be minimized by providing diagonal reinforcement. Moreover, diagonal reinforcement contributes to the flexural strength and improves the energy dissipation capacity. However, in practice, the diagonal reinforcement is replaced with horizontal and vertical reinforcement due to practical difficulties. Though sliding is not generally a desired failure mode, but appears to have happened widely, particularly at poorly formed and compacted construction joints. Since the gravity load carrying capacity is not altered in a sliding shear failure, it is not inherently an unsafe mechanism. The sliding shear failure can be minimized by maintaining high axial load to lateral load ratio.

1.3.5 Rocking failure mode

Rocking has probably saved many walls that would otherwise have failed if they had rigid foundations. The rocking failure for short/squat shear wall and slender shear wall are depicted in Fig. 1.10(d) and Fig. 1.11(d) respectively. Although inherently a simple mechanism, rocking is dynamically complex but considered a very safe mechanism of failure.

1.4 Methods of Analysis of Shear Wall

In the early days, several conventional analytical methods were developed and adopted for the elastic analysis, specifically to shear wall. The popular conventional methods may be enumerated as (i) Continuous Connection Method, (ii) Transfer Matrix Method, (iii) Wide Column Analogy or frame analysis, (iv) Discrete Force Method, etc. Nevertheless, these methods involve assumptions of linear elasticity and cannot be programmed to handle complex problems, especially under severe earthquake ground motion. The Finite Element Method (FEM) has been the most versatile and

successfully employed method of analysis to accurately predict the structural behavior of reinforced concrete shear walls in linear as well as in non-linear range under static and dynamic loading conditions. The analytical procedures of the shear wall may be broadly categorized into (i) Linear Elastic Procedure, (ii) Linear Dynamic Procedure, (iii) Non-linear Static Procedure, and (iv) Non-linear Dynamic Procedure.

1.4.1 Linear elastic procedure

In earlier days, the analysis of RC shear walls were based on the fact that the concrete remains uncracked and hence the linear elastic behavior was followed in predicting the response. Michael et al. (1970) used linear elastic finite element analysis with substructure approach to analyze the shear walls with and without openings and observed that the finite element results were in good agreement with experimental results in the linear elastic range (Michael et al. 1970). Petersson and Popov (1976) developed a special purpose finite element computer program for the analysis and design of structural walls with and without openings. This computer program was capable of predicting the behavior of structural walls with multiple openings. Nevertheless, several building codes including International Building Code (IBC 2000) considers the use of cracked section and recommends the use of reduced stiffness after the onset of cracking. Sometimes, the reduced stiffness is found to be 75 to 80% of the gross un-cracked cross section's stiffness. This procedure of analysis is incapable of capturing the higher modes of deformation.

1.4.2 Linear dynamic procedure

The linear dynamic procedure incorporates the effect of higher modes of deformation and considers actual distribution of forces in the elastic range in a better way as compared to linear static procedure (Mothei, 2005; Su and Wong, 2007). The use of linear dynamic procedures such as mode superposition and response spectrum method has been found extremely popular for linear systems. Nevertheless, in reality, during strong earthquakes, buildings are generally subjected to large inertia forces, which cause members of buildings to behave in a non-linear manner. In such scenarios, linear analysis fails to capture the actual strength of the structural members, which is only possible with non-linear static or non-linear dynamic analysis procedure (Naeim, 2001).

1.4.3 Non-linear static procedure

The non-linear static procedure is an improvement over the linear static analysis in the sense that it allows the inelastic behavior of the structure. In this method, the magnitude of the structural loading is incrementally increased in accordance with a certain predefined pattern. The non-linear static procedure gives accurate results for structures whose response is dominated by a fundamental mode. This method of analysis neglects the variation of loading with time, the influence of higher modes and the effect of resonance. For structures that are more flexible, the response quantities are strongly influenced by higher modes and hence non-linear static procedure predicts highly inaccurate results for such cases (Mothei, 2005). The non-linear dynamic procedure is the only method to describe the actual behavior of the structure during strong earthquakes (Su and Wong, 2007). This method is based on the direct numerical integration of the differential equation of motion.

1.4.4 Non-linear dynamic procedure

According to D'Alembert's principle, the unbalanced force is proportional to the acceleration of the structure and the constant of proportionality being the mass. Considering the free body diagram of rigid block shown in Fig. 1.12, the equation of motion of rigid block of mass 'm' in the lateral direction is given by

$$R(t) - ku - c\dot{u} = m\ddot{u} \quad \Rightarrow \quad m\ddot{u} + c\dot{u} + k u = R(t) \quad [1.1]$$

The above equation is the second order linear differential equation with constant coefficients. However for the non-linear case, the above equation is represented as

$$m\ddot{u} + c\dot{u} + f_s(u, \dot{u}) = R(t) \quad [1.2]$$

The constant coefficients m , c and k are the mass, damping and stiffness components respectively and $R(t)$ is an external force, which varies with time 't'. The term f_s represents the restoring force component which varies with time.

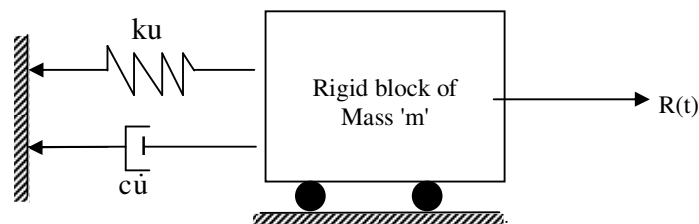


Fig. 1.12: Dynamics of rigid block

In order to define the motion of rigid block of mass m at various time intervals, it is normally suggested to use direct step-by-step time integration. The direct step-by-step time integration is computationally very demanding than response spectrum technique. Mothei (2005) observed that for RC structures, the inelastic time history method has been found to give displacements up to 10% higher than the spectral analysis (Mothei, 2005). The direct integration method is further classified into implicit and explicit methods. Both the methods are extensively used in determining the response of the structure at discrete time intervals. The various implicit and explicit direct integration methods are well described in the literature (Chopra, 2006; Clough and Penzien, 2003; Bathe, 1996). However, for completeness, the explicit and implicit time integration methods are discussed briefly.

Explicit time integration

In the explicit time integration methods the response at time ' $t + \Delta t$ ' is calculated from the equilibrium at time ' t '. The explicit method of integration is commonly used for determining the response of the structure subjected to blast or impact loads. Central difference method is the most popular explicit methods used in the time integration. The use of explicit central difference method in wave propagation problem is well documented in the literature (Bathe, 1996). The advantage of explicit time integration is that the stiffness matrix need not be assembled completely and hence diagonalization is completely avoided. This method is very advantageous provided mass matrix is diagonal. The diagonal mass matrix is obtained by lumping the masses at nodes. The major drawback of explicit time integration is that the time step ' Δt ' used for calculation of response has to be smaller than the critical time step ($\Delta t_{cr} = 2/\omega_{max}$) to ensure the stable solution. Hence, the time step is bounded by the largest natural circular frequency of the structure. If the time step is not strictly followed, then the solution can be unstable with very large displacements even in the case of linear analysis.

Implicit time integration

In the implicit time integration, the solution at time ' $t + \Delta t$ ' involves the equilibrium equation at ' $t + \Delta t$ ' and hence results in an iterative solution. The Newmark Beta method, also popularly known as trapezoidal rule, is the most common of all implicit methods, and is unconditionally stable and allows larger time step to be used in the computation of the response (Bathe, 1996).

1.5 Damping Characteristics in Structures

Damping can be defined as the characteristic in which certain energy is lost irrecoverably over the period of time, thus resulting in the decay of response. The free vibration response of the structure when subjected to initial displacement and velocity is depicted in Fig. 1.13(a) and Fig. 1.13(b) for undamped and damped cases respectively. For the undamped case, the response repeats after every cycle and continues forever, representing no energy loss [Fig. 1.13(a)]. Nevertheless, for damped case, some amount of energy loss is bound to occur and hence response decays with time [Fig. 1.13(b)].

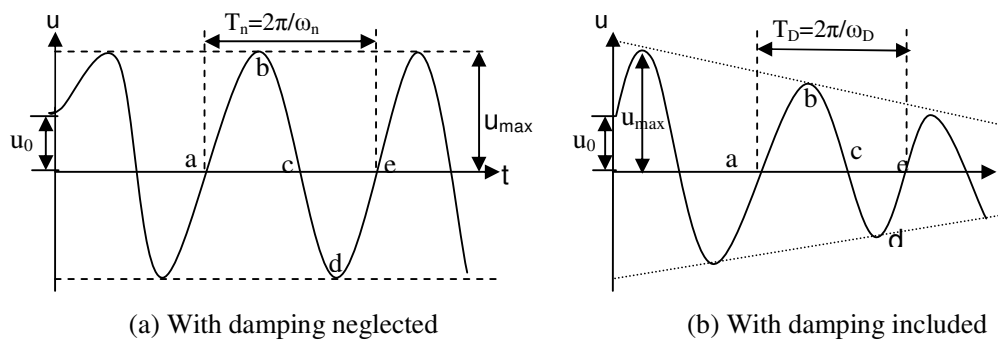


Fig. 1.13: Vibration of a system

The energy dissipation is a fundamental requirement of the structure subjected to severe earthquake. The greater energy is dissipated if a structure experiences stable inelastic response. The vibration amplitude, structural materials, fundamental natural period of vibration, mode shapes and structural configuration are some of the important factors affecting the damping of the structure. The structural damping is due to energy dissipation in materials of construction and structural components. The concrete, being a brittle material, is not a good source of energy dissipation. Sometimes, transfer of energy takes place from vibrating structure to the soil and such energy loss is known as foundation damping. The interaction of the structure with surrounding air and water are considered as aerodynamic and hydrodynamic damping, respectively. Charney considered the hydrodynamic dampers in the analysis of off-shore structures (Charney, 2008). It has been reported that the shape of the building has a strong influence on the aerodynamic damping response of structures (Taranath, 2010). The various aerodynamic modifications to the basic cross section of shear walls are depicted in Fig. 1.14.

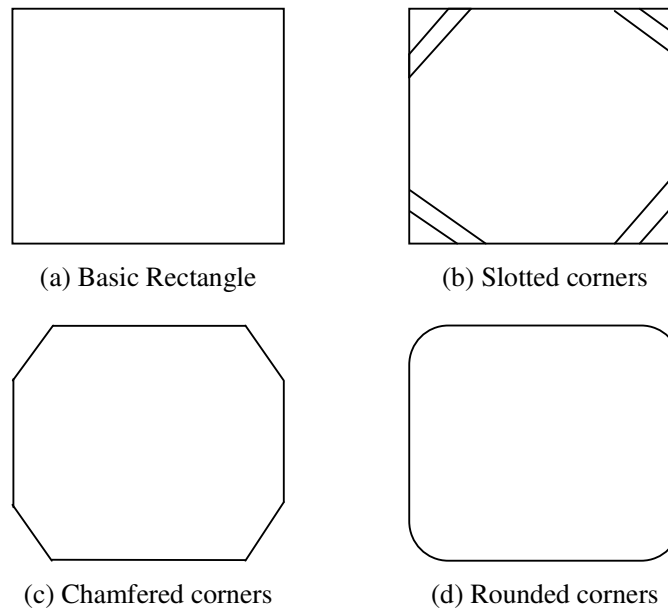


Fig. 1.14: Various aerodynamic modifications to corner geometry

It is suggested to have slotted corners, chamfered corners and rounded corners instead of regular basic shapes in order to mitigate the response of tall buildings especially in the case of wind effects. Rounding of a corner to a circular shape has resulted in a significant reduction in the response of structures. For very tall buildings, the inherent damping may not be sufficient in mitigation of structural response adequately. It has also been observed that the inherent damping of tall structures is less than 1% of critical damping. Hence such structures are extremely sensitive to lateral wind and earthquake vibrations. The use of supplemental or auxiliary dampers is vital in keeping the response of tall buildings to the desired level from safety and serviceability point of view. Damping helps in delaying the failure due to diagonal compression, diagonal tension and sliding shear and thus ensuring the full shear or flexural capacity before collapse.

1.6 Ductility in Shear Wall

The structures' response to ductility is one of the most important parameters in assessing the qualitative performance of building, especially from earthquake resistant point of view. The fundamental requirement of structural design is to prevent the sudden collapse of the structure. The sudden collapse of the structure due to high lateral loads may be avoided by allowing limited inelastic deformation before failure. A structure may achieve the required inelastic deformations provided it has inherent ductility. The ductility of the shear wall is majorly influenced by many parameters such as the aspect

ratio of the shear wall, reinforcing steel properties, quantity & location of reinforcing bars, openings in the shear wall etc. The aspect ratio's influence on ductility is well understood and relatively straight forward in the sense that the slender walls favor ductile behavior as compared to short/squat shear walls. The type of reinforcing steel has strong influence on the structural response of shear wall. It has been learnt from previous failures that mild steel possesses high ductility than the high strength steel. However, for a given quantity of steel, reinforcement location plays a crucial role on the structural response. In the shear walls with boundary elements, the degree of confinement has the strong effect on the strength and ductility of shear wall. However, it has been observed that beyond a certain extent, confinement may not necessarily result in increase in ductility (Paulay and Priestley, 1992). Ductility is usually expressed in terms of ductility ratio (μ), which is defined as the ratio of ultimate deformation to the deformation at yield. The ultimate deformation is the sum of the elastic deformation and the plastic deformation. The physical representation of displacements and rotations at yield, plastic and ultimate stages is shown in Fig. 1.15. The plastic hinge is expected to form at the bottom of the shear wall as shown in Fig. 1.15.

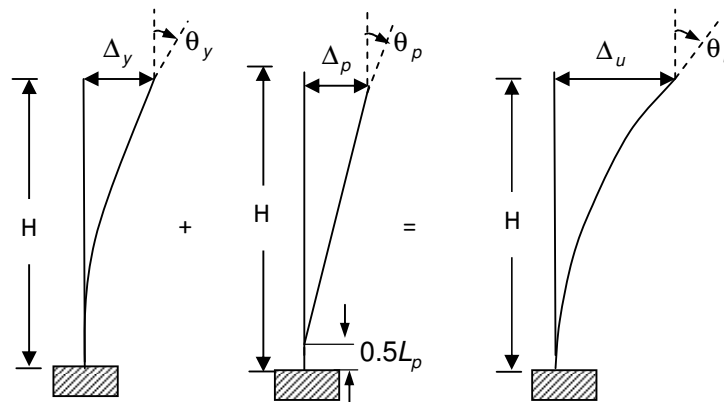


Fig. 1.15: Displacements and rotations at yield, plastic and ultimate stage

L_p = Length of plastic hinge

$\Delta_y, \Delta_p, \Delta_u$ = Displacement at yield, plastic, and ultimate stage

$\theta_y, \theta_p, \theta_u$ = Rotation at yield, plastic, and ultimate stage

The yield and failure/ultimate deformation of the structure are the two most difficult parameters to be captured analytically especially in the reinforced concrete structures. Researchers have suggested different ways to identify the yield and ultimate deformation (Park, 1988; Paulay and Priestley, 1992). Nevertheless, yield deformation is generally taken as the deformation corresponding to the first yield of vertical reinforcement in

tension. On the other hand, ultimate deformation is taken as the deformation corresponding to either (i) the significant load capacity after the peak, or (ii) the stage when reinforcing steel fractures or the longitudinal compression steel buckles. The typical models of ductility in terms of displacement, strain and curvature are shown in Fig. 1.16 (a), (b), (c) respectively.

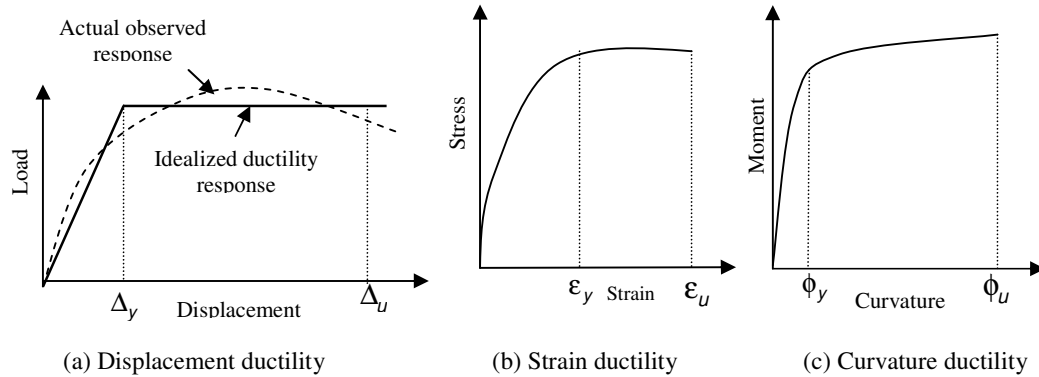


Fig. 1.16: Ductility models

The actual observed response through experimental/analytical investigations may not give clarity on the exact yield and ultimate point; hence, the actual observed responses are slightly modified and idealized as multi-linear model as shown in Fig. 1.16(a). The ductility ratio is expressed in terms of (i) displacement ductility (μ_{Δ}), (ii) strain ductility (μ_s), and (iii) curvature ductility (μ_{ϕ}), defined as:

$$\left. \begin{aligned} \text{Displacement Ductility, } \mu_{\Delta} &= \frac{\text{Displacement at ultimate } (\Delta_u)}{\text{Displacement at Yield } (\Delta_y)}; \\ \text{Strain Ductility, } \mu_s &= \frac{\text{Strain at ultimate } (\epsilon_u)}{\text{Strain at Yield } (\epsilon_y)}; \\ \text{Curvature Ductility, } \mu_{\phi} &= \frac{\text{Curvature at ultimate } (\phi_u)}{\text{Curvature at Yield } (\phi_y)} \end{aligned} \right\} \quad [1.3]$$

Ductility has a special concern in the reinforced concrete shear walls because concrete is a brittle material and may fail suddenly. It is essential to increase the ductility by providing proper reinforcement. It has been suggested that the ductility of the shear wall can be increased by (a) decreasing the tension steel content, (b) increasing compression steel content, (c) using low yield strength steel, and (d) increasing the transverse reinforcement (Helmut, 2007). It is also suggested that the structure can be designed for lower seismic shear forces in case if it possesses sufficient ductility.

1.7 Shear Wall with Openings

Several experimental and analytical studies confirm that the structural behavior of the shear wall with opening is complex due to stress concentration near the openings (Neuenhofer, 2006), leading to reduction in stiffness and strength of the wall. Moreover, openings in the shear wall result in the reduction in the concrete area and may result in the tremendous shear deformation even in the case of tall slender shear walls. Moreover, the force transfer gets disturbed in the shear wall with openings. The shear strength of the wall with openings should be examined along critical planes that pass through openings. Hence it is necessary to provide proper reinforcement in horizontal as well as in vertical direction around the openings. This vertical and horizontal reinforcement constitutes a steel band around openings thus resulting in strengthening (ductile detailing) of the shear wall. The diagonal reinforcement may also be provided around the openings as a part of strengthening process. The American Building Code Requirements for Structural Concrete (ACI 318-11) specifies that for walls with openings, the influence of the openings on the flexural and shear strengths are to be examined.

Depending upon the size, shape and location of openings, the response of the shear wall may get affected. The Architectural Institute of Japan (AIJ) specifies that the strength reduction factor of a shear wall due to the openings is limited to 0.6 by restricting the maximum ratio of opening dimensions to the corresponding wall dimensions. On the other hand, the seismic code of China specifies that the limiting value of the opening to be 15% of the area of wall. Nevertheless, these limits have been specified only to make the conventional methods applicable to wall structures as well. Most of the other codes are silent on the limiting percentage of openings in shear wall. This is partly due to lack of research on multiple openings in shear wall (AIJ, 2000; Kato, 1995). In order to determine the influence of openings on the structural response of reinforced concrete shear wall, many experimental and analytical investigations have been conducted in the past several decades as portrayed in the next chapter in detail. The research study on the shear wall panel by Tomii and Miyata (1963) revealed that the position of the openings in the shear wall did not greatly influence the response of the shear wall. Nevertheless, recent studies specify that the opening positions affect the performance of the shear wall (Neuenhofer, 2006). It is also suggested that the circular openings result in less severe stress concentration than rectangular openings. Nevertheless, due to practical difficulties as well as due to the

complexity in modeling circular shape openings, rectangular/square openings are generally provided and hence have been considered for the present analytical study.

1.8 Scope of the Present Study

The present research work involves the development and validation of finite element program for the static and dynamic analyses of squat and slender shear walls with and without openings. The non-linear finite element analysis has been employed with material non-linearity which includes the non-linearity due to concrete cracking, yielding of concrete and steel and crushing of concrete. To geometrically model the shear wall, the nine-noded locking free layered Lagrangian degenerated shell element with assumed strain approach has been adopted. The modeling of elastoplastic behavior concrete in compression is done using plasticity approach and Willam-Warnke five-parameter model is adopted to define the yielding/failure surface of concrete. For mathematical simplicity, only isotropic hardening with associated flow rule has been considered to define the strain hardening and plastic flow, respectively. The reinforcing steel bars are assumed to be in tension and modeled using bilinear stress-strain curve with elastic and strain hardening behavior. Since concrete is weak in tension, cracks form at early stages of loading and may result in non-linearity. In order to model the cracks, the fixed smeared crack approach has been adopted in the study. The tension stiffening effect has been incorporated by assuming the linear descending curve.

1.9 Organization of the Thesis

This thesis is divided into seven chapters. The Chapter 1 of thesis establishes the background along with scope and details of thesis organization. The Chapter 2 presents the various aspects of solid shear wall and shear wall with openings, as well as the influence of damping on the structural response of shear wall. The research gaps have been identified and objectives have been set in this chapter. The material modeling of RC structures is discussed in Chapter 3. The geometric modeling including element formulation and dynamic analysis are described in Chapter 4. The steps involved in the complete finite element formulation are also presented in Chapter 4. The validations of the developed finite element program with the standard analytical and experimental results are also presented in Chapter 4.

The Chapter 5 elaborates the response analysis of slender as well as squat shear walls with different opening sizes and locations for static monotonic loading conditions. The influence of ductile detailing (strengthening) around the openings and the displacement ductility index are discussed in this chapter. The Chapter 6 presents the time history response analysis of slender as well as squat shear walls with different opening sizes and locations for dynamic ground motions. The influence of damping on the structural response is also discussed in this chapter. In Chapter 7, findings, conclusions, and scope for further research are presented.

References:

1. ACI 318 (2011). “*Building code requirements for structural concrete and commentary.*” American Concrete Institute, Michigan, USA.
2. AIJ (2000). “*AIJ standards for structural calculation of steel reinforced concrete structures.*” Architectural Institute of Japan, Tokyo, Japan.
3. Atimtay, E., and Kanit, R. (2006). “Learning seismic design from the earthquake itself.” *ASCE Practice Periodical on Structural Design and Construction*, 11(3), 149-160.
4. Bathe, K.J. (1996). “*Finite element procedures.*” Prentice-Hall, Upper Saddle River, New Jersey.
5. Charney, F.A. (2008). “Unintended consequences of modeling damping in structures.” *ASCE Journal of Structural Engineering*, 134(4), 581-592.
6. Chopra, A. (2006). “*Dynamics of structures: Theory and application to earthquake engineering.*” 3rd Ed., Prentice-Hall, Englewood Cliffs, New Jersey, USA.
7. Clough, R.W., and Penzien, J. (2003). “*Dynamics of structures.*” McGraw-Hill Book Co, New York, USA.
8. Derecho, A.T, Ghosh, S.K., Iqbal, M., and Fintel, M. (1979). “Strength, stiffness, and ductility required in reinforced concrete structural walls for earthquake resistance.” *ACI Structural Journal*, 76(37), 875-896.
9. Elnashai, A., Pilakoutas, K., and Ambrayses, N. (1990). “Experimental behavior of reinforced concrete walls under earthquake loading.” *Journal of Earthquake Engineering and Structural Dynamics*, 43(11-12), 861-869.
10. Farvashany, F.E., Foster, S.J., and Vijaya Rangan, B. (2008). “Strength and deformation of high-strength concrete shearwalls.” *ACI Structural Journal*, 105(1), 21-29.
11. Fintel, M. (1977). “Performance of buildings with shear walls in earthquakes of the last thirty years.” *PCI Journal*, 95(2), 62-71.
12. Ghorbanirenani, I., Tremblay, R., Leger, P., and Leclerc, M. (2012). “Shake table testing of slender RC shear walls subjected to Eastern North America seismic ground motions.” *ASCE Journal of Structural Engineering*, 138(12), 1515-1529.
13. Helmut K. (2007). “Importance of good non-linear Analysis.” *The Structural Design of Tall and Special Buildings*, 15(5), 515-531.
14. IBC (2000). “*International Building Code.*” International Conference of Building Officials, Whittier, California.

15. IS 13920 (1993). “*Ductile detailing of reinforced concrete structures subjected to seismic forces.*” Bureau of Indian Standards, New Delhi, India.
16. IS 4326 (1993). “*Earthquake resistant design and construction of buildings.*” Bureau of Indian Standards, New Delhi, India.
17. Kato, D., Kabeyasawa, T., Otani, S., and Aoyama, H. (1995). “Earthquake resistant design of shear walls with one opening.” *ACI Structural Journal*, 92(4), 495-501.
18. Klinger, R.E., McLean, D.I., and Shing, P.B. (2012). “Masonry versus reinforced concrete shear walls- should they be designed differently.” *Structures Congress*, 1131-1142.
19. Lefas, I.D., Kotsovos, M.D., and Ambraseys, N.N. (1990). “Behavior of reinforced concrete structural walls: Strength, deformation characteristics, and failure mechanism.” *ACI Structural Journal*, 87(1), 23-31.
20. Michael, G., and Dickson, T., and Nilson, A.H. (1970). “Analysis of cellular buildings for lateral loads.” *ACI Structural Journal*, 67(12), 963-966.
21. Mothei, J.P. (2005). “Nonlinear analysis for performance based earthquake engineering.” *The Structural Design of Tall and Special Buildings*, 14(5), 385-400.
22. Mullapudi, R.T., Charkhchi, P., and Ayoub, A.S. (2009). “Evaluation of behavior of Reinforced Concrete shear walls through finite element analysis.” *ACI Special Publication*, 265, 73-100.
23. Murthy, C.V.R. (2004). “Why are buildings with shear walls preferred in seismic regions?” *IITK- BMTPC, Earthquake Tips*.
24. Naeim, F. (2001). “*The seismic design handbook.*” 2nd edition, Kluwer Academic Publishers, Boston, USA.
25. Neuenhofer, A. (2006). “Lateral stiffness of shear walls with openings.” *ASCE Journal of Structural Engineering*, 132(11), 1846-1851.
26. Paknahad, M., Noorzai, J., Jaafar, M.S., and Thanoon, W.A. (2007). “Analysis of shear wall structure using optimal membrane triangle element.” *Finite Elements in Analysis and Design*, 43(11-12), 861-869.
27. Park, R. (1988). “Evaluation of ductility of structures and structural assemblages from laboratory testing.” *Bulleting of the New Zealand National Society for Earthquake Engineering*, 22(3), 155-166.
28. Paulay, T., and Priestley, M. (1992). “*Seismic design of reinforced concrete and masonry buildings.*” Wiley, New York.

29. Petersson, H., and Popov, E.P. (1976). "Sub structuring and equation system solutions in finite element analysis." *Proceedings of a paper presented at the second National Symposium on Computerized Structural Analysis and Design*, George Washington University, March 29-31.
30. Rahimian, A. (2011). "Lateral Stiffness of Concrete Shear Walls for Tall Buildings." *ACI Structural Journal*, 108(6), 755-765.
31. Su, R.K.L., and Wong, S.M. (2007). "Seismic behavior of slender reinforced concrete shear walls under high axial load ratio." *Engineering Structures*, 29(8), 1957-1965.
32. Taranath, B.S. (2010). "*Reinforced concrete design of tall buildings*." CRC Press, Taylor & Francis Group, New York.
33. Thomsen, J.H., and Wallace, J.W. (1995). "Displacement-based design of RC structural walls: An experimental investigation of walls with rectangular and T-shaped cross-sections." *Report No. CU/CEE-95/06*, Department of Civil and Environmental Engineering, Clarkson University, Potsdam, New York.
34. Thomsen, J.H., and Wallace, J.W. (2004). "Displacement based design of slender RC structural walls-experimental verification." *ASCE Journal of Structural Engineering*, 130(4), 618-630.
35. Tomii, M., and Miyata, S. (1963). "Outline of shear tests concerning quake resisting walls having various openings." *Transactions of the Architectural Institute of Japan*, 66(1), 301-304.

RC Shear Wall: A State-of-the-Art

2.1 Background

Shear walls have been usually adopted as the lateral load resisting elements in Reinforced Concrete (RC) buildings. Since 1940s, a significant number of experimental investigations have been conducted in many countries on RC shear walls. The first experimental investigation on shear walls appears to have been conducted by Ban (1943). Most of these investigations focused on the determination of ultimate strength of walls subjected to various loading conditions such as monotonic, cyclic, dynamic and blast (high-speed monotonic). Significant experimental investigations on shear wall subjected to monotonic loading were conducted at Massachusetts Institute of Technology (MIT), USA in 1949 to develop design procedures for shear-wall structures as well as to prepare a basis for the evaluation of existing shear wall structures. In continuation to the above experimental investigations conducted at MIT, Benjamin and Williams (1953,1954) studied the behavior of RC shear walls surrounded by RC frames under monotonic loading to develop the analytical procedures for the design of shear wall framed structures, The major design variables considered in their study were aspect ratio, reinforcement ratio, and openings etc. In order to simulate the dynamic loading, in the 1970s, the dynamic loading began to replace the monotonic tests. The first dynamic tests on shear wall were conducted in early 1980s at the Los Alamos National Laboratory (LANL) in the United States using earthquake-simulator. Since then, many experimental and analytical investigations have been performed to determine the responses of shear walls under various loading conditions (Yanez, 1993; Kwak and He, 2001; Fragomeni, 2012).

For the analysis of shear wall, several analytical methods have been proposed by various researchers which range from simplified conventional approach to the sophisticated finite element approach. Due to the complexity of numerous factors which influence the overall behavior of RC shear walls, the validity of modeling and analysis techniques could only be established by comparing the same with experimental results. In this chapter several experimental and analytical investigations are presented pertaining to the assessment of the shear walls of different aspect ratios with and without openings and

subjected to different loading conditions. Furthermore, various codal provisions have also been reviewed to make a comparative study on design guidelines of shear walls with and without openings. In the end, the damping characteristics and the mathematical models are also discussed in detail.

2.2 Methods of Analysis of Shear Wall

During the past few decades, efforts have been directed towards the development of effective analytical techniques that are able to model the behavior of shear walls adequately. Simplified methods have been proposed by various researchers in the past: the simplified methods such as equivalent column model, lumped plasticity models, equivalent frame model, Rosman- approach, method of relaxation etc are quite popular among the engineering fraternity. However, these simplified models are applicable only to shear wall with regular geometry and with linear elastic behavior. On the other hand, finite element method is capable of analyzing shear wall of irregular geometry subjected to loads varying with time in the linear as well as non-linear regimes. The current section explains the various simplified methods and the finite element methods.

2.2.1 Simplified methods

One of the simplest ways to analyze the shear wall, shown in Fig. 2.1(a), is by using equivalent column approach. In earlier days, equivalent column approach has been adopted in analyzing the solid shear wall structures and results in simplified computation owing to unidirectional dimensionality, as shown in Fig. 2.1(b). In the equivalent column approach, the shear wall is modeled as a column element of equivalent stiffness and is analyzed as a 1-D column (line) member. Moreover, for the analysis of shear wall with openings using equivalent column approach, openings band(s) in the shear wall are idealized as an interaction of walls and beams. Although equivalent column approach has widely contributed to the basic understanding of the shear walled structures, it suffers due to the inability in capturing the non-linear strain distribution over the wall length during loading. This drawback is more pronounced in the case of squat and short shear walls where aspect ratio is less. Hence the application of equivalent column model is mostly restricted to slender shear walls.

Under severe seismic excitation of shear wall, the inelastic behavior of shear wall usually gets concentrated at certain locations, probably at the edges and at locations weakened by

openings. In order to simulate this behavior, Bolander and Wight (1991) used non-linear springs at those locations to represent plastic hinges of zero length as shown in Fig. 2.1(c). Since plastic hinges are concentrated at certain specified locations, this modeling technique is popularly known as lumped plasticity approach. The advantage of lumped plasticity modeling is that they reduce the computational degrees of freedom of a structure to a near minimum (Bolander and Wight, 1991). The lumped plasticity models have been found to be very efficient in predicting the load-deflection response of shear wall framed structures. It has also been observed that these models represent the behavior closer to experimental results. However, the lumped plasticity approach fails to simulate the behavior of real structures due to the uncertainties involved in choosing the adequate parameters.

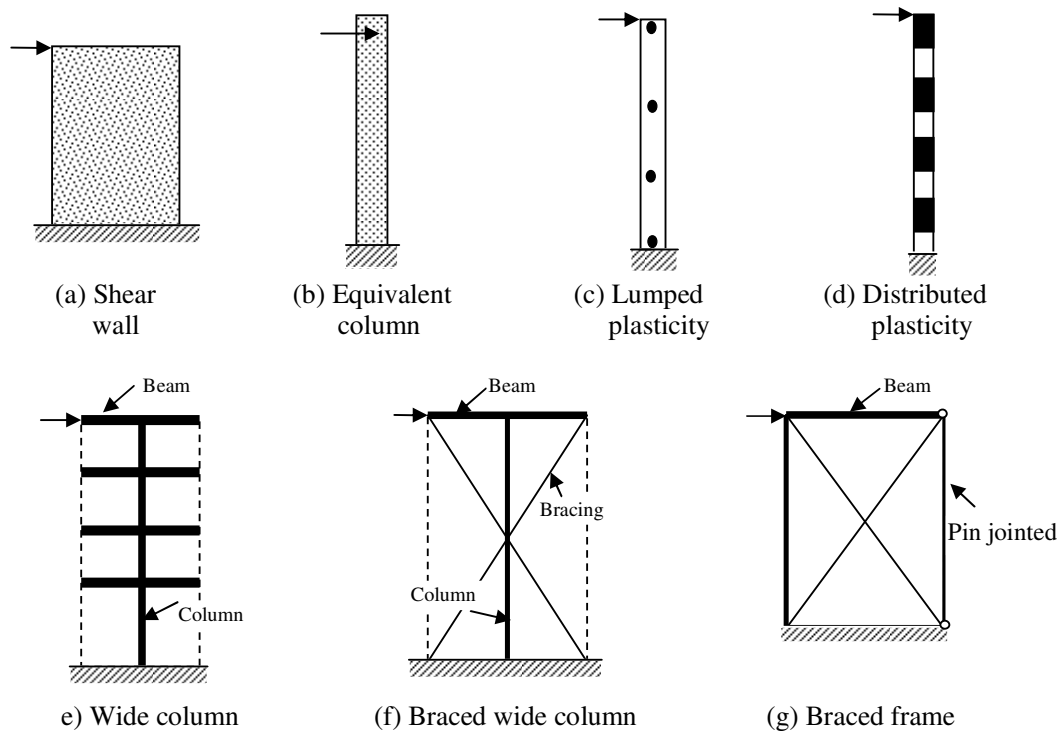


Fig. 2.1: Simplified methods of analysis of shear wall

To overcome the above drawbacks associated with the lumped plasticity model, Kunnath proposed a slightly complicated distributed plasticity approach in which the inelastic effects are distributed along a finite length (Kunnath, 1994) as shown in Fig. 2.1(d). The distributed plasticity models inherit uncertainty in the estimation of the length of the zone where inelastic effects are to be distributed. Invariably and justifiably, both lumped plasticity and distributed plasticity models possess certain inherent simplifying

assumptions, and cannot be applied to walls, plates and shells especially where shear deformation predominates (Bolander and Wight, 1991).

The equivalent frame model is another simplified method popularly used in design offices for the analysis of multistory shear wall-frame structures because of its simplicity and efficiency (Schwaighofer and Microys, 1969). In the equivalent frame model, the two-dimensional shear wall is replaced by an idealized framed structure consisting of a column located at wall's centroidal axis and rigid beams located at floor levels [Fig. 2.1(e)]. This method is popularly known as wide column analogy approach. The popularity of this method is largely attributed to the fact that it can be applied to almost any shear wall configuration (Nayar and Coull, 1976; Mattacchione, 1991). Schwaighofer and Microys (1969) used the equivalent frame model to analyze the shear wall with openings and observed that the equivalent frame method overestimates the flexural and shear deformations due to discrete modeling of continuous vertical joints and becomes impractical when the width of the columns are significant compared with their centre to centre distances.

To overcome the drawbacks posed by the equivalent frame model, Smith et.al. (1981) proposed two methods based on analogous frame method, namely (i) braced wide column analogy and (ii) braced frame analogy. The braced wide column analogy method is similar to the conventional wide column analogy method with the addition of diagonal braces, as shown in Fig. 2.1(f). In this method, the three structural components columns, beams and braces are effectively used to model the shear wall geometry. The properties of columns, beams and braces are estimated in such a way that it inherits the properties of shear wall.

In the braced frame analogy, the model consists of a column on the left hand side, rigid beams, a hinged link on the right hand side and diagonal braces as shown Fig. 2.1(g). In both braced wide column and braced frame analogies, it has been observed that there is a probability of obtaining negative stiffness values for the column and braces for certain aspect ratios of the shear wall. Considering the fact that most of the computer programs cannot perform analysis with negative stiffness values, these methods have been found to be ineffective.

Rosman (1964) developed a simple approximate method for the analysis of shear walls with single and two bands of openings of width 'b' and height 'h' subjected to lateral

loads. He used the continuous system approach, wherein the vertical line of openings are replaced by a continuous lamina of width 'b' throughout the height as shown in Fig. 2.2. Rosman in his formulation neglected the axial deformations of the beams and assumed the point of contraflexure to occur at the centre of the beams. Schwaighofer extended the Rosman's approach for three bands of openings. Schwaighofer also conducted an experimental investigation on shear walls with three bands of openings and compared his experimental results with the Rosman's analytical approach and found the results to be in close agreement. However, it has been observed that if both shear wall and frame are present, this method results in the undesirable effects (MacLeod and Hosny, 1977).

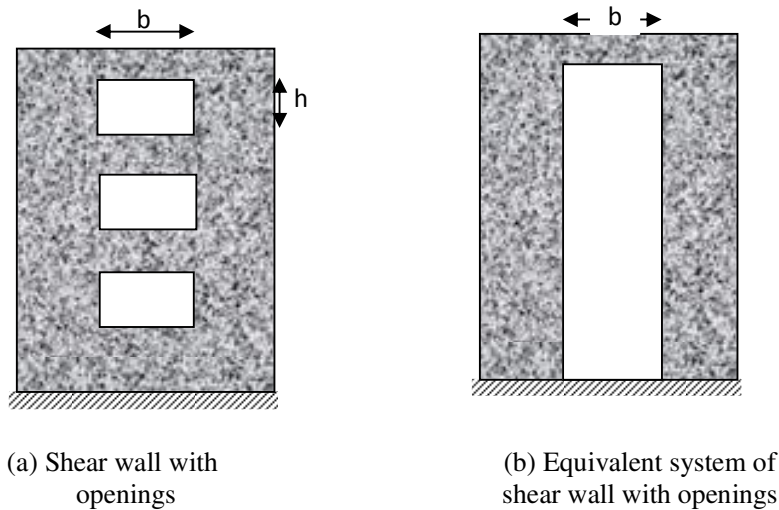


Fig. 2.2: Continuous system approach

Lindeburg and Baradar (2001) developed the simplified hand calculation method to analyze the shear walls with openings with varying assumptions (Lindeburg and Baradar, 2001). The accuracy of this simplified method was checked by Neuenhofer (2006) using the linear elastic finite element model of shear wall with conventional four-noded plane stress elements and observed that simplified method consistently underestimates the impact of the openings on the stiffness reduction, thus producing a lateral stiffness larger than that obtained using finite element analysis. Moreover, simplified methods have been found to produce remarkably poor results for shear walls with small aspect ratios where shear deformation controls the structural behavior (Neuenhofer, 2006). Hence, a more versatile method of analysis like finite element method is sought for the analysis of shear wall with varying geometry and subjected to different loading conditions.

2.2.2 Finite element methods

In order to circumvent the problems associated with simplified methods especially for shear walls, finite element analysis has been used to analyze the RC structures of any geometry and subjected to any loading conditions in linear as well as non-linear regimes since 1960. The earliest publication on the application of the finite element method for the analysis of RC structures was presented by Ngo and Scordelis (1967). They analyzed simple beams with a model in which the concrete and reinforcing steel were represented by constant strain triangular (CST) elements. This CST element is the simplest class of 2-D elements and is also known as linear triangular element. Since the strain is constant inside the finite element, it is necessary to use more number of CST elements in a critical zones, e.g. zones in which openings are located in a shear wall, to obtain reasonable accuracy. Nilson (1972) analyzed the RC structure with non-linear material properties of concrete and steel using quadrilateral element formed by combining four constant strain triangular elements. On the other hand, linear strain triangular (LST) element results in the better accuracy with less number of elements. Subsequently, the use of linear quadrilateral element, and quadratic quadrilateral elements were also effectively employed to model the 2-D structures. Quadrilateral elements with quadratic functions using iso-parametric approach are considered superior to model the 2-D structures because of its high accuracy in analysis. Iso-parametric elements are the class of elements, which are more arbitrary in shape and effectively used to model the curved geometry of the structure (Ahmad et al. 1970). Moreover, the iso-parametric elements are widely used in many structural applications related to plates and shells. Franklin (1970) used special frame-type elements, quadrilateral plane stress elements, axial bar elements, two-dimensional bond links with advanced non-linear capabilities to analyze the behavior of RC frames coupled with shear walls. Due to its simplicity, the use of plane stress elements are popular and used by numerous investigators to study the behavior of RC frame and wall systems. Cervenka (1970) analyzed the shear walls using plane stress elements and proposed a constitutive relationship for the composite concrete-steel material for uncracked, cracked and plastic stages. Nayak and Zienkiewicz (1972) also conducted the investigation on the elasto-plastic behavior of concrete in compression using plane stress finite elements. Dotroppe et al. (1973) used a layered finite element procedure in which slab elements were divided into layers to account for the progressive cracking through the slab thickness. Scanlon and Murray (1974) used

layered rectangular slab elements to analyze the slab by incorporating both cracking and time-dependent effects of creep and shrinkage in slabs. Lin and Scordelis (1975) used layered triangular finite elements in RC shell analysis by incorporating the membrane and bending effects, as well as the tension stiffening effect of concrete between cracks in the model.

The use of shell elements to model moderately thick structures like shear wall is well documented in the literature (Dvorkin and Bathe, 1984). Nevertheless, the general shell theory based on the classical approach has been found to be complex in the finite element formulation. In order to reduce the number of nodes, it was proposed to use degenerated shell element with nodes situated only at the mid plane of the element (Ahmad et al. 1970). The degenerated shell element derived from the three-dimensional element, has been quite successful in modeling moderately thick structures because of their simplicity and circumvents the use of classical shell theory. However, in the case of thin shells, the shear and membrane locking appeared to be disturbing the solutions (Zienkiewicz et al. 1971; Paswey and Clough, 1971) due to parasitic shear stresses (shear locking) and parasitic membrane stresses (membrane locking). In order to use these elements for thin walled structures such as shear walls, a locking free element is required. The assumed strain based degenerated shell element has been quite successfully adopted in modeling thin and moderately thick shear wall.

2.3 Structural Response of Solid Shear Wall

The structural response of RC shear wall has been investigated by several researchers in the past. Galletly (1952) conducted experimental investigations to determine the strength of RC shear walls under static monotonic loadings. Benjamin and Williams (1953; 1954) studied the behavior of squat RC shear walls surrounded by concrete frames under monotonic loading in which they tested ten different specimens of shear walls each having width 1.91 m (75.19 in) and thickness 102 mm (4 in). The first six specimens had aspect ratio of two and the seventh & eighth specimen had aspect ratio of four and six, respectively. The last two specimens had aspect ratio of two and subjected to load reversals while other specimens were subjected to monotonic loading. The boundary elements of size 610 mm (24 in) wide with 102 mm (4 in) thick are attached to each end of the shear wall to simulate cross walls or columns in a real structure. The amount of flexural reinforcement in boundary element was varied from 1.8% to 6.4% of the area of

the boundary element. Vertical and horizontal reinforcement used in the shear wall web area was varied from 0% to 5% of area of the shear wall. Each specimen was topped with a slab of 1.52 m (59.84 in) wide with 152 mm (5.98 in) thick simulating a floor or roof element. Based on the test results, it was observed that the shear walls with low aspect ratio possess higher shear strength than taller shear walls. Moreover, they assessed that shear walls subjected to load reversals had shear strength about 10% less than similar specimens subjected to monotonic loading. For the specimens with aspect ratio of two or less, it was found that the horizontal wall reinforcement did not contribute much to shear strength. Nevertheless, the horizontal wall reinforcement was effective in producing a more distributed cracking pattern and in reducing crack widths. Hence, it was found necessary to provide minimum horizontal reinforcement in shear walls. Moreover, lateral force was observed to be transmitted from the top slab to the base through the formation of compressive “struts” in the wall between cracks. Antebi et al. (1960) also conducted the experimental investigation to evaluate the strength of low-rise shear walls with boundary elements. The above studies laid the platform for the development of design criteria for RC shear walls (Anderson et al. 1964).

Portland Cement Association (1970) conducted the experimental investigations on thirteen shear walls out of which four were of rectangular type with cross-sectional size of width 1905 mm (75 in) and thickness 101.6 mm (4 in) and remaining nine were of bar bell type with increased thickness of 304.8 mm (12 in) at the ends to simulate the boundary elements. This investigation was conducted to determine the influence of cross-sectional shape as well as the amount of reinforcement on shear walls subjected to lateral load at the top of the shear wall (MacLeod, 1970).

Barda (1972) tested eight squat RC flanged shear walls to determine the overall behavior of shear walls in terms of strength, stiffness, and energy absorption characteristics under monotonic as well as cyclic loading. Out of eight shear wall specimens, two specimens were subjected to monotonic loading and the remaining six shear walls were subjected to cyclic loading. The key parameters considered in their study were (i) the reinforcement in the flanges, (ii) reinforcement in the web, and (iii) aspect ratio of the shear wall. They observed that the strength of a shear wall under cyclic loading was approximately 10% less than the identical shear wall loaded monotonically. They also observed that the flange reinforcement ratio did not have a significant effect on shear strength of shear

wall. On the other hand, the vertical reinforcement ratio was found to be more effective than the horizontal reinforcement ratio in resisting the lateral load. The strength reduction in the case of shear walls with aspect ratio 1.0 was around 20% as compared to the shear walls with aspect ratio 0.5. It was observed that there was no significant reduction in strength when the aspect ratio was changed from 0.50 to 0.25. However, the vertical reinforcement was more effective for the shear walls with aspect ratio 0.5 than for shear walls with aspect ratio 1.0. Hence, it was concluded that the vertical reinforcement has been found mandatory in the case of squat shear walls. Based on their study they concluded that shear walls should possess higher shear strength in order to have better energy absorption characteristics.

Iliya and Bertero (1980) studied the effects of amount and arrangement of reinforcement on hysteretic behavior of RC shear wall panels and observed that 45° arrangement of the wall reinforcing bars is more effective in resisting the effect of load reversals. They also indicated that conventional reinforcement failed by diagonal cracking whereas shear wall with diagonal reinforcement failed by flexural cracking. Nevertheless, the construction cost of diagonally reinforced shear walls was higher as compared to shear walls with vertical and horizontal bars.

Paulay et al. (1982) conducted a study on the shear walls with rectangular as well as flanged cross-sections without boundary elements and subjected to lateral static cyclic loading. In shear walls with rectangular and flanged cross-sections, the horizontal and vertical reinforcement ratios were kept at 1.6% and 0.8%, respectively. It was observed that the response of the shear wall was dominated by sliding shear and the shear wall performed better upto the displacement ductility of four beyond which the structural degradation occurred.

Maier and Thurlimann (1985) tested ten RC squat shear walls with an aspect ratio of 1.0 to investigate the effect of cross-section shape (flanged or rectangular), reinforcement ratio and arrangement, and loading (monotonic or cyclic) on the strength and deformation characteristics of shear wall. In their investigations, they considered two shear walls with different horizontal reinforcement ratios keeping the vertical reinforcement ratio constant. The first shear wall had a horizontal reinforcement ratio of 1.1% and the second shear wall had no horizontal reinforcement. Though the horizontal reinforcement had little influence on the magnitude of peak load, it was observed that the

shear wall with horizontal reinforcement failed due to diagonal compression and the one without horizontal reinforcement failed due to the diagonal tension. It was concluded that horizontal reinforcement had a negligible effect on the ultimate shear strength but found to have influenced deformation characteristics of shear wall. Moreover, it was concluded that the cyclic loading was not significantly influencing the strength and deformation.

A similar study was conducted by Lefas et al. (1990) to assess the effect of horizontal reinforcement on the behavior of shear wall with boundary elements having top and bottom slabs subjected to monotonic loading. The vertical reinforcement ratio in the web portion was around 2.4% and that of boundary element was 3.1%. The amount of horizontal reinforcement was varied from 0.37% to 1.1%. They observed that the shear wall specimens failed in diagonal compression mode and magnitude of horizontal reinforcement had little influence on the failure mode and peak load.

Sittipunt and Wood (1995) conducted an experimental investigation to assess the influence of diagonal web reinforcement on the hysteresis response in which four specimens were considered, two containing the inclined web reinforcement and other the two containing the conventional horizontal as well as vertical reinforcement. During the test, it was observed that both the shear wall specimens with conventional web reinforcement failed due to web crushing and pinched hysteresis curves were observed for top displacement as well as for shear distortion near the base. On the other hand, the walls with diagonal reinforcement failed due to crushing of the boundary elements and displayed rounded hysteresis curves. Though the choice of diagonal reinforcement did not produce a significant influence on the maximum lateral load carrying capacity, but measured crack widths were found less with significant energy dissipation capacity.

Palermo (1998) tested the 3-D RC flanged squat shear wall on high performance shaking table to experimentally investigate the dissipating capacity of shear wall. It was observed that the squat shear walls produced highly pinched hysteresis loops and hence the poor energy dissipating capacity. On the other hand, the ultimate lateral load resisting capacity has been found to be enhanced by increasing the axial load.

Salonikos et al. (1999) conducted an experimental investigation on rectangular shear walls with aspect ratios of 1.0 and 1.5 to determine the influence of magnitude of

web reinforcement, magnitude of boundary reinforcement and the presence of diagonal reinforcement on the failure characteristics of shear wall. Their study revealed that the reduction of vertical and horizontal reinforcement ratios from 0.57% to 0.28% and boundary reinforcement from 1.7% to 1.3% neither significantly affected the failure mode nor the observed drift. Nevertheless, due to absence of diagonal reinforcement, the sliding shear failure was evident and resulted in poor energy dissipation capacity.

Massone et al. (2004) conducted experimental investigations on four RC shear wall models, scaled approximately to 1/4th of the size of the actual shear wall. Out of four shear wall models, two were of rectangular cross-sections and remaining two was of T-shaped. The shear walls were 3.66 m (12 ft) tall and 101.6 mm (4 in) thick with web and flange widths of 1.22 m (4 ft). The floor slabs were provided at 0.91 m (3 ft) intervals over the height of the shear walls. The special boundary elements were provided over the bottom 1.22 m (4 ft) of each shear wall. Based on their investigations, it was revealed that the coupling between the inelastic flexural and shear deformations exist despite the shear wall having the shear strength of approximately two times the demand.

Su and Wong (2007) conducted the experimental investigation to assess the influence of Axial Load Ratio (ALR) on the behavior of slender shear walls with high aspect ratio and subjected to artificial earthquake loads. Three RC wall specimens of size 400 mm (width) × 80 mm (thickness) × 1640 mm (height) with high concrete strength of 60 MPa and high vertical as well as horizontal steel ratio of 2% and 0.5%, respectively were fabricated and tested under combined axial load, shear and moment. They observed that ALR has significant influence on the ductility and failure mode of the shear wall. However, the maximum rotational ductility was found to be decreased with increase in ALR. Moreover, it was also observed that an increase in ALR has a detrimental effect on shear walls with significant reduction in the strength and energy dissipation capacity.

Farvashany et al. (2008) conducted an experimental investigations on seven shear wall models each comprised two beams, one at the top and one at the bottom, and a shear wall panel bounded by two boundary elements to assess the influence of horizontal as well as vertical reinforcement on strength and deformation of high-strength RC shear

walls. The tested shear walls with the aspect ratio of 1.57 were scaled approximately to $1/3^{\text{rd}}$ of those in a real building and had a thickness of 76.2 mm (3 in), with a width of 701.04 mm (27.6 in) and a height of 1099.82 mm (43.3 in). The dimensions of edge columns (boundary elements) were 375.92×88.9 mm (14.8 in \times 3.5 in) with the same height of 1099.82 mm (43 in). The purpose of the top beam of size 1300.42 mm \times 200.66 mm \times 574.04 mm (51.2 in \times 7.9 in \times 22.6 in) and bottom beam of size 1800.86 mm \times 299.72 mm \times 574.04 mm (70.9 in \times 11.8 in \times 22.6 in) is to resist the stresses in the top and bottom portions, respectively. The two different amounts of horizontal reinforcement of 0.47% and 0.75% were used in conjunction with two different amounts of vertical reinforcement of 1.26% and 0.75%. The reinforcement ratio used for boundary elements in all specimens was kept at 4%. They observed that the increase in vertical reinforcement ratio increases the horizontal failure load. On the other hand, the effect of horizontal steel ratio was found to be not as significant as the vertical steel ratio. The shear strength of the shear wall was found to be increased only marginally with an increase in horizontal steel ratio.

2.4 Structural Response of Shear Wall with Openings

Many experimental and analytical investigations have been conducted in the last few decades to assess the performance of shear wall with openings under various loading conditions. The present section highlights few of the prominent experimental and analytical investigations that stimulated the research on shear wall with openings.

2.4.1 Experimental investigation

Benjamin and Williams (1953) conducted the experimental investigations on single story rectangular shear walls with boundary elements with different opening sizes and reinforcement ratios at Stanford University. A total of twenty one shear wall models, scaled approximately to $1/4^{\text{th}}$ of the real structure, having size 1727.2 mm \times 1409.7 mm \times 203.2 mm (68 in \times 55.5 in \times 8 in) with an aspect ratio of 0.816, were tested, out of which three models were of solid type and remaining were of shear walls with openings. Two different studies were conducted to assess the influence of openings on the response of shear wall, one with special reinforcement and other with conventional reinforcement. The reinforcement ratio in the case of conventional reinforcement pattern was around 0.5% in vertical as well as in horizontal direction, while in the case of special

reinforcement, the reinforcement pattern consist of conventional reinforcement plus two additional bars around openings in horizontal as well as vertical direction. Their experimental investigations revealed that the openings resulted in the reduction in both strength and rigidity and high stress concentration around the openings in shear wall irrespective of reinforcement patterns. Nevertheless, with the help of special reinforcement around the openings, it was observed that shear walls demonstrated a more uniform crack patterns thus resulted in the ductile behavior. Hence, they suggested that the vertical and horizontal reinforcement interrupted by openings should be replaced in equal amounts at the sides of the openings.

Yamada et al. (1974) tested a low-rise framed shear wall (aspect ratio 0.44) with openings subjected to monotonic loading. The strength and deformation characteristics of the RC shear wall were investigated at three stages of behavior, viz. cracked, peak and post-peak. Shiu et al. (1981) conducted an experimental investigation as a part of Portland Cement Association (PCA) research program on two 1/3rd scaled rectangular six-storeyed slender shear walls of 5.4864 m (18 ft) tall, 1.905 m (6.25 ft) wide with a uniform thickness of 100 mm (4 in). They compared the behavior of solid shear wall with shear wall with window openings of size 317.5 mm × 457.2 mm (12.5 in x 18 in) in all six storeys. It was concluded that the solid shear wall possessed 14% more load carrying capacity than the shear wall with openings. This was attributed to the interruption of diagonal compression strut in the case of shear wall with openings. Moreover, they observed that the solid shear wall failed due to horizontal sliding, however, shear wall with openings failed due to shear compression failure of the boundary elements. Chiba et al. (1985) tested the low-rise heavily reinforced shear walls with openings subject to lateral and axial loads. These shear walls were also provided with girders at top and bottom. Sotomura et al. (1985) studied ultimate shear strength of low-rise shear walls with numerous small openings subject to horizontal cyclic loads for a nuclear power plant. From the above studies, it is observed that openings resulted in tremendous shear deformation depending on the size of the openings.

Daniel et al. (1976) tested two 1/3rd scaled six storeyed shear wall models of height 5.48 m (18 ft), a horizontal length of 1.91 m (6 ft 3 in), and a uniform thickness of 102 mm (4 in). The height of each storey was 1.22 m (4 ft). Floor slabs were simulated by 64 mm (2.5 in)

thick stubs running full length on both sides of the specimens and the specimens were attached to the laboratory test floor through a rigid foundation block. In order to investigate the influence of openings, shear walls were penetrated with openings at every floor of size 304.8 mm × 457.2 mm (12 in × 18 in) and were located centrally. Kobayashi et al. (1995) tested 26 wall specimens to study the effect of small openings on the strength and stiffness of shear walls in reactor buildings. Based on the test results, they proposed the method for predicting the shear strength of walls. Johnson (1997) tested different wall configurations containing various openings and one control wall with no openings to determine the ultimate capacity and stiffness of shear walls.

On the basis of Chile earthquake in year 1960, which struck the city with a magnitude of 7.8, Wood et al. (1987) conducted a post-earthquake survey of 415 RC building structures, ranging in height from 5 to 23 storeys, and identified that only six buildings suffered massive substantial structural damage. Most of the buildings that withstood the damage were shear wall buildings and predominantly with openings. They concluded that the buildings with shear walls with staggered openings showed excellent performance in preventing the damage. Nevertheless, the special steel was provided adjacent to openings that resulted in a ductile performance along with special boundary elements.

Lin and Kuo (1988) tested various shear wall panels to investigate the effect of openings, its shapes and boundary elements on the structural behavior of shear wall subjected to lateral loading, both monotonic and cyclic. Two different types of shear wall panels were tested, one with opening and one without opening. In order to assess the influence of openings and boundary elements on the crack patterns, tests were conducted on the scaled model of shear wall having dimensions (250 mm × 172 mm × 20 mm) with opening size 300 mm × 400 mm as shown in Fig. 2.3. Based on the studies, it was concluded that in case of solid shear wall, the cracks initiated at bottom corner of the junction of wall and boundary element whereas for shear wall with openings, the crack initiated at the corner of the openings due to relatively low strength and propagated outward with an approximate 45° angle. Nevertheless, for shear wall with boundary elements, the crack remained almost horizontal until it failed, indicating that the cracks were primarily generated due to flexure.

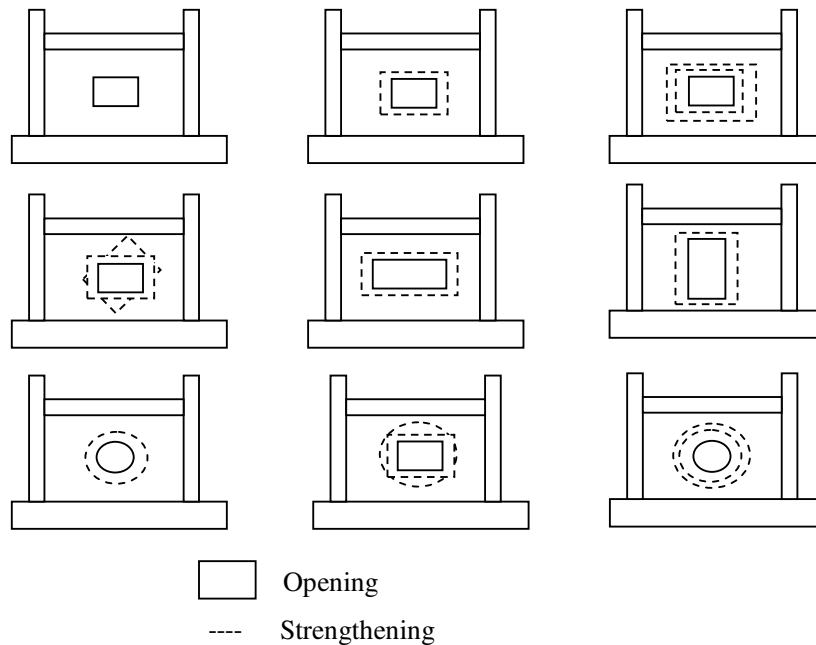


Fig. 2.3: Shear wall with openings (Lin and Kuo, 1988)

They also observed that not much significant difference was observed in the behavior of shear walls when subjected to cyclic loading and monotonic loading. For the same size of opening with two different reinforcement patterns, i.e. diagonal and combination of horizontal & vertical, it was observed that the reduction in the strength as compared to solid shear wall was found to be only 15% in the case of diagonal reinforcement and 25% in the case of horizontal & vertical pattern. The ductility and shear strength of the shear wall with opening was also found to be severely affected by the reinforcement around opening. Moreover, it was also observed that shear strength contributed by diagonal reinforcement around the opening reached 40% of its yield strength and that of rectangular arrangement is only of 20%. Hence, they suggested providing diagonal reinforcement around openings in the shear wall. Nevertheless, due to difficulty in construction, the rectangular arrangement is generally preferred.

Ali and Wight (1991) conducted tests on lightly reinforced barbell shaped slender walls (3.56 m high and 1.22 m wide) with staggered openings for moderate axial and shear loads. The horizontal and vertical reinforcement in the web portion and boundary element portion in shear walls were 0.3% and 3% respectively. The total opening area in the shear walls they considered was 13.4% of the area of shear wall. The openings were located in a staggered manner as shown in Fig. 2.4.

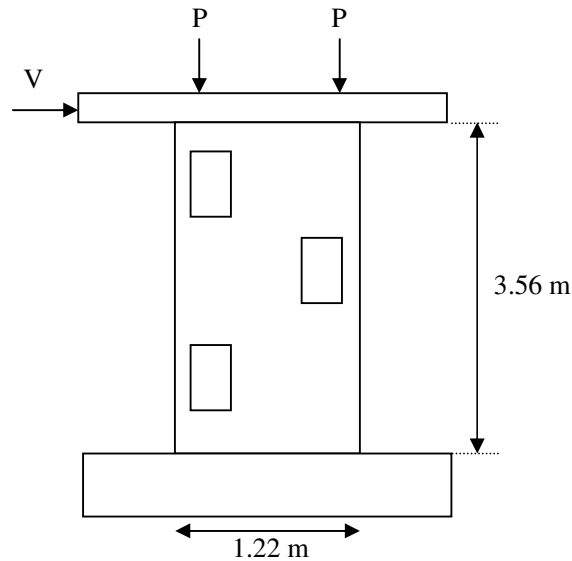


Fig. 2.4: Shear wall with staggered opening (Ali and Wight, 1991)

Based on the above study, it was observed that the staggered openings can be considered a feasible alternative to the straight openings. Nevertheless, door openings located too close to the edge of the boundary column results in the lack of confinement and can trigger an early shear-compression failure (Ali and Wight, 1991).

Saheb and Desayi (1990) conducted experimental investigations on twelve RC wall panels of size 900 mm long (L), 600 mm high (h) and 50 mm thick (t) subjected to in-plane vertical loads applied at an eccentricity to represent possible accidental eccentricity that occurs in practice due to constructional imperfections. They considered six different opening locations out of which three were three window openings two door openings and a window cum door opening as shown in Fig. 2.5. The typical sizes of window and door opening are 240 mm \times 240 mm and 210 mm \times 420 mm, respectively. The aspect ratio (H/W), slenderness ratio (H/T) and thickness ratio (W/T) for all the shear walls specimens were 0.67, 12, and 18, respectively. The percentage of horizontal and vertical reinforcement was kept same in all specimens. It was a well known fact that a rectangular wall panel hinged at top and bottom and carrying out-of plane vertical loads develop curvature in one direction (one-way action), while a wall panel supported on all four edges develop bi-axial curvatures (two-way action). It was concluded that the deflections of all panels in two-way action have been found smaller and about 40.5% to 78.7% of those in one way action at 75% of ultimate load.

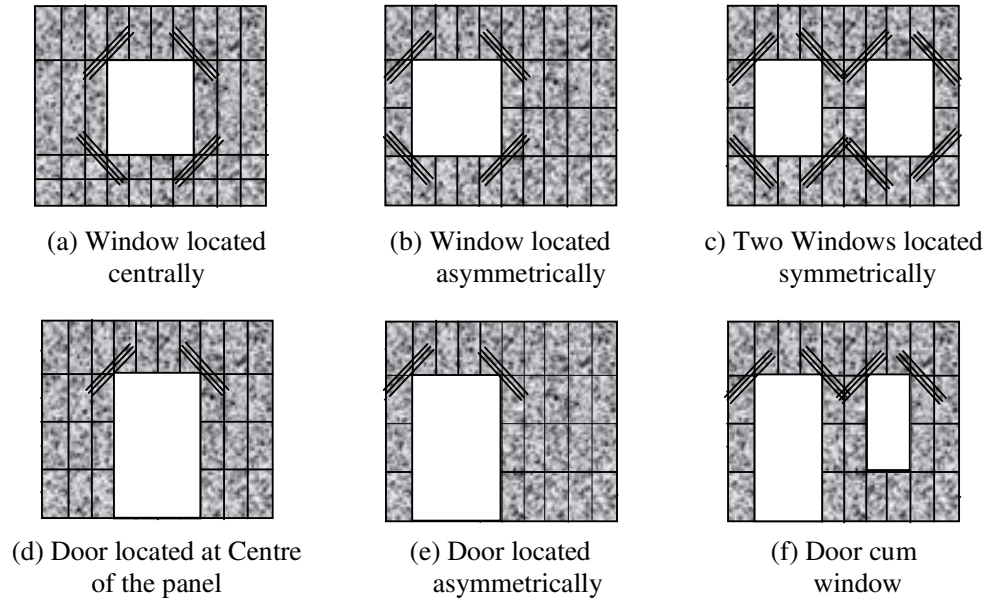


Fig. 2.5: Shear wall panel with different opening positions (Saheb and Desayi, 1990)

The cracking loads of panels in two-way action were about 7.3% to 16.2% more than those in one-way action. Moreover, the ultimate loads of panels in two way action were about 2.96% to 7.29% more than those in one way action. They also observed that the presence of openings had a considerable effect on cracking & ultimate loads and there was no significant difference between one-way and two-way actions. Hence, it was concluded that the advantage of the potential increase in the load-carrying capacity due to two-way action has been offset by the presence of openings.

Yanez (1993) conducted experiments on six three-story RC walls, scaled to about $1/3^{\text{rd}}$, under reversed cyclic lateral loading. The walls were 2000 mm wide, 2300 mm high and 120 mm thick. He concluded that the size and arrangement of the openings did not have a significant effect on the structural behavior of walls under cyclic lateral loading. Nevertheless, in the current design code of Architectural Institute of Japan (AIJ, 1999), the strength reduction factor of a shear wall due to the openings is limited to 0.6 by restricting the maximum ratio of opening dimensions to the corresponding wall dimensions.

Taylor et al. (1998) conducted the experimental investigations on the response of four storeyed slender shear wall of size (width \times height \times thickness) 1200 mm \times 3600 mm \times 100 mm (48 in \times 144 in \times 4 in) with base opening of sizes 300 mm \times 675 mm (12 in \times

27 in) and 225 mm × 500 mm (9 in × 20 in). Experimental results show that properly reinforced slender shear walls with openings at the base exhibit stable hysteretic behavior and significant ductility.

Kwan and He (2001) analyzed thirteen shear walls tested by Lefas (1990) to determine the strength, deformation characteristics and failure mechanism of shear walls under the combined action of a constant vertical load and a monotonically increasing horizontal load. Two different types of specimens were analyzed using finite element analysis, one with the size (width × height × thickness) 750 mm × 750 mm × 70 mm and other with the size 650 mm × 1300 mm × 65 mm. Fragomeni et al. (2012) tested seven RC shear walls with opening configurations in both one-way and two-way action. The RC panels of size 1200 mm × 1200 mm along with various opening configurations and sizes were similar to the one tested by Lee (2008). The vertical and horizontal reinforcement ratios were 0.31% for all the wall panels. On the basis of experimental study, it was observed that the failure loads and crack patterns depend on the opening configuration and support conditions. The failure loads of two-way panels with openings were observed to be about 2 to 4 times those of similar one-way panels with openings. Furthermore, the test results indicate that failure loads decreased when the number of openings was increased from one to two. Recently, Fragomeni et al. (2012) pointed out that the design of shear walls with openings is being given little importance in International codes of practice despite several experimental and analytical investigations.

Kabeyasawa et al. (2007) conducted the experimental investigations on six shear wall panels, scaled approximately to 1/5th of real shear wall, of size (width × height × thickness) 2000 mm × 2200 mm × 80 mm to assess the effects of boundary elements and openings on the structural response of shear wall. The web reinforcement ratio in vertical as well as horizontal direction was kept at 0.25%, which corresponds to the minimum requirements specified in the Japanese code (BSL, 2007) The boundary elements of size (width × height × thickness) 250 mm × 2200 mm × 250 mm were provided at the edges of the shear wall with the reinforcement ratio of 0.52% to provide the confining effect to the shear wall. The shear strength of a wall without boundary elements was found to be slightly less than that of the wall with boundary elements. In order to determine the influence of openings on the response of shear wall, the opening sizes were chosen according to the maximum prescribed one (i.e. 360 mm × 680 mm) mentioned in the

Japanese codes of practice (BSL, 2007). It was also suggested in the Japanese code that shear wall with openings beyond this size should be analyzed as frame elements with two columns and the wing walls. It was observed that the openings reduced the strength; nevertheless the deformability (ductility) of the wall with openings was observed to be much higher than that of the wall without openings.

Lee (2008) tested seven shear wall panels of size (width \times height \times thickness) 1200 mm \times 1200 mm \times 40 mm to assess the strength and deformability of the shear wall in the presence of window and door openings. The reinforcement ratio in the vertical as well as horizontal direction was kept at 0.31% as per the Australian Standards for Concrete Structures (AS3600-2009). In order to prevent shrinkage cracking, reinforcing bar strip of small length were diagonally placed at the corners of the opening. He observed that the size of the openings significantly affects the structural response of the shear wall. The next section deals with the state-of-the-art analytical studies in the shear wall with openings.

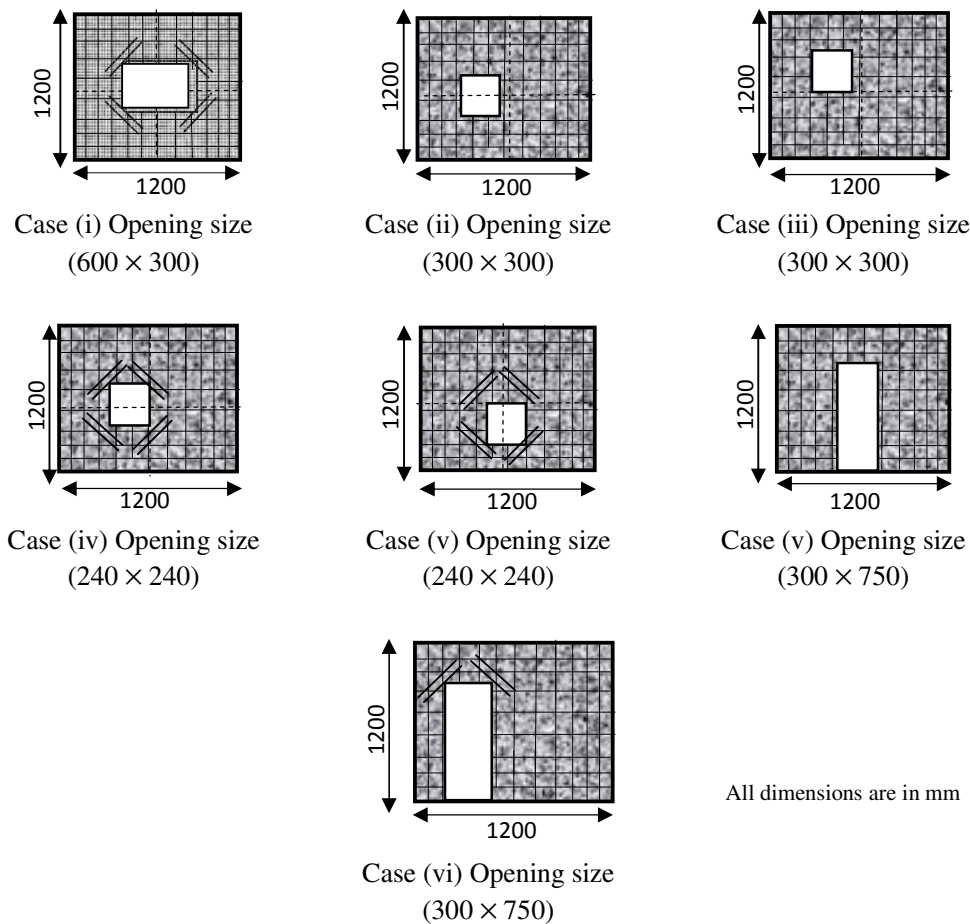


Fig. 2.6: Shear wall panels with openings of various sizes and locations (Lee, 2008)

2.4.2 Analytical investigation

Prior to the early 1960's, very little attention was paid to the development of analytical techniques for the analysis and design of shear walls. In the early sixties, a series of analytical studies were conducted by famous researchers to indicate the importance of shear walls in those days and coincidentally many of those analyses focus on the response of shear walls in the presence of openings (Schulz, 1961; Tomii and Miyata, 1963; Rosman, 1964; Magnus, 1965; Thadani, 1966; Kazimi, 1966; Girijavallabhan, 1969).

Tomii (1961) determined the load-deformation characteristics of various shear wall panels with openings at Kyushu University. He formulated a relatively simple empirical relationship between parameters representing the load and the relative size of the openings. Though he found that the size of the openings affect the behavior of the shear wall, he also observed the surprising fact that the position of the openings did not greatly affect the performance of shear wall. In the same year, Stiller (1961) carried out the theoretical study on stresses in shear walls with openings. He analyzed the shear walls with circular and rectangular openings and found that circular openings resulted in less stress concentration than rectangular openings. Beck (1962) initiated the research work on wall panels and Vierendeel girders with openings in which the individual columns were replaced by an equivalent laminar system to allow for significant axial and shear deformations in shear walls.

Rosman (1964) developed a linear elastic approach based on different assumptions to analyze the shear wall with single and double bands of openings in which he established the fundamental Eulerian differential equation of the problem. He chooses the solution in terms of the axial force in the shear walls and expressed this by trigonometric series. Nevertheless, he neither allowed for shear deformation nor considered the separation forces exerted by the spandrel beams. In 1969, Schwaighofer and Microys used this approach to analyze the shear wall with three rows of openings and observed that the Rosman's theory predicts the behavior of shear wall with three rows of openings with sufficient accuracy. Neuenhofer studied the response of the shear wall with and without opening using finite element approach and observed that the position of opening affects the structural behavior of shear wall (Neuenhofer, 2006). He also observed that if the opening is near the middle of the wall, it does not decrease the moment capacity of the shear wall to the

great extent; however, the shear strength reduces significantly. In contrast, he found that an opening near a wall boundary impacts both shear and flexural strengths depending on the size of the opening. Nevertheless, there was a strong consensus that openings in shear wall are to be located centrally. However, Kato et al. (1995) carried out analytical investigations on shear wall with openings and objected the provision recommended by the then Architectural Institute of Japan (AIJ, 1999) for not limiting the size of single opening in shear wall for flexural failing mechanism. This was partly due to lack of research on multiple openings in shear wall (AIJ, 1999; Kato et al. 1995).

Sittipunt and Wood (1995) conducted finite element analysis on slender reinforced concrete walls with and without openings subjected to lateral load reversals.

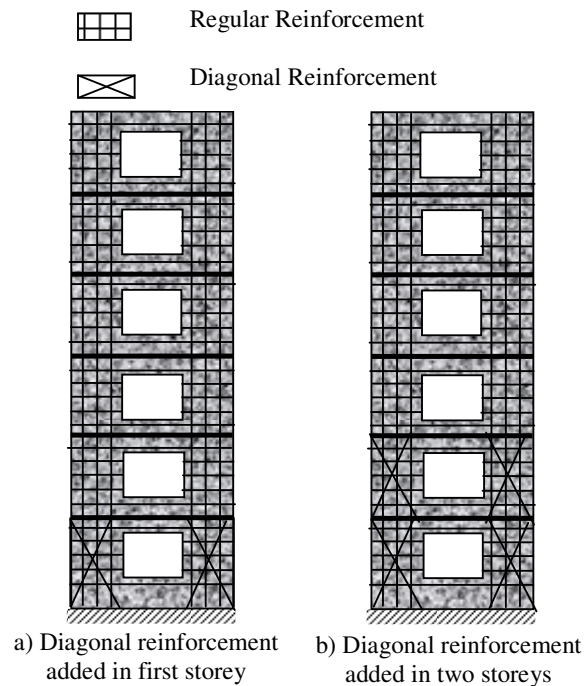


Fig. 2.7: Effect of diagonal reinforcement on the structural response of shear wall
Sittipunt and Wood (1995)

They considered 5.49 m (18 ft) high shear wall with rectangular cross section and having six openings in the web over its height and the wall was subjected to single lateral load at the top. For the finite element analysis, they used iso-parametric plane-stress elements to model the shear wall. To perform the non-linear analysis, they used fixed smeared crack approach to simulate the concrete cracking and modeled the steel bars using the two-

node truss elements. Based on the study, it was concluded that the shear distortions concentrates in the first-story of the wall. In order to investigate further the influence of reinforcement pattern in controlling the shear distortion, two arrangements were considered, as shown in Fig. 2.7. On the basis of cyclic loading, it was observed that adding diagonal reinforcement at the first story did not change the overall force-displacement response appreciably although it helped in controlling the shear distortion successfully. Moreover, when the diagonal reinforcement was placed in the lower two storeys, the hysteretic response improved considerably. It was also concluded that, the pinching was not observed in the overall force-displacement response or the story shear-distortion curves.

Qamaruddin (1998) proposed an approximate method to determine in-plane stiffness of shear walls with openings, in which spandrels are assumed flexible and can translate and rotate under lateral load. He concluded that the in-plane stiffness computed based on approximate method compares well with the stiffness computed by the elastic finite element method.

In order to predict the above results analytically, Doh and Fragomeni (2006) developed prediction equation for normal strength concrete shear walls with openings and found that the failure loads were reasonably well predicted and later found agreeable to the experimental investigations performed by Lee (2008).

Masood et al. (2012) conducted an finite element based analytical study using ANSYS (Version 5.4) to determine the response of shear wall with base opening and concluded that base opening beyond 60% resulted in tremendous decrease in strength and stiffness degradation. Even though base opening has always been a risky option considering its structural importance, because of the need to provide parking access, it has become an automatic functional requirement in the recent years.

On the basis of literature review carried above, it can be concluded that limited experimental and analytical work has been performed to investigate the influence of openings, its sizes and shapes on ductile response of shear wall under severe loading conditions until collapse. In order to develop the design guidelines, there is a necessity to analyze in detail the shear walls with openings.

2.4.3 Shear walls - Codal provisions

The design of any structure is bound by codal provisions. Since shear wall is a specialized component of the structure mainly meant to provide the lateral resistance of a structure, it is essential to review the various codal provisions evolved over the years and currently adopted in practice.

ACI 318 building code

Design criteria for the RC shear walls were first incorporated in the ACI Committee 318 Building Code in 1971 (ACI Committee 381-1971). Prior to the publication of the ACI 318-71, the only provisions for the design of shear walls in the United States were those contained in the Uniform Building Code (UBC) published in the year 1967 and 1970 (UBC 1967, 1970). Before 1970s, limited studies were available on the shear walls and hence most of the provisions in the early versions of the ACI code were based on the experimental investigations undertaken by the Portland Cement Association (PCA) in the late 1960s and the subsequent recommendations by Cardenas et al. (1973). The early provisions advocated by the codes were basically intended to ensure that the walls possessed adequate shear strength and the emphasis was on the evaluation of flexure and shear strength under monotonic loading only.

The ACI Code design requirements for shear walls located in regions of high seismicity suggests that the reinforcement in the shear walls typically contain distributed vertical and horizontal reinforcement spread uniformly over the width and the height of the wall, respectively. Well distributed reinforcement is generally preferred in the walls because it provides cracking control to the diagonal compression strut and improves the conditions for dowel action, which in turn enhances the sliding shear resistance at the base of the wall (Paulay et al. 1982). The minimum ratio of horizontal reinforcement area to the gross area of the wall is specified as 0.0025. Moreover, based on the research findings (Cardenas 1973; Wood 1990; Lefas et al. 1990), the ACI code recommends that for short shear walls, the amount of vertical reinforcement should not be less than the horizontal reinforcement because vertical reinforcement is more efficient than the horizontal reinforcement in controlling the width and growth of diagonal cracks.

Hong Kong code of practice for structural use of concrete

The code of practice for structural use of concrete prepared by Buildings department, Hong Kong (2013) has suggested that reinforced concrete shear walls contribute to the lateral stability of the structure. It suggests that the combined effects of axial loading and shear should be taken into account. This code also suggests that effect of sway of shear walls on the occupants of the structure should also be considered. The minimum percentage of vertical reinforcement based on the concrete cross-sectional area of a wall is 0.4%. It is also suggested that this minimum area of reinforcement should be distributed at each face. The distance between two adjacent vertical bars should not exceed three times the wall thickness or 400 mm whichever is the lesser. The minimum horizontal reinforcement is 0.30% for mild steel and 0.25% for high strength steel. The diameter of the horizontal bar should not be less than 1/4th of the diameter of the vertical bars. In any case, the diameter of horizontal reinforcing bar should not less than 6 mm. The code also suggests that the nominal reinforcement be provided around the openings.

Indian standards 13920-1993

The Indian Standard (IS 13920-1993) specifies the following requirements for shear wall.

- The thickness of any part of the wall should not be less than 150 mm to avoid very thin sections.
- The diameter of the bars to be used in any part of the wall should not exceed 1/10th of the thickness of that part.
- The minimum reinforcement in horizontal and vertical direction is 0.25% of gross area in each direction. The maximum spacing of vertical and horizontal reinforcement should not be more than the minimum of the following; a) 1/5th of the width of the shear wall, b) Thickness of the shear wall; c) 450 mm.
- Though the inherent characteristics of shear walls such as strength, stiffness and ductility are affected by many parameters such as aspect ratio, cross-sectional geometry and material type, the behavior alters significantly in the presence of openings, which may be unavoidable due to the functional requirement such as placement of windows, doors and ducts. In the case of shear wall with openings, reinforcements are provided along the edges of openings in walls. The area of the vertical and horizontal bars should be such as to equal that of the respective

interrupted bars. The vertical bars should extend for the full storey height. The horizontal bars should be provided with development length in tension beyond the sides of the opening.

2.5 Damping in Structures

The fundamental effect of damping is to reduce the peak amplitudes of the vibrating system with little alteration in natural frequency. In order to understand the phenomenon of damping, an energy dissipation capacity, various experimental investigations have been conducted over the period of years. The energy dissipation of a vibrating building cannot be quantified in terms of specific parameters. Numerous mechanisms such as hysteresis in the material and slip in connections may be present at any point of time contributing to damping and hence it is impossible to define it mathematically (Zareian and Medina, 2010). Moreover, these mechanisms are not well understood and, therefore, it is difficult to incorporate into the equations of structural dynamics. Hence, the damping has been modeled using single equivalent damping parameter including the effect of various complex sources. The treatment of damping in computational analyses can be categorized as (1) phenomenological damping methods, and (2) spectral damping methods. In the phenomenological damping methods, the actual physical dissipative mechanisms such as elastic-plastic hysteresis loss, structural joint friction, material micro-cracking etc. are considered.

In the spectral damping method of analysis, viscous damping is introduced by means of specified fractions of critical damping. The minimum amount of damping necessary to prevent the oscillations completely is known as critical damping (Taranath, 2010). The damping of a structure is measured in terms of percentage of critical damping. The percentage of critical damping varies between 1% to 10% for non-base isolated buildings and 25-30% for base-isolated buildings. Chopra (2006) proposed the damping values as 3-5% for considerable cracking case and 7-10% near the yield point. Farrar and Baker (1995) conducted experiments to measure the damping ratio of low-rise shear walls and found that for undamaged low-rise shear walls, the damping ratio was around 1-2%. However, as the damage level increased, the measured damping ratio shot up to 8%. Similar experimental studies have also been performed by Ile and Reynouard (2000) correlating the damping ratio with the increasing damage of shear

wall. It was found inevitable to use damping as a viable means of mitigating the structural damage.

Based on the inherent damping, the structures can be categorized as under damped, critically damped or over damped. Critically damped and over-damped structures don't vibrate and hence does not pose any problems. Most of the civil engineering structures fall in under-damped category where the building actually vibrates. Moreover, it is important to note that the inherent damping present in civil engineering structures is of the order of maximum 10%. Satake et al. (2003) determined the damping ratios for different building types based on the vibration tests reported in AIJ and concluded that the tall buildings possess the smaller fundamental damping ratio. The damping ratios are reported to be affected depending on the functional use of building. The damping ratios were found to be larger in a building where more infill partitions are available.

Very little information is available about variation of damping in linear and non-linear systems. However, the effect of damping is generally low as compared to inertial and stiffness effects in most of the practical situations. Therefore, it is reasonable to account for damping in the analysis using the simplified approximations. The following section describes the various damping models used in practice.

2.6 Damping Models

In order to represent damping analytically, various damping models have been in use to account for energy loss mechanism. These models are classified into four categories namely (i) viscous damping models, (ii) non-viscous damping models, (iii) active control damping models, and (iv) passive control damping models. The choice of damping model depends on the system behavior as well as on the computational expenses. These models are discussed briefly in the current section.

2.6.1 Viscous damping models

The representation of damping through viscous damping coefficient has been in use due to simplicity and accuracy. Viscous damping is a type of damping in which a system is said to be vibrating in a fluid. Hence, the viscous damping is a property of the computer model and is not a property of a real structure.

In viscous damping, the damping force, F is assumed to be proportional to velocity of the medium, \dot{u} ; i.e.

$$F \propto \dot{u} \Rightarrow F = c \dot{u} \quad [2.1]$$

where c is the constant of proportionality, commonly known as viscous damping coefficient.

For the multi-degrees of freedom system, the c becomes a matrix, known as damping matrix. The damping matrix can be formulated analogous to mass and stiffness matrices (Chopra, 2006). Comparisons of theoretical and experimental results show that the above mentioned approach of simulating viscous damping is sufficiently accurate in most of the cases. The typical viscous damping response in free vibration tests is shown in Fig. 2.8.

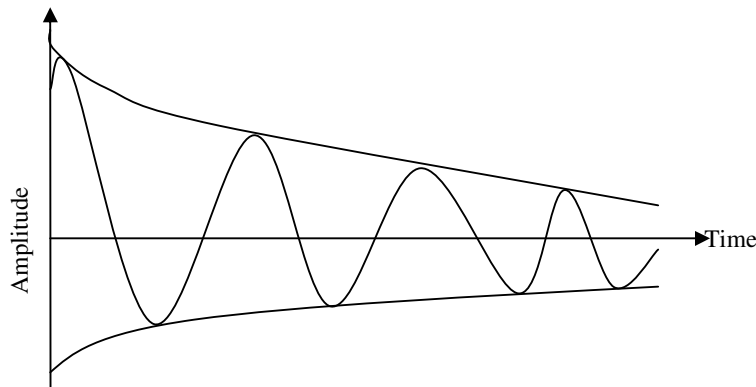


Fig. 2.8: Viscous damping response

Modal damping ratios are also frequently used in a computer model to approximate the nonlinear energy dissipation of the structure. Amick and Monteiro (2006) determined the modal damping in concrete beams experimentally to identify the material damping properties of concrete beams. Damping matrices based on modal damping ratios are known as classical or proportional damping (Bernal, 1994). Many damping models have evolved based on the concept of viscous damping such as Cauchy damping (Caughey, 1960), Rayleigh damping (a special case of Cauchy damping) and Wilson-Penzien damping (Wilson and Penzien, 1972). Both Cauchy and Wilson-Penzien damping models are computationally expensive and hence are not preferred for dynamic analysis (Carr, 2007). Thus, Rayleigh's proportional damping has the specific advantage that the equation of motion can be uncoupled when it is proportional to mass and stiffness matrices.

The representation of damping using Cauchy series is given by

$$[C] = [M] \sum_{k=0}^{p-1} a_k [M^{-1}]^k [K]^k \quad [2.2]$$

where the coefficients a_k ($k = 1, 2, \dots, p-1$) are obtained from $(p-1)$ simultaneous equations. $k = 0, 1$ yields mass and stiffness proportional damping, respectively. Alternatively, $k = 2$ yields the well-known Rayleigh damping which is proportional to both mass and stiffness. From the above equation, it is clear that for higher values of k , the damping can also be controlled by as many modes as possible instead of two parameters, as used by Rayleigh damping. On the other hand, the use of Rayleigh's proportional damping in the post yield stage may not be justified as the tangential stiffness properties are not the same as initial properties once the structure yields. Thus, the proportionality is lost after the onset of yielding (Bernal, 1994). Nevertheless, in the case of non-linear dynamic analysis, the dissipation of energy through inelastic deformation tends to supersede significantly the dissipation through viscous damping. Hence, the exact representation of damping is not as important in a non-linear system as in the linear system.

2.6.2 Non-viscous damping models

In viscous damping, it is assumed that damping force is dependent on the velocity of the structure and not on any other parameter. It has been mentioned in the literature that when the structure exhibits the property of non-viscosity, then the usage of viscous damping models results in the improper estimation of damping. In such cases, development of non-viscous damping becomes paramount importance. Adhikari and Woodhouse (2003) mentioned that the non-viscous damping models may be a better option in modeling the linear elastic behavior. Puthanpurayil et al. (2011) discussed the various issues related to modeling of in-structure damping and concluded that non-viscous damping has resulted in the larger peak response than the viscous damping (Puthanpurayil et al. 2011). Many investigations have been carried out to determine the response of the structure with different damping models. The choice of damping models affects the structural response of the system.

2.6.3 Active control damping models

For very tall buildings, the inherent damping may not be sufficient in mitigation of structural response adequately. Hence, the use of supplemental or auxiliary damping is vital in keeping the response of tall buildings to the desired level. Active control damping systems requires the power supply to activate such type of damping and hence cannot be considered a viable option especially in the seismically active zone. Nevertheless, the active damping system is being used as a method in dampening the response of tall buildings subjected to severe wind load effects.

2.6.4 Passive control damping models

On the other hand, passive damping control system can be incorporated in a structure to absorb a portion of seismic energy imparted and hence considered a potential candidate for the protection of buildings in a high seismic zone. The classification of active and passive system is mentioned in the form of flowchart in Fig. 2.9. Depending upon the type of dampers, the structural response differs significantly. Viscous dampers and viscoelastic dampers dampens the response essentially at all levels of deformation and cover broad frequency range.

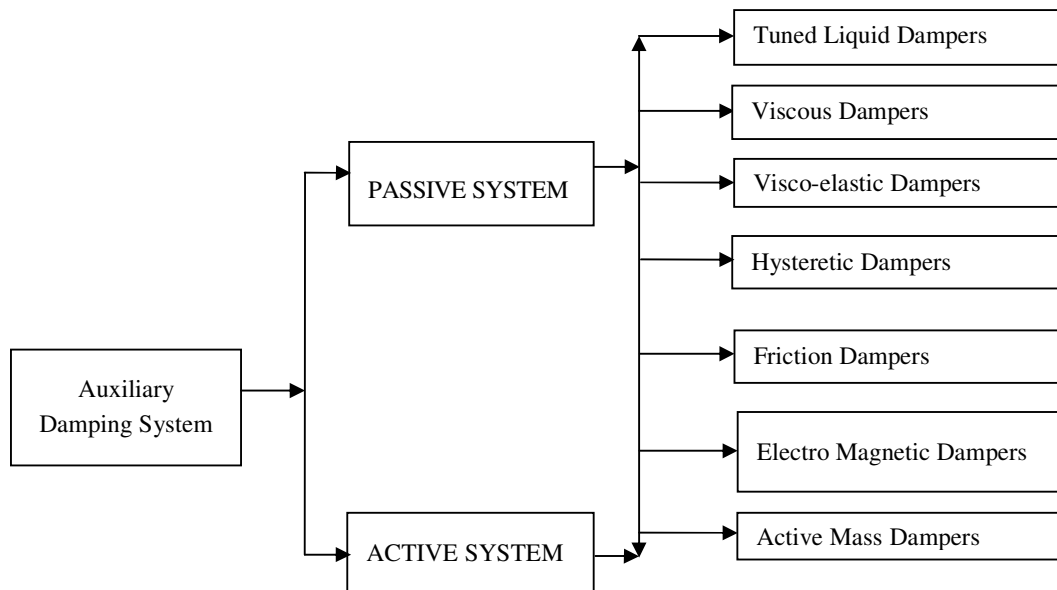


Fig. 2.9: Different types of auxiliary damping system

Friction dampers will get triggered when the slip force exceeds and metallic yield dampers dissipate energy through inelastic deformation. Sometimes, it may be necessary to incorporate the effect of all dynamic characteristics in a building to mitigate the

damping. Hybrid damping incorporates the effect of all the dampers and may be specifically installed in a building to damp out both high frequency and low frequency content.

Hence, it is concluded that the influence of damping can prove to be significant parameter in controlling the structural damage and may result in the desired structural response.

2.7 Gaps in Existing Research

Based on the literature review the following research gaps have been identified and intended to be performed in the current study.

- The literature advocates and captures the different failure modes to be adopted for the design of slender and squat shear walls. Nevertheless, limited analytical study has been conducted on the structural response of shear wall with different aspect ratio.
- Even though substantial experimental work has been done on the response of shear wall with openings, not much analytical study has been found in the literature pertaining to the structural response of shear wall with different opening sizes especially under severe dynamic ground motions.
- Very limited study has been found in the literature pertaining to the structural response of shear wall with different opening locations.
- The literature advocates the use of dampers in shear walls for better structural performance. However, limited analytical study has been found on the response of shear wall for different damping ratios.

2.8 Objectives of the Present Study

In order to assess the influence of aspect ratio of shear wall, sizes and locations of openings, and damping on the structural response of shear wall, the following objectives have been framed.

- To develop and validate the finite element program capable of analyzing static and dynamic analysis of RC shear wall in non-linear regimes.
- To assess the influence of opening size and opening location on the structural response of slender and squat shear walls.

- To assess the influence of strengthening around the openings on structural response of slender and squat shear walls.
- To examine the influence of damping on the structural response of slender and squat shear walls.

References:

1. ACI 318 (2011). “*Building code requirements for structural concrete and commentary.*” American Concrete Institute, Michigan, USA.
2. Adhikari, S., and Woodhouse, J. (2003). “Quantification of non-viscous damping in discrete linear systems.” *Journal of Sound and Vibration*, 260(1), 499-518.
3. Ahmad, S., Irons, B.M., and Zienkiewicz, O.C. (1970). “Analysis of thick and thin shell structures by curved finite elements.” *International Journal of Numerical Methods in Engineering*, 2(3), 419-451.
4. AIJ (1999). “*Architectural Institute of Japan Standard for RC Structures.*” Architectural Institute of Japan, Tokyo, Japan
5. Ali, A., and Wight, J.K. (1991). “RC structural walls with staggered door openings.” *ASCE Journal of Structural Engineering*, 117(5), 1506-1514.
6. Amick, H., and Monteiro, J. M. (2006). “Experimental determination of modal damping in concrete beams.” *ACI Materials Journal*, 103(3), 153-160.
7. Anderson, F.E., Hanson, R.J., Murphy, H.L., Newmark, N.M., and Merit, P.W. (1964). “Design of structures to resist nuclear weapons effects.” ASCE, New York.
8. Antebi, J., Utku, S., and Hansen, J.R. (1960). “The response of shear walls to dynamic loads.” Report, *Department of Civil and Sanitary Engineering, MIT, Cambridge Massachusetts.*
9. AS3600 (2009). “*Concrete structures.*” Australian Standards, Australia.
10. Ban, S. (1943). “Experimental study on the seismic resistance of walls with openings.” *Transactions of the Architectural Institute of Japan*, 30.
11. Barda, F. (1972). “*Shear strength of low-rise walls with boundary elements.*” Ph.D. University, Lehigh University, Bethlehem, Pennsylvania, USA.
12. BD (2008). “*Code of practice for structural use of concrete.*” Buildings Department, Kowloon, Hong Kong.
13. Beck, H. (1962). “Contribution to the analysis of coupled shear walls.” *ACI Journal, Proceedings*, 59, 1055-1069.
14. Benjamin, J.R., and Williams, H.A. (1953). “Investigation of shear walls, - Part 3- Experimental and Mathematical studies of the behavior of plain and reinforced concrete walled bents under static shear loading.” *Department of Civil Engineering, Stanford University, Stanford, California, July*, 142 pp.
15. Benjamin, J.R., and Williams, H.A. (1954). “Investigation of shear walls, - Part 6- Continued Experimental and Mathematical studies of reinforced concrete walled bents under static shear loading.” *Department of Civil Engineering, Stanford University, Stanford, California, August*, 59 pp.

16. Bernal, D. (1994). "Viscous damping in inelastic structural response." *ASCE Journal of Structural Engineering*, 120(4), 1240-1254.
17. Bolander, J and Wight, J (1991). "Finite element modeling of shear-wall-dominant buildings." *ASCE Journal of Structural Engineering*, 117(6), 1719-1739.
18. BSL (2007). "*The Building Standard Law of Japan.*" Ministry of Construction, Tokyo, India.
19. Cardenas, A.E., Hanson, J.M., Corley, W.G., and Hognestad, E. (1973). "Design provisions for structural walls." *ACI Journal Proceedings*, 70(3), 221-230.
20. Carr, A.J. (2007). "*Ruaumoko Manual-Theory.*" University of Canterbury. 3-14.
21. Caughey, T.K. (1960). "Classical normal modes in damped linear systems." *ASCE Journal of Applied Mechanics*, 27(2), 269-271.
22. Cervenka, V. (1970). "*Inelastic finite element analysis of reinforced concrete panels.*" Ph.D. Dissertation, University of Colorado, Boulder, USA.
23. Chiba, O., Fukuzawa, R., Hatori, T., and Yagishita, K. (1985). "Experimental study on heavily reinforced concrete shear walls." *Transactions of 8th SMiRT Conference*, H 4/1, 131-136.
24. Chopra, A. (2006). "*Dynamics of structures: Theory and application to earthquake engineering.*" 3rd Ed., Prentice-Hall, Englewood Cliffs, New Jersey, USA.
25. Daniel, J. I., Shiu, K.N., and Corley, W.G. (1976). "Openings in earthquake resistant structural walls." *ASCE Journal of Structural Engineering*, 112(7), 1660-1976.
26. Doh, J.H., and Fragonemi, S. (2006). "Ultimate load formula for reinforced concrete wall panels with openings." *Advances in Structural Engineering*, 9(1), 103-115.
27. Dotroppe, J.C., Schnobrich, W.C., and Pecknold, D.A. (1973). "Layered finite element procedure in inelastic analysis of reinforced concrete slabs." *IABSE Publication*, 33-11.
28. Dvorkin, E.N., and Bathe, K.J. (1984). "A continuum mechanics based four-node shell element for general nonlinear analysis." *Engineering Computations*, 1(1), 77-78.
29. Farrar, C.R., and Baker, W.E. (1993). "Experimental assessment of low-aspect-ratio, reinforced concrete shear wall stiffness." *Earthquake Engineering & Structural Dynamics*, 229(5), 373-387
30. Farvashany, F.E., Foster, S.J., and Vijaya Rangan, B. (2008). "Strength and deformation of high-strength concrete shearwalls." *ACI Structural Journal*, 105(1), 21-29.

31. Fragomeni, S., Doh, J.H., and Lee, D.J. (2012). "Behavior of axially loaded concrete wall panels with openings: An experimental study." *Advances in Structural Engineering*, 15(8), 1345-1358.
32. Franklin, H.A. (1970). "Non-linear analysis of reinforced concrete frames and panels." Ph.D. Dissertation, SEMM 70-5, *Division of Structural Engineering and Structural Mechanics, University of California, Berkeley, USA*.
33. Galletly, G.D. (1952). "Behavior of reinforced concrete shear walls under static load." *Report, Department of Civil and Sanitary Engineering, MIT, Cambridge Massachusetts, USA*.
34. Girijavallabhan, C.V. (1969). "Analysis of shear walls by finite element method." *Proceedings of the Symposium on Application of Finite Element Methods in Civil Engineering*, Vanderbilt University, Nashville, Tennessee, 631-641.
35. Ile, N., and Reynouard, J.M. (2000). "Nonlinear analysis of reinforced concrete shear wall under earthquake loading." *Journal of Earthquake Engineering*, 4(2), 183-213.
36. Iliya, R., and Bertero, V.V. (1980). "Effects of amount and arrangement on wall-panel reinforcement on hysteretic behavior of reinforced concrete walls." *Report No. UCB/EERC-80/04*, University of California, Berkeley.
37. IS 13920 (1993). "*Ductile detailing of reinforced concrete structures subjected to seismic forces.*" Bureau of Indian Standards, New Delhi, India.
38. Johnson, A.C. (1997). "Monotonic and cyclic performance of full-scale timber shear walls with openings, *thesis submitted in partial fulfillment of Master's of Science Degree in Civil Engineering, Virginia Polytechnic Institute and State University, Blacksburg, Virginia.*
39. Kabeyasawa, T., Matsumori, T., and Yousok, K. (2007). "Shake table tests on the three-story reinforced concrete buildings with flexible foundations." *Proceedings of the 2nd NEES/e-defense workshop on collapse simulation of reinforced concrete building structure, Miki*, 243-254.
40. Kato, D., Kabeyasawa, T., Otani, S., and Aoyama, H. (1995). "Earthquake resistant design of shear walls with one opening." *ACI Structural Journal*, 92(4), 495-501.
41. Kazimi, S.M.A. (1966). "The analysis of shear-wall buildings." *Building Science*, 1(4), 271-276.
42. Kobayashi, J., Korenaga, T., Shibata, A., Akino, K., and Taira, T. (1995). "Effect of small openings on strength and stiffness of shear walls in reactor buildings." *Nuclear Engineering and Design*, 156(1-2), 17-27.
43. Kunnuth, S.K. (1994). "Distributed flexibility models for non-linear analysis of RC structures in Analysis." *Proceedings of ASCE Structures Congress in Atlanta, ASCE Publishing, New York*, 145-154

44. Kwak, A.K.H., and He, X.G. (2001). "Finite element analysis of effect of concrete confinement on behavior of shear walls." *Computers & Structures, Elsevier*, 79(19), 1799-1810.
45. Lee, D.J. (2008). "Experimental and theoretical study of normal and high strength concrete wall panels with openings." *PhD Thesis, Griffith University*, Australia.
46. Lefas, I.D., Kosovos, MD., and Ambraseys, N.N. (1990). "Behavior of reinforced concrete structural walls, strength, deformation characteristics, and failure mechanism." *ACI Structural Journal*, 87(1), 23-31.
47. Lin, C.S., and Scordelis, A.C. (1975). "Nonlinear analysis of RC shells of general form." *ASCE Journal of Structural Division*, 101(3), 523-538.
48. Lin, C.Y., and Kuo, C.L. (1988). "Behavior of shear wall with openings." *Proceedings of Ninth world Conference on Earthquake Engineering, Tokyo-Kyoto, Japan, IV*, 535-540.
49. Lindeburg, M.R., and Baradar, M. (2001). "*Seismic design of building structures.*" 8th Ed, Professional Publications Inc., Belmont, California.
50. MacLeod, I. (1970). "Shear wall-frame interaction: a design aid." *Engineering Bulletin, Portland Cement Association*, 17 pp.
51. MacLeod, I. A., and Hosny, H. M. (1977). "Structural-analysis of wall systems." *Journal of Structural Engineering, ASCE*, 55(11), 487-495.
52. Magnus, D. (1965). "Pierced shear walls." *Concrete and Constructional Engineering*, LX(3), 89-98.
53. Maier, J., and Thurlimann, B. (1985). "Bruchversuche an stahlbetonscheiben, IBK Bericht 8003-1, ETH Zurich, *Institut für Baustatik und Konstruktion (IBK)*, Zurich.
54. Masood, M., Ahmed, I., and Assas, M. (2012). "Behavior of shear wall with base opening." *Jordan Journal of Civil Engineering*, 6(2), 255-266.
55. Massone, L.M., Orakcal, K., and Wallace, J.W. (2004). "Flexural and shear responses in slender RC shear walls." *Proceedings of the 13th World Conference on Earthquake Engineering, Vancouver, BC, Canada*, Paper 1067.
56. Mattacchine, A. (1991). "Equivalent frame method applied to concrete shear walls." *ACI Concrete International*, 13(11), 65-72.
57. Nayak, G.C., and Zienkiewicz, O.C. (1972). "Elasto-plastic stress analysis." *International Journal of Numerical Methods in Engineering*, 5, 113-135.
58. Nayar, K.K., and Coull, A. (1976). "Elastoplastic analysis of coupled shear walls" *Journal of Structural Division, ASCE*, 102(9), 1845-1860.
59. Neuenhofer, A. (2006). "Lateral stiffness of shear walls with openings." *ASCE Journal of Structural Engineering*, 132(11), 1846-1851.
60. Ngo, D., and Scordelis, A.C. (1967). "Finite element analysis of reinforced concrete beams." *ACI Journal*, 64(3), 152-163.

61. Nilson, A.H. (1972). "Internal measurement of bond slip." *ACI Journal*, 69(7), 439-441.
62. Palermo, D. (1998). "Testing of a 3-D shear wall under cyclic loading." *MASc thesis, Department of Civil Engineering, University of Toronto*, 240 pp.
63. Paswey, S.F., and Clough, R.W. (1971). "Improved numerical integration of thick shell finite elements." *International Journal for Numerical Methods in Engineering*, 3(4), 575-586.
64. Paulay, T., Priestley, M.J.N., and Singe, A.J. (1982). "Ductility in earthquake resisting squat shear walls." *ACI Journal*, 79(4), 257-269.
65. Puthanpurayil, A.M., Dhakal, R.P., and Carr, A.J. (2011). "Modeling of in-structure damping: A review of the state-of-the-art." *Proceedings of the Ninth Pacific Conference on Earthquake Engineering, Building an Earthquake-Resilient Society*, 14-16, April, Auckland, New Zealand.
66. Qamaruddin, M. (1998). "In-plane stiffness of shear walls with openings." *Building and Environment*, 34(1), 109-127.
67. Rosman, R. (1964). "Approximate analysis of shear walls subject to lateral loads." *Proceedings of ACI Journal*, 61(6), 717-732.
68. Saheb, S.M., and Desayi, P. (1990). "Ultimate strength of RC wall panels with openings." *ASCE Journal of Structural Engineering*, 116(6), 1565-1578.
69. Salonikos, T., Kappos, A., Tegos, A., and Penelis, G. (1999). "Cyclic load behavior of low slenderness reinforced concrete walls: design basis and test results." *ACI Structural Journal*, 96(4), 649-660.
70. Satake, N., Suda, K.I, Arakawa, T., Sasaki, A., and Tamura, Y. (2003). "Damping evaluation using full-scale data of buildings in Japan." *Journal of Structural Engineering, ASCE*, 129(4), 470-477.
71. Scanlon, A., and Murray, D.W. (1974). "Time dependent reinforced concrete slab deflections." *Journal of the Structural Division, ASCE*, 100(9), 1911-1924.
72. Schultz, M. (1961). "Analysis of reinforced concrete wall with openings." *The Indian Concrete Journal*, 35 (11), 432-433.
73. Schwaighofer, J., and Microys, H.F. (1969). "Analysis of shear walls using standard computer programmes." *ACI Journal, Proceedings*, 66, 1005-1007.
74. Shiu, K.N., Aristizabal, O.J.D., Barney, G.B., Fiorato, A.E., and Corley, W.G. (1981). "Earthquake resistant structural walls-coupled wall tests." *Report to National Science Foundation, Construction Technology Laboratories, A Division of Portland Cement Association, Stokie, Illinois, USA*.
75. Sittipunt, C., and Wood, S.L. (1995). "Influence of web reinforcement on the cyclic response of structural walls." *ACI Structural Journal*, 92(6), 745-767.

76. Smith, S.B., Kuster, M., and Hoenderkamp, J.C.D. (1981). "A generalized approach to the deflection analysis of braced frame, rigid frame and coupled wall structures, *Canadian Journal of Civil Engineering*, 8(2), 230-240.
77. Sotomura, K., and Murazumi, Y. (1985). "Nonlinear analysis of shear walls with numerous small openings." *Proceedings of Finite Element of Reinforced Concrete Structures, ASCE*, 300-307.
78. Stiller, M. (1961). "Beitrag zur Berechnung von Scheibensystemen bei Hochhausern unter Horizontalbelastung." *Dissertation, Technical University Berlin-Charlottenburg, Germany*.
79. Su, R.K.L., and Wong, S.M. (2007). "Seismic behavior of slender reinforced concrete shear walls under high axial load ratio." *Engineering Structures*, 29(8), 1957-1965.
80. Taranath, B.S. (2010). "Reinforced concrete design of tall buildings", CRC Press, Taylor & Francis Group, New York, USA.
81. Taylor C.P., Cote P.A., and Wallace J.W (1998). "Design of slender reinforced concrete walls with openings", *ACI Structural Journal*, 95(4), 420-433.
82. Thadani, B.N. (1966). "Analysis of shear wall structures." *The Indian Concrete Journal*, 40(3), 97-102.
83. Tomii, M., and Miyata, S. (1963). "Outline of shear tests concerning quake resisting walls having various openings." *Transactions of the Architectural Institute of Japan*, 66(1), 301-304.
84. UBC (1967). "*Uniform building code.*" International Conference of Building Officials, Whittier, California.
85. UBC (1970). "*Uniform building code.*" International Conference of Building Officials, Whittier, California.
86. Wilson, E. L., and Penzien, J. (1972). "Evaluation of orthogonal damping matrices." *International Journal of Numerical Methods and Engineering*, 4(1), 5-10.
87. Wood, S.L. (1990). "Shear strength of low-rise reinforced concrete walls." *ACI Structural Journal*, 87(1), 99-107.
88. Wood, S.L., Wight, J.K., and Moehle, J.P. (1987). "The 1985 Chile earthquake observations on earthquake-resistant construction in Vina del Mar." *Civil Engineering Studies, Structural Research Series, No. 532, University of Illinois, Urbana*.
89. Yamada, M., Kawamura, H., and Katagihara, K. (1974). "Reinforced concrete shear walls without openings, test and analysis." *ACI SP-42: Shear in Reinforced Concrete*, 1&2, 539-558.

90. Yanez, F.V. (1993). "Seismic behavior of reinforced concrete walls with irregular openings." *Ph.D dissertation, University of Canterbury, Christchurch, New Zealand.*
91. Yanez, F.V., Park, R., and Paulay, T. (1992). "Seismic behavior of walls with irregular openings." *Proceedings of the Earthquake Engineering Tenth World Conference, Balkema, Rotterdam.*
92. Zahrah, T.F., and Hall, W.J. (1984). "Earthquake energy absorption in SDOF structures." *Journal of Structural Engineering, ASCE*, 110(8), 1757-1772.
93. Zareian, F., and Medina, R.A. (2010). "A Practical Method for Proper Modeling of Structural Damping in Inelastic Plane Structural Systems." *Computers and Structures*, 88(1-2), 45-53.
94. Zienkiewicz, O.C., Taylor, R.L., and Too, J.M. (1971). "Reduced integration technique in general analysis of plates and shells." *International Journal of Numerical Methods and Engineering*, 3(2), 275-290.

Material Modeling of RC Structures

3.1 Background

Due to the advantage of its rigidity, RC shear walls which offer great resistance to lateral loads have been widely adopted in building structures as a lateral load resisting element. The material modeling of RC structures has been the subject of interest for many decades, because incorrect modeling results in poor characterization of its behavior. To cater to the increased demand for seismic design of RC structures, many experimental and analytical studies to capture the nonlinear response of RC structures under extreme loading conditions have been performed. Though the experimental investigation gives the required information close to reality, it is not always a viable alternative as experimental parametric studies incur huge cost and time. On the other hand, the design method envisaged in various codes based on many concepts often underestimates or over-estimates the structural response. Thus, there is a need for a reliable analytical model which predicts the behavior close to real behavior. Non-linear finite element analysis is an established analytical tool to evaluate response of RC structures.

The non-linearity in the reinforced concrete may be due to change in structural and material characteristics and may result in structural cracking of concrete, yielding of concrete and steel and crushing of concrete. Nevertheless, these non-linearities are considered to be instantaneous and assumed to be time independent. Such time independent non-linearities are usually incorporated in the analytical modeling of reinforced concrete. On the other hand, the non-linearity may also be caused due to creep and shrinkage effects which are time dependent. Such time dependent non-linearities are difficult to be incorporated analytically and hence not considered in the present study. The time independent behavior of materials can be further idealized into elastic behavior and plastic behavior. For an elastic material, there exists a one-to-one coordination between stress and strain. An elastic material is the material which returns to the original shape when the loads are removed. This is the minimal requirement for the material to qualify as elastic. The material which satisfies this minimal requirement is also known as hypo-elastic material. In a more restricted sense, an elastic material must also satisfy the

energy equation of thermodynamics. The elastic material characterized by this additional requirement is known as hyper-elastic.

On the other hand, the plastic material is the one in which the reversibility is not satisfied, i.e. the material undergoes some permanent deformation which cannot be retraced even after the removal of loads and stresses. Hence, the strain in the plastic material may be considered as the sum of the reversible elastic strain and the permanent irreversible plastic strain. The stress-strain law for a plastic material reduces, essentially, to a relation involving the current state of stress and strain and the incremental changes of stresses and plastic strains. This relation is generally assumed to be homogeneous and linear in the incremental changes of the components of stress and plastic strain. This assumption precludes viscosity effects, and thus contributes to the time-independent idealization. For the complete modeling of RC, constitutive laws representing elastic and plastic states are to be defined clearly. Elasticity based constitutive laws are required to define the behavior of the material in the elastic state while plasticity based constitutive laws are required to define the behavior of the material in the plastic state. Furthermore, the development of analytical models to determine the response of RC structures is complicated due to the following three factors:

a) Reinforced concrete is a composite material made up of concrete and steel, which have very different physical and mechanical behavior, b) concrete exhibits non-linear behavior even under low level of loading due to cracking of concrete and c) reinforcing steel and concrete interact in a complex way through bond-slip and aggregate interlock. Thus, for the finite element analysis of RC structures such as panels and shear walls, the analytical model must include (i) a strength criterion for concrete subjected to various stress combinations, (ii) concrete cracking and crack propagation, (iii) steel yielding, (iv) concrete crushing, and (v) the tension-stiffening behavior of reinforced concrete through bond-slip.

3.2 Experimental Behavior of Concrete

The behavior of plain concrete has been found to be complex due to inherent characteristics of the material. Several experimental works have been performed to examine mechanisms that lead to the propagation of failure from initial stage to ultimate collapse. Brestler and Pister (1958) suggested that the conditions responsible for local failure are essentially the same for both plain and reinforced concrete, thus highlighting

the importance of examining the behavior for plain concrete. Keeping in view the above-mentioned facts, a brief summary has been made on the various experimental investigations carried out on predicting the behavior of plain concrete under uni-axial, bi-axial and tri-axial loadings for different combinations of tension and compression.

3.2.1 Uni-axial behavior

In order to plot stress-strain curve for uni-axially compressed concrete, strength tests on cylindrical or cubical concrete specimens were conducted at the age of 28 days (Hognestad et al. 1955; Kwak and Filippou, 1990; Fardis et al. 1983; Tsai, 1988). The various stages of stress-strain curve, which characterizes different behavior of concrete, namely uni-axial compressive strength, strain corresponding to uni-axial compressive strength, initial tangent modulus and ultimate strain at failure can be regarded as the characteristic values for the stress-strain curve of concrete under uni-axial compression (Carreira and Chu, 1985). The direct tensile tests by various researchers (Hughes and Chapman, 1966, Ansari, 1987, Gopalarathnam and Shah, 1985) show that the load-elongation curve presents a peak followed by a softening branch. Since the structures are not generally subjected only to uni-axial loading conditions, it is imperative to know the behavior of concrete under bi-axial and tri-axial loading conditions.

3.2.2 Bi-axial behavior

Kupfer et al. (1969) conducted the test on concrete plate-type specimens ($20 \times 2 \times 5$ cms) under proportional monotonically increasing bi-axial compressive loading. Tasuji et al. (1978) conducted experimental investigations on thin plain concrete plates subjected to bi-axial loading, which includes all combinations of compressive and tensile loadings. It was reported that the concrete possesses higher compressive strength when subjected to biaxial compression as compared to uni-axial compression. On the other hand, when the concrete is subjected to combined compression and tension, the compressive strength has been reported to decrease linearly as the tensile stress increases (Tasuji et al. 1978; Kupfer et al. 1969; Kwak and Filippou, 1990). Nevertheless, concrete strength under bi-axial tension was found to be the approximately equal to the uni-axial tensile strength (Kupfer et al. 1969; Kwak and Filippou, 1990). Based on above-mentioned uni-axial and bi-axial tests on concrete, it is emphasized that the inclusion of the three basic parameters in any analytical model namely uni-axial compressive strength, uni-axial tensile strength, and biaxial compressive strength is indispensable.

3.2.3 Tri-axial behavior

To understand the behavior of concrete subjected to tri-axial loading, several experimental investigations have been done (Mills and Zimmerman, 1970; Imran and Pantazopoulou, 1991). Mills and Zimmerman (1970) reported that majority of investigations have been performed on cylindrical specimens where two principal stresses out of three retain the same value (Mills and Zimmerman 1970). They conducted the test on cubical specimens and concluded that cubical specimens provide a realistic estimation of failure strength as it incorporates the effect of intermediate stress component. It has been reported by Gardner (1969) that all mechanical properties can be improved with increase in the confinement. Gardner (1969) and Zhi et al. (1987) carried out the bi-axial and tri-axial experiments to investigate the influence of confinement on compressive strength of concrete and observed that confinement significantly enhances the compressive strength (Gardner 1969; Zhi et al. 1987). Linhua et al. (1991) found that strength of concrete under tri-axial compressive-compressive-tensile loading is higher compared to strength of concrete subjected to bi-axial Compression-tension loading.

Brestler and Pister (1958) performed experimental tests on 65 tubular specimens of plain concrete subjected to combined stresses to predict the failure of the concrete specimens. Based on experimental results they suggested that strength of the concrete is a function of the state of stress and cannot be predicted without considering the interaction of stresses. Therefore, it is essential to predict the behavior of concrete under multi-axial stress state to obtain the more generalized response (Kupfer and Gerstle, 1973; Darwin and Pecknold, 1977; Cedolin and Mulas, 1984; Hussein and Marzouk, 2000; Tasuji et al. 1978).

3.2.4 Cyclic behavior

On the other hand, cyclic loading occurs when there is a load reversal with several loading, un-loading and re-loading cycles. Loading, un-loading & re-loading constitutes a hysteresis loop. In order to understand the behavior of concrete under dynamic effects, it is essential to know the behavior of concrete under compressive and tensile cyclic loadings. The concrete, subjected to compressive loading of high amplitude and low cycle is predominantly significant from earthquake point of view. When the number of

cycles is large, the continuous growth of micro cracks can lead to the reduction in the strength of concrete (Sinha et al. 1964; Karsan and Jirsa, 1969). Vecchio (1998) discussed the importance of cyclic load modeling of reinforced concrete and analyzed the shear wall using non-linear elasticity model.

Several experimental investigations have been done on concrete subjected to uni-axial cyclic loading (Karsan and Jirsa, 1969; Sinha et al. 1964). Mlakar et al. (1985) examined the bi-axial tensile-compressive behavior of concrete under dynamic loading and concluded that the tensile stress at failure decreases while the compressive stress gets increased. This conclusion was similar to one observed under monotonic loading (Mlakar et al. 1985). It has been observed that strength envelope for cyclic and monotonic loading has not been found to show significant difference (Lan and Guo, 1999). Based on the above experimental works, it has been concluded that confinement of a concrete has a very strong influence on compressive strength and hence should be sufficiently incorporated in any analytical model. Moreover, since conditions responsible for local failure are essentially the same regardless of randomness of loading, information available on the monotonic loading can be used effectively in developing failure model capable of capturing the responses under monotonic and cyclic loading. The next section briefly describes the characteristics of the failure surface of concrete.

3.3 Characteristics of Failure Surface of Concrete

For the non-linear analysis of concrete, various material models- plasticity models, damage models, damage-plasticity models, micro plane models, and so on- have been developed. Based on numerous theoretical studies and test results, these models have been used to accurately describe the behavioral characteristics of concrete in various compressive stress states. Concrete shows various behavioral characteristics depending on its stress states. In uni-axial compression, the initial response is almost linear, and as the compressive stress reaches its maximum, micro cracking causes concrete to behave non-linearly. In the post-peak behavior, the concrete volume increases because of the unstable propagation of the micro cracks. In the bi-axial compression test by Kupfer et al. (1969), it was observed that maximum strength of concrete increases upto 125% of the uni-axial strength depending on the ratio of the two orthogonal stresses.

Comparable strength enhancement was also confirmed in other bi-axial compression tests (Liu et al. 1972; Tasuji et al. 1978). In the tri-axial compression tests conducted by various researchers (Kotsovos and Newman, 1978; Sfer et al. 2002), it was found that the strength and ductility of concrete increases significantly with the confinement effect. To describe these behavioral characteristics of concrete in compression, the plasticity model was frequently used because of its simple and direct representation of multi-axial stress. Many researchers have attempted to extend the application of the plasticity model to evaluate various stress states of concrete (Chen and Chen, 1975). The current section describes the overview of the development of yield/failure surface using plasticity approach.

The choice of yield/failure criteria considerably affects the estimation of strength characteristics of the material (Chen (1982), Yu (2002, 2004)). At every point inside the stressed body, there exist at least three planes called principal planes. The directions normal to these planes are called principal directions and the stresses along these directions are called principal stresses. Most of the failure criteria are expressed in terms of the principal stress invariants since it is generally acceptable that the macroscopic fracture behavior can be assumed to be isotropic, that is, in the form of following equation.

$$F(I_1, I_2, I_3) = 0 \quad [3.1]$$

where, $I_1 = \sigma_1 + \sigma_2 + \sigma_3$; $I_2 = \sigma_1\sigma_2 + \sigma_2\sigma_3 + \sigma_3\sigma_1$; $I_3 = \sigma_1\sigma_2\sigma_3$; σ_i are the principal stresses. It has also been reported in the literature that the failure criteria expressed by using separate functions for separate failure regions, in general, are better to predict the failure of concrete than those expressed by a simple function. Moreover, the failure criteria expressed by a simple single function are also different to apply to the failure form. The failure surface can also be represented in terms of three stress invariants (Chen, 1982) I_1, J_2 and J_3 as

$$F(I_1, J_2, J_3) = 0; J_2 = \frac{1}{3}(I_1^2 - 3I_2); J_3 = \frac{1}{27}(2I_1^3 - 9I_1I_2 + 27I_3) \quad [3.2]$$

The typical yield surface in 3-dimensional principal stress space is shown in Fig. 3.1.

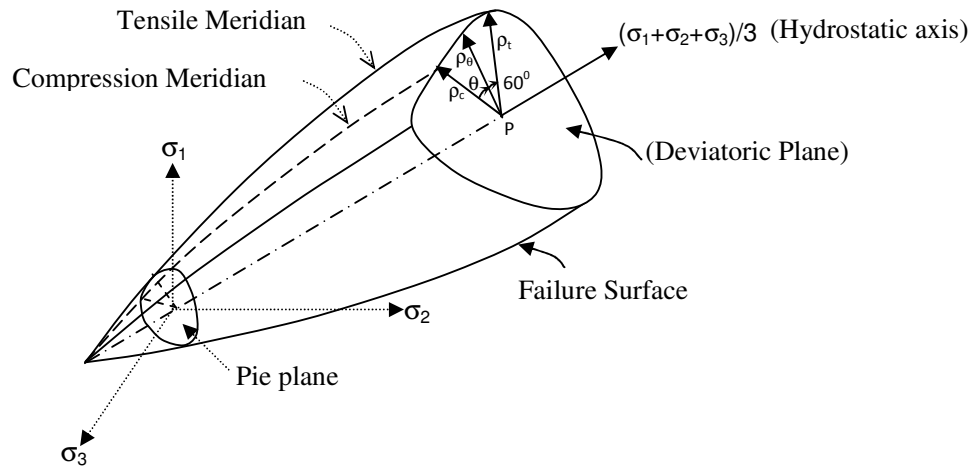


Fig. 3.1: Yield surface in 3-dimensional principal stress space

Hydrostatic axis is the axis which is equidistant from three principal axes ($\sigma_1 = \sigma_2 = \sigma_3$). Deviatoric plane is the plane perpendicular to the hydrostatic axis. Pie plane is the plane perpendicular to the hydrostatic axis, passes through the origin, and is considered as a special type of deviatoric plane. The meridians of the failure surface are the intersection curves between the failure surface and the plane containing the hydrostatic axis with constant θ . The meridian planes corresponding to $\theta=0^\circ$ and $\theta=60^\circ$ are called tensile and compressive meridians, respectively. The meridian plane corresponding to $\theta=30^\circ$ is known as shear meridian. The deviatoric plane and meridian planes are pictorially represented in Fig. 3.2.

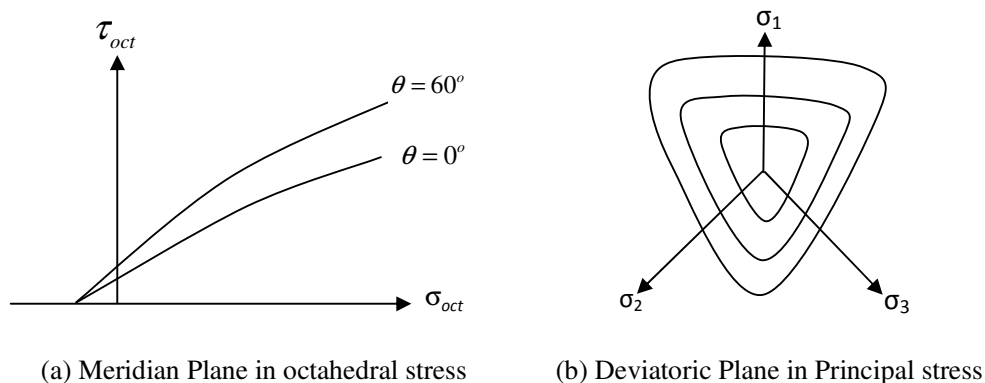


Fig. 3.2: Characteristics of failure surface

Nevertheless, for better geometric representation, the failure criterion may also be expressed using Haigh-Westergaard coordinate system (Han and Chen, 1987), which is defined in terms of three parameters namely hydrostatic stress invariant $\xi_s = (1/\sqrt{3}) \times I_1$, deviatoric stress invariant $\rho = \sqrt{2J_2}$ and deviatoric polar angle θ , which is also known as Lode angle. The Lode angle is expressed in terms of second and third deviatoric stress invariant (Nayak and Zeinkiewicz, 1972) as $\cos 3\theta = \frac{3\sqrt{3}}{2} \frac{J_3}{\sqrt{J_2^3}}$. The hydrostatic stress invariant ξ_s is an important index which determines the enhancement of strength and ductility in multi-axial compression. The failure surface is represented as $F(\xi_s, \rho, \theta) = 0$. In the Haigh-Westergaard coordinate system, the cross-section of the failure surface is represented in deviatoric plane and the meridians are described in the meridian plane. At any point within the failure surface, the principal stresses may be expressed in terms of Haigh-Westergaard coordinates as

$$\begin{pmatrix} \sigma_1 \\ \sigma_2 \\ \sigma_3 \end{pmatrix} = \frac{1}{\sqrt{3}} \begin{Bmatrix} \xi_s \\ \xi_s \\ \xi_s \end{Bmatrix} + \sqrt{\frac{2}{3}} \rho \begin{bmatrix} \cos \theta \\ \cos \left(\theta - \frac{2\pi}{3} \right) \\ \cos \left(\theta + \frac{2\pi}{3} \right) \end{bmatrix} \quad [3.3]$$

Based on the various experimental results, the following characteristics have been considered to be desirable and the same has to be reflected in any failure model. (i) Failure surface should be convex and should contain smooth edges, (ii) Cross-section in the deviatoric plane changes from triangular to circular with the increase in confinement, and (iii) Compressive and tensile meridians in the meridian plane should be parabolic in nature. Failure models have been developed in the past based on (i) the empirical approach, (ii) physical approach, and (iii) phenomenological approach. In the empirical approach, the tensile and compressive meridians in the meridian plane were derived through curve fitting over a cluster of experimental data points obtained by various researchers. To represent the failure surface in the deviatoric plane, the smooth interpolation between the two meridians were obtained to get the shape functions. It has also been reported by Fan and Wang (2002) that the formulations based on empirical approach lacks theoretical background on its hypothetical smooth interpolation between the meridians in the deviatoric plane although it has been found

to give satisfactory results. On the other hand, failure models have also been developed using physical approach based on the material structure, which has been claimed as the only true property of a material. The above approach captures the pressure sensitivity of the material. Failure models are also based on phenomenological approach where criterion is based on experimental observations of the global shape of the failure contour. Many failure models have been developed based on the phenomenological approach in the past according to the number of parameters associated with the failure models. The next section describes the modeling of concrete in compression with emphasis on failure criteria of concrete.

3.4 Modeling of Concrete in Compression

The experimental behavior of concrete paved the way for the development of non-linear theories which are available in literature. The non-linear behavior of concrete material is usually modeled by one of the three non-linear theories: non-linear elasticity, plasticity, or endochronic theory. The theory of plasticity is the most widely used method to describe the behavior of concrete (Chen, 1982). When the concrete is subjected to compressive stresses, experimental results (Sinha et al. 1964) have indicated that non-linear deformations of concrete are basically inelastic because upon un-loading only a portion of those strains can be recovered from the total strains. Therefore, the stress-strain behavior of the concrete material may be separated into recoverable and non-recoverable components. The recoverable part can be treated within the field of elasticity theory, while the irrecoverable part can be treated by the theory of plasticity. In general, models based on the theory of plasticity describe concrete as an elastic-perfectly plastic material (Hand et al. 1972), or, to account for the hardening behavior upto the ultimate strength, as an elastic strain-hardening plastic material (Chen and Chen, 1975). Since the elastic strain-hardening plastic model is more general and more accurate than the earlier elastic-perfectly plastic models, it is used in the present investigation. In order to apply the incremental theory of elastic strain-hardening plasticity, several aspects must be specified beforehand. The three main aspects are:

- i The yield function that defines the initial and subsequent yield surface during continuous loading.
- ii The hardening rules that describe the motion of the subsequent yield surface during continuous loading.
- iii The flow rule that relates the plastic strain increments to stress increments.

The early efforts to develop a plasticity model for concrete have been centered in search of a suitable failure surface. Then, the initial and subsequent yield surfaces are assumed in accordance with the shape of the failure surface. Since the failure surface serves as the strength criterion for concrete, it is the key element in the constitutive modeling of concrete. The following section reviews various failure models and describes the development of tri-axial failure surface using five parameter model proposed by Willam and Warnke (1974).

3.4.1 Failure models of concrete

The von-Mises, Tresca and Rankine failure criteria depend on only one parameter and it has been reported in the literature that these failure models fail to capture the behavior of concrete adequately. Addition of Rankine criterion to von-Mises and Tresca to include tension-cutoff condition makes these criteria two-parameter models. Nevertheless, these failure models are insensitive to hydrostatic pressure and hence are not used for concrete. The Mohr-Coulomb criterion, widely used as a failure criterion for concrete because of its hydrostatic pressure dependence, has straight edges and sharp corners in the failure surface in the deviatoric plane. The straight edges essentially mean that the linear interpolation has been used between the tensile and compressive meridian. The Drucker-Prager failure criterion gives better results than Mohr-Coulomb criterion because of the smoothness of the failure surface in the deviatoric section. The Mohr-Coulomb and Drucker-Prager criteria results to Tresca and von-Mises criteria respectively as special cases. Furthermore, the Rankine's criterion can be added to either Mohr-Coulomb or Drucker-Prager criteria to extrapolate these two-parameter models into three-parameter model. Several investigations have been conducted on the behavior of concrete subjected to bi-axial stress state of concrete and concluded that the biaxial compressive strength of concrete is higher than uni-axial compressive strength of concrete. Nevertheless, most of the researchers have suggested that not much variation was observed between the bi-axial tensile and uni-axial tensile strength of concrete. Thus, it has been reported that minimum three parameters, namely (i) uni-axial compressive strength, (ii) bi-axial compressive strength, and (iii) uni-axial tensile strength are required to predict the behavior of concrete. Thus, the use of Mohr-Coulomb, Drucker-Prager criteria have been found to be having limitations in predicting the response of concrete. On the basis of experimental investigations, various three-parameter models have been proposed. The Menetrey-Willam three-parameter model has been considered for the simplification of

Willam-Warnke five-parameter model and possesses the desired characteristics of a failure surface. Brestler and Pister (1958) have also proposed a three-parameter model. While Willam-Warnke failure model (Willam and Warnke, 1974) has the linear dependence between octahedral shear and normal stress, Brestler and Pister (1958) has the circular section in the deviatoric plane.

The extensive investigations lead to the representation of the failure surface with the help of four parameters (Chen and Chen, 1975). Ottosen and Hsieh-Ting-Chen model falls in this category. Hsieh-Ting Chen model is considered a computationally simpler than the one proposed by Ottosen; nevertheless, the failure model has edges in the failure surface in the deviatoric plane and hence not been considered superior. The Willam-Warnke five-parameter model has been the best pick over all the above mentioned failure criteria because of its versatility in satisfying all the characteristics of the failure surface and also its performance in predicting the behavior of concrete (Willam and Warnke, 1974). Hence, in this study, it has been decided to use five-parameter failure model to model the concrete.

3.4.2 Willam-Warnke five parameter failure model: mathematical formulation

In the Willam-Warnke five parameter failure model, a three dimensional failure surface is developed in stress-space plasticity assuming isotropic behavior of concrete. As required and portrayed in the characteristics of failure surface, the present failure surface is basically a cone with curved meridians and a non-circular base section. The limited tension capacity is responsible for tetrahedral shape in the tensile regime, while in compression a cylindrical form is ultimately reached. For the mathematical model, only a sextant of the principal stress space has been considered, if the stress components are ordered according to $\sigma_1 \geq \sigma_2 \geq \sigma_3$. The surface is conveniently represented by hydrostatic and deviatoric sections where the first one forms a meridian plane which contains equi-sectrix $\sigma_1 = \sigma_2 = \sigma_3$ as an axis of revolution. The deviatoric section lies in a plane normal to the equi-sectrix, the deviatoric trace being described by the polar coordinates (ρ, θ) . In addition, the convexity condition implies that the curve should have no inflection points in this interval, thus the approximation cannot be based on trigonometric functions or Hermitian interpolation. If the curve should also degenerate to

a circle for $\rho_t = \rho_c$, then an elliptic approximation has to be used for the functional variation of the deviatoric trace as shown in Fig. 3.3.

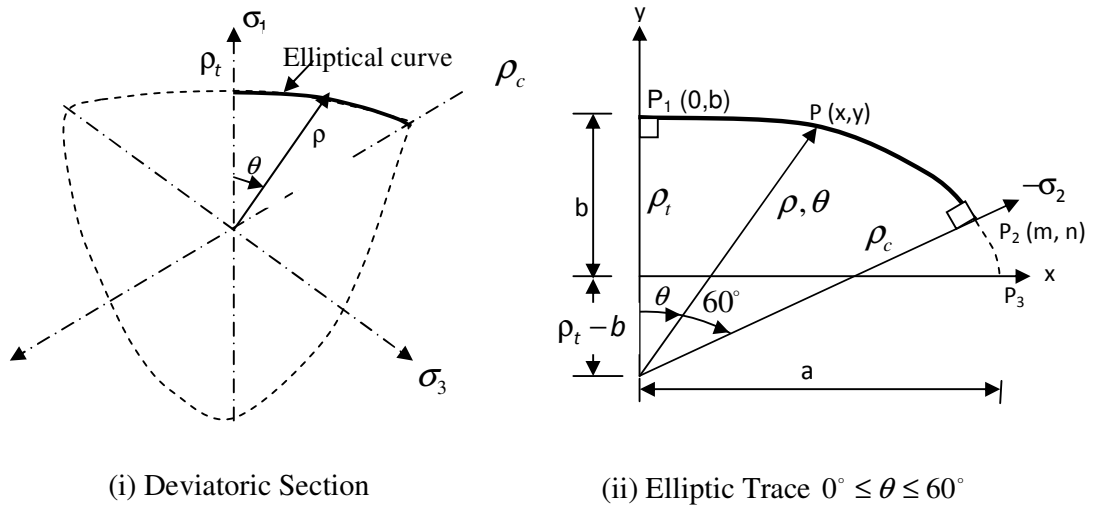


Fig. 3.3: Trace of the deviatoric section of Willam-Warnke five parameter failure surface

The ellipsoidal surface assures smoothness and convexity for all position vectors ρ satisfying $0.5 \rho_c \leq \rho < \rho_c$. The failure curve $P_1 - P - P_2$ with (ρ, θ) as polar co-ordinates is approximated by a quarter of an ellipse $P_1 - P - P_2 - P_3$ in the deviatoric section. The elliptic trace is expressed in terms of the polar coordinates (ρ, θ) by

$$\rho(\theta) = \frac{2\rho_c(\rho_c^2 - \rho_t^2)\cos\theta + \rho_c(2\rho_t - \rho_c) \left[4(\rho_c^2 - \rho_t^2)\cos^2\theta + 5\rho_t^2 - 4\rho_t\rho_c \right]^{1/2}}{4(\rho_c^2 - \rho_t^2)\cos^2\theta + (\rho_c - 2\rho_t)^2} \quad [3.4]$$

$$\Rightarrow \rho(\sigma_m, \theta) = \frac{s+t}{v}$$

where

$$\left. \begin{aligned} s &= s(\sigma_m, \theta) = 2\rho_c(\rho_c^2 - \rho_t^2)\cos\theta \\ t &= t(\sigma_m, \theta) = \rho_c(2\rho_t - \rho_c)u^{1/2} \\ u &= u(\sigma_m, \theta) = 4(\rho_c^2 - \rho_t^2)\cos^2\theta + 5\rho_t^2 - 4\rho_t\rho_c \\ v &= v(\sigma_m, \theta) = 4(\rho_c^2 - \rho_t^2)\cos^2\theta + (\rho_c - 2\rho_t)^2 \end{aligned} \right\} \quad [3.5]$$

The variations of the average shear stresses along tensile and compressive meridians are approximated by second-order parabolic expressions in terms of the average normal stresses, as follows:

$$\left. \begin{aligned} \frac{\tau_{mt}}{f'_c} &= \frac{\rho_t}{\sqrt{5}f'_c} = a_0 + a_1 \left(\frac{\sigma_m}{f'_c} \right) + a_2 \left(\frac{\sigma_m}{f'_c} \right)^2 & \theta = 0^\circ \text{ [Tensile]} \\ \frac{\tau_{mc}}{f'_c} &= \frac{\rho_c}{\sqrt{5}f'_c} = b_0 + b_1 \left(\frac{\sigma_m}{f'_c} \right) + b_2 \left(\frac{\sigma_m}{f'_c} \right)^2 & \theta = 60^\circ \text{ [Compressive]} \end{aligned} \right\} [3.6]$$

In the above equation, $\sigma_m = (I_1/3)$ is the mean stress, ρ_t and ρ_c are the stress components perpendicular to the hydrostatic axis at $\theta = 0^\circ$ and $\theta = 60^\circ$, respectively. a_0, a_1, a_2, b_0, b_1 and b_2 are material constants. The evaluation of the above six constants is explained in Appendix-1. All stress components are normalized by compressive strength (f'_c). The mathematical model expresses the failure surface in terms of average or hydrostatic stress σ_m (Change in volume), the average shear stress τ_m and the angle θ and the failure surface is defined as

$$F(\sigma_m, \tau_m, \theta) = \frac{\sqrt{5}}{\rho(\sigma_m, \theta)} \frac{\tau_m}{f'_c} - 1 = 0 \rightarrow \frac{\tau_m}{f'_c} = \frac{\rho(\sigma_m, \theta)}{\sqrt{5}} \quad [3.7]$$

The failure of the concrete is categorized into four domains:

- (a) $0 \geq \sigma_1 \geq \sigma_2 \geq \sigma_3$ (compression – compression – compression)
- (b) $\sigma_1 \geq 0 \geq \sigma_2 \geq \sigma_3$ (tensile – compression – compression)
- (c) $\sigma_1 \geq \sigma_2 \geq 0 \geq \sigma_3$ (tensile – tensile – compression)
- (d) $\sigma_1 \geq \sigma_2 \geq \sigma_3 \geq 0$ (tensile – tensile – tensile)

Yielding of concrete occurs when the equation (3.7) is satisfied. Cracking occurs as soon the principal stress exceeds the allowable tensile strength. The crushing condition can at best be ascertained using strain rather than stress. Hence, for crushing, Willam-Warnke five parameter model in strain space plasticity is employed to determine the equivalent strain. Crushing is said to occur if the equivalent strain exceeds the ultimate crushing strain.

3.4.3 Hardening rule

The plasticity theory defines the yield limit as the limit below which the material property remains elastic and any further loading beyond this yield limit results in plastic flow. In the case of elastic-perfectly plastic, the initial yield surface becomes a failure/bounding surface, reflecting the increase in strain without further change in stress.

Nevertheless, for concrete having elasto-plastic behavior, strain hardening behavior needs to be included. Strain hardening is the region between the yield and peak stress reflecting the hardening nature of concrete with the increase in stress value. Thus initial loading surface/yield surface is allowed to expand on the application of load reflecting the strain-hardening behavior of concrete and thus defining the subsequent loading surface.

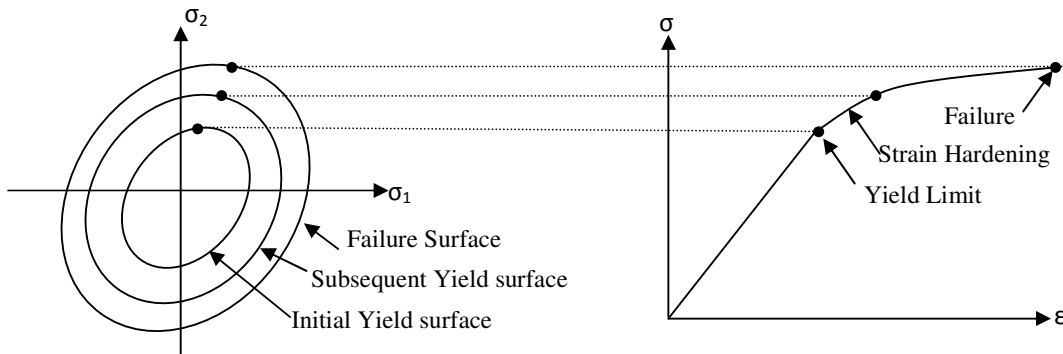


Fig. 3.4: Isotropic hardening with expanding yield surfaces and the corresponding uni-axial stress-strain curve

Hardening may be isotropic, kinematic or combination of both. Isotropic hardening assumes that the expansion of initial loading surface takes place uniformly thus completely neglecting Bauschinger effect. It essentially means that direction of strain and stress is assumed to progress in the same fashion. The typical isotropic hardening rule for the monotonic loading condition is shown in Fig. 3.4. On the other hand, the kinematic hardening assumes that the loading surface translates as a rigid body in stress space thus accounting for Bauschinger effect. At times, mixed hardening rule can be used which combines the isotropic and kinematic hardening. Nevertheless, isotropic hardening has yielded satisfactory results when used to model the hardening behavior of concrete with simplified mathematical approach (Smith et al. 1989) and hence is adopted in the present study.

To define the hardening rule, the relationship between the accumulated plastic strain and the current 'loading surface' is assumed to be the conventional 'Madrid Parabola'

$$\sigma = E_0 \varepsilon - \frac{1}{2} \frac{E_0}{\varepsilon_0} \varepsilon^2 \quad [3.8]$$

In the above equation, E_0 is the initial elasticity modulus, ε is the total strain and ε_0 is the total strain at peak stress f'_c . The total strain can be divided into elastic (ε_e) and plastic (ε_p) components as:

$$\varepsilon = \varepsilon_e + \varepsilon_p \quad [3.9]$$

Substituting the value of ε in equation (3.8), we get

$$\sigma = E_0 (\varepsilon_e + \varepsilon_p) - \frac{1}{2} \frac{E_0}{\varepsilon_0} (\varepsilon_e + \varepsilon_p)^2 \quad [3.10]$$

On expanding the equation (3.10)

$$\sigma = E_0 \varepsilon_e + E_0 \varepsilon_p - \frac{1}{2} \frac{E_0}{\varepsilon_0} \varepsilon_e^2 - \frac{1}{2} \frac{E_0}{\varepsilon_0} \varepsilon_p^2 - \frac{1}{2} \frac{E_0}{\varepsilon_0} \times 2 \times \varepsilon_e \times \varepsilon_p \quad [3.11]$$

Substituting the value of $\varepsilon_e = \frac{\sigma}{E_0}$ in equation (3.11)

$$\sigma = E_0 \frac{\sigma}{E_0} + E_0 \varepsilon_p - \frac{1}{2} \frac{E_0}{\varepsilon_0} \left(\frac{\sigma}{E_0} \right)^2 - \frac{1}{2} \frac{E_0}{\varepsilon_0} \varepsilon_p^2 - \frac{1}{2} \times \frac{E_0}{\varepsilon_0} \times 2 \times \left(\frac{\sigma}{E_0} \right) \times \varepsilon_p \quad [3.12]$$

On simplifying,

$$\sigma = \sigma + E_0 \varepsilon_p - \frac{1}{2} \frac{1}{\varepsilon_0} \frac{\sigma^2}{E_0} - \frac{1}{2} \frac{E_0}{\varepsilon_0} \varepsilon_p^2 - \frac{\sigma}{\varepsilon_0} \varepsilon_p \quad [3.13]$$

Equation (3.13) is quadratic equation, can be written in terms of

$$\left(\frac{1}{2\varepsilon_0 E_0} \right) \sigma^2 + \left(\frac{\varepsilon_p}{\varepsilon_0} \right) \sigma + \left(\frac{1}{2} \frac{E_0}{\varepsilon_0} \varepsilon_p^2 - E_0 \varepsilon_p \right) = 0 \quad [3.14]$$

This the quadratic equation in terms of σ ; on solving,

$$\sigma = -\frac{\varepsilon_p \times \varepsilon_0 E_0}{\varepsilon_0} \pm \frac{\sqrt{\left(\frac{\varepsilon_p}{\varepsilon_0} \right)^2 - \left(\frac{\varepsilon_p}{\varepsilon_0} \right)^2 + \frac{2\varepsilon_p}{\varepsilon_0}}}{\frac{1}{\varepsilon_0 E_0}} \quad [3.15]$$

$$\Rightarrow \sigma = -E_0 \varepsilon_p \pm \sqrt{2E_0^2 \varepsilon_0 \varepsilon_p}$$

Taking the feasible solution and simplifying, we get

$$\sigma = E_0 \left(-\varepsilon_p + \sqrt{2\varepsilon_0 \varepsilon_p} \right) \quad [3.16]$$

In the plasticity model adopted, the ductility increase due to the biaxial stress states cannot be represented. In order to overcome this drawback, the constant of 2.0 has been used as a strain multiplier to get the specified strain at the compressive strength.

$$\varepsilon_0 = \frac{2f'_c}{E_0} \quad [3.17]$$

Substituting the value of ε_0 in Eq. (3.16), we get

$$\sigma = E_0 \left(-\varepsilon_p + \sqrt{2 \times \frac{2f'_c}{E_0} \times \varepsilon_p} \right) \Rightarrow \sigma = E_0 \left(-\varepsilon_p + 2\sqrt{\frac{f'_c}{E_0} \times \varepsilon_p} \right) \quad [3.18]$$

The above equation is valid in the range $(0.3 f'_c < \sigma \leq f'_c)$ since the initial yield is assumed to begin when the stress exceeds 0.3 times compressive strength of concrete f'_c

$$\varepsilon = \varepsilon_e + \varepsilon_p \Rightarrow d\varepsilon = d\varepsilon_e + d\varepsilon_p \quad [3.19]$$

Dividing the above equation by incremental equivalent stress,

$$\frac{d\varepsilon}{d\sigma} = \frac{d\varepsilon_e}{d\sigma} + \frac{d\varepsilon_p}{d\sigma} \Rightarrow \frac{1}{E_T} = \frac{1}{E_0} + \frac{1}{H} \Rightarrow \frac{1}{H} = \frac{1}{E_T} - \frac{1}{E_0} \Rightarrow H = \frac{E_0 E_T}{E_0 - E_T} \quad [3.20]$$

The material initially deforms according to the initial elasticity modulus E_0 until the stress level reaches a value σ_y designated the uni-axial yield stress. On increasing the load further, the material is assumed to exhibit linear strain-hardening, characterized by the tangential modulus (E_T). The strain hardening parameter (H) can be interpreted as the slope of the strain hardening portion of the stress-strain curve after removal of the elastic strain component.

The total equivalent plastic strain is calculated by integrating the equivalent plastic strain as:

$$\varepsilon_p = \int d\varepsilon_p = \int \frac{d\sigma}{H} \quad [3.21]$$

The hardening parameter (H) is given as

$$H = \frac{\text{Incremental equivalent stress}}{\text{Incremental equivalent plastic strain}} = \frac{d\sigma}{d\varepsilon_p} \quad [3.22]$$

The hardening function is a function of the hardening parameter and its functional form is material dependent. The most common material test is performed under the uni-axial loading condition. The value of H is usually taken in the range $0 \leq H \leq 0.5$ with zero represents the elastic-perfectly plastic behavior. As always, the parameters necessary to describe hardening behavior in general loading are determined from this experiment. On the other hand, various researchers have analyzed the post peak region of concrete, also called strain-softening portion in addition to strain-hardening. However, the post peak behavior is not a material property and is very much dependent on the element size. Hence, it is not possible to universalize the strain softening for all kinds of structures. The stress-strain relations cannot precisely capture the behavior of descending portion. Hence, the present study does not include the modeling of softening portion of stress-strain curve.

3.4.4 Flow rule

During loading in the plastic range, the direction of the plastic deformation in the material (i.e., the unit normal vector in the direction of plastic flow) is defined mathematically through the plastic potential function. Though recent experimental evidence suggests that concrete demonstrates non-associativeness (Smith et al. 1989), only associated flow rule is employed in the present study because of mathematical simplicity. For small-strain elasto-plastic relation, the strain increments are decomposed into elastic component and a plastic component as

$$\{d\varepsilon\} = \{d\varepsilon_e\} + \{d\varepsilon_p\} \quad [3.23]$$

Based on this decomposition of strain increments, the incremental elastic stress-strain constitutive relationship can be expressed as

$$\{d\sigma_e\} = [D_e] (\{d\varepsilon\} - \{d\varepsilon_p\}) \Rightarrow \{d\sigma_e\} = [D_e] \{d\varepsilon_e\} \quad [3.24]$$

The incremental plastic strain is assumed to follow the relationship

$$\{d\varepsilon_p\} = d\lambda \{a\}, \quad \text{where } \{a\} = \left\{ \frac{\partial F}{\partial \sigma} \right\} \quad [3.25]$$

where F is the yield/plastic potential function. Since in this study, associated plasticity is adopted, the yield and potential function are same. $d\lambda$ is the consistency parameter, which represents the magnitude of the plastic flow and $d\lambda \geq 0$, a positive scalar; $\{a\}$ is the flow direction, which is obtained upon the differentiation of the yield function with respect to stress components, and is expressed as

$$\{a\}^T = \left[\frac{\partial F}{\partial \sigma_x} \quad \frac{\partial F}{\partial \sigma_y} \quad \frac{\partial F}{\partial \tau_{xy}} \quad \frac{\partial F}{\partial \tau_{xz}} \quad \frac{\partial F}{\partial \tau_{yz}} \right] \quad [3.26]$$

The use of an associated flow rule ensures that the plastic strain-increments are vectors perpendicular to the potential surface. Loading-unloading conditions, known as Kuhn-Tucker conditions (Chen, 1982) can be stated as

$$d\lambda \geq 0, \quad F \leq 0, \quad d\lambda F = 0 \quad [3.27]$$

The first of these indicates that the consistency parameter is non-negative while the second indicates that the stress states must lie on or within the yield surface as defined by hardening rule. The last condition assures that the stresses lie on the yield surface during plastic loading. From the loading-unloading conditions, the consistency condition can be rewritten as

$$d\lambda \Delta F = 0, \quad \text{if } F = 0 \quad [3.28]$$

$$\begin{aligned} \text{If } d\lambda \neq 0, \text{ then } \Delta F = 0 &\rightarrow \{a\}^T \{d\sigma_e\} = 0 \\ \Rightarrow \{a\}^T [D_e] \{d\varepsilon\} - \{d\varepsilon_p\} &= 0 \rightarrow \{a\}^T [D_e] \{d\varepsilon\} - d\lambda \{a\} = 0 \end{aligned} \quad [3.29]$$

The consistency parameter $d\lambda$, expressed in terms of the flow direction, is as follows

$$d\lambda = \frac{\{a\}^T [D_e] \{d\varepsilon\}}{\{a\}^T [D_e] \{a\}} \quad [3.30]$$

Since $\{a\}$ is dependent on the stress state, which is dependent on consistency parameter. Hence, eq. (3.30) is a non-linear equation. Substituting eq. (3.30) in to first of eq. (3.25),

$$\{d\varepsilon_p\} = \frac{\{a\}^T [D_e] \{d\varepsilon\}}{\{a\}^T [D_e] \{a\}} \{a\} \quad [3.31]$$

Substituting eq. (3.31) into eq. (3.24),

$$\{d\sigma_e\} = [D_e] \left(\{d\varepsilon\} - \{d\varepsilon_p\} \right) \Rightarrow \{d\sigma_e\} = [D_e] \{d\varepsilon\} - [D_e] \frac{\{a\}^T [D_e] \{d\varepsilon\}}{\{a\}^T [D_e] \{a\}} \{a\} \quad [3.32]$$

$$\{d\sigma_e\} = \{d\varepsilon\} \left[D_e - [D_e] \frac{\{a\}^T [D_e] \{a\}}{\{a\}^T [D_e] \{a\}} \right] \Rightarrow \{d\sigma_e\} = [D_{ep}] \{d\varepsilon\} \quad [3.33]$$

In eq. (3.33), $[D_{ep}]$ is the continuum elasto-plastic constitutive matrix given by

$$[D_{ep}] = [D] - \frac{[D] \{a\} \{a\}^T [D]}{\{a\}^T [D] \{a\}} \quad [3.34]$$

In the above equation, \mathbf{a} = flow vector, defined by the stress gradient of the yield function; \mathbf{D} = constitutive matrix in elastic range. The second term in eq. (3.34) represents the effect of degradation of material during the plastic loading.

The elasto-plastic constitutive matrix with strain-hardening behavior is given by the following expression

$$[D_{ep}] = [D] - \frac{[D] \{a\} \{a\}^T [D]}{H + \{a\}^T [D] \{a\}} \quad [3.35]$$

In general, the stress increments ($d\sigma_e = d\sigma$) are given by the relationship

$$\{d\sigma\} = [D_{ep}] \{d\varepsilon\} \quad [3.36]$$

The above equation represents the incremental elasto-plastic stress-strain curve considering the degradation in the stiffness due to yielding. The next section highlights the step-by-step procedure adopted in the compression modeling using incremental theory of plasticity.

3.4.5 Incremental theory of plasticity: Step-by-step procedure

The behavior of concrete may change during the course of loading from elastic to plastic frequently and vice-versa. It is essential to capture the state of stress and its behavior during the analysis. The incremental theory of plasticity relates stress increments to strain increments whereas the deformation theory relates total stress to total strain. In the present study, the incremental theory of plasticity has been adopted. The incremental theory of plasticity is capable of treating problems in which loading is

non-proportional whereas deformation theory cannot treat such problems. Stress integration represents calculation of stress change in an incremental step, corresponding to the strain increments. Not only should the integration algorithm reproduce accurately the mechanical response of the entire structure, but also should provide a computationally efficient algorithm because the stress integration is performed at all integration points.

During the application of an increment of load, an element or part of an element may yield. All stress and strain quantities are monitored at each Gaussian integration point in order to determine whether plastic deformation has occurred at such points. Consequently, an element can behave partly elastically and partly elasto-plastically if some, but not all, Gauss points indicate plastic yielding. For any load increment it is necessary to determine what proportion is elastic and which part produces plastic deformation and then adjust the stress and strain terms until the yield criterion and the constitutive laws are satisfied. In general, the following can be assumed depending on the value of failure function and the effective stress.

- (a) If $F < 0$ elastic behavior
- (b) If $F = 0$ and $d\sigma < 0$; this indicates elastic unloading occurs (elastic behavior) and the stress point returns inside the yield surface.
- (c) If $F = 0$ and $d\sigma > 0 \Rightarrow$ plastic loading; this indicates the plastic behavior for a strain hardening material and the stress point remains on the expanding yield surface.
- (d) If $F = 0$ and $d\sigma = 0 \Rightarrow d\varepsilon_p = 0$; this indicates the neutral loading (plastic behavior for a perfectly plastic material) and the stress point remains on the yield surface.
- (e) If $F > 0 \Rightarrow$ Go back to yield surface

The use of finite element discretization in a large class of non-linear problems results in a system of simultaneous equations of the form $K\varphi + f = 0$, in which φ is the vector of the basic unknowns, f is the vector of applied “loads” and K is the assembled “stiffness” matrix. For structural application, the terms 'load' and 'stiffness' are directly applicable, but for other situations the interpretation of these quantities varies according to the physical problem under consideration. If the coefficients of the matrix K depend on the

unknowns ϕ or their derivatives, the problem clearly becomes non-linear. In this case, direct solution of equation system is generally impossible and an iterative scheme must be adopted. Some of the most generally applicable methods are (i) Method of direct iteration (or successive approximation), (ii) The Newton-Raphson method, (iii) The tangential stiffness method, and (iv) The initial stiffness method. In the present study, Newton-Raphson method has been employed because of its versatility and simplicity. During any step of a Newton-Raphson iterative process of solution, A system of residual forces can be assumed to exist, so that

$$\psi = K\phi + f \neq 0 \quad [3.37]$$

These residual forces ψ can be interpreted as a measure of the departure of the equation from equilibrium. Since K is a function of ϕ and a possibly its derivatives, then at any stage of process, $\psi = \psi(\phi)$.

Consider the situation existing for the r^{th} iteration of any particular load increment. The solution algorithm employed is presented below:

- 1) The applied loads for the r^{th} iteration are the residual forces ψ^{r-1} calculated at the end of the $(r-1)^{\text{th}}$ iteration. These applied loads give rise to displacement increments $\Delta\phi^r$. Hence, calculate the corresponding increment of strain $\Delta\epsilon^r$.
- 2) Compute the incremental stress change assuming linear elastic behavior. This will introduce errors if the integration point has yielded and the material is behaving elasto-plastically. The stress change should be calculated according to $\Delta\sigma_e^r = \mathbf{D}\Delta\epsilon^r$ where the subscript e is used to denote that this stress is based on elastic behavior.
- 3) The next step in the process depends on whether or not the integration point had previously yielded during the $(r-1)^{\text{th}}$ iteration. This can be checked from the known value of the yield stress for the $(r-1)^{\text{th}}$ iteration. The stress limit for this cycle is expressed as

$$\sigma_y^{r-1} = \sigma_y + H \epsilon_p^{r-1} \quad [3.38]$$

Since the plastic strain will differ from point to point, each integration point will generally have a different permissible stress level.

- a) If $\sigma_y^{r-1} > \sigma_y + H \varepsilon_p^{r-1} \Rightarrow$ integration point had already yielded during the previous iteration.
 - b) If $\sigma_y^{r-1} \leq \sigma_y + H \varepsilon_p^{r-1} \Rightarrow$ integration point had not previously yielded.
- 4) *For the integration point which was yielded during the previous iteration:* If $\sigma_e^r > \sigma_y^{r-1} \rightarrow$ the integration point had reached the threshold stress during the previous iteration and the stress is still increasing. Therefore, all the excess stress $\sigma_e^r - \sigma_y^{r-1}$ must be reduced to the yield surface as indicated in Fig. 3.5. Therefore the factor, R, which defines the portion of the stress which must be modified to satisfy the yield condition, is equal to unity.

If $\sigma_e^r \leq \sigma_y^{r-1} \rightarrow$ the integration point is unloading which according to plasticity theory must take place elastically, and no further action need be taken. For elastic elements, the correct current stress is expressed as $\sigma^r = \sigma^{r-1} + \Delta\sigma_e^r$

- 5) *For the integration point which was not yielded during the previous iteration:* If $\sigma_e^r > \sigma_y \rightarrow$ the integration point yielded during the application of load in the current iteration, as shown in Fig. 3.6. Therefore the portion of the stress greater than the yield surface must be brought back to the yield surface. The removed portion will be included in the residual force vector for further calculation in the next iteration. The reduction factor R needs to be determined and is given by the expression

$$R = \frac{\sigma_e^r - \sigma_y}{\sigma_e^r - \sigma^{r-1}} \quad [3.39]$$

If $\sigma_e^r \leq \sigma_y \rightarrow$ the integration point is still elastic and no further action need be taken.

For elastic elements, the correct current stress is expressed as $\sigma^r = \sigma^{r-1} + \Delta\sigma_e^r$

- 6) *For the yielded integration points only:* Compute the portion of the total stress which satisfies the yield criterion as $\sigma^{r-1} + (1-R)d\sigma_e^r$. The remaining portion of stress $Rd\sigma_e^r$ must be effectively eliminated in some way. The point A must be

brought onto the yield surface by allowing plastic deformation to occur. Physically, this can be described as follows.

On loading from point C , the stress point moves elastically until the yield surface is met at B . Elastic behavior beyond this point would result in a final stress state defined by point A . However, in order to satisfy the yield criterion, the stress point cannot move outside the yield surface and consequently the stress point can only traverse the surface until both equilibrium conditions and the constitutive relation are satisfied.

$$d\sigma_r = D_e d\varepsilon^r - d\lambda Da \Rightarrow \sigma^r = \sigma^{r-1} + d\sigma_e^r - d\lambda Da \quad [3.40]$$

The above equation gives the total stresses σ^r satisfying elasto-plastic conditions when the stresses are incremented from σ^{r-1} . The above equation is illustrated vectorially in Fig. 3.5 and Fig. 3.6. It is seen that if a finite sized stress increment is taken, the final stress point D , corresponding to σ^r , may depart from the yield surface. This discrepancy can be partially eliminated by ensuring that the load increments considered in solution are sufficiently small. However, the point D can be reduced to the yield surface by simply scaling the vector σ^r .

$$\sigma^r = \sigma^r \left(\frac{\sigma_y^0 + H \bar{\varepsilon}_p^r}{\bar{\sigma}^r} \right) \quad [3.41]$$

This represents a scaling of the vector σ^r which implies that the individual stress components are proportionally reduced. The normality condition for the plastic strain increment is evident from Fig. 3.5 and Fig. 3.6 since $Dd\lambda a = Dd\varepsilon_p$

If relatively large load increment sizes are to be permitted the process described above can lead to an inaccurate prediction of the final point D on the yield surface if the stress point is in the vicinity of a region of large curvature of the yield surface. This is illustrated in Fig. 3.7 where the process of reducing the elastic stress to the yield surface is shown to end in the stress point D which is then scaled down to the yield surface to give point D' . Greater accuracy can be achieved by relaxing the excess stress to the yield surface in several stages. Fig. 3.7 shows the case where the excess stress is divided into three parts and each increment reduced to the yield surface in turn. After the three reduction cycles to the stress point E , the drift away from the yield surface can be

corrected by simple scaling to give the final stress point E' . It is seen that the final points D' and E' can be significantly different. An additional refinement which can be introduced is to scale the stress point to the yield surface after the reduction process for each cycle and not only after the final cycle as shown in Fig. 3.7. Obviously the greater the number of steps into which the excess stress AB is divided, the greater the accuracy. However, the computations for each step are relatively expensive since the vectors a and d_D have to be calculated at each stage. Clearly a balance must be sought and in this text the following criterion is adopted. The excess stress $Rd\sigma_e^r$ is divided into m parts where m is given by the nearest integer which is less than

$$\left(\frac{\bar{\sigma}_e^r - \sigma_y}{\sigma_y^0} \right) 8 + 1 \quad [3.42]$$

where $\bar{\sigma}_e^r - \sigma_y$ gives a measure of the excess stress AB and σ_y^0 is the initial uni-axial yield stress. This criterion can be readily amended by the user.

- 7) Finally, calculate the equivalent nodal forces from the element stresses according to

$$(f^e)^T = \int \mathbf{B}^T \boldsymbol{\sigma}^r d\Omega \quad [3.43]$$

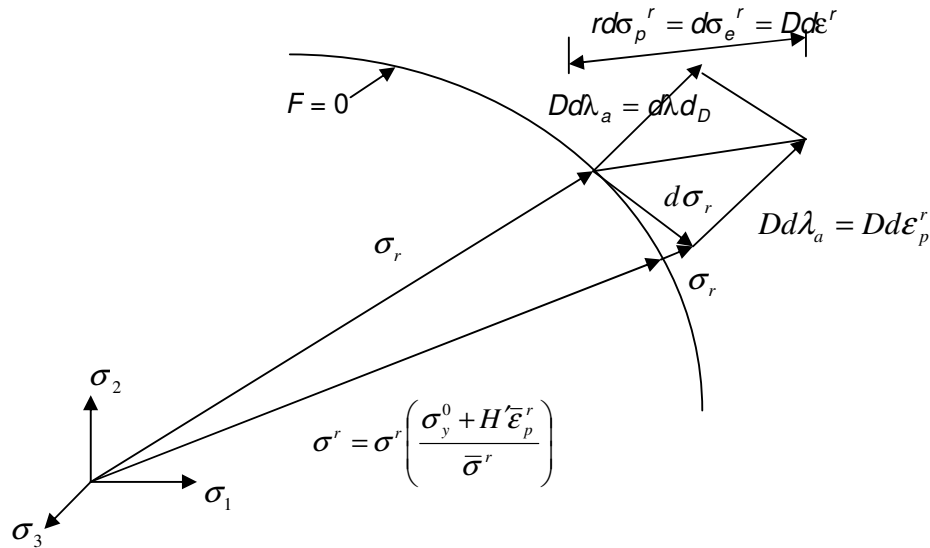


Fig. 3.5: Incremental stress changes in an already yielded point in an elasto-plastic continuum

usually found negligible in the analysis of concrete structures, much attention is being paid to the modeling of cracked concrete (Hinton and Owen, 1984) rather. In the analysis of reinforced concrete structures, the formation of cracks and their orientations play an important role. The methods of incorporating cracking mode of failure include the plasticity-based plastic fracture model (Bazant and Oh, 1983) and the simple tension cut-off model (Chen, 1982). The simple tension cut-off model is the most popular one and the basis for a cut -off may be strength, maximum strain, or energy. In most methods of analysis, a crack is formed when the major principal stress in the concrete exceeds the tensile strength assumed for the concrete. The crack direction is taken to be perpendicular to the direction of the major principal stress. In a finite element procedure, there are two distinct ways of representing cracks and are briefly discussed below.

3.5.1 Discrete crack modeling

This discrete crack model (Fig. 3.8) pioneered by Ngo and Scordelis (1967) represents cracks as inter-element discontinuities. Initially, this was implemented by letting a crack grow when the nodal force at the node ahead of the crack tip exceeded a tensile strength criterion. Then, the node is split into two nodes and the tip of the crack is assumed to propagate to the next node. When the tensile strength criterion is violated at this node, it is split and the procedure is repeated. This physically appealing representation of cracks has computational difficulties in that it requires node renumbering and there is restriction on the crack propagation direction depending on the mesh layout. Though this difficulty is tackled to certain extent through the use of automatic re-meshing, the continuous change in topology is inherent in the discrete crack approach and hence not being used in many finite element codes.

3.5.2 Smeared crack modeling

The alternative smeared crack approach (Fig 3.9), developed on the basis of equivalent theory of continuum mechanics, introduced by Rashid (1968), represents cracks as a change in the material property of the element over which the cracks are assumed to be smeared. It starts from the notion of stress and strain and permits a description in terms of stress-strain relations. It is sufficient to switch from the initial isotropic stress-strain law to an orthotropic law upon crack initiation.

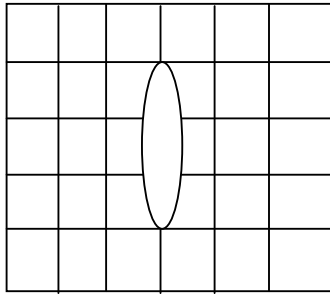


Fig. 3.8: Discrete crack approach

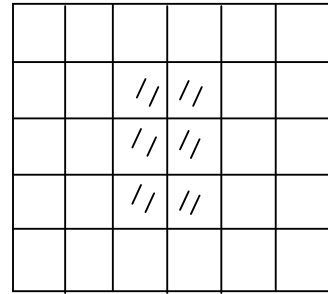


Fig. 3.9: Smeared crack approach

The procedure is attractive not only because it preserves the topology of the original finite element mesh, but also because it does not impose restrictions with respect to the orientation of the crack planes, i.e. the axes of orthotropy. Besides allowing any orientation of crack propagation direction, this procedure fits the finite element computation scheme well in the sense that smeared crack approach of modeling the cracking behavior of concrete is more straightforward than that of the discrete crack model. In the smeared crack approach, the stresses and strains of concrete and steel are evaluated by average or smeared values crossing several cracks. Though smeared crack approach cannot resolve individual crack numerically, it captures the overall response accurately. Sometimes, smeared crack approach seems to suffer from stress-locking in the vicinity of dominant discrete cracks; however, the difficulty can be easily overcome by assuming zero shear retention factor (β). In the context of the smeared crack model, two different representations of cracks, (i) the fixed smeared crack model, and (ii) the rotating smeared crack model, have emerged.

Fixed smeared crack model

In the fixed crack model proposed by Rashid (1968), a crack is formed perpendicular to the principal tensile stress direction when the principal stress exceeds the concrete tensile strength and the crack orientation does not change during subsequent loading and analysis. In some cases, a crack may close, and a new or secondary crack may be formed, but with restrictions relative to the initial crack direction. The ease of formulation and implementation of this model has led to its wide-spread used in early studies (Hand et al. 1973; Lin and Scordelis, 1975). Subsequent studies, however, showed that the model is associated with numerical problems caused by the singularity of the material stiffness matrix. Moreover, the crack pattern predicted by the finite element analysis using fixed

crack approach often shows considerable deviations from that observed in experiments (Jain and Kennedy, 1974). Furthermore, fixed crack model produces a stiffer response and hence overestimates the ultimate load.

The problem of the fixed crack model can be overcome by introducing a cracked shear modulus, which eliminates most numerical difficulties of the model and considerably improves the accuracy of the crack pattern predictions. It was also observed that results do not seem to be very sensitive to the value of the cracked shear modulus (Vebo and Ghali, 1977), as long as a value which is greater than zero is used, so as to eliminate the singularity of the material stiffness matrix and the associated numerical instability. Recent models use a variable cracked shear modulus to represent the change in shear stiffness, as the principal stresses in the concrete vary from tension to compression (Balakrishnan and Murray, 1988; Cervenka et al. 1990).

Rotating smeared crack approach

In the rotating crack model proposed by Cope et al. (1980), the crack direction is not fixed during the subsequent load history. Several tests by Vecchio and Collins (1982) have shown that the crack orientation changes with loading history and that the response of the specimen depends on the current crack direction rather than the original crack direction. The term “rotating crack” may also be taken in the abstract sense of the rotation of the anisotropy of the constitutive behavior. In the rotating crack model, the constitutive behavior of the complete load path may be reduced to a scalar relation with respect to the major principal stress. Due to the fact that the orientation of planes of degradation is aligned to the principal stress directions, only normal stresses occur on the crack surfaces, and the fictitious crack experiences pure Mode I (only tension). Therefore, no additional hypotheses are necessary to characterize the shear behavior. This model has been successfully used in analytical studies of RC structures whose purpose is to study the global structural behavior, rather than the local effects in the vicinity of a crack (Adeghe and Collins, 1986).

Indeed, smeared crack analyses are known to exhibit quite a number of cracks that unload, even close and sometimes reopen again in a later stage of the loading process (de Borst and Nauta, 1985). The unloading and reloading phenomena have been modeled using a secant approach, which implies that upon unloading the stress follows a straight

line back to the origin (Rots and de Borst, 1987). Nevertheless, a disadvantage of smeared crack approach is the difficulty in correlating the analytical results with experimental fracture mechanics research, which is at odds with the rotating crack concept (Kwak and Filippou, 1990). Hence, the present analytical study adopts only fixed smeared crack approach.

3.5.3 Tension stiffening in reinforced concrete

For the rational and accurate analysis of concrete structures, it is often important to include post-cracking resistance of concrete. When loaded in tension, plain concrete exhibits softening behavior after attaining the peak stress and is often referred to as tensile softening. As cracks start to develop in plain concrete, the energy stored in the concrete eventually gets converted to fracture energy. This fractured energy increases the cracks and causes the concrete to soften at relatively high rates. On the other hand, the existence of reinforcement in the concrete stiffens and engages the concrete between the cracks through local bond stress transfer associated with local bond-slip. Essentially, the tensile softening response is relatively improved due to the presence of reinforcement and some kind of stiffening effect takes place. This stiffening effect on the softening response is known as tension stiffening effect (Vecchio and Collins, 1986). This stiffening effect of post-cracking tensile stresses in the concrete between cracks has been recognized for quite some time. Neglecting the contribution of this tension stiffening can cause a significant overestimation of post-cracking deformation in reinforced concrete structures (Hsu and Zhang, 1996). Since the tension stiffening is caused due to interaction between concrete and steel, its characteristics depend on the crack spacing, reinforcement ratio, and interface bond transfer mechanism between concrete and steel (Balakrishnan and Murray, 1988).

The modeling of tension stiffening can be undertaken in one of the two ways: the first is to modify the stiffness of reinforcing bars; the second is to modify the concrete stiffness to carry the tension force after generation of cracks. Even though the first method seems to be beneficial to 1D problems, it has not been found satisfactory for 2D and 3D problems. The method, in which concrete stiffness gets modified, is assumed independent of the spacing of cracks, direction of reinforcing bars and reinforcement ratio. Hence the distribution of propagating cracks is assumed.

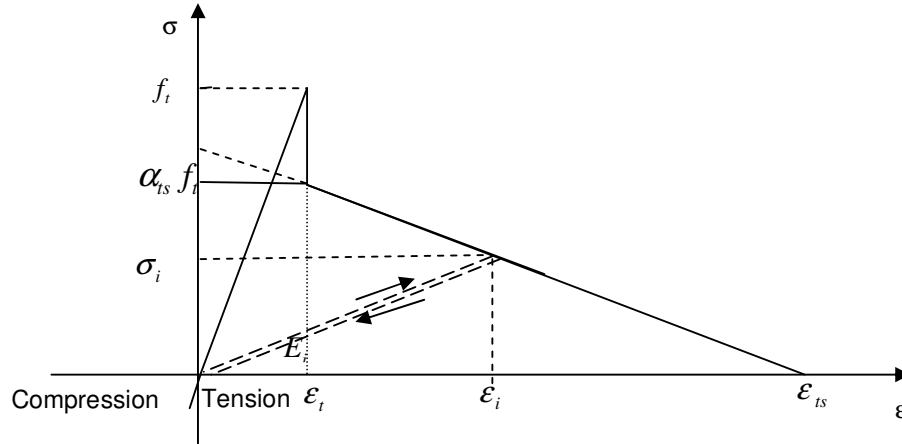


Fig. 3.10: Tension stiffening effect of cracked concrete

This is one of the reasons why this method has been considered most versatile in the analysis of cracked reinforced concrete. Many experimental investigations have been performed to simulate the tension stiffening effect (Lin and Scordelis, 1975; Gilbert and Warner, 1978). A gradual release of the concrete stress is adopted in this present study as shown in Fig. 3.10. The reduction in the tensile stress is given by the following expression

$$\sigma_i = \alpha_{ts} f_t \left(1 - \frac{\varepsilon_i}{\varepsilon_{ts}} \right); \quad \varepsilon_t \leq \varepsilon_i \leq \varepsilon_{ts} \quad [3.44]$$

Experimental studies on the tension stiffening behavior of concrete exhibit a large amount of scatter, and the stress-strain relationship for tension is not well defined (Daniel and Vecchio, 2004; Vecchio, 1999). Very few and scarce experimental data were available for the behavior of concrete under uni-axial tension (Gopalarathnam and Shah, 1985). The values of tension stiffening coefficients α_{ts} and ε_{ts} are generally taken to be 0.6 and 0.0020, respectively. It has also been reported that the influence of the tension stiffening on the response of the structures are generally small and hence the constant values are justified in the analysis (Hinton and Owen, 1984).

3.5.4 Shear transfer

It has been customary to consider the two constituents, concrete and steel reinforcement, as separate contributors to the overall stiffness and strength using the principle of superposition. It is normally assumed that full kinematic continuity between concrete and steel exists, at least at nodal points on element boundaries. Nevertheless, the two

materials are highly imbalanced in their behavior; Young's modulus for steel is one order higher than that of concrete, and unlike that for concrete, the stress-strain relation for steel is symmetric in tension and compression. This lack of material compatibility results in bond failure & sliding of reinforcement bars, and local deformations. Cracks in reinforced concrete are able to transmit large shear forces. Traditionally, this transfer has been neglected because of complexity and justified on the assumption that this would be a conservative simplification. Nevertheless, if a shear slip occurs along the crack, the crack will tend to dilate. If the crack dilatancy is prevented, forces normal to the crack faces will appear. These will have to be compensated by tensile forces on the reinforcement across the crack, increasing the potential for failure. Shear stresses can be transferred across the crack in three different ways: (i) by aggregate interlock as a result of the roughness of the crack faces, (ii) by dowel action or shear resistance of the reinforcement across the crack, and (iii) by the axial tensile force component in the reinforcement oblique to the plane of cracking. For members with low reinforcement and for small crack widths, aggregate interlock is the main mechanism of shear transfer. Tests carried out on beams without web reinforcement showed that aggregate interlock accounted for upto 75% of the shear transfer.

In the early attempts at modeling shear transfer in finite element methods, the shear stiffness of a cracked element was taken as $G_c = \beta G$ where G is the shear stiffness of the uncracked element and β is the shear stiffness reduction factor. This model does not reflect the decrease in shear transfer capability when the crack width increases. However, shear transfer eventually vanishes as the crack width approaches the aggregate size. The constant value of shear retention factor to model aggregate interlock has been considered as a coarse method by various researchers (Cedolin and Dei Poli 1977; Kolmar and Mehlhorn 1984). Even at large strains, the constant shear stress is being transmitted across the crack. In order to overcome this difficulty, β has been linked to the crack width and new expression has been suggested by Cedolin and Dei Poli as

$$G_c = G \left(1 - \frac{\varepsilon}{\varepsilon_c} \right) \text{ for } 0 < \varepsilon \leq \varepsilon_c ; G_c = 0 \text{ for } \varepsilon > \varepsilon_c \quad [3.45]$$

In the above equation, ε is the strain normal to the crack and ε_c is the value of ε after which there is no aggregate interlock.

3.5.5 Constitutive law of concrete

The constitutive law is defined for three cases (i) concrete in uncracked state, (ii) concrete cracked in one direction, and (iii) concrete cracked in two directions.

Concrete in uncracked state

The stress-strain relationship for uncracked concrete is given by

$$\begin{bmatrix} \sigma_1 \\ \sigma_2 \\ \tau_{12} \\ \tau_{13} \\ \tau_{23} \end{bmatrix} = \begin{bmatrix} D_1 & D_{12} & 0 & 0 & 0 \\ D_{12} & D_2 & 0 & 0 & 0 \\ 0 & 0 & D_3 & 0 & 0 \\ 0 & 0 & 0 & D_4 & 0 \\ 0 & 0 & 0 & 0 & D_5 \end{bmatrix} \begin{bmatrix} \varepsilon_1 \\ \varepsilon_2 \\ \gamma_{12} \\ \gamma_{13} \\ \gamma_{23} \end{bmatrix} \quad [3.46]$$

$$D_1 = \frac{E_1}{(1-\nu_{12}\nu_{21})} \quad D_3 = G_{12}$$

$$D_2 = \frac{E_2}{(1-\nu_{12}\nu_{21})} \quad D_4 = k_1 * G_{13}$$

$$D_{12} = \frac{E_2\nu_{12}}{(1-\nu_{12}\nu_{21})} \quad D_5 = k_2 * G_{23}$$

In the above equation, k_1 and k_2 are shear correction factors in the 1-3 (x-z) plane and 2-3 (y-z) planes respectively. For a homogeneous cross-section the shear correction factor is equal to 5/6;

Cracked in one direction

The stress-strain relationship for cracked concrete where cracking is assumed to take place in only one direction is given as

$$\begin{bmatrix} \sigma_1 \\ \sigma_2 \\ \tau_{12} \\ \tau_{13} \\ \tau_{23} \end{bmatrix} = \begin{bmatrix} 0 & 0 & 0 & 0 & 0 \\ 0 & E & 0 & 0 & 0 \\ 0 & 0 & G_{12}^c & 0 & 0 \\ 0 & 0 & 0 & G_{13}^c & 0 \\ 0 & 0 & 0 & 0 & G_{23} \end{bmatrix} \begin{bmatrix} \varepsilon_1 \\ \varepsilon_2 \\ \gamma_{12} \\ \gamma_{13} \\ \gamma_{23} \end{bmatrix} \quad \begin{aligned} G_{12}^c &= 0.25 \times G \left(1 - \frac{1}{0.004}\right) \text{ if } \varepsilon_1 < 0.004 \\ G_{12}^c &= 0 \text{ if } \varepsilon_1 \geq 0.004 \\ G_{13}^c &= G_{12}^c; G_{23} = \frac{5G}{6} \end{aligned} \quad [3.47]$$

Cracked in two directions

The stress-strain relationship for cracked concrete where cracking is assumed to take place in both directions is given as

$$\begin{bmatrix} \sigma_1 \\ \sigma_2 \\ \tau_{12} \\ \tau_{13} \\ \tau_{23} \end{bmatrix} = \begin{bmatrix} 0 & 0 & 0 & 0 & 0 \\ 0 & 0 & 0 & 0 & 0 \\ 0 & 0 & G_{12}^c/2 & 0 & 0 \\ 0 & 0 & 0 & G_{13}^c & 0 \\ 0 & 0 & 0 & 0 & G_{23}^c \end{bmatrix} \begin{bmatrix} \varepsilon_1 \\ \varepsilon_2 \\ \gamma_{12} \\ \gamma_{13} \\ \gamma_{23} \end{bmatrix} \quad \begin{aligned} G_{13}^c &= 0.25 \times G \left(1 - \frac{\varepsilon_1}{0.004} \right) \text{ if } \varepsilon_1 < 0.004 \\ G_{13}^c &= 0 \text{ if } \varepsilon_1 \geq 0.004 \\ G_{23}^c &= 0.25 \times G \left(1 - \frac{\varepsilon_2}{0.004} \right) \\ G_{12}^c &= 0.5 \times G_{13}^c \text{ if } G_{23}^c < G_{13}^c \end{aligned} \quad [3.48]$$

It has also been mentioned by Hinton and Owen (1984) that the tensile strength of concrete is a relatively small and unreliable quantity which is not highly influential to the response of structures. In the above stress-strain relationship, the cracked shear modulus (G^c) is assumed to be a function of the current tensile strain. In the above equation, G is the un-cracked concrete shear modulus. If the crack closes, the un-cracked shear modulus G is assumed in the corresponding direction. Even after the formation of initial cracks, the structure can often deform further without further collapse. In addition to the formation of new cracks, there may be a possibility of crack closing and opening of the existing cracks. If the normal strain across the existing crack becomes greater than that just prior to crack formation, the crack is said to have opened again; otherwise it is assumed to be closed. Nevertheless, if all cracks are closed, then the material is assumed to have gained the status equivalent to that of non-cracked concrete with linear elastic behavior.

3.6 Modeling of Steel Reinforcement

Reinforcing bars in structural concrete are generally assumed to be one-dimensional elements without transverse shear stiffness or flexural rigidity. The reinforcing bar can generally be treated as either discrete or smeared. The major advantage of discrete representation of reinforcing bar is existence of one-to-one correspondence between the real structure and model. In the smeared reinforcement, the average stress-strain relationship is calculated for an element area and incorporated directly as part of the overall concrete element stiffness matrix. In the present investigation, the smeared layered approach is adopted for simplicity. The bi-linear stress strain curve with linear elastic and strain hardening region is adopted in this study as shown in Fig. 3.11.

Typically, the hardening strain modulus is assumed to be 10% of initial elasticity modulus. The direction of steel (horizontal or vertical) can be set up by defining the angle with respect to local x-axis. There can only be two states of stress for the reinforcing bar, namely, elastic and linear strain hardening.

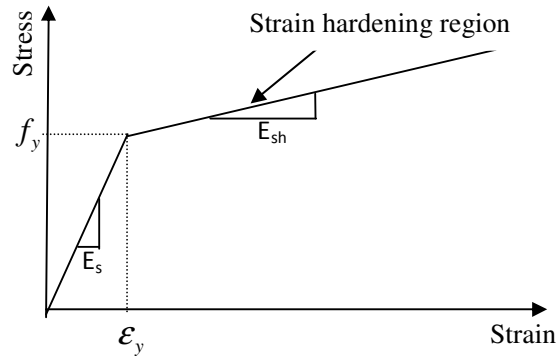


Fig. 3.11: Stress-strain curve for steel

3.7 Summary

In this chapter, the material modeling of reinforced concrete is broadly described. The experimental behavior of concrete under uni-axial, bi-axial, tri-axial and cyclic loading conditions is discussed. The various failure models developed on the basis of plasticity theory along with the characteristics of failure surface are also emphasized in this chapter. The formulation of five parameter failure model proposed by Willam-Warnke to define the yield criteria of concrete in compression is also described. The complete process of elasto-plastic analysis of RC structures is outlined including the hardening rule and flow rule. The step-by-step procedure of incremental theory of plasticity is discussed. The modeling of concrete in tension with emphasis of tension stiffening effect is also elaborated. In the end, the modeling of steel reinforcement is briefly discussed in the chapter.

References:

1. Adeghe, L.N. and Collins, M.P. (1986). "A finite element model for studying reinforced concrete detailing problems". *Publication No. 86-12*, Department of Civil Engineering, University of Toronto.
2. Ansari, F. (1987). "Stress-strain response of micro-cracked concrete in direct tension." *ACI Materials Journal*, 84(6), 481-490.
3. Balakrishnan S., and Murray D.W. (1988). "Concrete constitutive model for NLFE analysis of structures." *ASCE Journal of Structural Engineering*, 114(7), 1449-1466.
4. Bazant, Z.P., and Oh, B.H. (1983). "Crack band theory for fracture of concrete." *Materials and Structures*, RILEM, Paris, 155-176.
5. Borst, R. de., and Nauta, P. (1985). "Non-orthogonal cracks in a smeared finite element model." *Engineering Computations*, 2(1), 35-46.
6. Brestler, B., and Pister. (1958). "Behavior of concrete under triaxial compressive-compressive-tensile stresses." *ACI Materials Journal*, 8(2), 181-185.
7. Carreira, D.J., and Chu, K.H. (1985). "Stress-strain relationship for plain concrete in compression." *Proceedings of ACI Journal*, 82(6), 797-804.
8. Cedolin, L., and dei Poli, S. (1977). "Finite element studies of shear-critical R/C beams." *ASCE Journal of Engineering Mechanics Division*, 103(3), 395-410.
9. Cedolin, L., and Mulas, M.G. (1984). "Biaxial stress-strain relation for concrete." *ASCE Journal of Engineering Mechanics Division*, 110(2), 187-206.
10. Cervenka, V., Pukl, R., and Eligehausen, R. (1990). "Computer simulation of anchoring technique in reinforced concrete beams", *Proceedings of International Conference on Computer Aided Analysis and Design of Concrete Structures*, Part I, N. Bicanic et al., Ed., Pineridge Press, Swansea, Wales, 1-21.
11. Chen, A.C.T., and Chen, W.F. (1975). "Constitutive relations for concrete", *ASCE Journal of Engineering Mechanics Division*, 101(4), 465-481.
12. Chen, W.F. (1982). "*Plasticity in reinforced concrete.*" McGraw Hill, New York, USA.
13. Cope, R.J., Rao, P.V., Clark, L.A., and Norris, P. (1980). "*Numerical methods for non-linear problems.*" Pineridge press, Swansea, UK.
14. Daniel, P., and Vecchio F.J. (2004). "Compression field modeling of reinforced concrete subjected to reversed loading." *ACI Structural Journal*, 2004, 101(2), 155-164.

15. Darwin, D., and Pecknold, D.A. (1977). "Nonlinear biaxial stress-strain law for concrete." *ASCE Journal of Engineering Mechanics Division*, 103(2), 229-241.
16. Fan, S.C., and Wang, F. (2002). "A new strength criterion for concrete." *ACI Structural Journal*, 99(3), 317-326.
17. Fardis, M.N., Alibe, B., and Tasoulas, J.L. (1983). "Monotonic and cyclic constitutive law for concrete." *ASCE, Journal of Engineering Mechanics Division*, 109(2), 516-536.
18. Gardner, N.J. (1969). "Triaxial behavior of concrete." *Proceedings of ACI Journal*, 66(2), 136-146.
19. Gilbert, R.L., and Warner, R.F. (1978). "Tension stiffening in reinforced concrete slabs." *ASCE Journal of Structural Division*, 104(12), 1885-1900.
20. Gopalathnam, V.S., and Shah, S.P. (1985). "Softening response of plain concrete in direct tension." *ACI Structural Journal*, 82(2), 310-323.
21. Han D.J. and Chen W.F. (1987). "Constitutive modeling in analysis of concrete structures." *ASCE Journal of Engineering Mechanics Division*, 113(4), 577-593.
22. Hand, F.R., Pecknold, D.A., and Schnobrich, W.C. (1973). "Nonlinear layered analysis of RC plates and shells." *ASCE Journal of Structural Division*, 99(7), 1491-1505.
23. Hinton, E., and Owen, D.R.J. (1984). "*Finite Element Software for Plates and Shells*." Pineridge Press, UK.
24. Hognestad, E., Hansen, N.W., and McHenry, D. (1955). "Concrete stress distribution in ultimate strength design." *ACI Journal*, 52(4), 455-480.
25. Hughes, B.P., and Chapman, G.P. (1966). "The complete stress-strain curve for concrete in direct tension." *RILEM Bulletin*, 30, 95-97.
26. Hussein, A., and Marzouk, H. (2000). "Behavior of high-strength concrete under biaxial stresses." *ACI Materials Journal*, 97(1), 27-36.
27. Hsu, T.T.C., and Zhang, L.X. (1996). "Tension stiffening in reinforced concrete membrane elements." *American Concrete Institute Structural Journal*, 93(1), 108-115.
28. Imran I. and Pantazopoulou S.J. (2001). "Plasticity model for concrete under triaxial compression." *ASCE Journal of Engineering Mechanics Division*, 127(3), 281-290.
29. Jain, S.C., and Kennedy, J.B. (1974). "Yield criterion for reinforced concrete slabs." *ASCE Journal of Structural Division*, 100(3), 631-644.
30. Karsan, I.D., and Jisra, J.O. (1969). "Behavior of concrete under compressive loadings." *ASCE, Journal of Structural Division*, 95(12), 2543-2563.

31. Kolmar, W., and Mehlhorn, G. (1984). "Comparison of shear stiffness formulations for cracked reinforced concrete elements." *Proceedings of International Conference on Computer Aided Analysis and Design of Concrete Structures*, F. Damjanic et al., eds., Part 1, Pineridge Press, Swansea, 133-147.
32. Kotsovos M.D., and Newman J.B. (1977). "Behavior of concrete under Multiaxial Stress." *Proceedings of ACI Journal*, 74(9), 443-446.
33. Kupfer, H., and Gerstle (1973). "Behavior of concrete under biaxial stresses." *ASCE Journal of Engineering Mechanics Division*, 99(4), 853-866.
34. Kupfer, H., Hilsdorf, H.K., and Rusch, H. (1969). "Behavior of concrete under biaxial stresses." *Proceedings of ACI Journal*, 66(8), 656-666.
35. Kwak, H.G., and Filippou, F.P. (1990). "Finite element analysis of reinforced concrete structures under monotonic loads." Report No. *UCB/SEMM-90/14, Earthquake Engineering Research Centre, University of California, Berkeley*.
36. Lan, S., and Guo, Z. (1999). "Biaxial compression behavior of concrete under repeated loading." *ASCE Journal of Materials in Civil Engineering*, 105(11), 105-115.
37. Lin, C.S., and Scordelis, A.C. (1975). "Nonlinear analysis of RC shells of general form." *ASCE Journal of Structural Division*, 101(3), 523-538.
38. Linhua, J., Dahai, H., and Nianxiang, X. (1991). "Behavior of concrete under triaxial compressive-compressive tensile stresses." *ACI Materials Journal*, 88(2), 181-185.
39. Liu, T.C.Y., Nilson, A.H. and Slate, S.F.O. (1972). "Stress-strain response and fracture of a concrete in uniaxial and biaxial compression." *Proceedings of ACI Journal*, 69(5), 291-295.
40. Ngo, D., and Scordelis, A.C. (1967). "Finite element analysis of reinforced concrete beams." *ACI Journal*, 64(3), 152-163.
41. Mills, L.L., and Zimmerman, R.M. (1970). "Compressive strength of plain concrete under multiaxial loading conditions." *Proceedings of ACI Journal*, 67(10), 802-807.
42. Mlakar, P.F., Vitaya-Udom, K.P., and Cole, R.A. (1985). "Dynamic tensile-compressive behavior of concrete." *ACI Journal*, 86(5), 484-491.
43. Nayak, G.C., and Zienkiewicz, O.C. (1972). "Elasto-plastic stress analysis." *International Journal of Numerical Methods in Engineering*, 5(1), 113-135.
44. Rashid, Y.R. (1968). "Analysis of prestressed concrete pressure vessels." *Nuclear Engineering and redesign*, 7(4), 334-344.
45. Rots, J.G., Borst, R. de. (1987). "Analysis of mixed-mode fracture in concrete." *ASCE Journal of Engineering Mechanics*, 113(11), 1739-1956.

46. Sfer, D., Carol, I., Gettu, R. and Etse, G. (2002). "Study of the behavior of concrete under triaxial compression." *ASCE Journal of Engineering Mechanics*, 128(2), 156-163.
47. Smith, S.S., Willam, K.J., Gerstle, K.H., and Sture, S. (1989). "Concrete over the top, or Is there life after peak." *ACI Materials Journal*, 86(5), 491-497.
48. Sinha, B.P., Gerstle, K.H., and Tulin, L.G. (1964). "Stress-strain relations for concrete under cyclic loading." *Proceedings of ACI Journal*, 61(2), 195-212.
49. Tasuji, M.E., Slate, F.O., and Nilson, A.H. (1978). "Stress-strain response and fracture of concrete in biaxial loading." *Proceedings of ACI Journal*, 75(7), 306-312.
50. Tsai, W.T. (1988). "Uniaxial compressional stress-strain relation of concrete." *ASCE Journal of Structural Division*, 114(9), 2133-2166.
51. Vebo, A., and A. Ghali. (1977). "Moment-curvature relation of reinforced concrete slabs." *ASCE Journal of Structural Engineering*, 103(3), 515-531.
52. Vecchio F.J. (1999). "Towards cyclic load modeling of reinforced concrete." *ACI Structural Journal*, 96(2), 132-202.
53. Vecchio, F., and Collins, M.P. (1982). "The response of reinforced concrete to in-plane shear and normal stress." *Publication No. 82-03, Department of Civil Engineering, University of Toronto, Toronto, Canada.*
54. Vecchio, F.J., and Collins, M.P. (1986). "The modified compression field theory for reinforced concrete elements subjected to shear." *ACI Journal*, 82(2), 219-231.
55. Willam, K., and Warnke, E. (1974). "Constitutive model for triaxial behavior of concrete." *Proceedings of the International Association for Bridge and Structural Engineering*, 19, Zurich, Switzerland, 1-30.
56. Yu, M.H. (2002). "Advances in strength theories for materials under complex stress state in the 20th century." *ASME Applied Mechanics Reviews*, 55(3), 169-218.
57. Yu, M.H. (2004). "*Unified strength theory and its applications.*" Springer, Berlin, Germany.
58. Zhi, W.C., Hai, G.Z. and Qin, Z.X. (1987). "Experimental investigation of biaxial and triaxial compressive concrete strength." *ACI Materials Journal*, 84(2), 92-100.

Finite Element Analysis of RC Structures: Programming & Validation

4.1 Background

The experimental results are generally considered highly accurate and reliable since they replicate the real behavior of the tested structure. It is a well known fact that the experimental testing of structures, if not impossible, is time consuming as well as costly and, therefore, it is desirable to rely on numerically simulated models which can substitute the experimental investigation in a fairly accurate manner. Finite Element Method (FEM) is a firmly well established good choice for the numerical simulation of complex structures which is increasingly used for investigating the behavior of complex structures and their designing (Meyer et al. 1985). One of the principal advantages of the FEM is the unifying approach which it offers the solution to a wide variety of engineering problems. The finite element method heavily relies on the physical interpretation in which the structure is assumed to be composed of non-overlapping regions known as elements over which the main variables are interpolated. These elements are connected at a discrete number of points along their periphery known as nodal points. The finite element method gives an approximate solution with an accuracy that depends mainly on the type of element and the fineness of the finite element mesh. In general there are several approaches to formulate the finite element problem namely, (i) Direct formulation, (ii) The minimum total potential energy formulation, and (iii) weighted residual formulations. It is important to note that the basic steps involved in the analysis using the above methods are similar. In general, the engineering problems that can be analyzed using FEM, can be classified into three categories: (i) equilibrium problems, (ii) Eigen value problems, and (iii) propagation problems. *Equilibrium problems* are the problems in which the response of the system does not vary with time, a classic example being the stress analysis of linear elastic systems. *Eigen value problems* are extensions of equilibrium problems in which specific or critical values of certain parameters are ascertained. The stability of structures and determination of the natural

frequencies of linear elastic systems are typical examples of such problems. *Propagation problems* include problems associated with the time-dependent phenomena. The dynamic transient analysis of shear wall, a present study, is a classic example of propagation problems.

Reinforced concrete shows very complex behavior primarily due to material inelasticity, concrete cracking as well as due to interactions between cracked concrete and steel. The linear behavior of reinforced concrete structures is usually ceased even at service loads mainly due to cracking and the non-linearity becomes noticeable at higher loads due to subsequent yielding of concrete and steel. With the advent of computers it is now possible to carryout the non-linear behavior of RC structures simulating such non-linear behavior. Nonlinear finite element method is a unique tool for the analysis of reinforced concrete structures to include their deformational characteristics not only at service load conditions but near the failure stage also. The first application of FEM to analyze the RC structures dates back to late 1960s (Ngo and Scordelis, 1967). Since then rapid and great advances have been made to simulate the concrete behavior more precisely.

In order to simulate the complex behavior of concrete, several commercial packages have been developed. These softwares provide good graphical representation of the results, however, the main drawbacks of these softwares are that they require huge input data and produce voluminous output data since they have been developed for general use. Moreover, the user cannot incorporate the recent developments in the material modeling and the user has to wait for the updated version of software. On the other hand, perhaps the biggest benefit of the developed computer programs is that they provide the full technical understanding to the developer/user and the input and output data may be customized in the desired format. Several computer programs have been developed in the past for the analysis of RC structures. Hinton and Owen (1984) developed a computer program in FORTRAN to the study the elasto-plastic behavior RC structures subjected to static loads. Huang (1989) modified this program to incorporate the dynamic analysis. These programs were developed primarily for the analysis of RC structures on no-crack basis using the Owen-Figurius yield/failure criterion. In the present study the Hinton-Owen-Huang program has been modified to incorporate the concrete cracking and the state of the art in yield/failure criterion to model the concrete in compression. To this end, several subroutines have been incorporated and modified to fulfill the above requirement.

The non-linear finite element programming essentially consists of two major steps, viz. material modeling and geometrical modeling. The material modeling of concrete and steel has already been discussed in detail in Chapter three of the thesis. On the other hand, the geometric modeling deals with the identification of suitable finite element to model the structure to be analyzed. Since the present investigation deals with the response analysis of shear walls with and without openings subjected to static and dynamic loading conditions, the use of shell element has been found to be best suited to model the geometry of shear wall with moderate thickness. In the present study, the layered degenerated shell element with assumed strain approach has been adopted to discretize the shear wall. The assumed strain based degenerated shell element is capable of analyzing thin as well as moderately thick shear wall structures. In order to perform the time-history analysis of shear wall, different methods have evolved over the years. It is well documented in the literature that non-linear implicit direct integration time history analysis is more accurate and predicts the results closer to the experimental results. In the present study the Newmark-Beta method (Trapezoidal rule) of direct implicit time integration has been used to perform the time-history analysis of shear wall. In this study a code has been developed to perform the **Non-Linear Dynamic Analysis of Shear wall** and hereafter referred as NLDAS. The code NLDAS has been validated against the standard benchmark problems available in the literature.

4.2 Finite Element Selection

The choice of selecting suitable element to model a particular geometry is very crucial in attaining the desired results. Several finite elements have been developed so far and they are categorized on the basis of its dimensionality as well as its behavior. Bar and beam elements are considered 1-D elements. These elements are typically used to model the truss structures and the steel reinforcement in a RC structure. On the other hand, the beam element is primarily being used to model deflection and rotation of the beam. Except for the above cases, it is difficult to use 1-D elements for many practical problems. The 2-D elements such as Constant Strain Triangular (CST) element, Linear Strain Triangular (LST) element as well as rectangular elements (MacLeod 1969) are being used to model the structure with regular geometry. On the other hand, 3-D elements such as brick elements and solid elements are used to model the thick structures. However, analyst generally prefers the use of 2-D elements because of less

computational demand. Nevertheless, the structural problems may involve complex geometry, which may not be represented by simple elements such as triangular or rectangular elements. Since there is no single element which is universally best suited to model all geometry, the careful selection of element depending on the type of problem at hand is mandatory keeping in view the accuracy as well as the computational demand. In general, it is strongly believed that the elements must be allowed to take the general shapes in order to model the irregular geometry especially near openings.

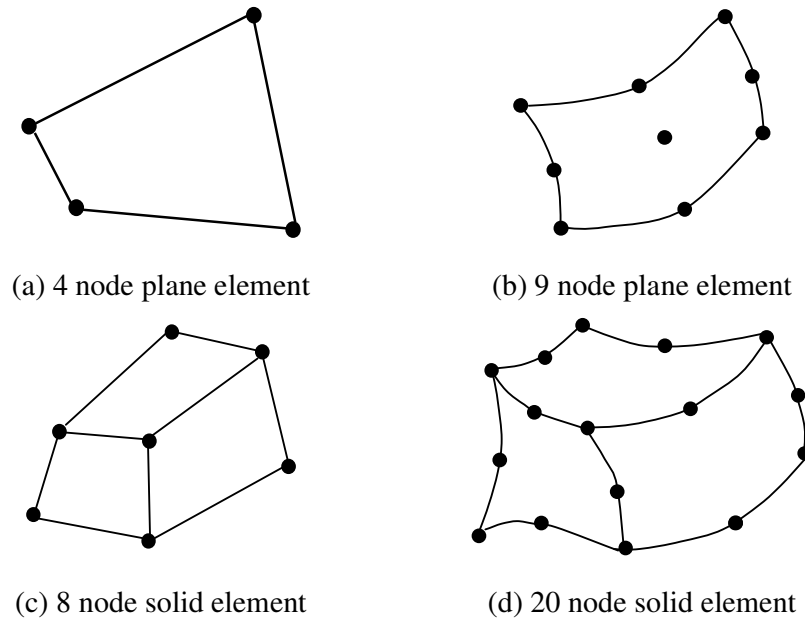


Fig. 4.1: Isoparametric class of finite elements

In sequel to that, more generic finite elements came into picture in the recent years and have revolutionized the element technology to a greater level. Iso-parametric elements are the class of elements, which are more arbitrary in shape (Fig. 4.1) and thus can effectively be used to model the curved geometry of the structure (Zienkiewicz et al. 2013). The concept of iso-parametric element is based on the transformation of the parent element from local or natural coordinate system to an arbitrary shape in Global coordinate system. The iso-parametric elements are widely used in many structural applications related to plates and shells. In the iso-parametric elements the variation of displacements and geometry within the element are defined using the similar shape functions.

The modeling of the shear wall geometry has been the subject of great interest over the past few decades. In the past, shear walls were modeled using beam elements or by plane stress elements. Nevertheless, the performances were not found to be good enough due to the poor convergence. On the other hand, shell elements are being used predominantly in modeling the shear wall geometry and resulted in a better performance. The use of shell element to model moderately thick structures like shear wall is well documented in the literature (Dvorkin and Bathe, 1984). A complete survey on the use of shell elements has been found in the literature (Yang et al. 2000).

4.3 Evolution of Shell Elements

In order to develop a simple, efficient and versatile shell element, several shell elements have been developed over the years and most of them can be put into three distinct classes namely flat elements, curved shell elements based on classical theories, and the degenerated shell elements (Liu and Teng, 2008) according to the basic mathematical principles involved and are explained below.

4.3.1 Curved shell elements

Curved elements based on exact or approximate shapes of shells began to appear in the late 1960s. In this approach, the actual surface is replaced by an assemblage of curved elements formulated on the basis of classical shell theories. The range of application of these elements is limited since the shell element formulation is dependent on the shell theory employed as well as on the geometrical description of shell surface. Gallagher (1969) observed that there are many difficulties in selecting a particular shell theory for a particular problem. Moreover, he observed that the many classical shell theory based finite element formulation are complex in terms of satisfying the continuity of displacements as well as in representing the rigid body modes.

4.3.2 Flat shell elements

In order to avoid the complex formulation of shell elements based on classical shell theory, the actual surface of the shell is replaced by an assemblage of flat faceted plate elements which are either triangular or quadrilateral in shape. Due to the simplicity of the formulation and easier implementation, the flat elements became more popular for the analysis of shell structures. The flat element matrices are constructed by adding plane

stress and plate bending element matrices. Assembly of these elements gives a geometry which only approximates the actual shell surface. This approach has been successfully applied for cylindrical shells by Hrennikoff (1966) and for general shells by Zienkiewicz and Cheung (1967). However, the difficulties and the shortcomings of the flat plate element used for the analysis of shells have been pointed out by Gallagher (1969) as mentioned below.

- The behavior of the shells as represented by the differential equations is not approached in the limit of refinement of flat plate approximation.
- The discontinuities of slope between adjacent plate elements may produce bending moments in the region of shells where they do not exist.
- The coupling of membrane and bending effects due to curvature of the shell is absent in the interior of the individual elements and consequently a large number of elements must be used to achieve satisfying accuracy.

Moreover, he mentioned the requirements which should be met in the development of a reliable and effective shell finite element as follows:

- The element should satisfy the usual isotropy and convergence requirements.
- The element should be formulated without the use of specific shell theory so that it is applicable to any plate/shell situation.
- The element should be simple and inexpensive to use with.
- The element should not be based on numerically adjusted factors.
- The element should be relatively insensitive to distortions.

4.3.3 Three-dimensional solid element for shell analysis

In this approach, the actual three-dimensional (3-D) continuum is replaced by an assemblage of 3-D solid elements such as 4-noded tetrahedron elements, 8-noded hexahedron or 20 noded curved solid elements. Nevertheless, in such discretization, more than one layer of elements may be needed across the thickness to simulate the bending behavior of shell. The use of this technique for shell analysis results in many degrees of freedom and results in the huge computational demand and makes them inefficient. Moreover, this approach for shell analysis is found unsatisfactory especially in case of thin shells wherein the strain normal to mid-surface is associated with very large stiffness coefficients and as a result the equations become ill-conditioned. In order

to circumvent the shortcomings of curved, flat and 3-D solid elements, the conversion of 3-D element into an equivalent 2-D element seemed to have gained momentum in the 1970s through the concept of degeneration.

4.3.4 Degenerated shell elements

The degenerated shell element is derived from 3-D continuum theory by introducing the assumption that the original normals to the shell mid-surface are inextensible and essentially straight after deformation. The use of degenerated solid elements for the analysis of structures has become more and more popular due to the fact that they are not based on any particular shell theory and are therefore more versatile when compared with the other shell elements. The degenerated shell elements can be easily used to analyze shell structures with non-uniform thickness or with anisotropic material properties as well as with more than one material layer such as in reinforced concrete shear walls where the steel mesh may be modeled as a steel layer of uniform thickness. In addition, the solution obtained by using degenerated shell elements can be considered to be more realistic and closer to the solution obtained by using the true 3-D continuum approach. By using the iso-parametric mapping technique, degenerated shell elements are more accurate than flat shell elements. The implementation of the degenerated shell elements is relatively easy due to the iso-parametric and displacement-based formulation.

The degenerated shell element is a C^0 shell element in which the assumed displacement function is continuous and need not satisfy the continuity of any derivatives and is the simplest class of finite elements. The nine noded Lagrangian displacement Interpolation has been used as a common type of degenerated shell elements. This element has been quite successful in modeling moderately thick structures because of their simplicity as well as in circumventing the use of classical shell theory. The popularity of these elements has grown enormously, as is obvious from the numerous publications devoted to them (Ahmad et al. 1970; Belytschko et al, 1985; Huang and Hinton 1986; Kant et al. 1994) and from their implementation in most of the available commercial finite element codes. The detailed description of the element and its mathematical formulation is discussed in the next section.

4.4 Formulation of Degenerated Shell Element

In this section, the underlying basic ideas in the formulation of the degenerated curved shell element are described. Two assumptions are made in the formulation of the curved shell element which is degenerated from three-dimensional solid. First, it is assumed that, even for thick shells, the normal to the middle surface of the element remains straight after deformation. Secondly, the strain energy corresponding to stresses perpendicular to the middle surface is disregarded, i.e. the stress component normal to the shell mid-surface is constrained to be zero. Five degrees of freedom are specified at each nodal point, corresponding to its three translations and two rotations of the normal at each node. The independent definition of the translational and rotational degrees of freedom permits the transverse shear deformation to be taken into account during the formulation of the element stiffness, since rotations are not necessarily normal to the slope of the mid-surface.

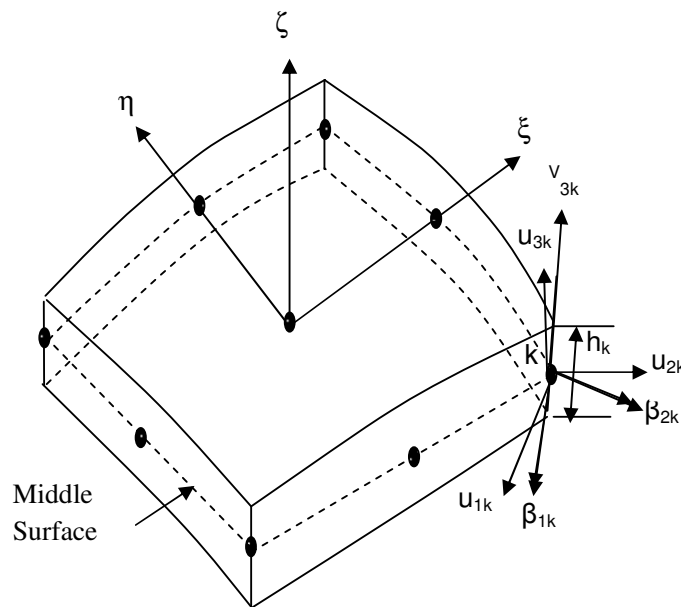


Fig. 4.2: Geometry of 9-noded degenerated shell element

Coordinate systems

The geometry of the shell can be represented by the coordinates and normal vectors of its middle surface as Fig. 4.2. The geometry of the degenerated shell element and kinematics of deformation are described by using four different coordinate systems, i.e. global, natural, local, and nodal coordinate systems. The global coordinate system

(x, y, z) is used to define the shell geometry. The shape functions are expressed in natural curvilinear coordinates (ξ, η, ζ) . In order to easily deal with the thin shell assumption of zero normal stress in the z -direction, the strain components are defined in terms of local coordinate set of axes (x', y', z') . At each node of shell element, the nodal coordinate set $\mathbf{V}_{1k}, \mathbf{V}_{2k}, \mathbf{V}_{3k}$ with unit vectors $(\bar{\mathbf{V}}_{1k}, \bar{\mathbf{V}}_{2k}, \bar{\mathbf{V}}_{3k})$ is defined. The four coordinate sets employed in the present formulation are now described.

Global coordinate set (x, y, z)

This is a Cartesian coordinate system, freely chosen, in relation to which the geometry of the structure is defined in space. Nodal coordinates and displacements, as well as the global stiffness matrix and applied force vector are referred to this system. The displacements corresponding to x, y, z directions are u, v, w , respectively.

Nodal coordinate Set $(\bar{\mathbf{V}}_{1k}, \bar{\mathbf{V}}_{2k}, \bar{\mathbf{V}}_{3k})$

A nodal coordinate system is defined at each nodal point with origin at the reference surface (mid-surface). The vector \mathbf{V}_{3k} is constructed from the nodal coordinates at top and bottom surfaces at node k and is expressed as

$$\begin{Bmatrix} V_{3k}^x \\ V_{3k}^y \\ V_{3k}^z \end{Bmatrix} = \begin{Bmatrix} x_{3k}^{top} - x_{3k}^{bot} \\ y_{3k}^{top} - y_{3k}^{bot} \\ z_{3k}^{top} - z_{3k}^{bot} \end{Bmatrix} \quad [4.1]$$

\mathbf{V}_{3k} defines the direction of the normal at any node ' k ', which is not necessarily perpendicular to the mid surface. The major advantage of the definition of \mathbf{V}_{3k} with normal not necessary to be perpendicular to mid surface is that, there are no gaps or overlaps along element boundaries.

The vector \mathbf{V}_{1k} is constructed perpendicular to \mathbf{V}_{3k} and parallel to the global x - z plane. Hence

$$\mathbf{V}_{ik} = \mathbf{j} \times (V_{3k}^x \mathbf{i} + V_{3k}^y \mathbf{j} + V_{3k}^z \mathbf{k}) \Rightarrow \mathbf{V}_{ik} = V_{3k}^z \mathbf{i} + 0\mathbf{j} - V_{3k}^x \mathbf{k} \Rightarrow V_{1k}^x = V_{3k}^z, V_{1k}^y = 0, V_{1k}^z = -V_{3k}^x \quad [4.2a]$$

However, if the vector \mathbf{V}_{3k} is in the y -direction, i.e. $(V_{3k}^x = V_{3k}^z = 0)$, the vector \mathbf{V}_{1k} is defined as:

$$\mathbf{V}_{ik} = \mathbf{i} \times (V_{3k}^x \mathbf{i} + V_{3k}^y \mathbf{j} + V_{3k}^z \mathbf{k}) \Rightarrow \mathbf{V}_{ik} = 0\mathbf{i} + V_{3k}^y \mathbf{j} - V_{3k}^z \mathbf{k} \Rightarrow V_{1k}^x = 0, V_{1k}^y = V_{3k}^y, V_{1k}^z = -V_{3k}^z \quad [4.2b]$$

The superscripts refer to the vector components in the global coordinate system.

The vector \mathbf{V}_{2k} is constructed perpendicular to the plane defined by \mathbf{V}_{1k} and \mathbf{V}_{3k} , i.e. $\mathbf{V}_{2k} = \mathbf{V}_{1k} \times \mathbf{V}_{3k}$. The unit vectors in the directions of \mathbf{V}_{1k} , \mathbf{V}_{2k} , \mathbf{V}_{3k} are represented by $\bar{\mathbf{V}}_{1k}$, $\bar{\mathbf{V}}_{2k}$, $\bar{\mathbf{V}}_{3k}$ respectively. The unit vectors $\bar{\mathbf{V}}_{1k}$ and $\bar{\mathbf{V}}_{2k}$ define the rotations of the β_{2k} and β_{1k} , respectively at node k .

Natural coordinate set (ξ, η, ζ)

In this coordinate system, ξ and η are the two curvilinear coordinates in the middle plane of the shell element and ζ is a linear coordinate in the thickness direction. It is assumed that ξ, η and ζ vary between -1 and +1 on the respective faces of the elements. It should also be noted that the ζ direction is only approximately perpendicular to the shell-surface, since ζ is defined as a function of $\bar{\mathbf{V}}_{3k}$.

Local coordinate set (x', y', z')

This is the Cartesian coordinate system defined at the sampling points wherein stresses and strains are to be calculated. The direction z' is taken perpendicular to the surface $\zeta = \text{constant}$, being obtained by the cross product of the tangential vectors in the ξ and η directions. The direction of x' can be taken along the tangent to the ξ direction at the sampling point and the direction y' is defined by the cross product of the z' and x' -directions.

$$z' = \begin{bmatrix} \frac{\partial x}{\partial \xi} \\ \frac{\partial y}{\partial \xi} \\ \frac{\partial z}{\partial \xi} \end{bmatrix} \times \begin{bmatrix} \frac{\partial x}{\partial \eta} \\ \frac{\partial y}{\partial \eta} \\ \frac{\partial z}{\partial \eta} \end{bmatrix} \quad x' = \begin{bmatrix} \frac{\partial x}{\partial \xi} \\ \frac{\partial y}{\partial \xi} \\ \frac{\partial z}{\partial \xi} \end{bmatrix} \quad y' = z' \times x' \quad [4.3]$$

The local coordinate system varies throughout the shell and it is used to define the direction cosine matrix which enables transformation between the local and global coordinate system. The transformation matrix is now defined as

$$\mathbf{T} = \begin{bmatrix} l_1 & l_2 & l_3 \\ m_1 & m_2 & m_3 \\ n_1 & n_2 & n_3 \end{bmatrix} \quad [4.4]$$

where l_i , m_i and n_i ($i = 1, 2, 3$) are the direction cosines of the unit vectors along the x' , y' and z' , respectively.

Element geometry

The global coordinates of pairs of points on the top and bottom surface at each node are usually input to define the element geometry. Alternatively, the mid-surface nodal coordinates and the corresponding directional thickness at each node can be furnished. In the iso-parametric formulation, the coordinates of a point within an element are obtained by interpolating the nodal coordinates through the element shape functions and are expressed as

$$\begin{Bmatrix} x \\ y \\ z \end{Bmatrix} = \underbrace{\sum_{k=1}^9 N_k(\xi, \eta) \begin{Bmatrix} x_k^{mid} \\ y_k^{mid} \\ z_k^{mid} \end{Bmatrix}}_{\text{mid-surface only}} + \underbrace{\sum_{k=1}^9 N_k(\xi, \eta) \frac{\zeta h_k}{2} \begin{Bmatrix} V_{3k}^x \\ V_{3k}^y \\ V_{3k}^z \end{Bmatrix}}_{\text{effect of shell thickness}} \quad (4.5)$$

where x_k^{mid} , y_k^{mid} and z_k^{mid} are the coordinates of the shell mid-surface and h_k is the shell thickness at node k. In the above expression $N_k(\xi, \eta)$ are the element shape functions at the point considered within the element (ξ, η) and ζ tells the position of the point in the thickness direction. The unit vector in the directions of \mathbf{V}_{3k} is represented by $\bar{\mathbf{V}}_{3k}$.

The element shape functions are calculated in the natural coordinate system as

$$\begin{aligned} N_1 &= \frac{1}{4} \xi(1+\xi)\eta(1+\eta); & N_2 &= \frac{1}{2} (1+\xi)(1-\xi)\eta(1+\eta); & N_3 &= -\frac{1}{4} (1-\xi)\eta(1+\eta); \\ N_4 &= -\frac{1}{2} \xi(1-\xi)(1+\eta)(1-\eta); & N_5 &= \frac{1}{4} (1-\xi)\eta(1-\eta); & N_6 &= -\frac{1}{2} (1+\xi)(1-\xi)\eta(1-\eta); \\ N_7 &= -\frac{1}{4} \xi(1+\xi)\eta(1-\eta); & N_8 &= \frac{1}{2} \xi(1+\xi)(1+\eta)(1-\eta); & N_9 &= (1+\xi)(1-\xi)(1+\eta)(1-\eta) \end{aligned} \quad [4.6]$$

Based on the two assumptions of the degeneration process previously described, the element displacement field can then be expressed by the five degrees of freedom at each node. The global displacements are determined from mid surface nodal displacements u_k^{mid} , v_k^{mid} and w_k^{mid} and the relative displacements are caused by the two rotations of the normal as

$$\begin{Bmatrix} u \\ v \\ w \end{Bmatrix} = \sum_{k=1}^9 N_k \begin{Bmatrix} u_k^{mid} \\ v_k^{mid} \\ w_k^{mid} \end{Bmatrix} + \sum_{k=1}^9 N_k \zeta \frac{h_k}{2} \begin{bmatrix} V_{1k}^x & -V_{2k}^x \\ V_{1k}^y & -V_{2k}^y \\ V_{1k}^z & -V_{2k}^z \end{bmatrix} \begin{bmatrix} \beta_{1k} \\ \beta_{2k} \end{bmatrix} \quad [4.7]$$

where β_{1k} and β_{2k} are the rotations of the normals which results in the relative displacements and V_{1k} and V_{2k} are the unit vectors defined at each node.

4.4.1 Strain displacement relationship

In order to easily deal with the thin shell assumption of zero stress in the z' direction ($\sigma'_z=0$), the strains need to be expressed in terms of local coordinate system $x' - y' - z'$ where z' is perpendicular to the material surface layer. For the small deformations, the in-plane and transverse shear strain components are defined as

$$\boldsymbol{\varepsilon}' = \begin{Bmatrix} \boldsymbol{\varepsilon}'_f \\ \boldsymbol{\varepsilon}'_s \end{Bmatrix} = \begin{Bmatrix} \boldsymbol{\varepsilon}_{x'} \\ \boldsymbol{\varepsilon}_{y'} \\ \boldsymbol{\gamma}_{xy'} \\ \boldsymbol{\gamma}_{xz'} \\ \boldsymbol{\gamma}_{yz'} \end{Bmatrix} = \begin{Bmatrix} \frac{\partial u'}{\partial x'} \\ \frac{\partial v'}{\partial y'} \\ \frac{\partial u'}{\partial y'} + \frac{\partial v'}{\partial x'} \\ \frac{\partial u'}{\partial z'} + \frac{\partial w'}{\partial x'} \\ \frac{\partial v'}{\partial z'} + \frac{\partial w'}{\partial y'} \end{Bmatrix} \quad [4.8]$$

In Eq. 4.8, $\boldsymbol{\varepsilon}'_f$ and $\boldsymbol{\varepsilon}'_s$ are the in-plane and transverse shear strains respectively and u', v', w' are the displacement components in the local coordinate system $x' - y' - z'$. The derivatives of u', v', w' in local coordinate system are obtained from the derivatives of displacements, u, v, w in global coordinate system as

$$\begin{bmatrix} \frac{\partial u'}{\partial x'} & \frac{\partial v'}{\partial x'} & \frac{\partial w'}{\partial x'} \\ \frac{\partial u'}{\partial y'} & \frac{\partial v'}{\partial y'} & \frac{\partial w'}{\partial y'} \\ \frac{\partial u'}{\partial z'} & \frac{\partial v'}{\partial z'} & \frac{\partial w'}{\partial z'} \end{bmatrix} = [\mathbf{T}]^T \begin{bmatrix} \frac{\partial u}{\partial x} & \frac{\partial v}{\partial x} & \frac{\partial w}{\partial x} \\ \frac{\partial u}{\partial y} & \frac{\partial v}{\partial y} & \frac{\partial w}{\partial y} \\ \frac{\partial u}{\partial z} & \frac{\partial v}{\partial z} & \frac{\partial w}{\partial z} \end{bmatrix} [\mathbf{T}] \quad [4.9]$$

Where, transformation matrix $[\mathbf{T}]$ is given by

$$\mathbf{T} = \begin{bmatrix} l_1 & l_2 & l_3 \\ m_1 & m_2 & m_3 \\ n_1 & n_2 & n_3 \end{bmatrix} \quad [4.10]$$

In the iso-parametric elements, the conversion of derivatives of displacements with respect to Cartesian coordinate system into derivatives of displacements with respect to natural coordinate system is attained through Jacobian matrix as

$$\begin{bmatrix} \frac{\partial u}{\partial x} & \frac{\partial v}{\partial x} & \frac{\partial w}{\partial x} \\ \frac{\partial u}{\partial y} & \frac{\partial v}{\partial y} & \frac{\partial w}{\partial y} \\ \frac{\partial u}{\partial z} & \frac{\partial v}{\partial z} & \frac{\partial w}{\partial z} \end{bmatrix} = \mathbf{J}^{-1} \begin{bmatrix} \frac{\partial u}{\partial \xi} & \frac{\partial v}{\partial \xi} & \frac{\partial w}{\partial \xi} \\ \frac{\partial u}{\partial \eta} & \frac{\partial v}{\partial \eta} & \frac{\partial w}{\partial \eta} \\ \frac{\partial u}{\partial \zeta} & \frac{\partial v}{\partial \zeta} & \frac{\partial w}{\partial \zeta} \end{bmatrix} \quad [4.11]$$

where, $[\mathbf{J}]$ is the Jacobian matrix defined as

$$\mathbf{J} = \begin{bmatrix} \frac{\partial x}{\partial \xi} & \frac{\partial y}{\partial \xi} & \frac{\partial z}{\partial \xi} \\ \frac{\partial x}{\partial \eta} & \frac{\partial y}{\partial \eta} & \frac{\partial z}{\partial \eta} \\ \frac{\partial x}{\partial \zeta} & \frac{\partial y}{\partial \zeta} & \frac{\partial z}{\partial \zeta} \end{bmatrix} \quad [4.13]$$

Now the relation between the strains and nodal displacements may be established as

$$\boldsymbol{\varepsilon}' = \mathbf{B} \boldsymbol{\delta} \quad [4.14]$$

where, \mathbf{B} is known as strain-displacement matrix and $\boldsymbol{\delta}$ is a vector of nodal displacements defined as

$$\{\boldsymbol{\delta}\} = \{u \ v \ w \ \beta_1 \ \beta_2\}^T \quad [4.15]$$

It is convenient to write Eq. (4.14) in partitioned form as

$$\begin{Bmatrix} \boldsymbol{\varepsilon}'_f \\ \boldsymbol{\varepsilon}'_s \end{Bmatrix} = \begin{Bmatrix} \sum_{k=1}^9 \mathbf{B}_{fk} \boldsymbol{\delta}_k \\ \sum_{k=1}^9 \mathbf{B}_{sk} \boldsymbol{\delta}_k \end{Bmatrix} \quad [4.16]$$

The finite element analysis of RC shear wall can be carried out by adopting a layered element approach, which is very prominent for modeling of composite section. The layered approach divides the shell element into several concrete and steel layers through the thickness, and each layer has its own independent material properties. The layered element formulation (Teng et al. 2005) allows the numerical integration through the element thickness direction. For the numerical integration along the thickness direction, each layer is assumed to have one integration point at its mid surface. The steel layers are used to model the in-plane reinforcement only. The strain-displacement matrix \mathbf{B} and the material constitutive matrix \mathbf{D} are evaluated at the midpoint of each layer, and for all integration points in the plane of the layer. Using the principle of minimum potential energy, the element stiffness matrix \mathbf{K}^e may be determined as:

$$\mathbf{K}^e = \iiint \mathbf{B}^T \mathbf{D} \mathbf{B} \, dV \quad [4.17]$$

In the above equation, the integration is made over the entire volume of the element. Since material non-linearity is only considered in the present study, the strain-displacement matrix \mathbf{B} remains constant throughout the analysis and the material constitutive matrix \mathbf{D} changes due to non-linearity.

In the Euclidean space, the volume of the element is given as the product of the differentials of the Cartesian coordinates and is expressed as $dV = dx dy dz$. The transformation of integrals from the global coordinate system to the local coordinate system is performed with the use of determinant of the Jacobian matrix.

$$dV = dx dy dz = |\mathbf{J}| d\xi d\eta d\zeta$$

For the numerical integration of the element stiffness matrix, the volume integration is converted into area integration using Jacobian and is expressed as

$$K^e = \iint \mathbf{B}^T \mathbf{D} \mathbf{B} |\mathbf{J}| d\zeta dA \quad [4.18]$$

where

$$\int dA = |\mathbf{J}| \int_{-1}^{+1} \int_{-1}^{+1} d\xi d\eta \quad [4.19]$$

With the help of Eq. (4.16), the stiffness matrix may be decomposed into in-plane and transverse shear strain stiffness matrices as

$$\mathbf{K}^e = \mathbf{K}_f^e + \mathbf{K}_s^e \quad [4.20a]$$

where,

$$\mathbf{K}_f^e = \iint \mathbf{B}_f^T \mathbf{D} \mathbf{B}_f |\mathbf{J}| d\zeta dA \quad [4.20b]$$

$$\mathbf{K}_s^e = \iint \mathbf{B}_s^T \mathbf{D} \mathbf{B}_s |\mathbf{J}| d\zeta dA \quad [4.20c]$$

Further, the in-plane stiffness matrix \mathbf{K}_f^e may be decomposed into in-plane bending stiffness matrix \mathbf{K}_b^e and in-plane membrane stiffness matrix \mathbf{K}_m^e as

$$\mathbf{K}_f^e = \mathbf{K}_b^e + \mathbf{K}_m^e \quad [4.20d]$$

where,

$$\mathbf{K}_b^e = \iint \mathbf{B}_b^T \mathbf{D} \mathbf{B}_b |\mathbf{J}| d\zeta dA \quad [4.20e]$$

$$\mathbf{K}_m^e = \iint \mathbf{B}_m^T \mathbf{D} \mathbf{B}_m |\mathbf{J}| d\zeta dA \quad [4.20f]$$

The internal force vector f^e , may be expressed as

$$f^e = \iint \mathbf{B}^T \boldsymbol{\sigma} |\mathbf{J}| d\zeta dA \quad (4.21)$$

The stiffness matrix and force vector are evaluated by carrying out numerical integration using the Gauss- quadrature rule, which is one of the most widely used methods of numerical integration. The assembling of the element stiffness matrix and element load vector results in structural stiffness matrix \mathbf{K} and structural load vector \mathbf{f} respectively. The structural stiffness matrix \mathbf{K} relates the structural force vector \mathbf{f} with the global displacement vector δ as

$$\mathbf{f} = \mathbf{K} \delta \quad [4.22]$$

Once the displacements are determined, the strains and stresses may be calculated using strain-displacement matrix and material constitutive matrix respectively. The formulation of degenerated shell element is completely described in Huang (1987). The finite element programming sequence comprising the various modules is shown in Appendix-2.

4.4.2 Element locking

The degenerated shell element was found promising when it was first developed for the analysis of moderately thick plates and shells. Soon after the introduction of the degenerated concept, it was realized that the fully integrated stiffness matrix (3×3) overestimates the stiffness of the shell element as its thickness decreases. Thus, the degenerated formulations possess strong deficiencies in reproducing the behavior of thin structures, leading to locking phenomena. Though conventional shell elements with six degrees of freedom can be analyzed accurately either by full or reduced integration, it is an inherent disadvantage in the case of degenerated shell element with only five degrees of freedom, especially in thin shell conditions. For very thin elements, it is very difficult to avoid these locking phenomena theoretically. There are two drawbacks outlined below with respect to degenerated shell element.

a) *Transverse shear locking* occurs when elements of lower interpolation order cannot reproduce pure bending states without an activation of transverse shear. Shear locking is a phenomenon associated with the development of spurious transverse shear strains and it is difficult to reproduce the thin shell conditions (zero transverse shear strains). Shear locking is essentially due to the inability of the assumed displacement fields to model the zero shear stress condition in the limit as the thickness of the shell tends to zero.

The transverse shear matrix \mathbf{K}_s^{ij} is of the order $(h/L)^2$ higher than the remaining terms. Thus, as span/depth ratio increases, the computed shear stiffness, \mathbf{K}_s^{ij} completely dominates and no effect of the bending stiffness remains with the finite length of the computer word. This actually causes the element stiffness \mathbf{K}^{ij} to over-stiff and leads to shear dominated solutions (shear locking). This defect can be overcome using selective/reduced integration and assumed transverse shear strain fields.

b) Membrane locking occurs due to the same mechanism as transverse shear locking. Membrane locking is a phenomenon associated with the development of spurious membrane strains and it is difficult to reproduce pure bending strains. A distinguishing feature of the curved elements, as compared to the flat shell elements, is the presence of membrane-flexural coupling within each element. This coupling is achieved in the elements based on shell theory through the explicit presence of the curvature terms in the strain-displacement relationships, while for the degenerated element this is effected through the variation in the Jacobian. The presence of membrane-flexural coupling, although desirable, again leads to the phenomena of membrane locking, in which a bending-dominated response is replaced with a membrane-dominated response. This defect leads to additional stiffening of the solution. Elimination of membrane locking can be done via reduced integration of the membrane terms and also by using assumed membrane strain fields.

Techniques to alleviate locking

In order to alleviate locking problems, the reduced/selective integration techniques have been suggested and adopted by many authors (Zienkiewicz et al. 1971; Paswey and Clough, 1971; Malkus and Hughes 1978; Hughes et al. 1978). Zienkiewicz et al. (1971) used the reduced integration scheme in order to improve the degenerated shell element proposed by Ahmad et al. (1970) and found that the use of reduced integration results in spurious mechanisms or zero energy modes. Subsequently, in the same year, Paswey and Clough (1971) successfully employed the selective integration scheme to avoiding the locking by adopting different integration rule for calculating bending, shear and membrane stiffnesses \mathbf{K}_b^e , \mathbf{K}_m^e and \mathbf{K}_s^e respectively. The order of integration is reduced for membrane and shear stiffness matrices to underestimate their effects in thin situations. Nevertheless, the selective integration schemes also suffer from the

mechanisms such as spurious mode/hourglass mode/zero energy mode. However, if these spurious modes are incompatible (or non-communicable) between adjacent elements, they do not cause any numerical instability. Moreover, it is not easy to find an appropriate reduced or selective integration rule which can eliminate both locking and undesirable kinematic modes at the same time.

In order to suppress the spurious kinematic modes, a stabilization matrix may be added to the element stiffness matrix evaluated by a reduced integration rule (Belytschko et al. 1984; Liu et al. 1985; Hughes 1987). In doing so, great care is needed to avoid reintroducing the effect of locking through excessive stabilization. Belytschko et al. (1985) described the implementation of a 9-noded Lagrangian element with uniform reduced integration with stabilization matrix (spurious mode control) for plates and shells. From their study, it was observed that the rate of convergence of this element is significantly superior and also the effectiveness of stabilization matrix in avoiding the zero energy modes. Nevertheless, such stabilization matrix, employed to alleviate locking, needs artificial damping or stiffness, both with user-determined coefficients. The default values are usually set in the commercial software after extensive studies with various examples, but the parameters are not able to work perfectly for all the applications that contain various meshes, loading conditions, and materials. Working along similar lines, some of the mixed/hybrid elements based on the first order shear deformation theory, such as shear-flexible element by Wilt et al. (1990) and the shear-locking-free element by Auricchio and Sacco (1999), seem to be efficient in removing shear-locking. However, their complex formulation and high computational cost render their usage less attractive in practical applications.

The assumed strain approach has been successfully adopted by many researchers (Huang and Hinton, 1986; Huang, 1987) as an alternative to avoid locking. Assumed Natural Strain (ANS) and the Enhanced Assumed Strain (EAS) are the two methods of assumed strain approach popularly used in the finite element application to avoid the locking phenomena. Though enhanced assumed strain approach (Simo & Rifai, 1990) has been successfully employed in removing shear and volumetric locking, it has not been used as prominently as assumed natural strain approach (MacNeal 1982). Huang and Hinton (1986) developed eight- and nine-noded Mindlin plate elements and degenerated shell elements with assumed natural strain approach in which the interpolation of the

transverse shear strains is done in the natural coordinate system and the membrane strains in the local coordinate system at the assumed sampling points. Lee and Han (2001) presented an assumed strain based eight-noded shell element for the analysis of laminated plates and shells and found that the elements based on assumed natural strain approach are capable of removing the locking phenomenon (both shear & membrane locking) and performed well in the modeling of thin plates and shell structures. Teng et al. (2005) successfully analyzed the concrete slabs with assumed natural strain approach using Finite Element Analysis.

4.4.3 Assumed natural strain formulation

The key idea of the ANS method is the replacement of the selected displacement-related strains by independently assumed strain fields in element natural coordinates. In general, the application of the ANS method needs: (i) the positions of the sample points; (ii) the strain components at these points; and (iii) the interpolation functions to interpolate the strains from the sampling points to the Gaussian points.

The appropriately chosen polynomial terms and sampling points ensure the elimination of risk of spurious zero energy modes. The location of the sampling points for shear strains $\gamma_{\xi\zeta}$ and $\gamma_{\eta\zeta}$ are shown in Fig. 4.3. The membrane and shear strains are interpolated from identical sampling points even though the membrane strains are expressed in orthogonal curvilinear coordinate system and transverse shear strains are expressed in natural coordinate system.

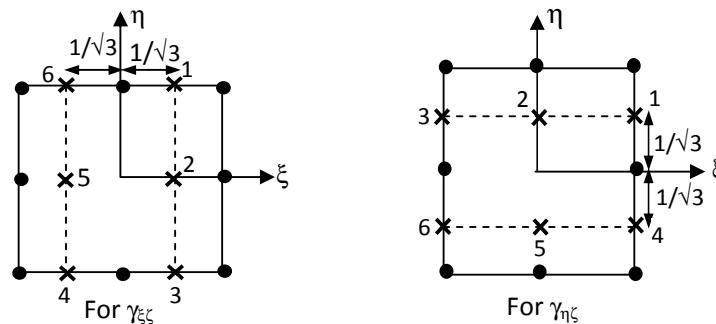


Fig. 4.3: Sampling point locations for assumed shear/membrane strains

If $\gamma_{\xi\zeta}^{ij}$ and $\gamma_{\eta\zeta}^{ij}$ are the shear strains at sampling points obtained from Lagrangian shape functions, the assumed shear strains at all nine Gaussian points (for 3×3 integration rule) may be interpolated as

$$\left. \begin{aligned} \bar{\gamma}_{\xi\zeta} &= \sum_{i=1}^3 \sum_{j=1}^2 P_i(\eta) \cdot Q_j(\xi) \gamma_{\xi\zeta}^{ij} \\ \bar{\gamma}_{\eta\zeta} &= \sum_{i=1}^3 \sum_{j=1}^2 P_i(\xi) \cdot Q_j(\eta) \gamma_{\eta\zeta}^{ij} \end{aligned} \right\} \quad [4.23]$$

where, the $P_i(z)$ and $Q_j(z)$ are the interpolating functions along ξ direction (for $z = \xi$) and η direction (for $z = \eta$) respectively and they are defined as

$$\left. \begin{aligned} P_1(z) &= \frac{z}{2}(z+1), & P_2(z) &= 1-z^2, & P_3(z) &= \frac{z}{2}(z-1) \\ Q_1(z) &= \frac{1}{2}(1+\sqrt{3}z), & Q_2(z) &= \frac{1}{2}(1-\sqrt{3}z) \end{aligned} \right\} \quad [4.24]$$

The assumed strain may be considered a special case of integration scheme wherein, for function $\bar{\gamma}_{\xi\zeta}$ full integration is employed in η direction and reduced integration is employed in ξ direction. On the other hand, for function, $\bar{\gamma}_{\eta\zeta}$ reduced integration is employed in η direction and full integration is employed in ξ direction. Moreover, it may be observed that $\bar{\gamma}_{\xi\zeta}$ is linear in ξ direction and quadratic in η direction, while $\bar{\gamma}_{\eta\zeta}$ is linear in η direction and quadratic in ξ direction. The flexural membrane *strains* are evaluated in the local coordinate system $x' - y' - z'$ using the following expressions as

$$\begin{aligned} \bar{\epsilon}_{m,x'x'} &= \sum_{i=1}^3 \sum_{j=1}^2 P_i(\eta) \cdot Q_j(\xi) e_{m,x'x'}^{ij} && \text{(along } x - \text{ direction)} \\ \bar{\epsilon}_{m,y'y'} &= \sum_{i=1}^3 \sum_{j=1}^2 P_i(\xi) \cdot Q_j(\eta) e_{m,y'y'}^{ij} && \text{(along } y - \text{ direction)} \\ \bar{\epsilon}_{m,x'y'} &= \sum_{i=1}^3 \sum_{j=1}^2 P_i(\eta) \cdot Q_j(\xi) e_{m,x'y'}^{ij} && \text{(along } x - \text{ direction)} \\ \bar{\epsilon}_{m,x'y'} &= \sum_{i=1}^3 \sum_{j=1}^2 P_i(\xi) \cdot Q_j(\eta) e_{m,x'y'}^{ij} && \text{(along } y - \text{ direction)} \end{aligned} \quad [4.25]$$

4.5 Dynamic Analysis of RC Structures

In the present section, the dynamic analysis of RC structures is discussed. In a dynamic analysis, the governing equation of motion can be expressed by the following equation which is a second order non-linear differential equation with constant coefficients. This equation is non-linear because the restoring force component varies with time.

$$\mathbf{M} \ddot{\mathbf{u}} + \mathbf{C} \dot{\mathbf{u}} + \mathbf{f}_s(\mathbf{u}, \dot{\mathbf{u}}) = \mathbf{R}(t) \quad [4.26]$$

The coefficients \mathbf{M} , \mathbf{C} and \mathbf{f}_s are the mass, damping and restoring force components respectively and $\mathbf{R}(t)$ is an external force, which varies with time 't'. The restoring force (stiffness component) varies depending on the non-linearity present in the structure and the formulation has been discussed in detail in chapter three (Material Modeling of RC Structures). The present section concentrates on the development of mass matrix and damping matrix. In the end, the complete formulation of the Newmark Beta method of direct integration is discussed in detailed followed by the validation of the developed finite element program NLDAS with the bench mark problems.

4.5.1 Formulation of mass matrix

In a dynamic analysis, a correct estimate of mass matrix is very important in predicting the dynamic response of RC structures. There are two different ways, namely (i) consistent approach and (ii) lumped approach, by which the element mass matrix can be developed. In the case of consistent approach, the masses are assumed to be distributed over the entire finite element mesh. In this approach, the shape functions (N_i) used for the computation of mass matrix is the same shape functions used for the development of stiffness matrix and hence the name ‘consistent’ approach. The mass matrix developed using the consistent approach is known as consistent mass matrix. The consistent element mass matrix (\mathbf{M}_e) is given by

$$\mathbf{M}_e = \int_V \rho_m N_i [N_i]^T dV \quad [4.27]$$

where ρ_m is the mass density, 'i' is the node number and the integration is performed over the entire volume of the element. The shape-functions for the nine-noded degenerated shell element have been mentioned in Eq. (4.6). The consistent mass matrix contains off-diagonal terms and hence is computationally expensive.

On the other hand, the lumped mass matrix is purely diagonal and hence computationally cheaper than the consistent mass matrix. Nevertheless, the diagonalization of the mass matrix from the full mass matrix results in the loss of information and accuracy (Huang 1987). Nodal quadrature, row sum and special lumping are the three lumping procedures available to generate the lumped mass matrices. All the three methods of lumping lead to the same mass matrix for nine-node rectangular elements. Nevertheless, one of the most efficient means of lumping is to distribute the element mass in proportion to the diagonal

terms of consistent mass matrix (Archer and Whalen, 2006) and also discarding the off-diagonal elements. This way of lumping has been successfully used in many finite element codes in practice.

The advantage of this special lumping scheme is the assurance of positive definiteness of mass matrix. The use of lumped mass matrix is mostly employed in lower order elements. For higher order elements, the use of lumped mass matrix may not be an appropriate option and hence the present study uses only consistent mass matrix. Moreover, the lumped mass matrix may be an ideal option in the case RC framed structures in which the masses can be lumped at floor level. As RC shear wall is the concrete structure, it may be appropriate to use consistent mass matrix. The element mass matrix for consistent and lumped mass matrices are as mentioned below.

$$[M_e^c] = \begin{bmatrix} I_1 & 0 & 0 & 0 & I_2 \\ 0 & I_1 & 0 & -I_2 & 0 \\ 0 & 0 & I_1 & 0 & 0 \\ 0 & -I_2 & 0 & I_3 & 0 \\ I_2 & 0 & 0 & 0 & I_3 \end{bmatrix} \quad [4.28]$$

$$[M_e^L] = \begin{bmatrix} I_{L1} & 0 & 0 & 0 & 0 \\ 0 & I_{L1} & 0 & 0 & 0 \\ 0 & 0 & I_{L1} & 0 & 0 \\ 0 & 0 & 0 & I_{L2} & 0 \\ 0 & 0 & 0 & 0 & I_{L2} \end{bmatrix} \quad [4.29]$$

Eq. (4.27) is very general and can be used to develop the consistent mass matrix for any displacement-based finite element. In Eq. (4.28), ' I_1 ' represents the contribution of mass in resisting the linear or translational motion and is defined as $I_1 = \int \rho_m dz$. Hence, masses corresponding to translational degrees of freedom are represented by ' I_1 '. On the other hand, ' I_3 ' represents the contribution of mass in resisting the change in the rotatory motion and is expressed mathematically as $I_3 = \int \rho_m z \times z dz$. $I_2 = \int \rho_m z dz$. The total mass matrix \mathbf{M} is the sum of the element mass matrices \mathbf{M}_e . The term z is the position of layer middle surface from shell middle surface. Eq. (4.29) represents the lumped mass matrix which is not used in the present analytical study.

4.5.2 Formulation of damping matrix

Mass and stiffness matrices can be represented systematically by overall geometry and material characteristics. However, damping can only be represented in a phenomenological manner and thus making the dynamic analysis of structures in a state of uncertainty. The quantification and representation of damping is certainly complicated by the relationship between its mathematical representation and the physical sources. The damping may be assumed to be contributed through friction, hysteretic and viscous characteristics. There is no single universally accepted methodology for representing damping because of the nature of the state variables, which control damping. Nevertheless, several investigations have been done in making the representation of damping in a simplistic yet logical manner (Charney, 2008). Only for the mathematical convenience, the damping has been modeled as equivalent viscous damping, represented as the percentage of critical damping. The governing equation of motion second order differential equation with constant coefficients is rewritten as

$$\mathbf{M}\ddot{u} + \mathbf{C}\dot{u} + \mathbf{K}u = \mathbf{R}(t) \quad [4.30]$$

The trial solution is given by

$$u = ce^{st} \quad [4.31]$$

On substituting the trial solution and simplifying, the roots of quadratic equation are as

$$\left. \begin{aligned} s &= \frac{-c}{2m} \pm \sqrt{\left(\frac{c}{2m}\right)^2 - \omega^2} \\ \left(\frac{c}{2m}\right)^2 - \omega^2 > 0 &\Rightarrow 2 \text{ real roots (over damped)} \\ &\rightarrow s_1 = -\xi\omega + \omega\sqrt{\xi^2 - 1}; \\ &\quad s_2 = -\xi\omega - \omega\sqrt{\xi^2 - 1} \\ \left(\frac{c}{2m}\right)^2 - \omega^2 = 0 &\Rightarrow 1 \text{ real root (critically damped)} \\ &\rightarrow s_1 = -\xi\omega \\ \left(\frac{c}{2m}\right)^2 - \omega^2 < 0 &\Rightarrow 2 \text{ complex roots (under damped)} \\ &\rightarrow s_1 = -\xi\omega + i\omega\sqrt{1 - \xi^2}; \\ &\quad s_2 = -\xi\omega - i\omega\sqrt{1 - \xi^2} \end{aligned} \right\} \quad [4.32]$$

In Eq. (4.32), the damping ratio ξ is given by

$$\xi = \frac{c}{2m\omega} \Rightarrow \frac{c}{2m} = \xi\omega; \quad \xi = \frac{c}{c_{cr}} \quad [4.33]$$

Over damped system does not vibrate at all. The classical example is automatic door closing. Critical damping has the linear exploding function and hence the amplitude is higher than the over damped system, and then followed by exponentially exploding function resulting in the fast movement over the time. The bottom line is both over damped and critically damped does not vibrate at all. Nevertheless, in a building structure, critically damped and over damped situation may not arise. Damping matrix can be formulated analogous to mass and stiffness matrices (Duggal, 2007). It is also important to note that the damping matrix should be formulated from damping ratio and not from the member sizes. Rayleigh dissipation function assumes that the dissipation of energy takes place and can be idealized as the function of velocity. When Rayleigh Damping is used, the resultant damping matrix is of same size as stiffness matrix. Rayleigh damping is being used conveniently because of its versatility in segregating each mode independently. The damping can be defined as the linear combination of mass and stiffness matrices as

$$[C] = \alpha[M] + \beta[K] \quad [4.34]$$

$$\zeta_i = \frac{\alpha}{2\omega_i} + \frac{\beta\omega_i}{2} \quad [4.35]$$

It is to be noted that the damping is controlled by only two parameters [Fig. 4.4]. From Eq. (4.35), it is observed that if β is zero, the higher modes of the structure will be assigned very little damping. When α alpha is zero, the higher modes will be heavily damped, as the damping ratio is directly proportional to circular frequency (ω) (Clough and Penzein, 1993). Thus, the choice of damping is problem dependent. Hence, it is inevitable to perform modal analysis to determine the different frequencies for different modes.

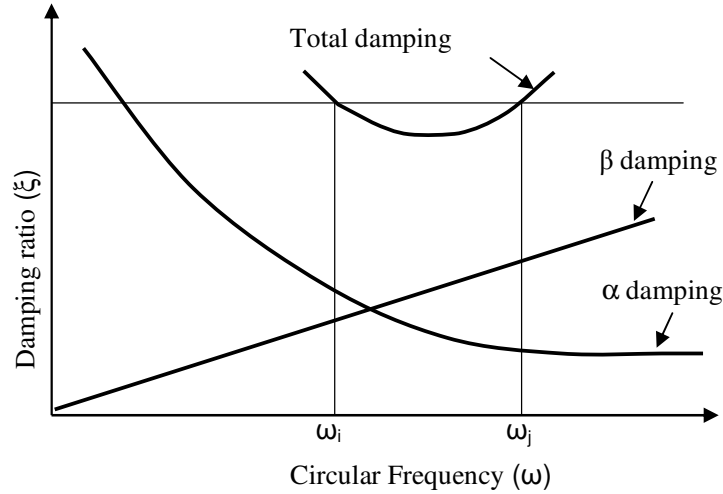


Fig. 4.4: Variation of damping with circular frequency

4.6 Formulation of Newmark Method

For the dynamic time history analysis of RC structures, the Newmark Beta (β) method of direct time integration (Newmark, 1959), an implicit integration algorithm, has been used to solve the below mentioned equation of motion

$$\mathbf{M} \ddot{\mathbf{u}}^{t+\Delta t} + \mathbf{C} \dot{\mathbf{u}}^{t+\Delta t} + \mathbf{K} \mathbf{u}^{t+\Delta t} = \mathbf{R}^{t+\Delta t} \quad [4.36]$$

where \mathbf{M} is the mass matrix; \mathbf{C} is the damping matrix; \mathbf{K} is the stiffness matrix.

The truncated form of Taylor series is given below for the velocity and displacements.

$$\left. \begin{aligned} \dot{\mathbf{u}}_{n+1} &= \dot{\mathbf{u}}_n + \frac{\Delta t}{2} (\ddot{\mathbf{u}}_n + \ddot{\mathbf{u}}_{n+1}) \\ \mathbf{u}_{n+1} &= \mathbf{u}_n + \Delta t \dot{\mathbf{u}}_n + \frac{1-2\beta}{2} \Delta t^2 \ddot{\mathbf{u}}_n + \beta \Delta t^2 \ddot{\mathbf{u}}_{n+1} \end{aligned} \right\} \quad [4.37]$$

The following assumptions are made in the linear acceleration method.

$$\left. \begin{aligned} \dot{\mathbf{u}}^{t+\Delta t} &= \dot{\mathbf{u}}^t + \left[(1-\delta) \ddot{\mathbf{u}}^t + \delta \ddot{\mathbf{u}}^{t+\Delta t} \right] \Delta t \\ \mathbf{u}^{t+\Delta t} &= \mathbf{u}^t + \dot{\mathbf{u}}^t \Delta t + \left[\left(\frac{1}{2} - \alpha \right) \ddot{\mathbf{u}}^t + \alpha \ddot{\mathbf{u}}^{t+\Delta t} \right] \Delta t^2 \end{aligned} \right\} \quad [4.38]$$

In the above equations, α is the accuracy parameter and δ is the stability parameter.

Expanding Eq. (4.38),

$$\left. \begin{aligned} \mathbf{u}^{t+\Delta t} &= \mathbf{u}^t + \dot{\mathbf{u}}^t \Delta t + \frac{1}{2} \ddot{\mathbf{u}}^t \Delta t^2 - \alpha \ddot{\mathbf{u}}^t \Delta t^2 + \alpha \ddot{\mathbf{u}}^{t+\Delta t} \Delta t^2 \\ \mathbf{u}^{t+\Delta t} - \mathbf{u}^t - \dot{\mathbf{u}}^t \Delta t - \frac{1}{2} \ddot{\mathbf{u}}^t \Delta t^2 + \alpha \ddot{\mathbf{u}}^t \Delta t^2 &= \alpha \ddot{\mathbf{u}}^{t+\Delta t} \Delta t^2 \\ \ddot{\mathbf{u}}^{t+\Delta t} &= \frac{1}{\alpha \Delta t^2} \left[\mathbf{u}^{t+\Delta t} - \mathbf{u}^t - \dot{\mathbf{u}}^t \Delta t - \frac{1}{2} \ddot{\mathbf{u}}^t \Delta t^2 + \alpha \ddot{\mathbf{u}}^t \Delta t^2 \right] \end{aligned} \right\} [4.39]$$

Substituting the value of $\ddot{\mathbf{u}}^{t+\Delta t}$ from Eq. (4.39) in $\dot{\mathbf{u}}^{t+\Delta t}$ of Eq. (4.38)

$$\dot{\mathbf{u}}^{t+\Delta t} = \dot{\mathbf{u}}^t \Delta t - \delta \ddot{\mathbf{u}}^t \Delta t + \delta \left[\frac{1}{\alpha \Delta t^2} \left(\mathbf{u}^{t+\Delta t} - \mathbf{u}^t - \dot{\mathbf{u}}^t \Delta t - \frac{1}{2} \ddot{\mathbf{u}}^t \Delta t^2 + \alpha \ddot{\mathbf{u}}^t \Delta t^2 \right) \Delta t \right] [4.40]$$

Using Eq. (4.38) and (4.39), the equation of motion in Eq. (4.36) is modified as

$$\left. \begin{aligned} \mathbf{M} \left[\frac{1}{\alpha \Delta t^2} \left(\mathbf{u}^{t+\Delta t} - \mathbf{u}^t - \dot{\mathbf{u}}^t \Delta t - \frac{1}{2} \ddot{\mathbf{u}}^t \Delta t^2 + \alpha \ddot{\mathbf{u}}^t \Delta t^2 \right) \right] + \\ \mathbf{C} \left[\begin{aligned} &\dot{\mathbf{u}}^t + \ddot{\mathbf{u}}^t \Delta t - \delta \ddot{\mathbf{u}}^t \Delta t + \\ &\frac{\delta}{\alpha \Delta t} \left(\mathbf{u}^{t+\Delta t} - \mathbf{u}^t - \dot{\mathbf{u}}^t \Delta t - \frac{1}{2} \ddot{\mathbf{u}}^t \Delta t^2 + \alpha \ddot{\mathbf{u}}^t \Delta t^2 \right) \end{aligned} \right] + \mathbf{K} \mathbf{u}^{t+\Delta t} = \mathbf{R}^{t+\Delta t} \end{aligned} \right\} [4.41]$$

On expanding the above Eq. (4.41), we get

$$\left. \begin{aligned} \frac{\mathbf{M}}{\alpha \Delta t^2} \mathbf{u}^{t+\Delta t} - \frac{\mathbf{M}}{\alpha \Delta t^2} \mathbf{u}^t - \frac{\mathbf{M}}{\alpha \Delta t^2} \dot{\mathbf{u}}^t \Delta t - \frac{\mathbf{M}}{\alpha \Delta t^2} \frac{\ddot{\mathbf{u}}^t \Delta t^2}{2} + \frac{\mathbf{M}}{\alpha \Delta t^2} \alpha \ddot{\mathbf{u}}^t \Delta t^2 \\ + \mathbf{C} \dot{\mathbf{u}}^t + \mathbf{C} \ddot{\mathbf{u}}^t \Delta t - \mathbf{C} \delta \ddot{\mathbf{u}}^t \Delta t + \frac{\mathbf{C} \delta}{\alpha \Delta t} \mathbf{u}^{t+\Delta t} - \frac{\mathbf{C} \delta}{\alpha \Delta t} \mathbf{u}^t - \frac{\mathbf{C} \delta}{\alpha \Delta t} \dot{\mathbf{u}}^t \Delta t \\ - \frac{\mathbf{C} \delta}{2 \alpha \Delta t} \ddot{\mathbf{u}}^t \Delta t^2 + \frac{\mathbf{C} \alpha \delta}{\alpha \Delta t^2} \Delta t^2 \ddot{\mathbf{u}}^t + \mathbf{K} \mathbf{u}^{t+\Delta t} = \mathbf{R}^{t+\Delta t} \end{aligned} \right\} [4.42]$$

In order to simplify the above Eq. (4.42), the following constants are defined using accuracy parameter and stability parameter.

$$\left. \begin{aligned} a_0 &= \frac{1}{\alpha \Delta t^2}; & a_1 &= \frac{\delta}{\alpha \Delta t}; & a_2 &= \frac{1}{\alpha \Delta t}; & a_3 &= \frac{1}{2\alpha} - 1 \\ a_4 &= \frac{\delta}{\alpha} - 1; & a_5 &= \frac{\Delta t}{2} \left(\frac{\delta}{\alpha} - 2 \right); & a_6 &= \Delta t (1 - \delta); & a_7 &= \delta \Delta t \end{aligned} \right\} [4.43]$$

Using the constants defined in Eq. (4.43), the Eq. (4.42) is rewritten as

$$\left. \begin{aligned} [a_0 \mathbf{M} + a_1 \mathbf{C} + \mathbf{K}] \mathbf{u}^{t+\Delta t} &= [\mathbf{R}^{t+\Delta t} + \mathbf{M} (a_0 \mathbf{u}^t + a_2 \dot{\mathbf{u}}^t + a_3 \ddot{\mathbf{u}}^t) + \mathbf{C} (a_1 \mathbf{u}^t + a_4 \dot{\mathbf{u}}^t + a_5 \ddot{\mathbf{u}}^t)] \\ \Rightarrow \mathbf{K}^* \mathbf{u}^{t+\Delta t} &= \mathbf{R}^{*t+\Delta t} \Rightarrow \mathbf{LDL}^T \mathbf{u}^{t+\Delta t} = \widehat{\mathbf{R}}^{t+\Delta t} \end{aligned} \right\} [4.44]$$

In Eq. (4.44), the effective stiffness matrix (\mathbf{K}^*) and the effective load vector ($\hat{\mathbf{R}}$) is expressed as

$$\mathbf{K}^* = a_o \mathbf{M} + a_1 \mathbf{C} + \mathbf{K} \quad [4.45]$$

$$\hat{\mathbf{R}}^{t+\Delta t} = [\mathbf{R}^{t+\Delta t} + \mathbf{M}(a_0 \mathbf{u}^t + a_2 \dot{\mathbf{u}}^t + a_3 \ddot{\mathbf{u}}^t) + \mathbf{C}(a_1 \mathbf{u}^t + a_4 \dot{\mathbf{u}}^t + a_5 \ddot{\mathbf{u}}^t)] \quad [4.46]$$

The acceleration and velocities at time $t + \Delta t$

$$\begin{aligned} \ddot{\mathbf{u}}^{t+\Delta t} &= a_o (\mathbf{u}^{t+\Delta t} - \mathbf{u}^t) - a_2 \dot{\mathbf{u}}^t - a_3 \ddot{\mathbf{u}}^t \\ \dot{\mathbf{u}}^{t+\Delta t} &= \dot{\mathbf{u}}^t + a_6 \ddot{\mathbf{u}}^t + a_7 \ddot{\mathbf{u}}^{t+\Delta t} \end{aligned} \quad [4.47]$$

The complete steps of Newmark β direct time integration (Chopra, 2006) are outlined in Table 4.1. The parameters β and γ are chosen to arrive at a numerical approximation to the actual Taylor series expansion. It is also to be noted that any value of γ less than 0.5 results in a numerically unstable solution. On the other hand, the γ value other than 0.5 introduces spurious damping mechanism. The value of β varies from 0 to 0.5 representing the explicit and implicit conditions respectively. The implicit condition is numerically stable.

Table 4.1: Step by step Newmark β method of time integration

Step	Step description	Equations
1	Set the iteration counter	$i = 0$
2	Begin the predictor phase	$u_{n+1}^{[i]} = u_n + \Delta t \dot{u}_{n+1} + \Delta t^2 (1 - 2\beta) \ddot{u} / 2$ $\dot{u}_{n+1}^{[i]} = \dot{u}_{n+1} = \dot{u}_n + \Delta t (1 - \gamma) \ddot{u}$ $\ddot{u}_{n+1} = \frac{u_{n+1}^{[i]} - u_{n+1}}{\Delta t^2 \beta}$
3	Evaluation of residual forces	$\psi^{[i]} = f_{n+1} - M a_{n+1}^{[i]} - p(u_{n+1}^{[i]}, \dot{u}_{n+1}^{[i]})$
4	Evaluation of effective stiffness matrix & solving the equation	$K^* = \frac{M}{\Delta t^2 \beta} + \frac{\gamma C_T}{\Delta t \beta} + K_T(u_{n+1}^{[i]})$ $K^* \Delta u^{[i]} = \psi^{[i]}$
5	Begin the corrector phase	$u_{n+1}^{[i+1]} = u_{n+1}^{[i]} + \Delta u^{[i]};$ $\dot{u}_{n+1}^{[i+1]} = \dot{u}_{n+1} + \Delta t \gamma \ddot{u}_{n+1}^{[i+1]};$ $\ddot{u}_{n+1}^{[i+1]} = \frac{u_{n+1}^{[i+1]} - u_{n+1}}{\Delta t^2 \beta}$
6	Setting up the initial values for next step once the convergence is achieved	$u_{n+1} = u_{n+1}^{[i+1]}; \dot{u}_{n+1} = \dot{u}_{n+1}^{[i+1]}; \ddot{u}_{n+1} = \ddot{u}_{n+1}^{[i+1]}$

4.7 Solution Algorithms

Direct methods and iterative methods are the two methods generally employed for the solution of non-linear finite element static equations. The direct method, typically based on the Gaussian elimination, is the best since the amount of computational effort required is known prior to the analysis. Various direct methods have evolved over the period of years for the static solution such as Cholesky, LDL^T , Crout's method, Static Condensation etc., Nevertheless, all direct methods invariably depends on Gaussian elimination. On the other hand, iterative methods are more popular these days in nonlinear analysis. The solution algorithms namely (i) Euler-Cauchy forward integration and (ii) Newton-Raphson method have been the most successful of all techniques to solve the non-linear incremental equations. The Newton-Raphson method requires the non-zero and finite tangent stiffness function and its derivatives.

4.7.1 Euler - Cauchy forward integration

It is considered as the simplest of incremental methods for solving the non-linear problem. However, the response obtained using Euler-Cauchy forward integration generally appears to be stiffer than the actual one. Also, the solution may rapidly shift away from the true solution as no check is made to insure the structural equilibrium against external loading after each load increment. In order to estimate the accuracy of the procedure, analysis is repeated several times using successively smaller time increments. Nevertheless, the analysis becomes expensive.

4.7.2 Newton - Raphson iterative procedure

The Newton-Raphson procedure is a well-known method for the solution of nonlinear algebraic equation (Bathe, 2006). In the Newton's method, the linearization of the discrete equations results in tangent moduli, which relates a stress rate to a strain rate. The resulting material tangent stiffness matrix is called the continuum tangent stiffness matrix (Owen and Hinton, 1980). The two main types of solution procedures that can be adapted to model material non-linearity are (i) constant stiffness iterations, and (ii) variable stiffness (tangent) iterations. In the case of constant stiffness iterations, the non-linearity is introduced by iteratively modifying the right hand side "loads" vector. The (usually elastic) global stiffness matrix in such an analysis is formed at the beginning of the solution. Convergence is said to occur if the stresses generated by the loads satisfy some stress-strain law in terms of yield or

failure criterion within the specified tolerances. Nevertheless, constant stiffness approach requires much iteration towards failure load as shown in Fig. 4.5(a). On the other hand, variable stiffness approach (modified Newton-Raphson method) takes care of material degradation as stiffness gets modified frequently and hence takes less iteration as shown in Fig. 4.5(b).

Incremental displacements are computed and are added to the displacements at the end of the previous time step. The process is repeated till the desired convergence is reached. The Newton-Raphson method possesses excellent convergence characteristics (quadratic convergence rate). The tangent stiffness matrix is updated and triangularized for each iteration step. Prior to each solution, the Newton-Raphson approach assesses the out-of-balance load vector, which is the difference between the restoring forces (the loads corresponding to the element stresses) and the applied loads. The program carries out a linear solution, using the out-of-balance loads, and checks for convergence. If convergence criteria are not satisfied, the out-of-balance load vector is re-evaluated, the stiffness matrix is updated, and a new solution is attained. This iterative procedure continues until the problem converges. The constant stiffness approach (Newton Raphson method) and variable stiffness approach (Modified Newton Raphson method) are depicted in Fig. 4.5.

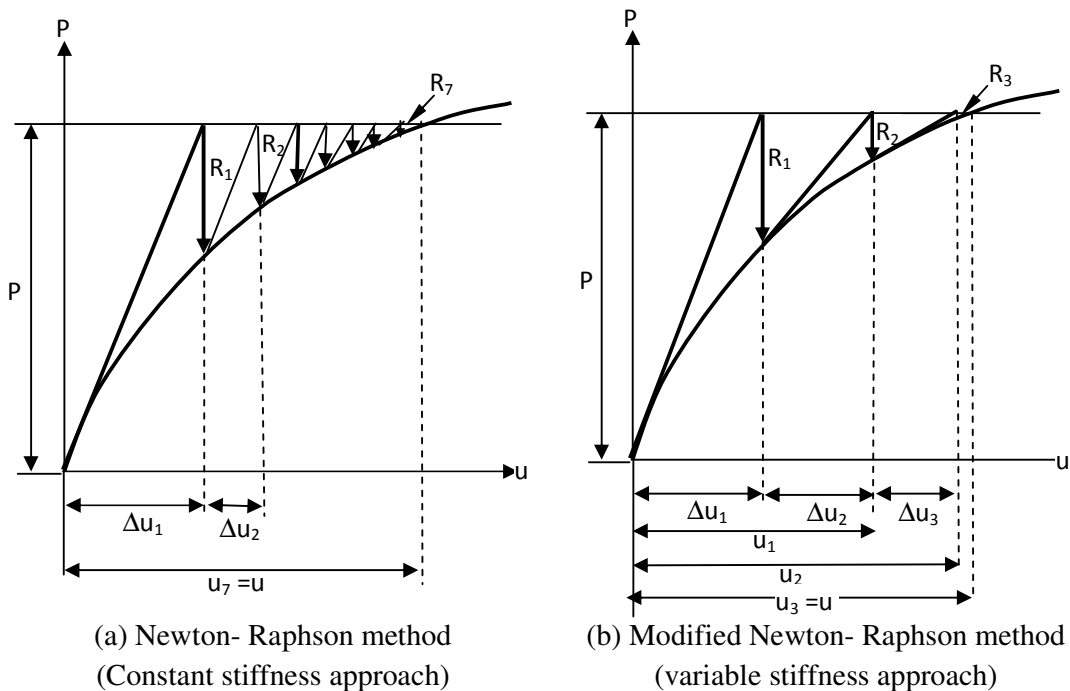


Fig. 4.5: Iterative algorithm

The realistic criteria are to be used for termination of the iteration in order to attain appropriate solution and also to avoid unnecessary computational expenditure. At the end of iteration, the solution obtained should be checked to verify the convergence within the present tolerance limit. Inaccurate results may be resulted because of very relaxed tolerance limit. On the other hand, very tight tolerance limit may result in needless accuracy (Bathe 2006).

$$\left| \frac{\sqrt{\left[\sum (\phi_i^r)^2 \right]} \sqrt{\left[\sum (\phi_i^{r-1})^2 \right]}}{\sqrt{\left[\sum (\phi_i^1)^2 \right]}} \right| \times 100 \leq \text{tolerance limit (0.0025)} \quad [4.48]$$

The global convergence check has been employed in order to check the convergence. In the above equation, $r-1$ and r denote successive iterations. The multiplication factor of 100 on the left-hand side allows the specified tolerance factor to be considered as a percentage term. Equation (4.48) states that convergence is assumed to have occurred if the difference in the norm of the unknowns between the two successive iterations and the first iteration. Nevertheless, the size of the load increments is not a critical parameter in tracing out the deformational response provided that an appropriate solution algorithm is employed (Hinton and Owen, 1984). The norm can be defined in terms of (i) force, (ii) displacement, and (iii) energy. Nevertheless, displacement based tolerance is usually adopted in practice due to its simplicity.

4.8 Development of Computer Program

In the present study an analysis module, NLDAS was developed using Fortran 77 and used to perform the non-linear dynamic finite element analysis of RC shear walls. The computer codes developed by Huang (1989) and Owen & Hinton (1984) for the static and dynamic elasto-plastic analysis of RC structures based on simple Owen-Figurius yield/failure criterion have been taken as the base programs in this study.

These programs have been merged and modified to include state of the art five-parameter yield/failure model and concrete cracking. A modular approach has been adopted for the program development. To this end several new subroutines have been incorporated and few subroutines have been enhanced.

The program consists of 19 subroutines which are developed to perform various operations. In the program NLDAS, though the input files for static and dynamic analysis are different, all the data sets have to be read in at the beginning of the program. The program mainly consisted of the following subroutines: input, loading, incremental loading, stiffness, mass and damping matrices development and assembly, solution of equations, residual force calculations, convergence check and output results, in addition to modules for storage of global arrays such as nodal coordinates, element connectivity, material properties, and boundary conditions. Fig. 4.6 shows the program layout explaining the process of the program.

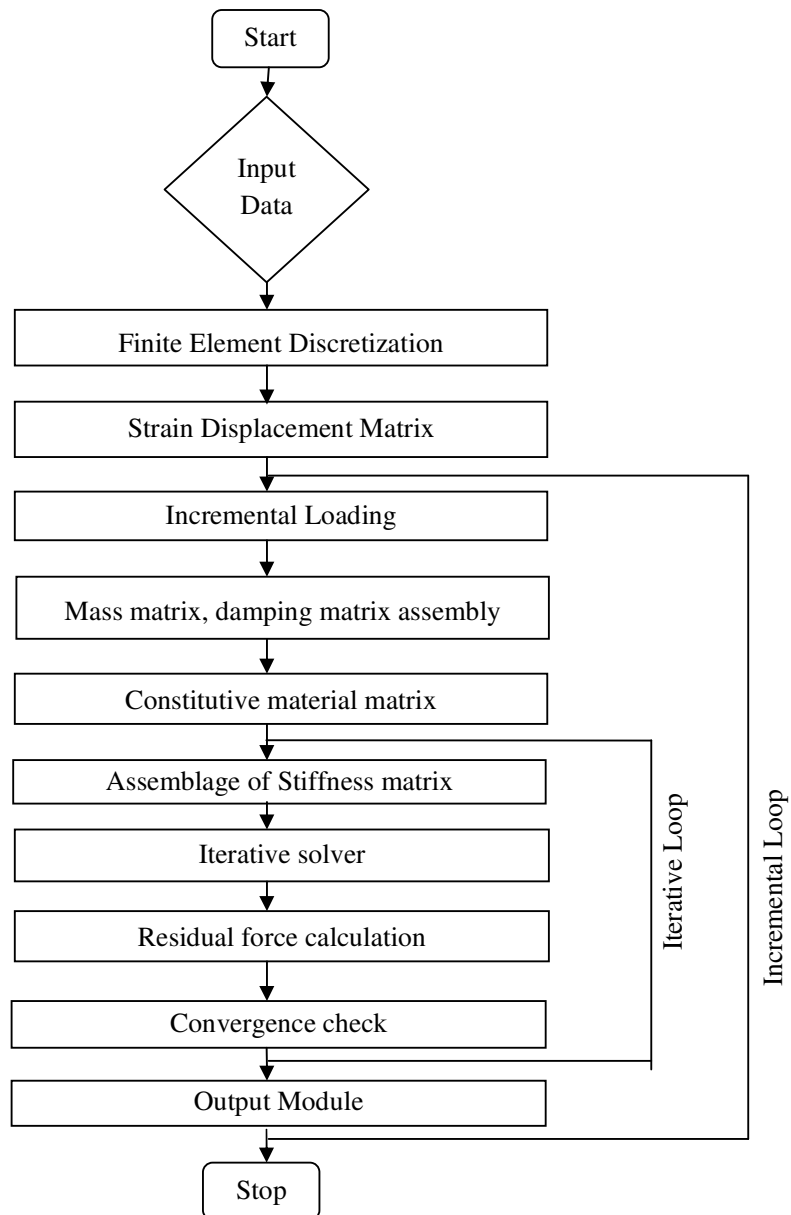


Fig. 4.6: Program layout – NLDAS

4.9 Program Validation

The finite element program developed is validated against standard experimental and analytical investigations and is divided into two parts. The first part deals with the validation of problems pertaining to static analysis, while the second part deals with the validation of problems related to dynamic analysis.

4.9.1 Analysis of structures subjected to static loads

In order to validate the program for analysis of RC structures, three problems have been identified for static analysis as mentioned below.

- Linear static analysis of clamped square plate with uniform loading
- Linear static analysis of cantilever beam subjected to concentrated load
- Non-linear static analysis of shear wall subjected to concentrated load

The analysis of first two problems aims at validating the efficiency of assumed strain based degenerated shell element used in the present analytical study with respect to two other elements. The third problem signifies the accuracy of the present analytical study in predicting the load-deformation response of RC shear wall with top and bottom beams subjected to static monotonic loading. It also validates the degenerated shell element, geometric modeling of shear wall, and material modeling of concrete and steel.

Analysis of clamped square plate under uniform loading

In order to validate the performance of assumed strain based degenerated shell element for thick as well as thin structures, a completely clamped square plate (Fig. 4.7) of size 2 feet ($a = 0.6096$ m), subjected to uniform loading of 10 psi (0.0689 MPa), has been considered with different thicknesses.

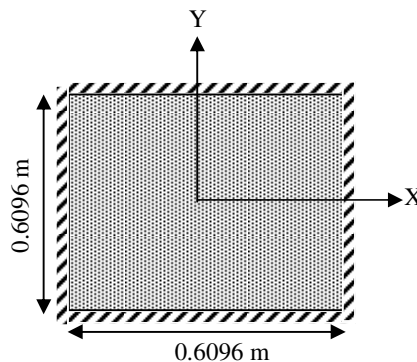


Fig. 4.7: Clamped square plate under uniform loading

The plate is analyzed for four different thicknesses, viz. (i) 5.08 mm, (ii) 0.508 mm, (iii) 0.0508 mm, and (iv) 0.00508 mm. The square plate is made out of material which has the elasticity modulus (E) as 68947.5 MPa and Poisson's ratio (ν) = 0.3. The deflection at the centre of the plate has been determined using linear elastic finite element analysis by discretizing the square plate into four equal elements and the solution is compared with (i) the exact solution and (ii) the analytical finite element solution using Lagrangian element. The exact solution for the deflection (w) at the center of the square plate is given by the following expression (Timoshenko and Krieger, 1959):

$$w = \frac{0.00126 q a^4}{D} \Rightarrow \frac{0.00126 q a^4}{Et^3 / 12 (1 - \nu^2)} \quad [4.49]$$

The solutions obtained using the finite element analyses are normalized with respect to the exact solution for an easy comparison. Table 4.2 shows the exact solution, the normalized finite element solutions based on (i) degenerated shell element with assumed strain approach and (ii) Lagrangian element.

Table 4.2: Displacement of square plate under uniform loading

Span/ depth ratio (a/t)	Exact displacement (Timoshenko & Krieger, 1959) (inch)	Normalized displacement (calculated/exact) based on	
		Degenerated shell element (used in present Study)	Lagrange element
10	0.0000027518	1.2630	1.1361
100	0.00275	1.1144	0.7640
1000	2.75184	1.1130	0.2966
10000	2751.84	1.1129	0.0048

The displacement at the centre of the plate obtained using assumed strain based degenerated shell element has been found to be closer to the exact solution than other two elements. The performance of Lagrange element has not been found to be satisfactory especially for very thin plates.

Analysis of plain concrete cantilever beam

In order to assess the performance of assumed strain based degenerated shell element with full and reduced integration, the concrete cantilever beam, shown in Fig. 4.8, of length 10 ft (3 m) subjected to concentrated load (30 N) at the free end has been analyzed by discretizing the cantilever beam into three finite elements. The cross-sectional size of a cantilever beam is $0.25 \text{ m} \times 0.25 \text{ m}$. The elasticity modulus (E) is taken as $6.89 \times 10^5 \text{ kN/m}^2$ and Poisson's ratio (ν) is taken as 0.3.

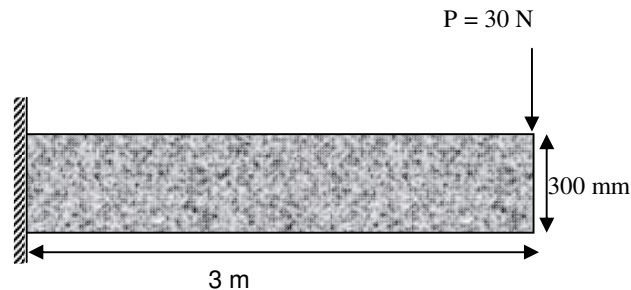


Fig. 4.8: Cantilever beam subjected to point load at the free end

The linear elastic analysis has been performed and the displacement at free end is calculated and normalized with respect to the exact solution, as predicted by Euler Bernoulli beam theory.

Table 4.3: Normalized vertical displacement at the free-end of cantilever beam

Degenerated shell element with layered approach		Lagrange element		
Integration Rule	$3 \times 3 \times 3$	$2 \times 2 \times 2$	3×3	2×2
Normalized Displacement	0.97279	1.0054	0.9467	0.9991

Table 4.3 shows the normalized vertical displacement at the free end of the cantilever beam for two different finite elements, namely (i) assumed strain based degenerated shell element, (ii) Lagrange element. It has been observed from Table 4.3 that the normalized displacements predicted by degenerated shell element (proposed to be used in this study) with full integration and reduced integration schemes are better than the corresponding solutions obtained by Lagrangian element with full integration and reduced integration. This signifies that the degenerated shell element predicts the displacement response

reasonably accurately for both full and reduced integration and element is unaffected by locking phenomena and spurious mechanisms.

Analysis of RC shear wall-nonlinear static analysis

In order to validate the developed finite element program, the RC shear wall panel of size 650 mm wide \times 1300 mm high \times 65 mm thick with aspect ratio of two has been analyzed by subjecting it to the monotonically increasing load. The shear wall panel is sandwiched between upper beam (to provide anchorage for vertical reinforcement) and bottom beam (to provide the base for shear wall panel), and the lateral load is applied at the middle of the upper beam as shown in Fig. 4.9. The lower end of the shear wall is constrained in all degrees of freedom. The same problem was analyzed by Lefas et al. 1990 under same loading conditions and hence been considered as a bench mark problem for the present analytical study. The entire RC shear wall is discretized into 156 elements using assumed strain based degenerated shell element with layered approach. The material properties of concrete and steel are as follows:

Elasticity modulus of concrete = 32710 MPa

Poisson's ratio of concrete = 0.20

Compressive strength of concrete = 42.8 MPa

Tensile strength of concrete = 2.15 MPa

Hardening modulus of concrete = 3271 MPa

Ultimate crushing strain of concrete = 0.0035

Elasticity modulus of steel = 2×10^5 MPa

Poisson's ratio of steel = 0.3

Hardening modulus of steel = 20000 MPa

Yield stress of steel in x -direction = 520 MPa (for both zone I and zone II)

Yield stress of steel in y -direction = 470 MPa (for both zone I and zone II)

Percentage of steel reinforcement in x -direction = 0.8 for zone I and 1.2 for zone II

Percentage of steel reinforcement in y -direction = 2.1 for zone I and 3.3 for zone II

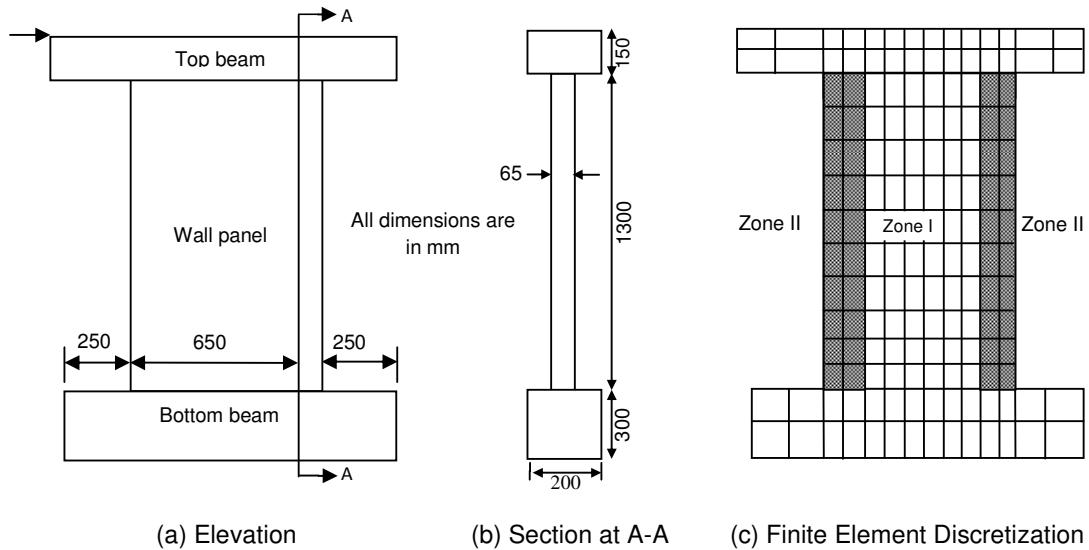


Fig. 4.9: Geometry of solid RC shear wall

The material non-linearity has been considered which includes concrete cracking, yielding of concrete and steel, crushing of concrete. The modeling of concrete in compression has been formulated using plasticity theory with Willam-Warneke five-parameter failure criterion to define the yield/failure surface. The isotropic hardening with associated flow rule has been adopted in defining the strain-hardening behavior of the concrete. The smeared crack modeling has been adopted in which cracks are assumed to be smeared over the element. To represent the capacity of the intact concrete between neighboring cracks, the linearly descending branch of tension stiffening has been adopted in the present investigation. The modeling of reinforcement has been done assuming steel reinforcement assumed to be smeared in a particular layer. The bilinear stress-strain curve has been adopted in defining the steel in tension as well as in compression.

The load-displacement response at the top of the shear wall predicted using degenerated shell element by the present finite element analytical study is compared with experimental and analytical results reported by Lefas et al. (1990) and is shown in Fig. 4.10.

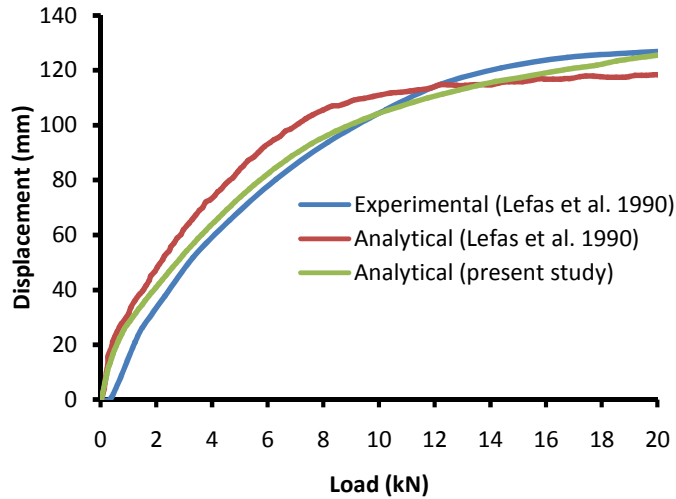


Fig. 4.10: Load deformation response of shear wall subjected to monotonically increasing load

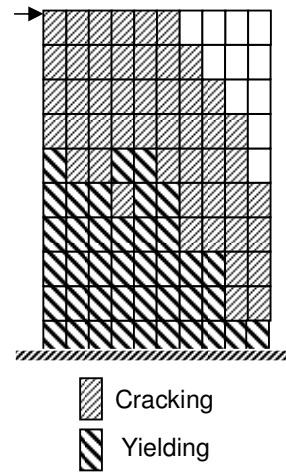


Fig. 4.11: Crack and yield patterns

It is observed that the load-displacement response predicted by the present analytical study is much closer to the experimental results. In fact, for most part of the curve, the present analytical study is better than the analytical study reported at Lefas et al. 1990. Moreover, the crack and yield patterns (Fig. 4.11) are also consistent with the experimental results reported by Lefas et al. (1990). The collapse load of the RC shear wall predicted by the present analytical study is 126.42 kN as against 127.37 kN determined experimentally. The error associated in predicting the collapse load is less than 1%. The collapse displacement has been characterized by heavy yielding of the steel reinforcement. Hence, it is concluded that the finite element program developed for the present analytical study using assumed strain based degenerated shell element with layered approach has been found to be predicting the results with acceptable accuracy. The part II of the validation with respect to dynamic analysis is discussed in the next section.

4.9.2 Analysis of structures subjected to dynamic loads

The finite element program developed is validated for dynamic analysis by taking two specific problems as mentioned below.

- Non-linear dynamic analysis of flanged RC shear wall subjected to artificial ground motion
- Non-linear dynamic analysis of rectangular RC shear wall subjected to earthquake ground motion.

Since the present investigation deals with the response analysis of RC shear wall, the validation of the developed finite element program has been done with RC shear walls, one of flanged type and other of rectangular type. The validation of program with respect to three problems is mentioned below.

Analysis of flanged shear wall- non-linear dynamic analysis

The international standard problem (ISP) reinforced concrete shear wall, shown in Figs. (4.12 - 4.15) has been analyzed using finite element analysis by discretizing the entire shear wall with assumed strain based degenerated layered shell element. The total number of elements used in the analysis is 316 and the number of nodes is 1349. In the 2D Analysis, the total number of elements used is 168 and the number of nodes is 725. The base of the shear wall is completely fixed. In the experimental investigation, it has been mentioned that the top slab is also fitted with four lead blocks on upper and lower side of top slab in order to simulate appropriate gravity load on the wall. To incorporate that effect, the weight of top slab is increased from 29.1 tonf to 122.0 tonf by increasing the density of top slab by keeping the dimensions of top slab as it is.

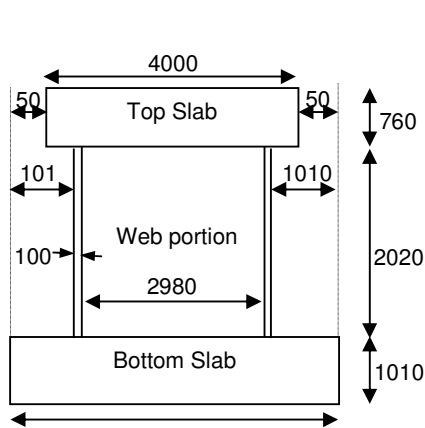


Fig. 4.12: Web side elevation of international standard problem

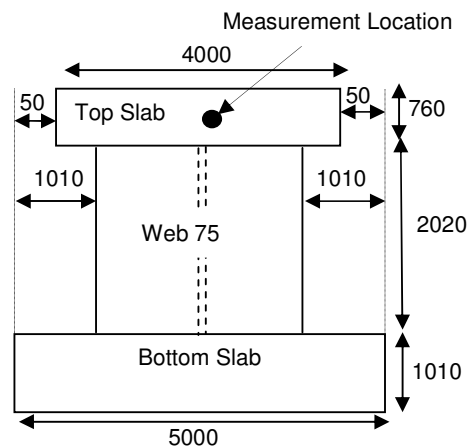


Fig. 4.13: Flange side elevation of international standard problem

The elasticity modulus and Poisson's ratio, of concrete are 2337.5 kg/mm^2 , and 0.155, respectively while that of steel are 18800 kg/mm^2 and 0.300, respectively. The yield stress of steel is taken as 38.4 kg/cm^2 . The diameter of steel used is 6.35 mm and at a spacing of 170 mm for flange and at 70 mm for web. At junction, extra steel was provided to provide confinement effect. The thickness of steel layers was calculated based on amount of steel provided in the horizontal and vertical direction. The concrete cover has been assumed 18 mm. The damping is assumed 1% in all cases.

Rayleigh damping has been assumed by considering only stiffness proportional damping component in order to provide damping proportional to frequency.

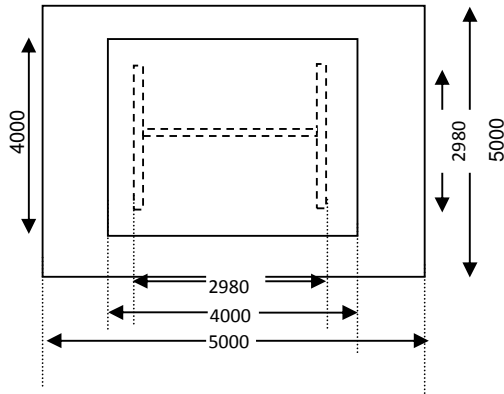


Fig. 4.14: Top view of shear wall

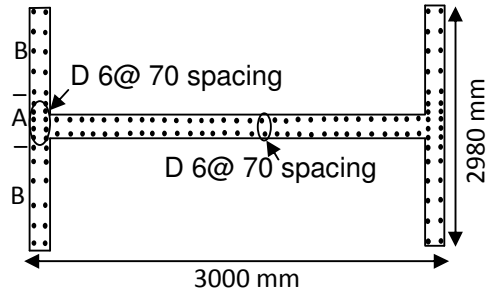


Fig. 4.15: Reinforcement pattern for ISP shear wall

In this study, an attempt has been made to verify the results of the finite element analysis with the actual experimental results and analytical results reported by Jagd (1996). The nonlinear dynamic analysis is performed RC flanged shear wall for two different earthquake ground motions [RUN1 & RUN2]. The duration of the ground motion for both runs (RUN1 and RUN 2) is 10 seconds. The waveforms used for both the runs are almost similar and hence the shape of the input ground acceleration has been shown only for RUN 2 (Fig. 4.16). The peak ground acceleration considered for RUN 1 and RUN 2 are 530 mm/s^2 and 1120 mm/s^2 shown in Table 4.4. The displacement time history response measured at the middle of the top slab of flanged shear wall has been computed using the Newmark Beta method of direct time integration and for brevity; only the maximum displacements have been shown in Table 4.4. The response has been computed at discrete time interval of 0.01 seconds. The total steps used for the computation of response are 1000.

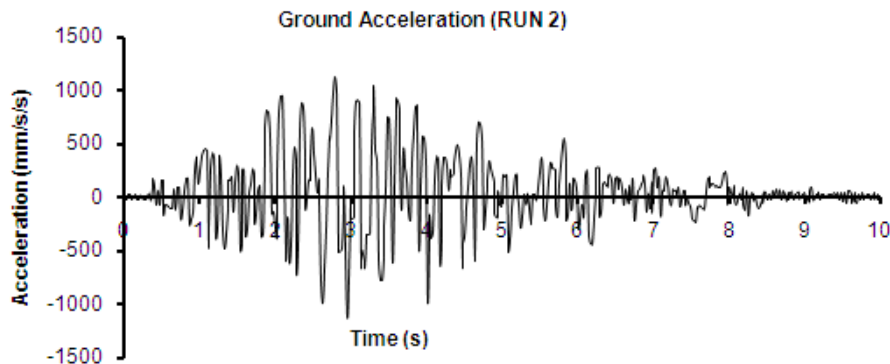


Fig. 4.16: Earthquake ground motion applied at the base of the structure

Table 4.4: Comparison of displacement response of present study with Jagd (1996)

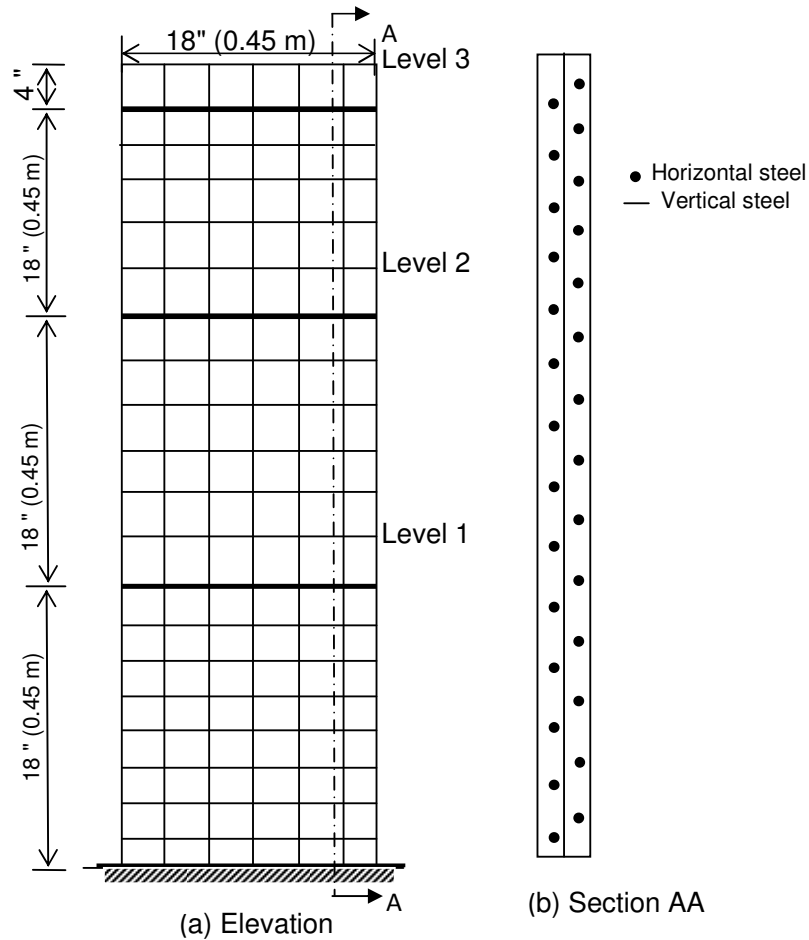
RUN	Peak Ground Acceleration (mm/s ²)	Displacements at the middle of the top slab (mm)			
		Jagd (1996) (Experimental)	Jagd (1996) (Analytical)	Present study (Analytical)	
				3-D Analysis	2-D Analysis
1	530	0.290	0.250	0.272	0.283
2	1120	0.580	0.735	0.418	0.492

Table 4.4 shows the comparison of the displacement response obtained via the present analytical study with the experimental and analytical investigations reported by Jagd (1996). It is observed that the present analytical study predicts the maximum displacement response closer to the experimental results than the analytical study reported by Jagd (1996). Hence, it is concluded that the assumed strain based degenerated shell element is capable of modeling the complex geometry such as flanged shear wall with reinforcements. It is also interesting to note that with 2D analysis, the results have been found to be much closer to the experimental results. On the other hand, the 2-D analysis can be considered a viable alternative to the time consuming 3-D analysis. Nevertheless, it remains to be seen whether 2-D analysis still possess same accuracy in predicting the displacement response of RC shear wall under non-linear dynamic loading conditions.

Analysis of slender shear wall- non-linear dynamic analysis

In order to perform the non-linear analysis of RC shear wall under dynamic loading conditions, the rectangular shear wall, shown in Fig. 4.19, has been discretized into 120 finite elements using 9-noded 5-dof assumed strain based degenerated shell element with layered approach. The geometry of the shear wall, its elevation [Fig. 4.17(a)] and longitudinal section [Fig. 4.17(b)] are the same as analyzed by Agarwal et al. (1981).

The material properties of RC shear wall are as mentioned in Table 4.5. The reinforcement is provided in two layers in horizontal direction and a single layer in vertical direction. The diameter of the reinforcing bar used as vertical and horizontal reinforcement is 4 mm diameter. In order to incorporate the effect of steel reinforcement, the layered approach is adopted in this study.


Fig. 4.17: Finite element idealization of rectangular shear wall
Table 4.5: Material properties of concrete and steel

Concrete				Reinforcing Steel			
Units	Elasticity Modulus	Yield strength in compression	Tensile strength	Elasticity Modulus	Strain hardening modulus	Yield stress	
						Vertical	Horizontal
psi	3.8×10^6	4720	409	2.9×10^7	7.03×10^4	53,500	53,500
MPa	26200	32.54	2.82	199947.9	48.5	368.8	368.8

The steel is modeled as a smeared layer of equivalent thickness. The properties of the steel are assumed constant in that layer. The bi-linear stress strain curve with linear elastic and strain hardening region is adopted in this study. The simulated EL Centro earthquake, shown in Fig. 4.18, is applied at the base of the shear wall with maximum amplitude or 1.05g.

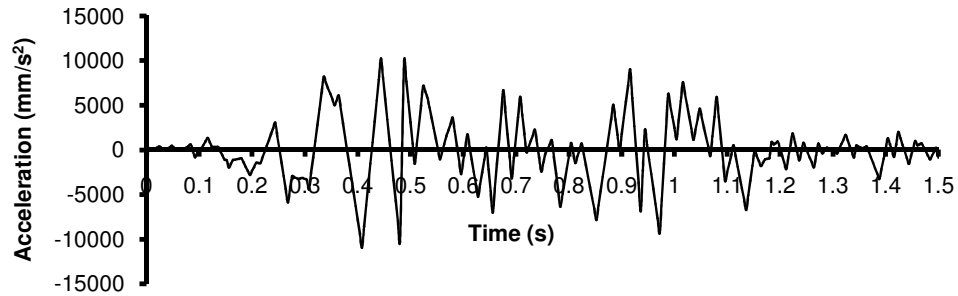


Fig. 4.18: Input ground acceleration applied at the base of shear wall

The response of the structure is traced for 1.5 seconds of duration. Several investigators have also adopted this way of response calculation by predicting the response only for the most intense earthquake period in order to simplify the computation. Fig. 4.19(a) and Fig. 4.19(b) show the experimental and analytical displacement time history responses, respectively, of RC shear wall subjected to scaled EI Centro ground motion as reported by Lefas et al. (1990). There is a considerable difference between the observed experimental response and analytical response reported by Agarwal et al. (1981). Though the maximum displacement response from both analytical and experimental approach is not much different, the shape of the displacement time history is different, especially for the duration from 0.4 seconds to 1.0 seconds. Fig. 4.20 shows the displacement time history response of RC shear wall proposed in the present study. The proposed analytical study also matches more with their analytical study reported by Lefas et al. (1990) than the experimental results.

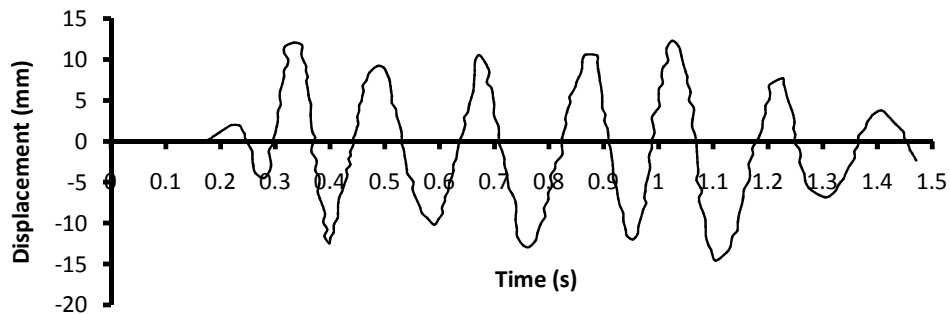


Fig. 4.19(a): Experimental displacement time history of the shear wall (Hsu et al. 1981)

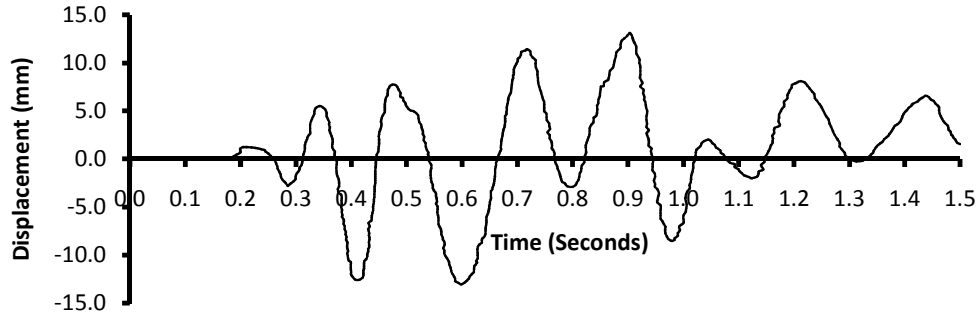


Fig. 4.19(b): Analytical displacement time history of the shear wall (Agarwal et al. 1981)

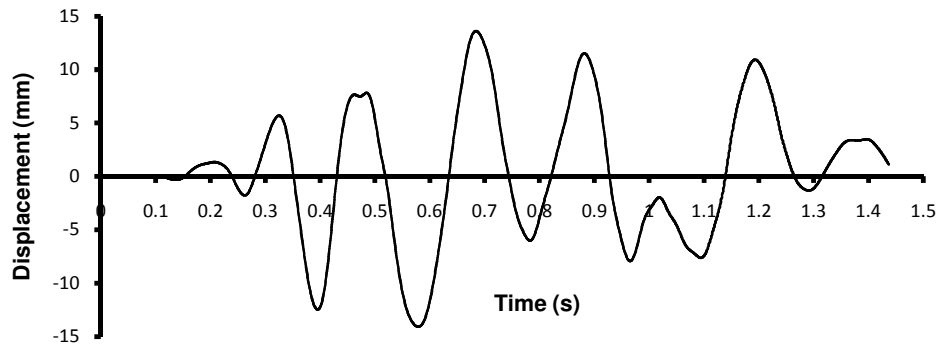


Fig. 4.20: Displacement response history response of shear wall subjected to scaled EL Centro earthquake 1940 (Present study)

It is concluded that the present proposed analytical study predicts the displacement time-history response of RC shear wall reasonably well for most of the duration. There is not much variation in the profile of the time-history as well.

Table 4.6: Displacement responses at different times

Time	Displacement (mm) (Agarwal et al. 1981)	Displacement (mm) (Present study)
0.1	0	0
0.2	1	1
0.3	-1	1
0.4	12.5	13.0
0.5	5	3
0.6	12	14
0.7	11	14

Time	Displacement (mm) (Agarwal et al. 1981)	Displacement (mm) (Present study)
0.8	2	5
0.9	13	12
1.0	8	4
1.1	2	6
1.2	8	11
1.3	0	1
1.4	4	4
1.5	1	0

4.10 Element Sensitivity Analysis

The sensitivity analysis has been performed by analyzing the 5-storeyed shear wall using 9-noded 5-degree of freedom degenerated shell element for three different mesh sizes. The mesh sizes considered in the present study are $2\text{ m} \times 0.5\text{ m}$ (140 elements), $1\text{ m} \times 0.5\text{ m}$ (280 elements), and $0.5\text{ m} \times 0.5\text{ m}$ (560 elements). Fig. 4.21 shows the load-displacement response of shear wall with three different mesh sizes. Table 4.7 shows the ultimate load carrying capacity and ultimate displacement of shear wall subjected to three different mesh sizes.

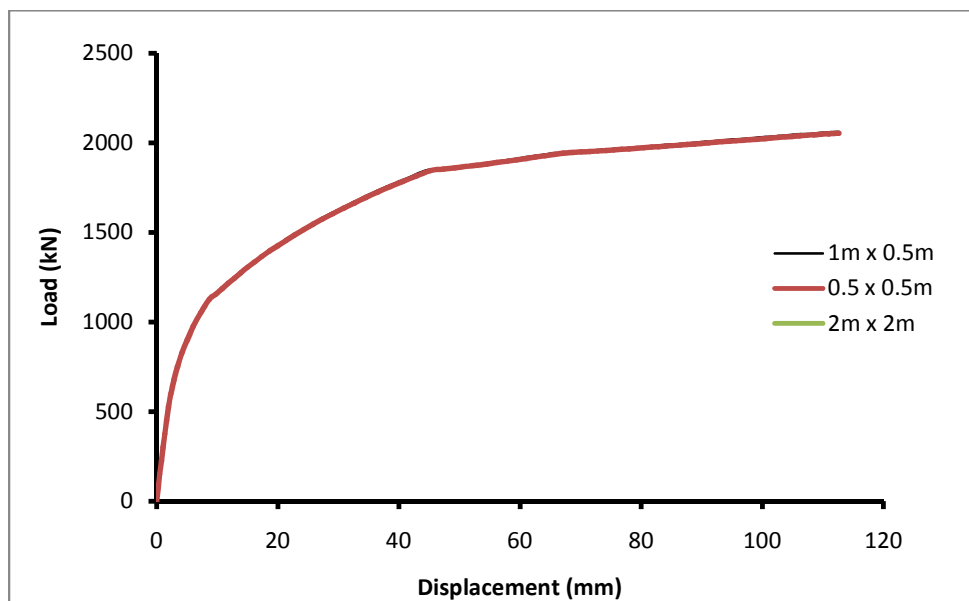


Fig. 4.21: Load-displacement response of squat shear wall for different mesh sizes

Table 4.7: Comparison of responses for different mesh sizes

Mesh size	No. of elements	Ultimate Load carrying capacity (kN)	Ultimate displacement (mm)
2 m × 0.5 m	140	2083.5	124.2
1 m × 0.5 m	280	2062.5	112.6
0.5 m × 0.5 m	560	2053.5	112.6

The ultimate load carrying capacity and ultimate displacement of shear wall discretized with 140 elements is 2083.5 kN. However, when the number of elements is doubled, the ultimate load carrying capacity is 2062.5 kN and ultimate displacement is 112.6 mm. The decrease in the ultimate load carrying capacity and ultimate displacement is 1% and 10% respectively when the number of elements is doubled (increased to 280 from 140). It essentially means that as the number of elements is increased, the ultimate load carrying capacity gets decreased and so as ultimate displacement. Further increase in number of elements decreases the ultimate load carrying capacity further only by 0.5%, but there is no further change in the ultimate displacement. Hence, it suggested going either for 280 elements or 560 elements.

4.11 Summary

In this chapter, the assumed strain based degenerated shell element formulation is discussed. The formulation of mass and damping matrices have been discussed. The step-by-step formulation of Newmark Beta method of direct time integration has also been discussed. The validation of finite element software is done for both static and dynamic analyses by comparing the response against standard bench mark problems. It has been concluded that the developed finite element program works well for linear and nonlinear static and dynamic analysis. At the end, the sensitivity analysis has been conducted to identify the mesh size to be adopted to discretize the shear wall.

References:

1. Agrawal, A.B., Jaeger, L.G., and Mufti, A.A. (1981). "Response of RC shear wall under ground motion." *ASCE Journal of the Structural Division*, 107(2), 395-411.
2. Ahmad, S., Irons, B.M., and Zienkiewicz, O.C. (1970). "Analysis of thick and thin shell structures by curved finite elements." *International Journal of Numerical Methods in Engineering*, 2(3), 419-451.
3. Archer G.C., and Whalen, T.M. (2006). "Development of rotationally consistent diagonal mass matrices for plate and beam elements." *Computational Methods Applied Engineering*, 194: 675-689.
4. Auricchio, F., and Sacco, E. (1999). "A mixed-enhanced finite element for the analysis of laminated composite plates." *International Journal for Numerical Methods in Engineering*, 44(10), 1481-1504.
5. Bathe, K.J. (2006). "*Finite element procedures*." Prentice-Hall, Upper Saddle River, New Jersey.
6. Bathe, K.J., Wilson, E.L., and Iding, R.H. (1974). "NONSAP A Structural Analysis Program for Static and Dynamic Response of Nonlinear Systems." *Report No. UC SESM 74-3, Structures and Materials Research, Department of Civil Engineering, University of California, Berkeley*.
7. Belytschko, T., Liu W.K., and Ong, J.S.J. (1985). "Implementation and application of a 9-node Lagrangian shell element with spurious mode control." *Computers & Structures*, 20(1-3), 121-128.
8. Belytschko, T., Ong, W., and Kennedy, J. (1984). "Hourglass control in linear and non-linear problems." *Computer Methods in Applied Mechanics and Engineering*, 43(3), 251-276.
9. Charney, F.A. (2008). "Unintended consequences of modeling damping in structures." *ASCE Journal of Structural Engineering*, 134(4), 581-592.
10. Chopra, A. (2006). "*Dynamics of structures: Theory and application to earthquake engineering*." 3rd Ed., Prentice-Hall, Englewood Cliffs, N.J.
11. Clough, R.W., and Penzien, J. (1993). "*Dynamics of structures*", McGraw-Hill Book Co, New York.
12. Duggal, S.K. (2007). "*Earthquake resistant design of structures*." Oxford Higher Education, Oxford University Press, New Delhi.

13. Dvorkin, E.N., and Bathe, K.J. (1984). "A continuum mechanics based four-node shell element for general nonlinear analysis." *Engineering Computations*, 1(1), 77-78.
14. Gallagher, R.H. (1969). "Analysis of Plate and Shell Structures.", *Proceedings of the Symposium on Application of Finite Element Method in Engineering*, Vanderbilt University, Nashville, USA.
15. Hinton, E., and Owen, D.R.J. (1984). "*Finite Element Software for Plates and Shells*." Pineridge Press, UK.
16. Hrennikoff, A., and Tezcan, S.S. (1966). "Analysis of cylindrical shells by the finite element method." *Symposium of problems of interdependence of design and construction of large span shells for industrial and civic buildings, Leningrad, Russia*.
17. Huang, H.C. (1987). "Implementation of assumed strain shell elements." *Computers & Structures*, 25(1), 147-155.
18. Huang, H.C., and Hinton, E. (1986). "A new nine node degenerated shell element with enhanced membrane and shear interpolation." *International Journal for Numerical Methods in Engineering*, 22(1), 73-92.
19. Huang, H.C. (1989). "*Static and dynamic analyses of plates and shells: theory, software and applications*." Springer-Verlag, New York, USA.
20. Hughes, T.J.R. (1987). "*The finite element method: Linear static and dynamic finite element analysis*." Prentice-Hall, Englewood Cliffs, New Jersey.
21. Hughes, T.J.R., Cohen, M., and Haroun, M. (1978). "Reduced and selective integration techniques in the finite element analysis of plates." *Nuclear Engineering and Design*, 46(1), 203-222.
22. Jagd, L.K. (1996). "Non-linear Seismic Analysis of RC shear wall." *OECD/NEA Seismic Shear wall International Standard Problem on Japanese Seismic Ultimate Response Test*, 5, 515-524.
23. Kant, T., Kumar, S., and Singh, U.P. (1994). "Shell dynamics with three-dimensional degenerate finite elements." *Computers & Structures*, 50(1), 135-146.
24. Lee, W.H., and Han, S.C. (2006). "Free and forced vibration analysis of laminated composite plates and shells using a 9-node assumed strain shell element." *Computational Mechanics*, 39(1), 41-58.
25. Lefas, I.D., Kosovos, M.D., Ambraseys, N.N. (1990). "Behavior of reinforced concrete structural walls, strength, deformation characteristics, and failure mechanism." *ACI Structural Journal*, 87(1), 23-31.

26. Liu, W.K., Belytschko, T., Ong, J.S.J., and Law, S.E. (1985). "Use of stabilization matrices in non-linear analysis." *Engineering Computations*, 2(1), 47-55.
27. Liu, Y., and Teng, S. (2008). "Nonlinear analysis of reinforced concrete slabs using non-layered shell element." *ASCE Journal of Structural Engineering*, 134(7), 1092-1100.
28. MacLeod, I.A. (1969). "New rectangular finite element for shear wall analysis." *ASCE Journal of Structural Division*, 95(3), 399-409.
29. MacNeal, R.H. (1982). "Derivation of element stiffness matrices by assumed strain distributions." *Nuclear Engineering Design*, 70(1), 3-12.
30. Malkus, D.S., and Hughes, T.J.R. (1978). "Mixed finite element methods, reduced and selective integration techniques: a unification of concepts." *Computational Methods in Applied Mechanics & Engineering*, 15(1), 63-81.
31. Meyer, C., and Okamura, H. (1985). "Finite element analysis of reinforced concrete structures." *Proceedings of the US-Japan Joint Seminar on Finite Element Analysis of Reinforced Concrete*, Tokyo, Japan.
32. Newmark, N.M. (1959). "A method of computation for structural dynamics." *ASCE Journal of Engineering Mechanics*, 85(3), 67-94.
33. Ngo, D., and Scordelis, A.C. (1967). "Finite element analysis of reinforced concrete beams." *Journal of American Concrete Institute*, 64(14), 152-163.
34. Owen D.R.G, and Hinton E (1980). "*Finite elements in plasticity, Theory and Practice.*" Pineridge Press Limited, UK.
35. Paswey, S.F., and Clough, R.W. (1971). "Improved numerical integration of thick shell finite elements." *International Journal for Numerical Methods in Engineering*, 3(4), 575-586.
36. Simo, J.C., and Rifai, M.S. (1990). "A class of mixed assumed strain methods and the methods of incompatible modes." *International Journal of Numerical Methods and Engineering*, 29(8), 1595-1638.
37. Teng, S., Liu, Y., and Soh, C.K. (2005). "Flexural analysis of reinforced concrete slabs using degenerated shell element with assumed strain and 3-D concrete model." *ACI Structural Journal*, 102(4), 515-525.
38. Timoshenko, S., and Krieger, S.W. (1959). "*Theory of plates and shells.*" McGraw Hill Publishing Company, pp. 580, USA.
39. Wilt, T.E., Saleeb, A.F., and Chang, T.Y. (1990). "A mixed element for laminated plates and shells." *Computers & Structures*, 37(4), 597-611.

40. Yang, H.T.Y., Saigal, S., Masud, A., and Kapania, R.K. (2000). "A survey of recent shell finite elements." *International Journal for Numerical Methods in Engineering*, 47(1-3), 101-127.
41. Yunhua, L., and Eriksson, A. (1999). "An alternative assumed strain method." *Computational Methods in Applied Mechanics and Engineering*, 178(1-2), 23-37.
42. Zienkiewicz, O.C., and Cheung, Y.K. (1967). "*The finite element method in continuum and structural mechanics.*" McGraw Hill, pp. 272, New York, USA.
43. Zienkiewicz, O.C., Taylor, R.L., and Fox, D.D. (2013). "*The finite element method for solid and structural mechanics.*" 7thEd, Butterworth-Heinemann, Elsevier publication, pp. 672, USA.
44. Zienkiewicz, O.C., Taylor, R.L., and Too, J.M. (1971). "Reduced integration technique in general analysis of plates and shells." *International Journal of Numerical Methods and Engineering*, 3(2), 275-290.

Non-Linear Static Response of RC Shear Wall

5.1 Background

Reinforced Concrete (RC) Shear wall has been considered one of the most viable lateral load resisting elements in resisting wind and earthquake loads. The behavior of RC shear walls is influenced by many factors such as aspect ratio, opening size and its locations. It is generally perceived that the aspect ratio of shear wall plays a crucial role on its structural response, slender being more flexible and squat being more rigid. As outlined in Chapter 2, to meet the functional requirements, shear walls are penetrated with openings of different sizes and at different locations. Though there is a strong consensus that shear walls be penetrated only with smaller openings in order to get the desired structural response, but there is no clarity on the optimum size of openings in shear walls from strength and ductility point of view. Moreover, for a given size of opening in shear wall, it is also essential to investigate the influence of opening location on the strength and ductility responses of RC shear wall. Furthermore, the influence of ductile detailing (strengthening) around the openings on the structural response of RC shear walls is also needed to be investigated. In this chapter, an attempt has been made to determine the response of RC shear walls for its sensitivity to above mentioned parameters by static (pushover) non-linear finite element analysis considering only the material non-linearity.

As discussed in Chapter 4, the assumed strain based locking free 9-noded layered degenerated shell element has been used for the discretization of RC shear wall. The mesh size has been kept uniform throughout the height of the shear wall. For the non-linear finite element analysis, the material non-linearities considered in the analysis are concrete cracking and yielding, yielding of steel and crushing of concrete. The plasticity based five parameter Willam-Warke failure model with associated flow rule and isotropic hardening has been used to define the yield/failure criteria of concrete in compression. The tension modeling of concrete is augmented by the Rankine's tension cut-off criterion with tension stiffening. The modeling of cracks is considered using fixed smeared crack approach. The bi-linear modeling of steel reinforcement has been adopted in the present study to idealize

the steel behavior. To this end, the shear wall panel and five storeyed (squat) & ten storeyed (slender) RC shear walls have been considered and analyzed for different opening sizes and locations. In this chapter, the displacement responses of RC shear walls with and without openings have been predicted by plotting load-deformation response of shear walls without and with strengthening. The parameters viz., ultimate load carrying capacity, displacement at failure and displacement ductility index are considered to assess the performance of shear wall.

5.2 Influence of Openings on the Static Response of Shear Wall Panel

The reinforced concrete shear wall tested by Lefas et al. (1990) has been considered for the present study in order to assess the influence of opening location on the displacement response of shear wall panel with top and bottom beams. The geometry and section of shear wall specimen is as shown in Fig. 5.1(a) and (b). The wall panel is 650 mm wide \times 1300 mm high \times 65 mm thick. The height to width ratio of wall panel (aspect ratio) is two, thus representing the squat type of shear wall. While the upper beam provides anchorage for vertical reinforcement, lower beam provides the base for wall panel. The element size used to discretize the shear wall panel is 65 mm \times 130 mm which is kept same for the entire structure. The number of degenerated shell elements used to discretize the shear wall panel and beams is 100 and 56 respectively.

The bottom beam has been constrained in all degrees of freedom. The discretized finite element model is shown in Fig. 5.1(c). The elasticity modulus of concrete is 3.27×10^4 MPa and Poisson's ratio is taken as 0.17. The concrete compressive and tensile strengths are as 42.8 MPa and 2.15 MPa, respectively and the crushing strain of concrete is 0.0035. While in the central portion of the shear wall referred as zone I, the conventional reinforcement is provided, the edges of the shear wall are strengthened by providing the additional reinforcement and are identified as zone II. The percentages of reinforcement of steel in x-direction and y-direction are 0.8 & 2.1 in zone I and 1.2 & 3.3 in zone II. Irrespective of the zones, the yield stresses of steel in the x- and y-direction are 520 MPa and 470 MPa respectively. The hardening modulus of concrete and steel are assumed to be 3.27×10^3 MPa and 2.00×10^4 MPa, respectively. The vertical reinforcement (y-direction) is provided in two layers and horizontal reinforcement (x-direction) is concentrated in single layer. For the finite element modeling the reinforcement is considered to be smeared within the

element. The lateral load has been applied at the middle of top slab and has been incrementally increased till the failure of the shear wall panel. The displacement response has also been ascertained at the loaded point. For the non-linear analysis, the stiffness matrix is modified at the end of every load step.

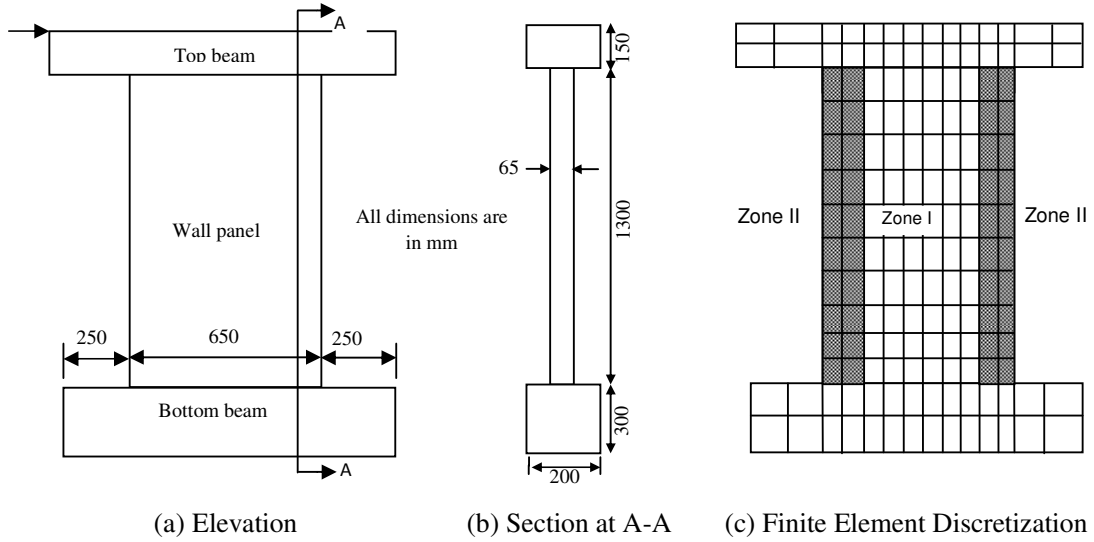


Fig. 5.1: Geometry of solid RC shear wall panel

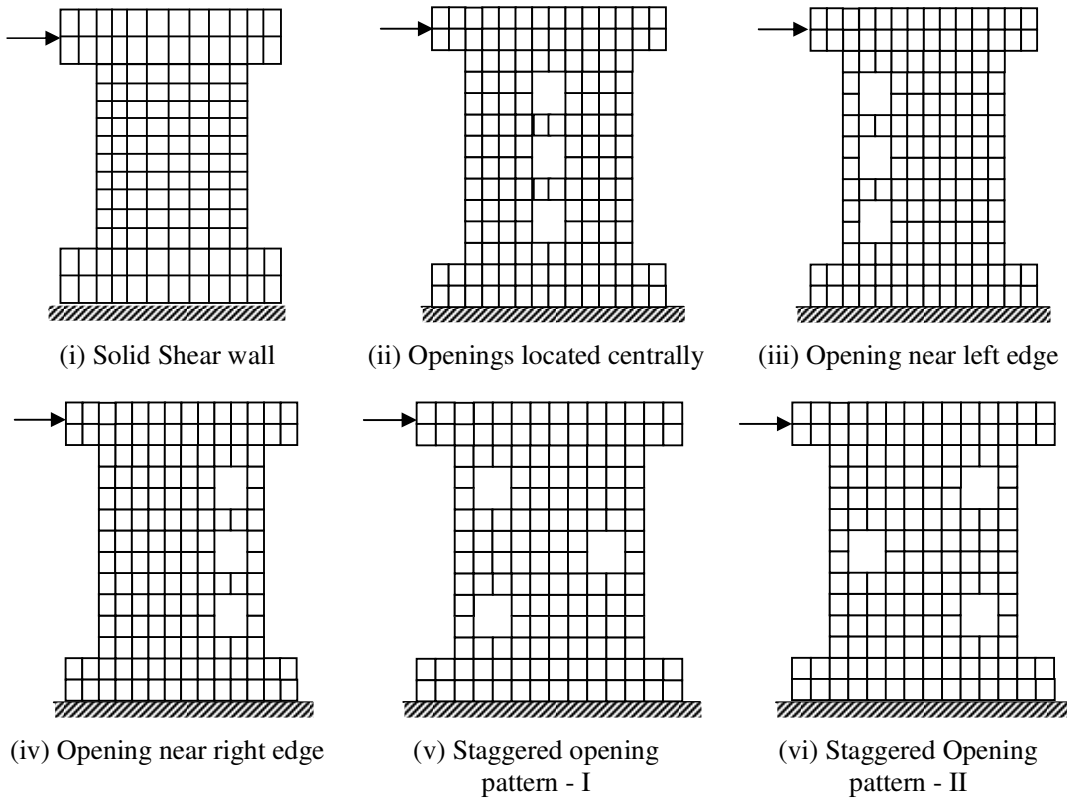


Fig. 5.2: Shear wall panel with different opening locations

As outlined in Chapter 3, the tension stiffening constants α_{ts} and ε_{ts} are taken as 0.8 and 0.0020 respectively. In order to determine the influence of opening locations on the structural response, the shear wall panel has been pierced with 12% opening. The number of openings considered for each shear wall panel is three and the size of each opening is 130 mm \times 130 mm, thus resulting in aspect ratio of opening equal to unity. The openings are positioned at different locations of shear wall panel as shown in Fig. 5.2. Fig 5.2 (i) has been considered as the control specimen with respect to which the behavior of other specimens (Figs. ii - vi) has been ascertained. In present study the failure stage of shear wall has been arrived at when there is severe cracking and yielding and consequently, converged solution could not be achieved even after several iterations for a time step.

The load-deformation response of shear wall with various opening locations has been plotted in Fig. 5.3. Fig. 5.4 shows the yield pattern predicted for shear wall with different opening locations. The complete summary in terms of ultimate load carrying capacity, collapse displacement and ductility index is given in Table 5.1. It is observed from Fig. 5.3 when the openings are provided, the ultimate load carrying capacity decreases with respect to solid shear wall. Though cracking of shear wall started at early stages of loading, however, the failure of all shear wall panels took place due to the yielding of steel reinforcement followed by severe crushing of concrete regardless of the location of opening.

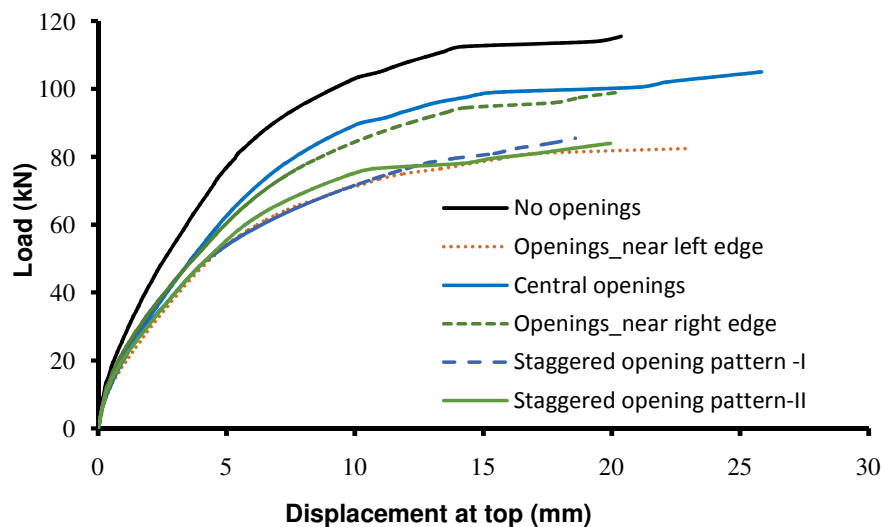


Fig. 5.3: Load-displacement response of RC shear wall panel

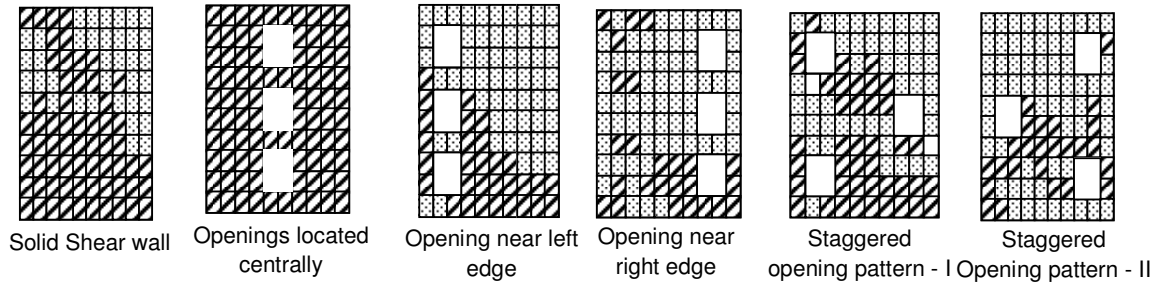


Fig. 5.4: Yield pattern of shear wall panel with various opening locations

Table 5.1: Ductility index and strength ratio of shear wall panel with various opening locations

Opening locations	Elements yielded in panel (out of 100)	Load (kN) at		Displacement (mm) at		Ductility index $\mu_{\Delta} = \Delta_u / \Delta_y$	Strength ratio, (P_u / P_y)
		Yield (P_y)	Collapse (P_u)	Yield (Δ_y)	Collapse (Δ_u)		
No opening	63	49.5	112.5	2.45	20.08	8.20	2.27
Central opening	100	34.5	99.0	2.13	25.69	12.06	2.87
Left opening	30	34.5	79.5	2.41	20.03	8.31	2.30
Right opening	25	37.5	85.5	2.62	20.78	7.93	2.28
Staggered opening pattern-I	41	37.5	84.0	2.58	20.62	7.99	2.24
Staggered opening pattern-II	25	36.0	87.0	2.46	20.95	8.52	2.42

From Table 5.1, it may be observed that the ultimate load carrying capacity and collapse displacement of solid shear wall are 112.5 kN and 20.08 mm respectively. On the other hand, when the shear wall is penetrated with central opening, the ultimate load carrying capacity is 88% of solid shear wall, while the collapse displacement is 21% higher than that of solid shear wall. There is a significant increase in the ductility index of shear wall with central opening. Moreover, the number of yielded elements at the collapse stage is 100, which signifies the fact that the entire shear wall is effective in resisting the lateral loads and in producing the higher collapse displacement. This reflects upon the fact that the ductile failure dominates in the case of shear wall with central opening.

When the shear wall is penetrated with openings located near left edge, the ultimate load carrying capacity is only 70% of the solid shear wall, while the collapse displacement is almost same as that of solid shear wall and hence, there is only a marginal increase in the ductility index of shear wall. In fact, the collapse load of shear

wall with left opening has been found to be the lowest amongst all opening locations. This is partly due to the fact that openings are located on the tension side of shear wall and hence resulted in early collapse. Moreover, the number of elements yielded at collapse is only 30% and hence the complete shear wall is not utilized in resisting lateral loads and displacements.

When the shear wall is penetrated with right opening, the load carrying capacity is 76% of solid shear wall. Nevertheless, only 25% elements yielded in comparison to central opening. Moreover, around 40% of total yielded elements have been concentrated on the compression zone and most of them are located near the bottom of the panel. The ductility index has also been found to be the lowest amongst all cases, signifying the sudden failure as compared to central opening.

When the shear wall is penetrated with staggered openings I, yield displacement has been comparatively higher than that of central opening. But, the ultimate load carrying capacity is reduced substantially with respect to central opening. 41% of elements yielded at the collapse stage. On the other hand, in the case of staggered opening-II, only 25% elements yielded and the behavior is closer to that of right opening.

Since the response of shear wall with central opening resulted in the maximum number of yielded elements apart from possessing higher ultimate load carrying capacity, higher ultimate displacement and higher ductility than other opening locations, it is suggested to provide central openings in the shear wall panel.

5.3 Influence of Opening Size on Structural Response of Slender and Squat Shear Wall

The behavior of the shear wall is strongly influenced by the presence of openings. It is essential to know the limiting size of openings in shear wall beyond which it becomes unserviceable or unsafe. Since the short shear walls have been found to possess very high load carrying capacity, the presence of openings in short shear wall may not alter the behavior significantly. Moreover, from the functional point of view, short shear walls with one or two storeys are not normally provided with openings and hence short shear walls with openings are not the part of this study. Since openings result in stress concentration, the portion of shear wall around the openings is generally strengthened by

providing reinforcements around the openings as per codal provisions (IS 13920-1993) and the same is shown in Fig. 5.5.

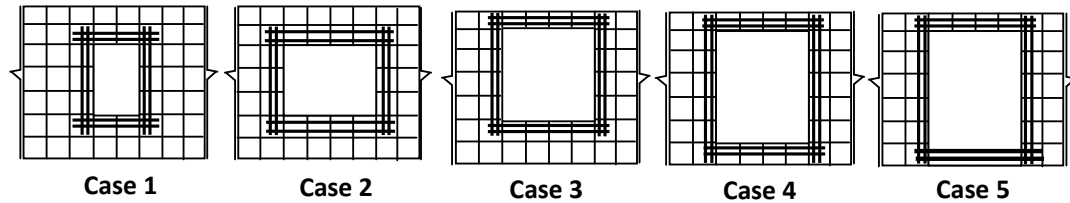


Fig. 5.5: Ductile detailing (strengthening) around openings for a typical storey

The present section investigates the influence of opening size and strengthening on the displacement structural response of squat shear walls (5 storeys) and slender shear walls (10 storeys). In each storey, only one opening is provided and the size of the opening has been kept uniform throughout the height of shear wall. The width, thickness, and storey height of squat and slender shear walls are 8 m, 0.3 m, and 3.5m respectively. The total height of squat and slender shear walls considered in this study is 17.5 m and 35 m respectively as shown in Fig. 5.6 and Fig. 5.7. The aspect ratio of slender shear wall is 4.4 while that of squat shear wall is 2.2. The shear walls have been analyzed for five different opening sizes at each storey viz, (i) $1\text{ m} \times 1.5\text{ m}$, (ii) $2\text{ m} \times 1.5\text{ m}$, (iii) $2\text{ m} \times 2\text{ m}$, (iv) $2\text{ m} \times 2.5\text{ m}$, (v) $2\text{ m} \times 3\text{ m}$, which correspond to approximately 5%, 11%, 14%, 18% and 21% openings in each storey.

Shear walls have been discretized using 9-noded 5 degree of freedom assumed strain based locking free degenerated shell elements. For the discretization of shear walls with openings; the mesh size is kept at $0.5\text{ m} \times 0.5\text{ m}$ which has been kept uniform throughout the shear wall geometry due to computational effort involved in preparing customized input data. In order to model steel reinforcement, the layered approach is adopted in this study, wherein, the steel is modelled as a smeared layer of equivalent thickness and the material properties are assumed to be constant in that layer. The bi-linear stress strain curve with linear elastic and strain hardening region is adopted for steel in compression and tension. The horizontal steel reinforcement is provided in two layers and vertical steel reinforcement is provided in single layer. As per the requirements of IS 13920-1993, shear walls are provided with minimum reinforcement ratio of 0.0025 of the gross area in both longitudinal (vertical) and transverse (horizontal) directions in the plane of the wall and the same has been adopted in the present study. For the strengthening of shear walls with openings, the

amount of vertical and horizontal reinforcement provided on the sides of openings is equal to that of the respective interrupted bars. For the pushover analysis, the triangular distribution of lateral loads has been considered and equivalent concentrated lateral loads are applied at the floor levels with maximum load at the top floor and zero at the ground level. The material properties adopted for the shear walls are as mentioned in Table 5.2. The details of geometry for a typical storey of shear wall such as the actual size & percentage of opening, number of elements, in slender as well as in squat shear wall is depicted in Table 5.3.

Table 5.2: Material properties used for the analysis

Material Property	Magnitude
<i>Concrete</i>	
Elasticity modulus	$2.7 \times 10^{10} \text{ N/m}^2$
Hardening modulus	$2.7 \times 10^9 \text{ N/m}^2$
Poisson's ratio	0.17
Uni-axial compressive strength of concrete	$30 \times 10^6 \text{ N/m}^2$
Tensile Strength of Concrete	$3 \times 10^6 \text{ N/m}^2$
Ultimate crushing strain of concrete	0.0035
Tension stiffening coefficient (α_{ts})	0.8
Tension stiffening strain (ϵ_{ts})	0.0020
<i>Steel</i>	
Elasticity modulus	$2.0 \times 10^{11} \text{ N/m}^2$
Hardening modulus	$2.0 \times 10^{10} \text{ N/m}^2$
Yield stress of steel	$50 \times 10^7 \text{ N/m}^2$

Table 5.3: Summary of different opening sizes considered

Case No.	1	2	3	4	5
Opening Size (W × H)	1 m × 1.5 m	2 m × 1.5 m	2 m × 2 m	2 m × 2.5 m	2 m × 3 m
Opening %	5.35% ≈ 5%	10.71% ≈ 11%	14.28% ≈ 14%	17.86% ≈ 18%	21.43% ≈ 21%
Number of elements per storey	106	100	96	92	88

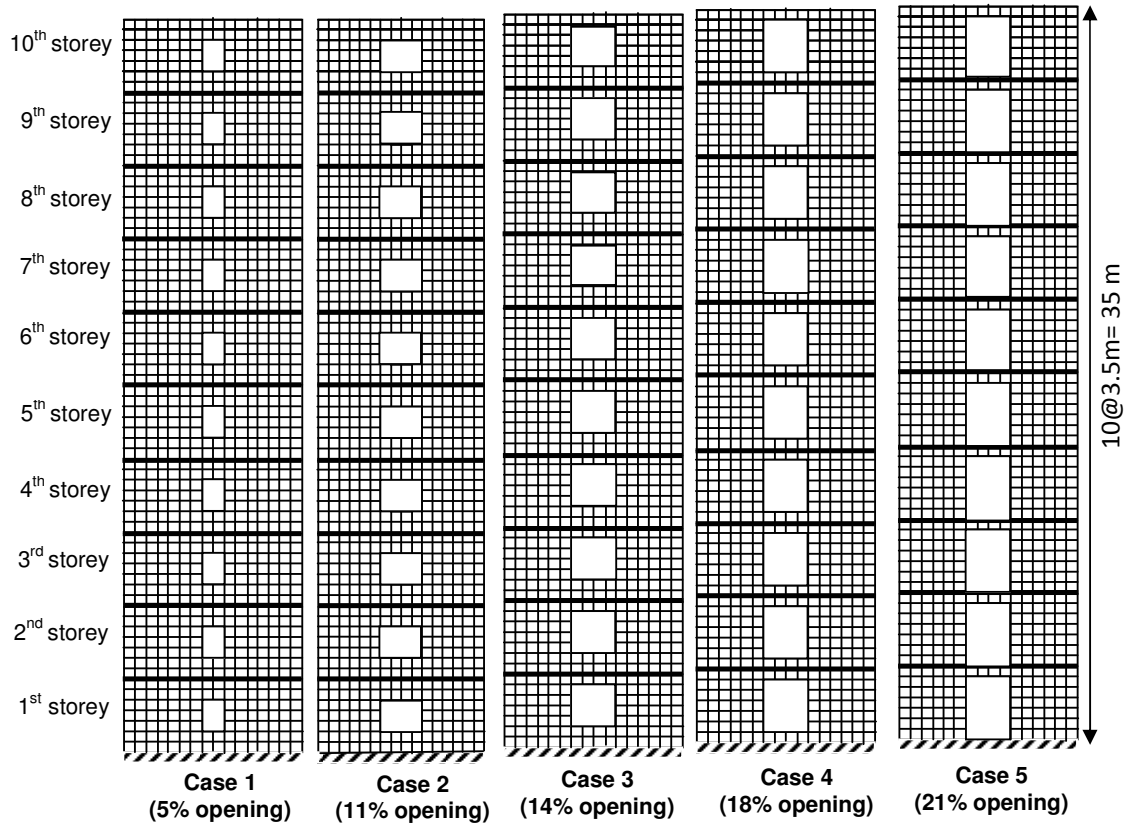


Fig. 5.6: Discretization of slender shear wall with various opening sizes

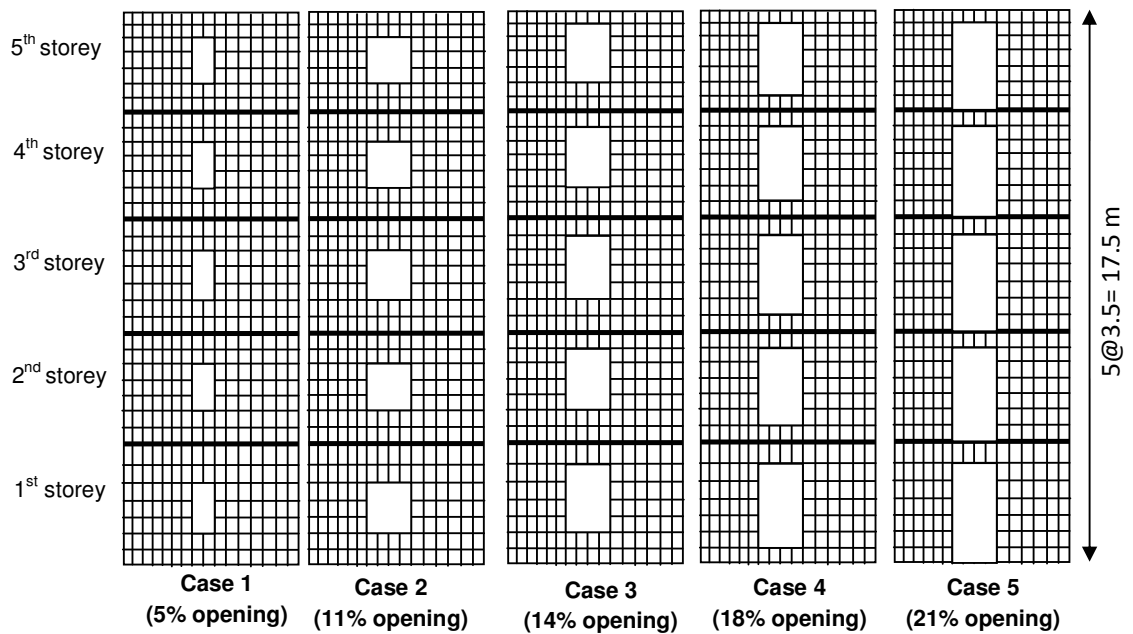


Fig. 5.7: Discretization of squat shear wall with various opening sizes

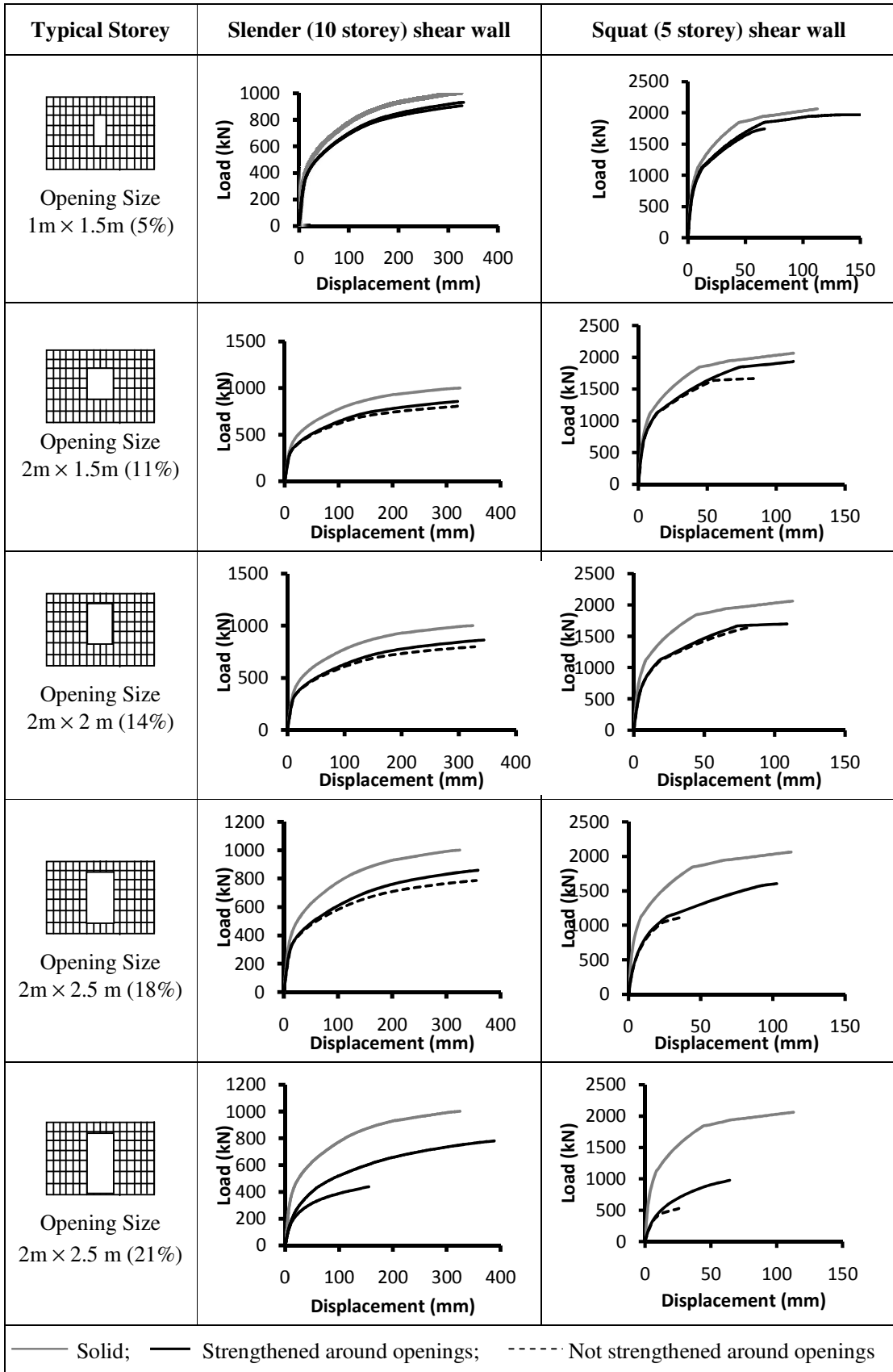


Fig. 5.8: Influence of opening size on the response of slender and squat RC shear wall

5.3.1 Influence of opening size on the ultimate load carrying capacity

Fig. 5.8 shows the load-displacement response of RC slender and squat shear walls for various opening sizes mentioned in Table 5.3. For each opening size, the response of shear wall with opening (with and without strengthening) is compared with solid shear wall. Table 5.5 and 5.6 shows the displacements and loads at yield and ultimate stages for slender and squat shear walls respectively.

From Tables 5.4 and 5.5, it observed that the ultimate load carrying capacity of RC solid shear wall is 1001 kN and 2062 kN for slender and squat respectively. It implies that load carrying capacity of the slender shear wall is around 50% of squat shear wall. It may be observed from the Table 5.4 & 5.5 that in general, when the shear walls are penetrated with openings, the load carrying capacity of shear wall gets decreased with the increase in the opening size. Moreover, when the shear walls are not strengthened around the openings, the ultimate load carrying capacity gets affected to the great extent especially in larger opening sizes, as explained in this section.

Table 5.4: Response of slender shear wall with different opening sizes

Opening size	Not strengthened around openings				Strengthened around openings			
	Yield Disp.	Ult. Disp.	Duct. Index	Ult. Load	Yield Disp.	Ult. Disp.	Duct. Index	Ult. Load
Nil	120	324.7	2.71	1001.0	120	324.7	2.71	1001.0
5%	132	329.1	2.49	907.5	132	330.8	2.51	932.3
11%	129	320.4	2.48	808.5	130	319.9	2.46	858.0
14%	132	327.8	2.48	797.5	140	343.8	2.46	863.5
18%	145	355.1	2.45	786.5	158	358.3	2.27	858.0
21%	80	159.0	1.99	440.0	185	387.9	2.10	781.0

Table 5.5: Response of squat shear wall with different opening sizes

Opening size	Not strengthened around openings				Strengthened around openings			
	Yield Disp.	Ult. Disp.	Duct. Index	Ult. Load	Yield Disp.	Ult. Disp.	Duct. Index	Ult. Load
Nil	34	112.6	3.31	2062	34	112.6	3.31	2062
5%	33	70.8	2.15	1755	44	127.7	2.90	1970
11%	29	83.4	2.88	1665	46	112.3	2.44	1935
14%	39	80.6	2.07	1635	42	108.7	2.59	1695
18%	18	38.3	2.13	1125	49	102.6	2.09	1605
21%	12	25.5	1.59	600	38	64.1	1.69	975

Slender shear wall:

The ultimate load carrying capacity of slender shear wall with 5% opening is 907.5 kN (90% strength of solid shear wall) when not strengthened, but increased to 932.3 kN (93% strength of solid shear wall) when strengthened. As expected, the strengthening of shear wall around openings results in the increase in the ultimate load carrying capacity but only marginally. However for slender shear wall with 11% opening, the ultimate load carrying capacity of shear wall without and with strengthening is 808.5 kN (80% of solid shear wall) and 858 kN (86% of solid wall) respectively which shows that the load carrying capacity of slender shear gets reduced as the opening is increased from 5% to 11%. For slender shear wall with 14% opening without strengthening, the ultimate load carrying capacity is close to 80% of solid shear wall, and strengthening results only in marginal increase of around 6% in the ultimate load carrying capacity. For slender shear wall with 18% opening, the ultimate load carrying capacity is close to 80% of the solid shear wall, but increased to 85% upon strengthening. It may be interpreted that the presence of additional steel provided around the openings is not significantly influencing the load carrying capacity of shear wall up to 18% opening. The load carrying capacity of slender shear wall with 21% opening is only 40% of the load carrying capacity of solid shear wall. However, the strengthening of shear wall around the openings resulted in increased load carrying capacity, 78% of solid shear wall which indicates that strengthening around opening is very essential in case of shear wall with 21% opening.

Thus it may be concluded that even without strengthening, for a given shear wall geometry and material characteristics, the opening up to 18% can be considered to be safe from the point of view of ultimate load carrying capacity.

Squat shear wall:

For squat shear wall with small opening (5% opening), the ultimate load carrying capacity of shear wall without and with strengthening is 85% and 95% of solid wall, respectively. It may be noted that for the squat shear wall with 5% opening, strengthening around openings results in increased load carrying capacity. For squat shear wall with 11% opening, the ultimate load carrying capacity of shear wall without and with strengthening is 80% and 93% of solid wall. The stiffened response upon strengthening is clearly visible for squat shear wall for 11% opening. For squat shear wall with 14% opening, the ultimate load carrying capacity is close to 80% of solid shear

wall without strengthening, and strengthening results only in negligible increase of only 2%. However for squat shear wall with 18% opening, the ultimate load carrying capacity is close to 55% of the solid shear wall, but increased to 78% upon strengthening. It may be interpreted that the presence of strengthening is influencing the load carrying capacity of squat shear wall significantly for 18% opening. Hence strengthening is considered essential and beneficial for squat shear walls for 18% opening for better load carrying capacity. The load carrying capacity of squat shear wall with 21% opening is only 29% of the load carrying capacity of solid shear wall. However, the strengthening of shear wall around the openings resulted in increased load carrying capacity, 47% of solid shear wall. That means, even by strengthening the shear wall around openings, 21% opening is not desirable for squat shear walls because of drastic reduction in the load carrying capacity of more than 50%.

On the basis of above discussion, it may be concluded that even without strengthening, for a given shear wall geometry and material characteristics, the 14% opening can be considered to be safe for squat shear wall from the point of view of ultimate load carrying capacity. However, when strengthened around the openings, 18% opening may also be adopted.

5.3.2 Influence of opening size on the displacement response of shear wall

The influence of opening sizes on the ultimate displacement (deformability) and displacement ductility index have been discussed in this section. The displacement ductility index is calculated as the ratio of yield to ultimate displacement. Since the well defined yield point may be very difficult to identify, many researchers have suggested different methods of arriving at the yield displacement. The present study adopts the one based on reduced stiffness equivalent elasto-plastic yield as shown in Fig. 5.9 [Park, 1988]. In this method, the yield displacement is found as the displacement where the secant line drawn at 75% of the ultimate load meets the horizontal line drawn at ultimate load as shown in Fig. 5.9. This way of representing the yield displacement has been considered the most realistic definition for reinforced concrete structures [Park, 1988]. The ultimate displacement and ductility index of slender and squat shear walls are shown in Table 5.4 and 5.5 respectively. For an easier comparison of the ultimate displacement and ductility index of shear wall with different opening sizes, the responses are normalized with respect to solid shear wall.

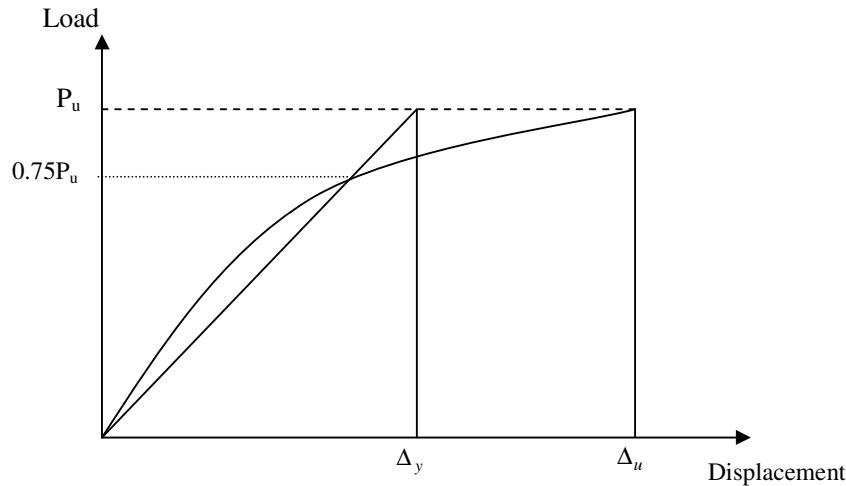


Fig. 5.9: Ductility based on reduced stiffness equivalent elasto-plastic yield

Slender shear wall:

Figs. 5.10 & 5.11 show the ultimate load, ultimate displacement, and ductility index in normalized form for slender shear wall without and with strengthening, respectively. For slender shear wall with 5% opening, the yield displacement and ultimate displacement of slender shear wall are approximately same for both un-strengthened and strengthened cases and hence, there is not much variation in the displacement ductility index (Table 5.4). The ductility index is 2.49 when not strengthened, but increased slightly to 2.51, when strengthened. The normalized ultimate displacement and ductility index is only 1.01 and 0.92 when not strengthened, but remains at 1.02 and 0.91 when strengthened. As expected, the strengthening does not increase in the ductile behavior.

For slender shear wall with 11% opening, the ductility index is only 2.48 when not strengthened, but decreased slightly to 2.46, when strengthened. This is due to the fact that the ultimate displacement and yield displacement of slender shear wall are approximately same for both un-strengthened and strengthened. The normalized ultimate displacement and ductility index is only 0.99 and 0.92 when not strengthened, but remains at 0.99 and 0.91 when strengthened. It may be interpreted that the strengthening does not result in impacting the ductile behavior.

From Table 5.4, it may be observed that for slender shear wall with 14% opening, the ductility index is only 2.48 when not strengthened, but decreased slightly to 2.46, when strengthened. The ultimate displacement of slender shear wall is 328 mm when un-

strengthened, but increased to 344 mm when strengthened. The normalized ultimate displacement and ductility index are 1.01 and 0.92 when not strengthened, but changed to 1.06 and 0.91 when strengthened. Hence, for shear wall with 14% opening, the increase in the ultimate displacement is offset by the corresponding increase in yield displacement, thus resulting in an unaltered displacement ductility index. However, it may be interpreted that the strengthening results in the ductile behavior for 14% opening.

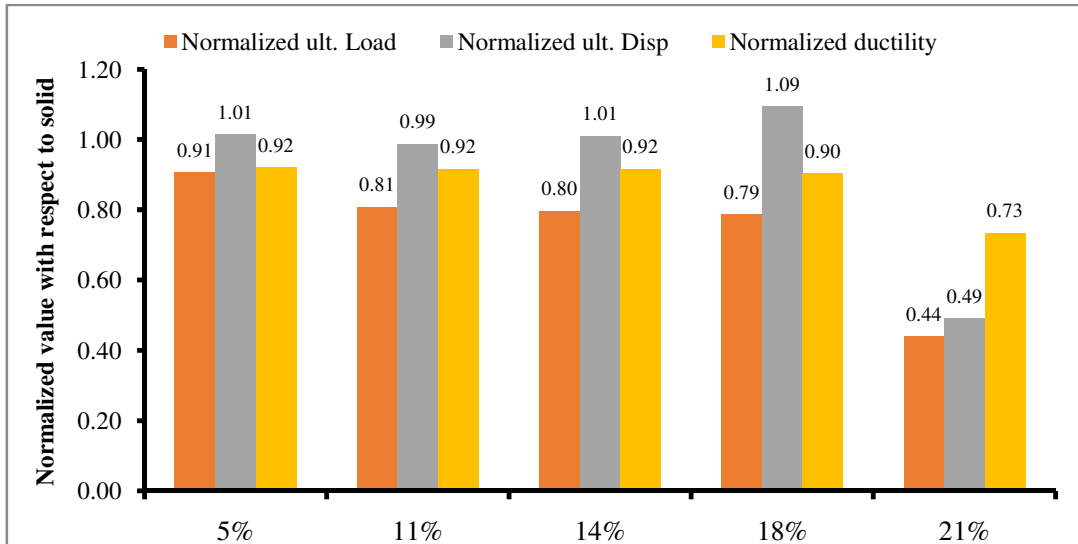


Fig. 5.10: Normalized ultimate load, ultimate displacement and ductility of slender shear wall with different openings without strengthening

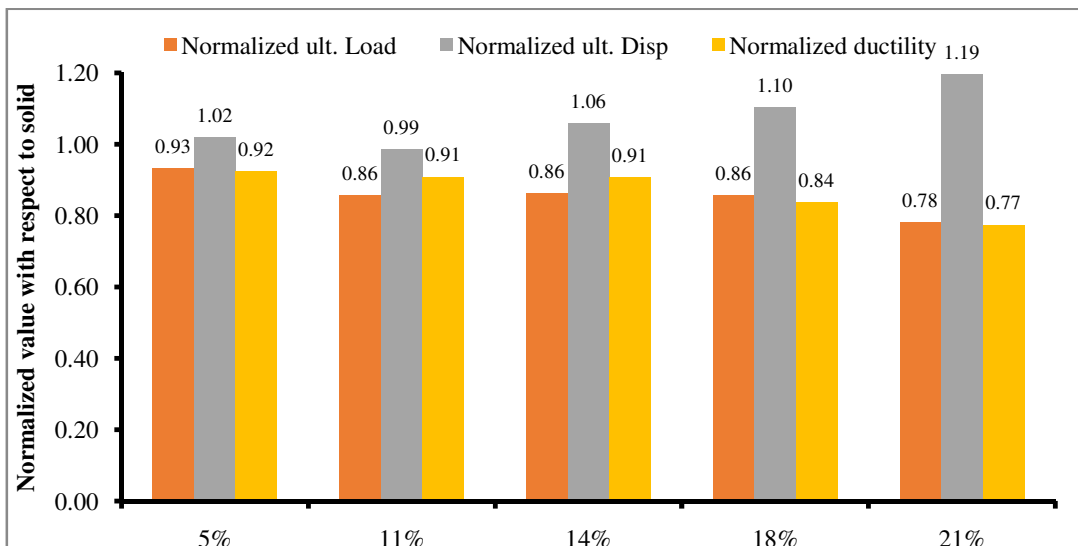


Fig. 5.11: Normalized ultimate load, ultimate displacement, ductility of RC slender shear wall with different openings with strengthening

For slender shear wall with 18% opening, the ductility index is 2.45 when not strengthened, but decreased to 2.27, when strengthened. The ultimate displacement of slender shear wall is 355 mm when un-strengthened, but only increased to 358 mm when strengthened. That means, not much change is observed in the ultimate displacement upon strengthening. The normalized ultimate displacement and ductility index are only 1.09 and 0.90 when not strengthened, but changed to 1.10 and 0.84 when strengthened. The displacement ductility index when strengthened has been found to be reduced due to the higher yield displacement. It is clear that the strengthening results in stiffening effect but not enhancing the ductility as such.

For slender shear wall with 21% opening, the ductility index is 1.99 when not strengthened, but slightly increased to 2.10, when strengthened. The ultimate displacement of slender shear wall is 159 mm when un-strengthened, but shot up to 387.5 mm when strengthened. The normalized ultimate displacement and ductility index are only 0.49 and 0.73 when not strengthened, but rose to 1.19 and 0.77 when strengthened. It is clear that the strengthening has been considered very essential in enhancing significantly the ultimate displacement and marginally the displacement ductility index.

Squat shear wall:

Figs. 5.12 & 5.13 show the ultimate load, ultimate displacement, and ductility of squat shear wall in normalized form without and with strengthening, respectively.

From Table 5.5, it may be observed that for squat shear wall with 5% opening, the ductility index is 2.15 when not strengthened, but increased to 2.90, when strengthened. The ultimate displacement of squat shear wall is 70 mm when un-strengthened, but shot upto 128 mm when strengthened. The normalized ultimate displacement and ductility index are only 0.63 and 0.65, respectively when not strengthened, but rose to 1.13 and 0.88 when strengthened. It is clear that the strengthening has been considered very essential in enhancing the ultimate displacement apart from enhancing ductility index. It may be interpreted that with the help of strengthening around the openings, the ultimate displacement has been satisfactorily increased to some extent with the desired ductile response.

For squat shear wall with 11% opening, the ductility index is 2.88 when not strengthened, but decreased to 2.44, when strengthened. The ultimate displacement of squat shear wall is 83 mm when un-strengthened, but shot upto 112 mm when strengthened. The normalized ultimate displacement and ductility index are only 0.74 and 0.87, respectively when not strengthened, but changed to 1.00 and 0.74 when strengthened. It is clear that the strengthening has been considered very essential in enhancing the ultimate displacement but not much useful to the ductility index. Since the yield displacement went several notches higher, there is a considerable decrease in the ductility index. It may be interpreted that with the help of strengthening around the openings, the ultimate displacement has been satisfactorily increased to some extent but has not helped in getting the desired ductile response.

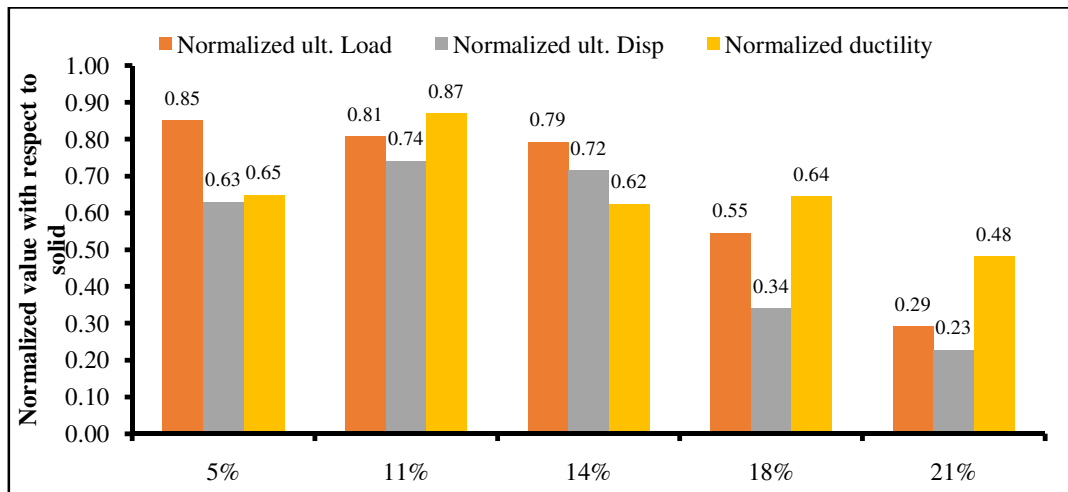


Fig. 5.12: Normalized ultimate load, ultimate displacement, ductility of RC squat shear wall with different openings without strengthening

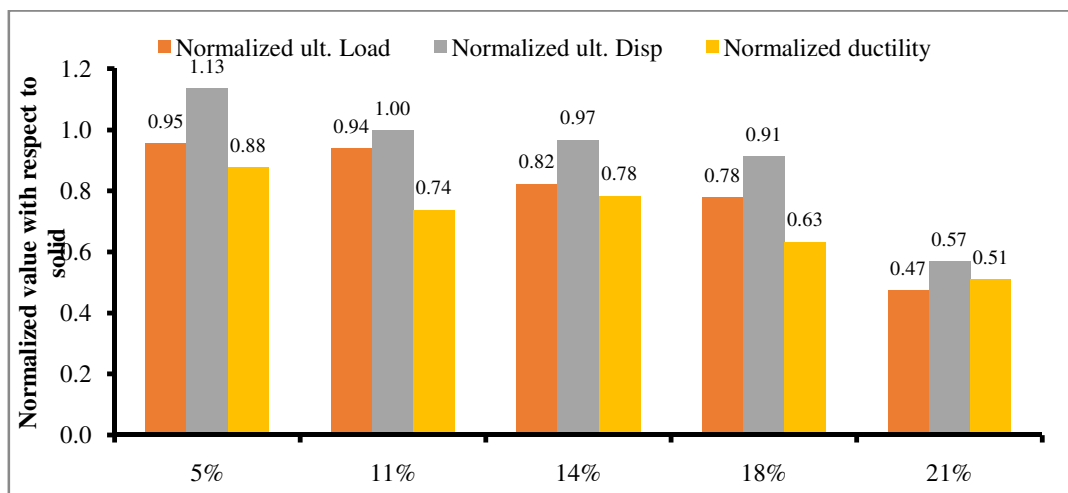


Fig. 5.13: Normalized ultimate load, ultimate displacement, ductility of RC squat shear wall with different openings with strengthening

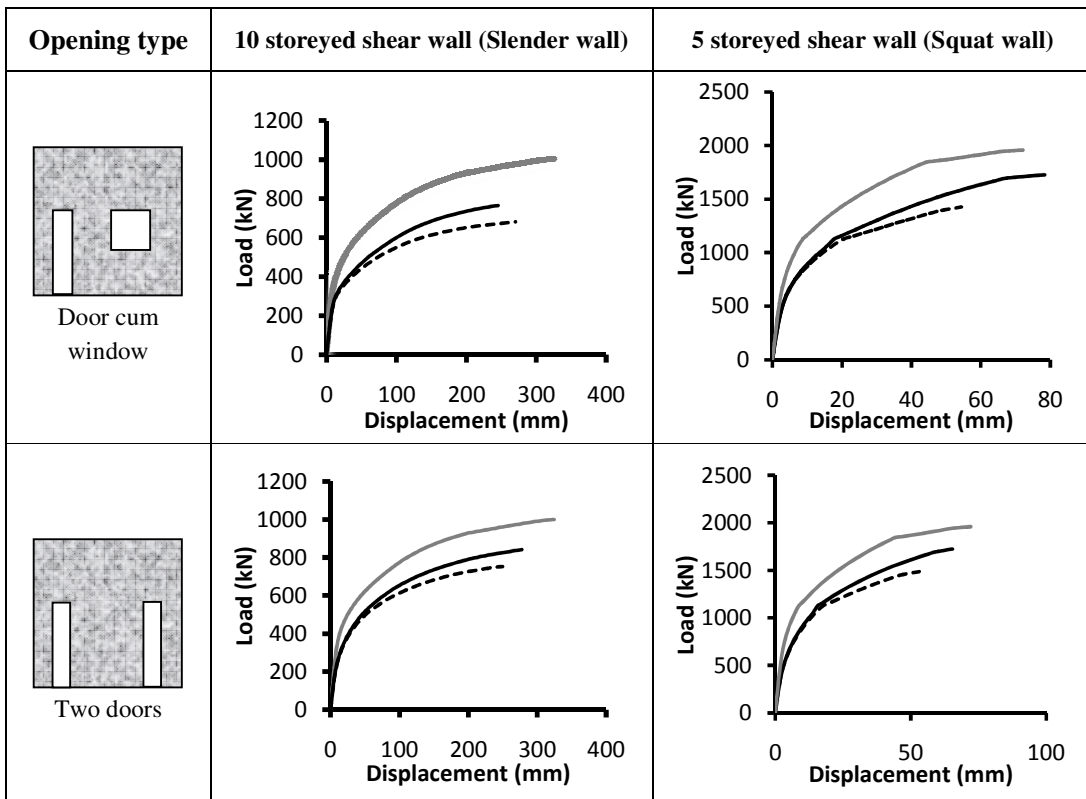
For squat shear wall with 14% opening, the ductility index is 2.07 when not strengthened, but slightly decreased to 2.59, when strengthened. The ultimate displacement of squat shear wall is 80 mm when un-strengthened, but shot upto 109 mm when strengthened. The normalized ultimate displacement and ductility index are only 0.72 and 0.62 when not strengthened, but rose to 0.97 and 0.78 when strengthened. It is clear that the strengthening has been considered very essential in enhancing the ultimate displacement as well as displacement ductility index. Though the yield displacement went few notches higher, it is the ultimate displacement which has gone multi-fold thus resulting in the significant increase in displacement ductility index. It may be interpreted that with the help of strengthening around the openings, the ductility and ultimate displacement have been significantly increased and thus idealizing the desired ductile response.

For squat shear wall with 18% opening, the ductility index is 2.13 when not strengthened, but slightly decreased to 2.09, when strengthened. The ultimate displacement of squat shear wall is 38 mm when un-strengthened, but shot upto 102 mm when strengthened. The normalized ultimate displacement and ductility index are only 0.34 and 0.64 when not strengthened, but rose to 0.91 and 0.63 when strengthened. It is clear that the strengthening has been considered very essential in enhancing the ultimate displacement but displacement ductility index remains unaltered primarily due to higher yield displacement due to strengthening. Nevertheless, it may be interpreted that only with strengthening around the openings; the ductility and ultimate displacement have been satisfactory, elongating the ultimate displacement.

For squat shear wall with 21% opening, the ductility index is only 1.59 when not strengthened, but slightly increased to 1.69, when strengthened. The ultimate displacement of squat shear wall is 25 mm when un-strengthened, but shot upto 64 mm when strengthened. The normalized ultimate displacement and ductility index are only 0.23 and 0.48 when not strengthened, but rose to 0.57 and 0.51 when strengthened. It is clear that the strengthening has been considered very essential in enhancing significantly the ultimate displacement and marginally the displacement ductility index. Nevertheless, it may be interpreted that even with strengthening around the openings, the ductility and ultimate displacement has not been considered satisfactory, characterized by the sudden failure.

5.4 Influence of Door Window Openings on the Response of Slender and Squat Shear Walls

As observed from the last section, when the 14% opening is provided at the centre of each storey, the strength and displacement response of shear wall is not significantly affected due to the strengthening effect and hence 14% opening has been concluded to be the safe opening size. Nevertheless, sometimes, due to practical considerations, it may not be possible to keep openings always at the centre of geometry and multiple openings may need to be located in a building. Hence, the present section investigates the load-displacement response of RC shear walls under various opening combinations and locations. Two representative problems of ten storey (35 m high, 8 m wide and 0.3 thick) and five storey (17.5 m high, 8 m wide, 0.3 thick), behaviorally slender and squat type respectively are chosen and analyzed for monotonic static loading conditions. In total, there are six opening cases considered as the possible opening locations prevailed in practice, viz. (i) door cum window, (ii) two doors (iii) two windows (regular), (iv) three windows, (v) four windows and (vi) two windows (staggered). The mesh size is kept at 1 m × 0.5 m. The geometry and material properties of the shear wall are the same as the previous section. The opening size is kept at 14% for all the cases.



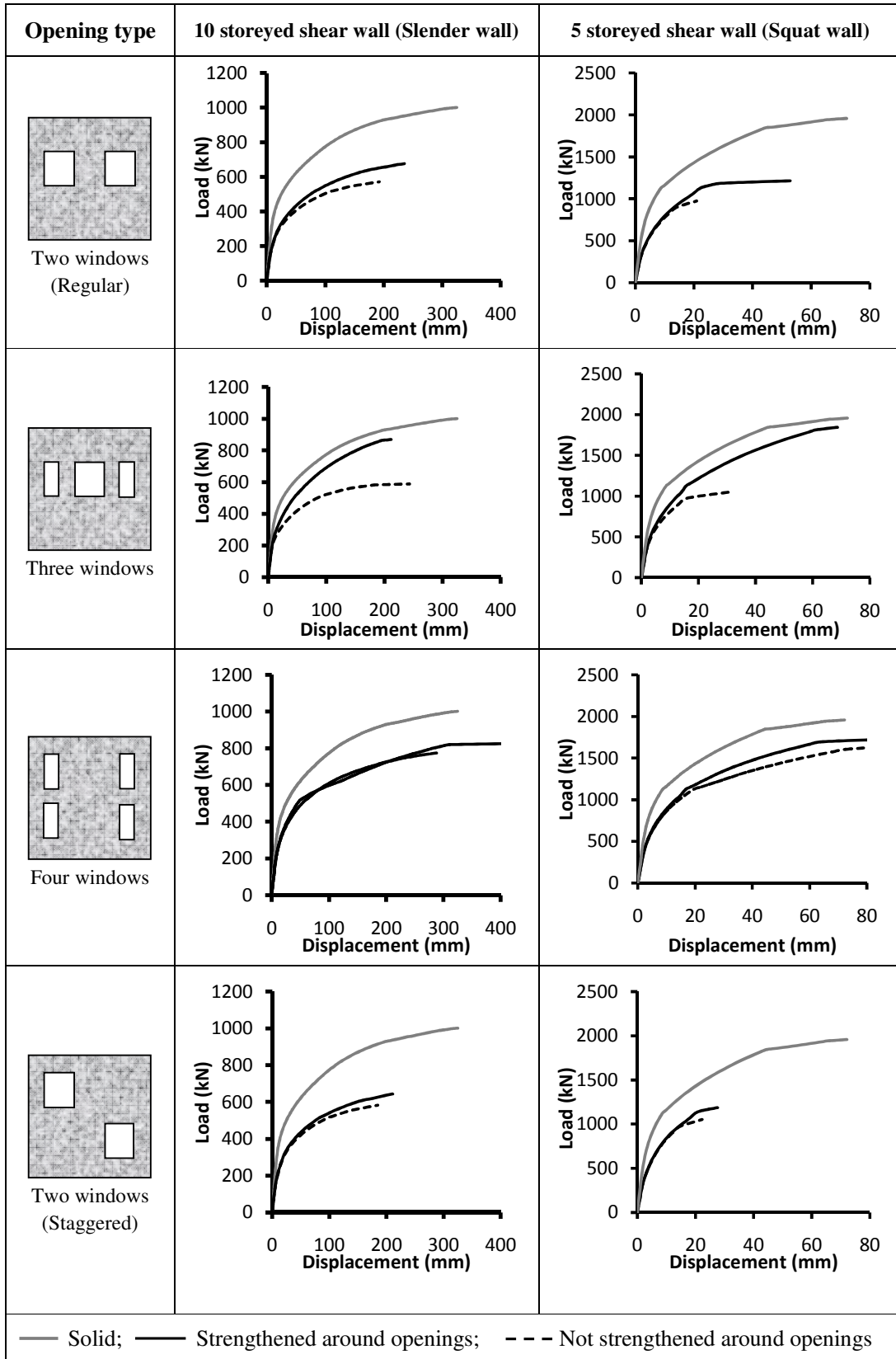


Fig. 5.14: Influence of door window openings on the displacement response of slender and squat shear wall

Fig. 5.14 shows the displacement response of RC shear wall with different opening combinations of doors and windows. Table 5.6 and Table 5.7 show the ultimate load carrying capacity, ultimate displacement, and ductility index of slender shear wall and squat shear wall respectively

Table 5.6: Response of slender shear wall with different door window opening combinations

Opening type	Not strengthened around openings				Strengthened around openings			
	Yield Disp.	Ult. Disp.	Ductility Index	Ult. Load	Yield Disp.	Ult. Disp.	Ductility Index	Ult. Load
No Opening	120.00	324.70	2.71	1001.00	120.00	324.70	2.71	1001.00
Single Central opening	132.00	327.80	2.48	797.50	140.00	343.80	2.46	863.50
Door cum window	102.00	270.50	2.65	682.00	115.00	245.40	2.13	764.50
Two doors	95.00	249.90	2.63	753.50	115.00	277.90	2.42	841.50
Two windows (Regular)	77.00	192.50	2.50	572.00	103.00	235.10	2.28	676.50
Three windows	81.00	243.10	3.00	588.50	113.00	211.70	1.87	869.00
Four windows	110.00	290.70	2.64	775.50	154.00	419.70	2.73	825.00
Two windows (staggered)	78.00	185.00	2.37	583.00	90.00	211.20	2.35	643.50

Table 5.7: Response of squat shear wall with different door window opening combinations

Opening type	Not strengthened around openings				Strengthened around the openings			
	Yield Disp.	Ult. Disp.	Ductility Index	Ult. Load	Yield Disp.	Ult. Disp.	Ductility Index	Ult. Load
No opening	34.00	112.60	3.31	2062.00	34.00	112.60	3.31	2062.00
Single Central opening	39.00	80.59	2.07	1635.00	42.00	108.70	2.59	1695.00
Door cum window	23.00	54.42	2.37	1425.00	39.00	78.40	2.01	1725.00
Two doors	23.00	53.10	2.31	1485.00	33.00	65.34	1.98	1725.00
Two windows (Regular)	11.50	20.92	1.82	975.00	19.00	52.82	2.78	1215.00
Three windows	12.50	30.59	2.45	1050.00	37.00	68.68	1.86	1845.00
Four windows	37.00	85.38	2.31	1635.00	37.00	84.99	2.83	1725.00
Two windows (staggered)	11.70	22.31	1.91	1050.00	15.50	27.58	1.78	1185.00

It may be observed from Table 5.6 & 5.7, when the single square opening is provided in each storey, the load carrying capacity of both squat and slender shear wall is close to 80% of the solid shear wall, increased to 86% when strengthened for slender and increased to 82% for squat as already elaborated in previous section. The following section highlights the behavioral performances of squat and slender shear wall in terms of ultimate load carrying capacity, ultimate displacement and ductility index for different opening combinations keeping the opening size constant.

5.4.1 Influence of door window openings on the load carrying capacity of shear wall

Slender shear wall:

When the openings are provided in the form of door cum window, the load carrying capacity of slender shear wall is around 68% of solid shear wall, when not strengthened, but shot upto 76% upon strengthening. In the door cum window opening, the strengthening significantly increases the load carrying capacity primarily due to the longitudinal steel provided on the sides of the openings. But, openings are not symmetrically located and hence such openings are not desirable in the shear wall.

When openings are provided in the form of two doors without strengthening, the load carrying capacity of slender shear wall is close to 75% of solid wall but shot up to 84% when strengthened. Again, the presence of vertical steel around the openings is critical in enhancing the load carrying capacity. The load carrying capacity of shear wall in the presence of two door openings is significantly better due to the symmetric openings and also due to the vertical steel around the openings. The aspect ratio of opening is also influencing in restricting the damage caused to the shear wall.

When the openings are provided in the form of two windows placed symmetrically without strengthening, the load carrying capacity of slender shear wall is only 57% of solid wall, but increased only to 67% when strengthened. This tremendous reduction in the load carrying capacity is partly due to the fact that the two openings are located at the same level and positioned near the edges of the shear wall. The strengthening of the shear wall around the openings increases the load carrying capacity, but only to some extent. Hence, shear wall with two windows are not desirable from the point of load carrying capacity.

When the openings are provided in the form of two staggered openings without strengthening, the load carrying capacity of slender shear wall is only 58% of solid shear wall, increased only marginally to around 64% when strengthened and hence, the staggered opening suffers from severe degradation in load carrying capacity. The strength degradation is primarily due to the aspect ratio of the opening where the longer side of the opening is located in the direction of loading.

When the openings are provided in the form of three windows without strengthening, the load carrying capacity of slender shear wall is only around 59% of solid wall, but rose to

86% when strengthened. The longer side of the openings is provided in the perpendicular direction of loading and hence the presence of additional vertical steel around the openings results in the significant increase in the load carrying capacity. Moreover, out of 14% opening, 7% is located in the middle portion of the shear wall and 3.5% opening is kept near the edges. Hence, the load carrying capacity is increased significantly upon strengthening, which was not the case in the case of two window openings.

When the openings are provided in the form of four windows without strengthening, the load carrying capacity of slender shear wall is around 78% of solid wall, increased only marginally to 82% when strengthened. Even without strengthening, the load carrying capacity of shear wall is good enough in the presence of four window openings. Such types of openings are desirable in shear wall as the performance is not overly dependent on the strengthening around the openings and there is no weak storey effect on the shear wall due to position of openings.

Squat shear wall:

For squat shear wall with door cum window opening, the load carrying capacity of squat shear wall is close to 70% of solid shear wall, when not strengthened, but shot up to 84% when strengthened. For the two door openings, the load carrying capacity is close to 72% of solid wall but shot up to 84% when strengthened. However, the load carrying capacity of squat shear wall with two window opening is 47% of solid wall, but increased to 60% when strengthened. As envisaged earlier, the longer side of the opening is in the direction of the loading and hence the load carrying capacity is significantly reduced. Moreover, in the presence of two window openings, the severity in the degradation in load carrying capacity is more than that of slender shear wall.

For squat shear wall with three window opening, the load carrying capacity is around 50%, of solid wall, but rose to 90% when strengthened. The softening effect of shear wall observed when not-strengthened is turned significantly into stiffening effect due to strengthening. The strengthening of the openings near edges simulates the boundary elements and hence resulting in the increased load carrying capacity upon strengthening. Nevertheless, such openings are not desirable in shear walls especially without strengthening.

For squat shear wall with four window openings, the load carrying capacity is around 80% of solid wall, increased only marginally to 84% when strengthened. Though the windows are located 1m away from the vertical sides of the shear wall, the aspect ratio of opening is unity and hence the performance of shear wall with four window opening is considered to be possessing good load carrying capacity, as was the case in shear wall with single square opening. Moreover, in this case openings are symmetrically located with respect to the centre line and hence the direction of loading becomes inconsequential on the load and displacement behavior. The openings are not located at one particular level, thus avoiding the storey mechanism of failure.

For squat shear wall with two window openings (staggered), the load carrying capacity is only 51% of solid shear wall, increased only marginally to around 57% and hence, the staggered opening suffers from severe degradation in load carrying capacity even with strengthening and hence such openings are to be avoided.

The behavior of shear wall with two window regular and staggered openings is not very different in terms of load carrying capacity. Since two window openings possess less load carrying capacity even with strengthening, it is suggested to avoid such openings.

5.4.2 Influence of door window openings on the displacement response of shear wall

Fig. 5.15 and Fig. 5.16 show the normalized ultimate load carrying capacity, ultimate displacement and displacement ductility index of squat shear wall without and with strengthening, respectively.

Slender shear wall:

The ultimate displacement of slender shear wall with *door cum window* when not strengthened is 270 mm, but reduced to 245 mm due to strengthening. Hence, strengthening results in slightly stiff behavior of the shear wall and hence there is a reduction in the ultimate displacement when strengthened. The normalized ultimate displacement of shear wall in the presence of door cum window opening is 0.83 when un-strengthened, and reduced to 0.76 when strengthened. Since vertical steel is provided around the door opening and the fact is that the door opening is located on the tension side of the shear wall, strengthening in a way provides the confining effect to some extent. The strengthening results in the reduced ductility (25% reduction) of 2.13 as

against 2.65 when not strengthened. The normalized ductility index for un-strengthened and strengthened is 0.98 and 0.79 respectively. This is consistent to the fact that the ductility decreases with increase in the amount of tension steel at the location. As far as possible, it may be better to keep the openings slightly towards the central region to avoid any undesirable effect.

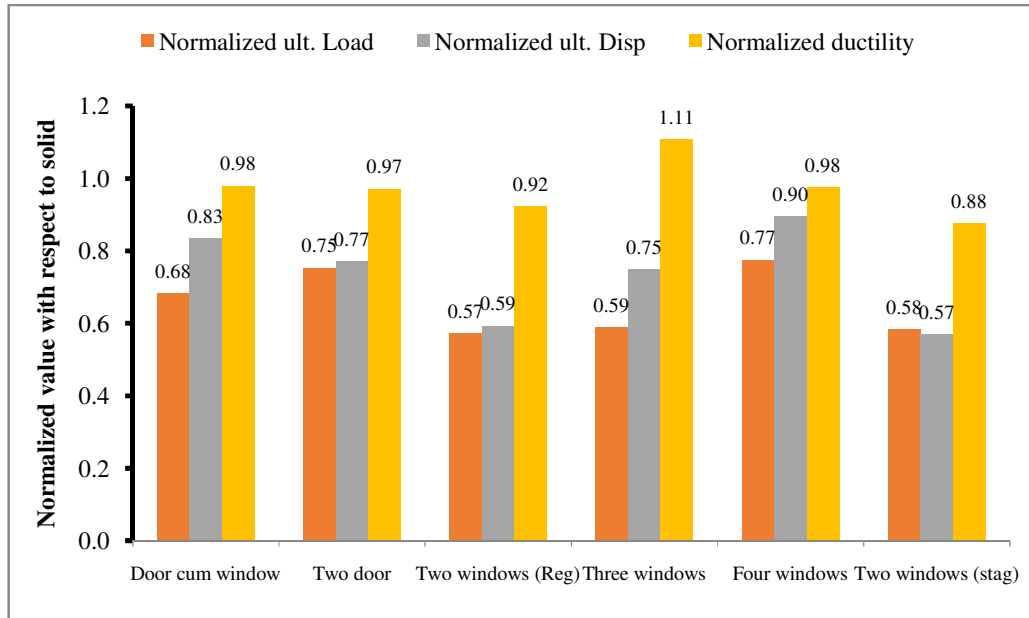


Fig. 5.15: Normalized ultimate load, ultimate displacement, ductility of RC slender shear wall with different door window opening combinations without strengthening

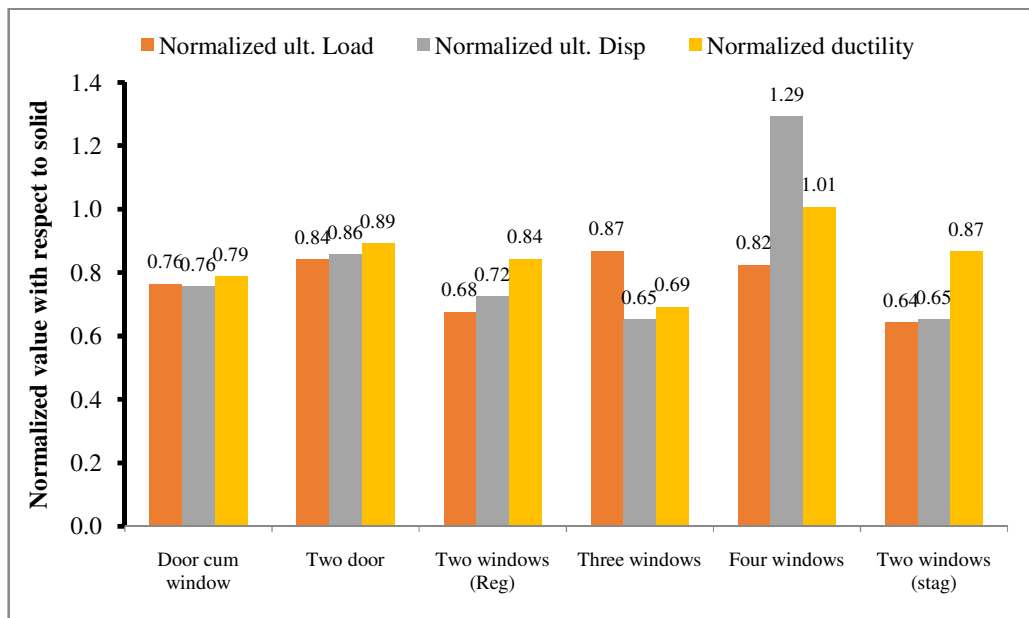


Fig. 5.16: Normalized ultimate load, ultimate displacement, ductility of RC slender shear wall with different door window opening combinations with strengthening

The ultimate displacement of slender shear wall with *two doors* when not strengthened is 249.9 mm, but increased to 277.9 mm due to strengthening. There is a good increase in the yield displacement (21%) and ultimate displacement (11%) when shear wall is strengthened around the openings. When strengthened, the ultimate displacement has not been as affected as the yield displacement and hence there is a reduction in the displacement ductility index of around 9%. The normalized ultimate displacement of shear wall in the presence of door cum window opening is 0.77 when un-strengthened, and increased to 0.86 when strengthened. The normalized ductility index of shear wall for un-strengthened and strengthened is 0.97 and 0.89 respectively. There is not much variation in the ultimate displacement and ductility index due to strengthening partly because the door openings are located symmetrically with respect to the centre line. The amount of tension steel provided on the left vertical edge is offset by the amount of compression steel provided on the right vertical edge. Nevertheless, it may be interpreted that the performance is reasonably satisfactory in terms of load carrying capacity as well as ductility.

The ultimate displacement of slender shear wall with *two window* openings, when not strengthened is 192.5 mm, but increased to 235.1 mm due to strengthening. There is a good increase in the yield displacement (34%) and ultimate displacement (22%) when shear wall is strengthened around the openings. The normalized ultimate displacement of shear wall in the presence of two window opening is 0.59 when un-strengthened, and increased to 0.72 when strengthened. The normalized ductility index of shear wall for un-strengthened and strengthened is 0.92 and 0.84 respectively. When strengthened, the ultimate displacement has not been as affected as the yield displacement and hence there is a reduction in the displacement ductility index of around 9%. Nevertheless, the ultimate displacement of two window opening is way too low as compared to solid shear wall and hence not preferred from displacement point of view.

The ultimate displacement of slender shear wall with *three window* openings, when not strengthened is 243.1 mm, but decreased to 211.7 mm due to strengthening. There is an increase in the yield displacement (40%) and decrease in the ultimate displacement (13%) when shear wall is strengthened around the openings. The normalized ultimate

displacement of shear wall in the presence of door cum window opening is 0.75 when un-strengthened, and decreased significantly to 0.65 when strengthened. Strengthening the shear wall around the openings actually resulted in the reduction of the displacement ductility index by a massive 38%. It is a matter of concern that the strengthening results in reduction in the ultimate displacement and ductility index. Out of three openings, two openings are of size $1\text{ m} \times 1\text{ m}$ and are located at a distance of exactly 1m from the vertical edge of the shear wall. The independent strengthening of those zones around the openings results in the brittle behavior of the shear wall. Such openings are not recommended.

The ultimate displacement of slender shear wall with *four window openings*, when not strengthened is 290.7 mm, but increased to 419.7 mm due to strengthening. There is a good increase in the yield displacement (40%) and ultimate displacement (44%) when shear wall is strengthened around the openings. The normalized ductility index of shear wall for un-strengthened and strengthened is 0.90 and 1.29 respectively. Strengthening the shear wall around the openings resulted in the increase in the ductility index only around by 3%. The good performance of this shear wall is attributed to the fact that the aspect ratio of openings is unity and the openings are symmetrically located with respect to the centre line and hence the direction of loading becomes inconsequential on the load and displacement behavior. As expected, the ductility index also has gone slightly higher upon strengthening.

The ultimate displacement of slender shear wall with *two windows (staggered)*, when not strengthened is 185 mm, but increased to 211.2 mm due to strengthening. There is an increase in the yield displacement (15%) and ultimate displacement (14%) when shear wall is strengthened around the openings. Nevertheless, strengthening the shear wall around the openings resulted in negligible change in the ductility index. The normalized ultimate displacement of shear wall in the presence of two window staggered type opening is 0.57 when un-strengthened, and increased to 0.65 when strengthened. Though there is an increase ultimate displacement, the direction of loading is conducive to create the diagonal cracks, and the fact that openings are also located diagonally, the possibility of cracks getting bridged together is inherently easier in the case of staggered openings. Hence, staggered openings are to be avoided in the shear walls.

Squat shear wall:

Fig. 5.17 and Fig. 5.18 show the normalized responses of squat shear wall with and without strengthening with respect to solid shear wall.

The ultimate displacement of squat shear wall with *door cum window opening* when not strengthened is 54.42 mm but increased to 78.4 mm. Upon strengthening, there is an increase of around 70% and 44 % in the yield displacement and ultimate displacement, respectively. Since, the yield displacement is magnified much higher than the ultimate displacement due to strengthening; there is a reduction in the ductility index to some extent. The normalized ductility index of shear wall for un-strengthened and strengthened is 0.71 and 0.61 respectively.

The ultimate displacement of squat shear wall with *two door opening* when not strengthened is 53.1 mm but increased to 65.34 mm. Upon strengthening, there is an increase of around 43% and 23% in the yield displacement and ultimate displacement respectively. Since, the yield displacement is magnified much higher than the ultimate displacement due to strengthening; there is a reduction in the ductility index to significantly by around 17%. The normalized ductility index of shear wall for un-strengthened and strengthened is 0.70 and 0.60 respectively. The presence of vertical steel around the openings is critical in enhancing the yield displacement more than the ultimate displacement. Essentially, not much difference in responses have been observed between shear wall with door cum window opening and shear wall with two door opening. The slight reduction in the ductility of shear wall with two door opening as against door cum window opening is probably due to the aspect ratio of the opening.

The ultimate displacement of slender shear wall with *two window opening*, when not strengthened is 20.92 mm, but increased to 52.82 mm due to strengthening. There is a good increase in the yield displacement (65%) and ultimate displacement (152%) when shear wall is strengthened around the openings. When strengthened, the ultimate displacement has been increased significantly as compared to yield displacement and hence there is an increase in the displacement ductility index of around 53%.

The ultimate displacement of squat shear wall with *three window opening*, when not strengthened is 30.59 mm, but increased to 68.68 mm due to strengthening. There is a good increase in the yield displacement (196%) and ultimate displacement (124%) when shear wall is strengthened around the openings. The normalized ultimate displacement of shear wall in the presence of three window opening is 0.27 when un-strengthened, and increased significantly to 0.61 when strengthened. Strengthening the shear wall around the openings resulted in the reduction of the ductility index by 25%. The normalized ductility index of shear wall for un-strengthened and strengthened is 0.74 and 0.56 respectively. Since the openings are located at the same level, the aspect ratio of the opening is crucial in attaining better performance. In this case, the longer openings are provided perpendicular to the direction of loading and hence the strengthening results in significant increase in yield displacement due to provision of vertical steel, but ultimate displacement has not increased in the same proportion as yield displacement.

The ultimate displacement of squat shear wall with *four window opening*, when not strengthened is 85.38 mm, but changed slightly to 84.99 mm due to strengthening. There is a negligible change in the yield displacement and ultimate displacement when shear wall is strengthened around the openings. In sequel to that, strengthening the shear wall around the openings has resulted in negligible change in the ductility index. Nevertheless, the normalized ductility index of shear wall for un-strengthened and strengthened is 0.70 and 0.69 respectively.

The ultimate displacement of squat shear wall with *two windows (staggered)*, when not strengthened is 22.31 mm, but increased to 27.58 mm due to strengthening. There is more increase in the yield displacement (32%) and less increase in the ultimate displacement (24%) when shear wall is strengthened around the openings. The normalized ultimate displacement of shear wall in the presence of staggered openings is 0.20 when un-strengthened, and increased marginally to 0.24 when strengthened. The normalized ductility index for un-strengthened and strengthened is 0.58 and 0.54 respectively. Strengthening the shear wall around the openings resulted in 7% decrease in ductility index. The performance of shear wall in the presence of staggered openings has not been considered satisfactory.

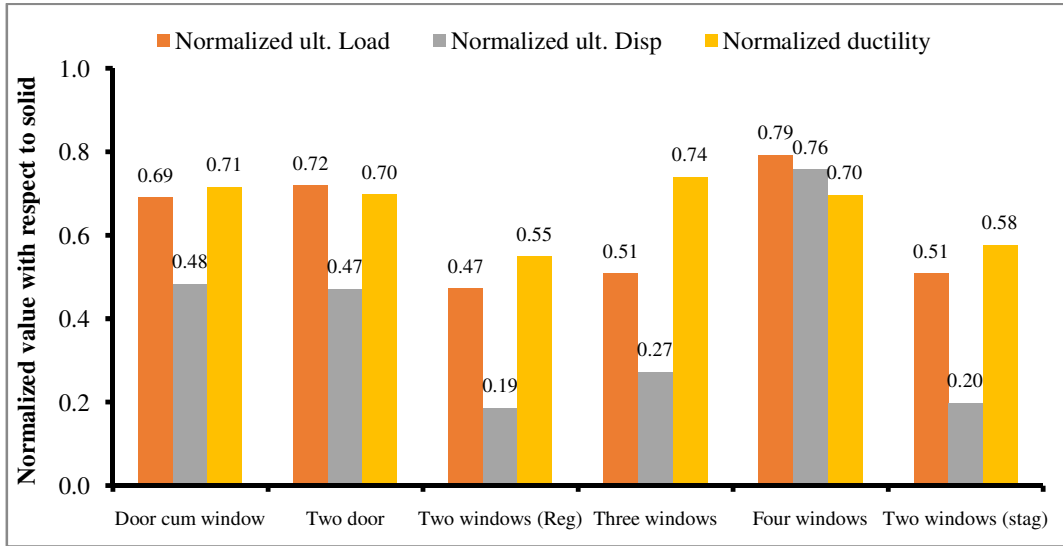


Fig. 5.17: Normalized ultimate load, ultimate displacement, ductility of RC squat shear wall with different door window opening combinations without strengthening

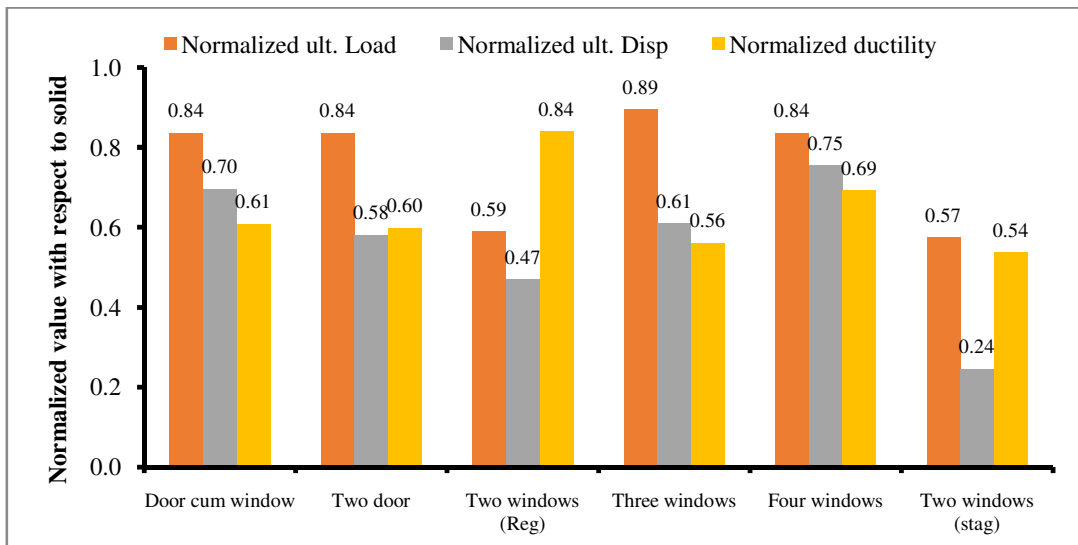


Fig. 5.18: Normalized ultimate load, ultimate displacement, ductility of RC squat shear wall with different door window opening combinations with strengthening

5.5 Summary

On the basis of non-linear static analysis of slender and squat shear walls with different sizes and opening locations, the following concluding remarks have been made.

- For the shear wall panel, the openings located away from the loading side (compression zone) resulted in better load carrying capacity compared to openings located near loaded side (tension zone). Hence, as far as possible, openings in the shear wall should be avoided in the tension zone.

- For a given cross-section of shear wall, the aspect ratio of shear wall significantly affects the load carrying capacity as well as the displacement response. The ten storey slender shear wall was found to possess around 50% of the load carrying capacity of five storey squat shear wall.
- The load carrying capacity of slender as well as squat shear wall with openings gets significantly affected as compared to solid shear wall. In both the cases, strengthening around openings has been found beneficial in improving the load carrying capacity.
- For the slender and squat shear walls, 14% opening was found safe even when shear wall is not strengthened around openings. The shear wall with 18% opening may be reasonably safe in the case of slender shear wall for both strengthen and not strengthen around the openings; however, the same is not true in the case of squat shear wall. For slender as well as squat shear walls, an increase in opening beyond 18% results in tremendous reduction in the load carrying capacity as well as ductility.
- The opening locations play a significant role on the load-displacement response of both slender as well as squat RC shear walls. The shear wall with single central opening resulted in the better performance as compared to other locations.
- The aspect ratio of opening plays significant role on the response of shear wall. The consistent performance of the shear wall with single central opening and four symmetrically placed window openings is partly to the square openings.
- The load carrying capacity gets severely affected for shear wall with openings located in the form of two windows or three windows. The two window (staggered) opening resulted in the significantly decrease in load carrying capacity for both slender as well as squat shear walls even with strengthening. The strengthening of the walls provided for two windows (regular) and three window openings resulted in brittle failure with reduced ductility index. Such openings are not recommended.
- The shear wall with two door openings resulted in the better load carrying capacity even without strengthening. Hence, it is beneficial to provide longer side of opening in the perpendicular to loading direction in order to minimize the degradation in the load carrying capacity.

References:

1. Lefas, I.D., Kotsovos, M.D., and Ambraseys, N. N. (1990). "Behavior of reinforced concrete structural walls: Strength, deformation characteristics, and failure mechanism." *ACI Structural Journal*, 87(1), 23-31.
2. IS 13920 (1993). *Code of Practice for Ductile Detailing of Reinforced Concrete Structures subjected to Seismic Forces*, Bureau of Indian Standards, New Delhi.
3. Park, F.V., Park, R., Paulay, T. (1998). "State-of-the Art Report Ductility evaluation from laboratory and analytical testing." *Proceedings of the Earthquake Engineering Ninth World Conference*, Tokyo, Japan.

Non-Linear Dynamic Response of RC Shear Wall

6.1 Background

Reinforced Concrete (RC) Shear wall has been considered one of the most viable lateral load resisting elements in resisting wind and earthquake loads. The behavior of RC shear wall is influenced by many factors such as aspect ratio, opening size and locations. It is generally perceived that the aspect ratio of shear wall plays a crucial role on its structural response, slender being more flexible and squat being more rigid. As outlined in the chapter two, to meet the functional requirements, shear walls are sometimes penetrated with openings of different sizes and at different locations. Though there is a strong consensus that shear walls be penetrated only with smaller openings in order to get the desired structural response, but there is no clarity on the optimum size of openings in shear walls from the strength and ductility point of view. Moreover, for a given size of opening in shear wall, it is also essential to investigate the influence of opening location on the strength and ductility of RC shear wall. Furthermore, the influence of strengthening (ductile detailing) around the openings on the structural response of RC shear walls has also been investigated. In this chapter, an attempt has been made to analyze RC shear walls for its sensitivity to above mentioned parameters by employing the non-linear time history analysis using Newmark- β direct method of time integration considering material non-linearities.

As mentioned in the Chapter 4, the assumed strain based locking free 9-noded layered degenerated shell element has been used for the discretization of RC shear wall. The mesh size has been kept constant throughout the height of the shear wall. In the material modeling, the non-linearities considered in the analysis are concrete cracking and yielding, yielding of steel and crushing of concrete. The compression modeling of concrete has been formulated using plasticity based five parameter Willam-Warnke failure model to define the yield/failure criteria of concrete in compression with associated flow rule and isotropic hardening. The tension modeling

of concrete is augmented by the Rankine's tension cut-off criterion with tension stiffening. The modeling of cracks is considered using fixed smeared crack approach. The bi-linear modeling of steel reinforcement has been adopted in the present study to define the steel behavior. To this end, a five storeyed RC shear wall (squat shear wall) and ten storeyed RC shear wall (slender shear wall) have been considered and analyzed for different opening sizes and locations. The displacement time history response of RC shear wall with and without openings has been plotted and the analysis has been conducted for two different damping ratios with and without ductile detailing (strengthening).

6.2 Influence of Openings on Dynamic Response of Shear Wall Panel

The reinforced concrete shear wall tested by Lefas et al. (1990) has been considered for the present study in order to assess the influence of opening location on the displacement response of shear wall panel with top and bottom beams. In each shear wall, three openings are provided which amounts to 12% opening. The geometry and section of shear wall specimen is as shown in Fig. 6.1(a) and (b). The wall panel is 650 mm wide \times 1300 mm high \times 65 mm thick. The height to width ratio of wall panel is two, thus representing the squat type of shear wall. While the upper beam provides anchorage for vertical reinforcement, lower beam provides the base for wall panel. The element size used to discretize the shear wall panel is 65 mm \times 130 mm which is kept same for the entire structure. The number of degenerated shell elements used to discretize the shear wall panel and beams is 100 and 56 respectively.

The bottom beam has been constrained in all degrees of freedom. The elasticity modulus of concrete is 3.27×10^4 MPa and Poisson's ratio is taken as 0.17. The concrete compressive and tensile strengths are 42.8 MPa and 2.15 MPa respectively and the crushing strain of concrete is 0.0035. The central portion of the shear wall referred as zone I, where the conventional reinforcement is provided, the edges of the shear wall are strengthened by providing the additional reinforcement and are identified as zone II. The percentages of steel reinforcement in x-direction and y-direction are 0.8 & 2.1 in zone I and 1.2 & 3.3 in zone II. However, irrespective of the zones, the yield stresses of steel in the x- and y-direction are 520 MPa and 470 MPa respectively. The hardening modulus of concrete and steel are assumed to be 3.27×10^3 MPa and 2.00×10^4 MPa ($1/10^{\text{th}}$ of

elasticity modulus) respectively. The vertical reinforcement (y-direction) is provided in two layers and horizontal reinforcement (x-direction) is concentrated in single layer. For the finite element modeling of steel, the reinforcement is considered to be smeared within the element. For the non-linear analysis, the stiffness matrix is modified at the end of every load step.

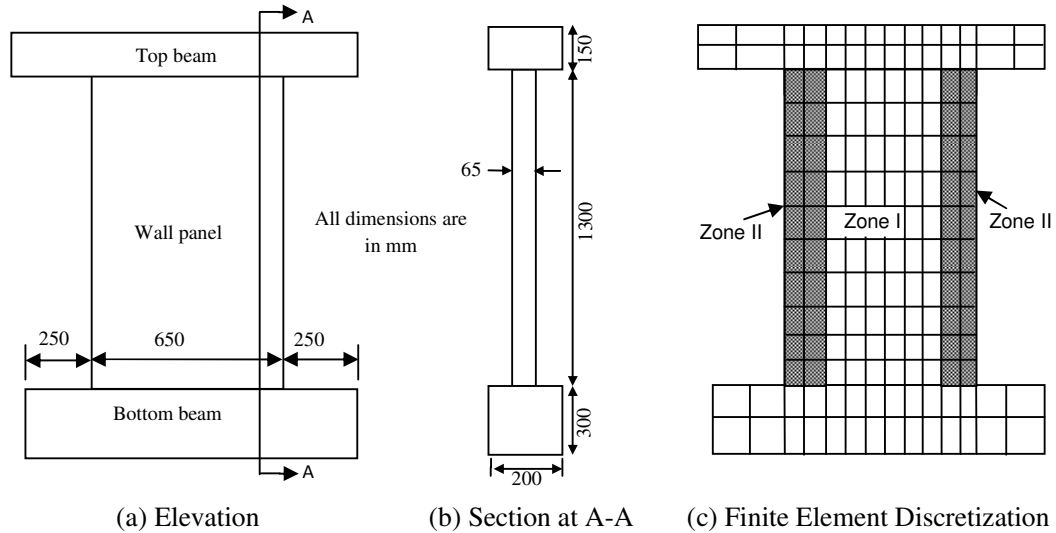


Fig. 6.1: Geometry of solid RC shear wall panel

The earthquake ground motion, which is applied at the base of the shear wall, is as shown in Fig. 6.2. The waveform considered here is the NS component of the well known EL Centro Earthquake occurred on May 18, 1940 (Pecknold version) for the duration of 31.18 seconds with the maximum acceleration of +0.29g. This is one of the first records of strong ground motion and has been widely used by structural engineers in assessing the seismic response of structures.

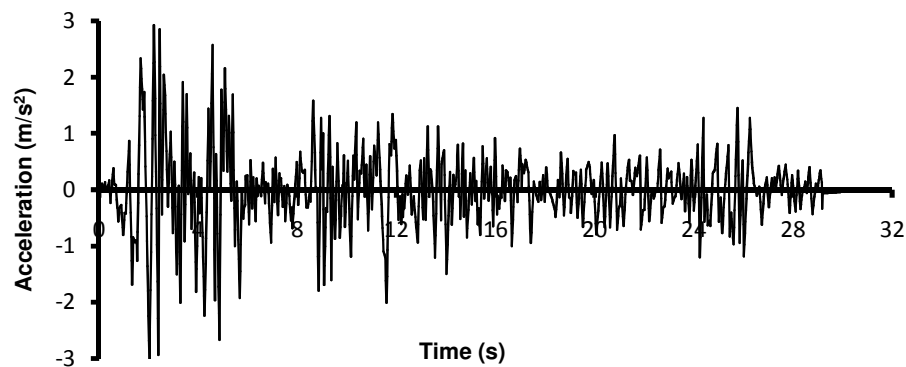


Fig. 6.2: Input ground acceleration

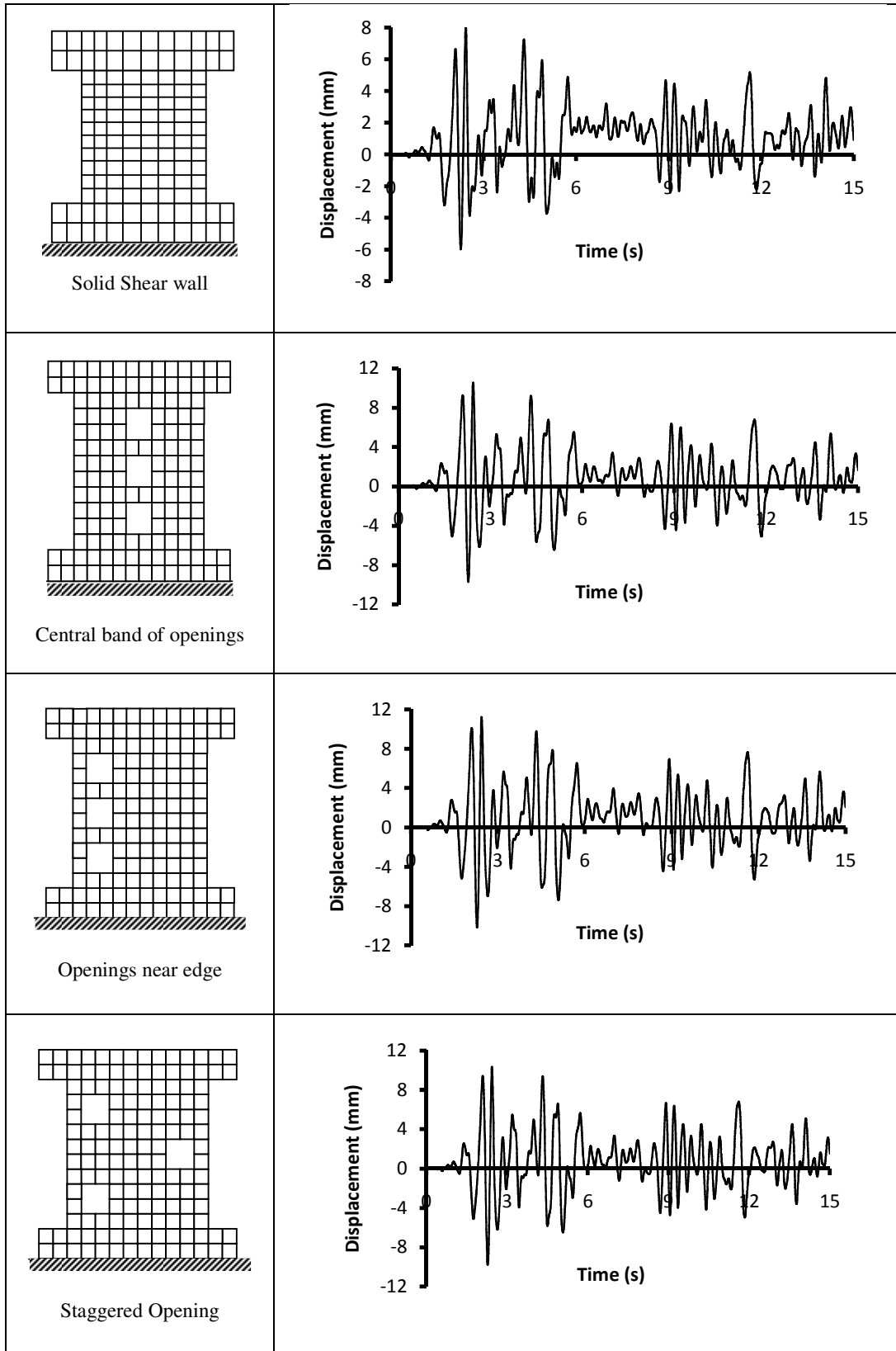


Fig. 6.3(a): Displacement time history response of shear wall panel for various opening locations (5% damping)

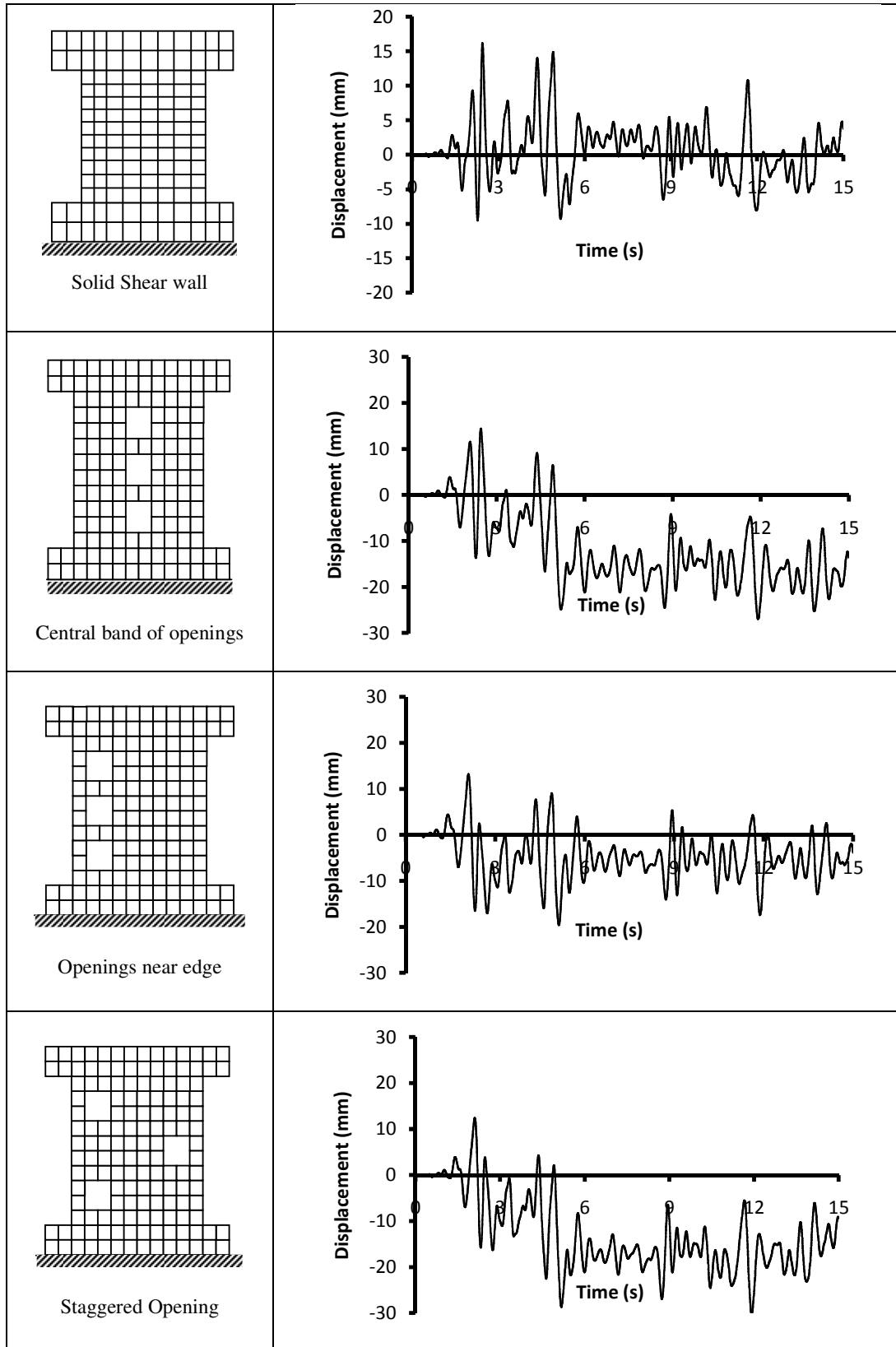


Fig. 6.3(b): Displacement time history response of shear wall panel for various opening locations (2% damping)

The entire ground acceleration data is discretized into a time interval of 0.02 seconds. The unconditionally stable Newmark β method of direct time integration has been employed to determine the displacement time history response. The time step for the analysis has been taken as 0.005 seconds. Since the peak load as well the displacement response occur in first 15 seconds, the response has been plotted only for 15 seconds and in total, 3000 time steps are required to complete the analysis. The maximum iterations have been kept at 50 and the displacement convergence norm has been kept at 0.0025. The analysis is conducted for 2% and 5% damping and damping is represented as Rayleigh damping with stiffness proportionality. The natural time period assumed for the shear wall is 10.73 seconds and the circular frequency is computed as 0.58 rad/sec. In order to simulate the actual dead loads present in the shear wall, dead load of 20 kN is assumed to be lumped at the top beam. The equivalent base shear is computed as $m \times \omega_n^2 \times u_{\max}$. The displacement time histories of all cases have been presented in Fig. 6.3(a) and (b). Table 6.1 shows the maximum displacement response of RC shear wall panel with various opening locations.

Table 6.1: Dynamic response of RC shear wall panel

Opening locations	Maximum displacement (mm)	
	5% damping	2% damping
No opening	8.18	16.21
Central opening	10.54	26.95
Left opening	11.20	19.60
Staggered opening	10.33	30.09

From Fig. 6.3(a) it may be observed that there is not much difference in the displacement time history response of shear wall with various opening locations and hence it may be concluded that 5% damping is sufficient enough to provide stable displacement time history irrespective of opening locations. Though solid shear wall results in least displacement, there is hardly any influence of opening locations on the maximum displacement response (Table 6.1). However, when the damping is reduced from 5% to 2%, the displacement time history of shear wall provided with central opening and staggered opening has resulted in one sided displacement response (Fig. 6.3(b)). For 2% damping, the shear wall with left opening resulted in less

displacement than central opening and staggered opening. Since edges of the shear walls are confined with heavy reinforcement, the response of shear wall with opening located near left edge resulted in less displacement. However, the staggered opening resulted in maximum displacement of 30.09 mm, 46% increase with respect to solid shear wall. However, the displacements are not alarming for this particular opening size & locations and hence there is a need to investigate further by subjecting the shear wall to different opening sizes and at different locations. The next section deals with the identification of safe opening sizes and opening locations.

6.3 Influence of Opening Size on Displacement Time History Response of Slender and Squat Shear Wall

The behaviour of the shear wall is strongly influenced by the presence of openings. It is essential to know the limiting size of openings in shear wall beyond which it becomes unserviceable or unsafe. Since the short shear walls have been found to possess very high load carrying capacity, the presence of openings in short shear wall may not alter the behaviour significantly. Moreover, from the functional point of view, short shear walls with one or two storeys are not normally provided with openings and hence short shear walls with openings are not the part of this study. Since openings result in stress concentration, the portion of shear wall around the openings is strengthened by providing reinforcements around the openings as per IS 13920-1993 as shown in Fig. 5.5.

The present section investigates the influence of opening size and strengthening on the displacement structural response of squat shear walls (5 storeys) and slender shear walls (10 storeys) for two different damping ratios 2% and 5%. In each storey, only one opening is provided and the size of the opening has been kept uniform throughout the height of shear wall. The width and thickness of shear walls are 8 m and 0.3 m, respectively. The height of each storey is 3.5 m which results in height of squat & slender shear walls as 17.5 m and 35 m respectively as shown in Fig. 6.4 and Fig. 6.5. The shear walls have been analyzed for five different opening sizes at each storey viz, (i) 1 m × 1.5 m, (ii) 2 m × 1.5 m, (iii) 2 m × 2 m, (iv) 2 m × 2.5 m, (v) 2 m × 3 m, which correspond to approximately 5%, 11%, 14%, 18% and 21% openings in each storey.

For the finite element analysis, the Shear walls have been discretized into finite element mesh using 9-noded 5 degrees of freedom assumed strain based locking free degenerated shell elements. For the discretization of shear walls with openings; the mesh size is kept at $0.5 \text{ m} \times 0.5 \text{ m}$ which has been kept uniform throughout the shear wall geometry to minimize the computational effort involved in preparing customized input data. In order to model steel reinforcement, the layered approach is adopted in this study, wherein, the steel is modelled as a smeared layer of equivalent thickness and the material properties are assumed to be constant in that layer. The bi-linear stress strain curve with linear elastic and strain hardening region is adopted for steel in compression and tension.

The horizontal steel reinforcement is provided in two layers and vertical steel reinforcement is provided in single layer. As per the requirements of IS 13920-1993, shear walls are provided with minimum reinforcement ratio of 0.0025 of the gross area in both longitudinal (vertical) and transverse (horizontal) directions in the plane of the wall and the same has been adopted in the present study. For the strengthening of shear walls with openings, the amount of vertical and horizontal reinforcement provided on the sides of openings is equal to that of the respective interrupted bars. The opening may result in the large displacement and instability which necessitated the need to dampen the response appropriately. In general, all RC structures may possess some amount of damping (1-2%) inherently. Nevertheless, most of the codal provisions suggest that concrete structures can be analyzed assuming 5% damping. Hence, the present study also aims to assess the influence of 2% and 5% damping on the displacement time history response of shear wall in the presence of openings. Only stiffness proportional (Beta) damping has been adopted in the present investigation in order to keep the damping proportional to frequency. The fundamental natural period (T) has been calculated using the formula mentioned in IS: 1893-2002. The natural time period of the system is determined using the expression $T_n = 0.09 h / \sqrt{d}$. The equivalent base shear is computed as $m \times \omega_n^2 \times u_{\max}$. In order to simulate the dead loads present in the building, 70 kN load is assumed to be lumped at each storey as an additional mass. The shear walls are subjected to earthquake ground acceleration for first 15 seconds as shown in Fig. 6.2. The influence of strengthening around openings is also examined. The material properties are as mentioned in Table 6.2.

Table 6.2: Material properties used for the analysis

Material Property	Magnitude
Concrete	
Elasticity modulus	$2.7 \times 10^{10} \text{ N/m}^2$
Hardening modulus	$2.7 \times 10^9 \text{ N/m}^2$
Poisson's ratio	0.17
Uni-axial compressive strength of concrete	$30 \times 10^6 \text{ N/m}^2$
Tensile Strength of Concrete	$3 \times 10^6 \text{ N/m}^2$
Ultimate crushing strain of concrete	0.0035
Tension stiffening coefficient (α_{ts})	0.8
Tension stiffening strain (ϵ_{ts})	0.0020
Steel	
Elasticity modulus	$2.0 \times 10^{11} \text{ N/m}^2$
Hardening modulus	$2.0 \times 10^{10} \text{ N/m}^2$
Yield stress of steel	$50 \times 10^7 \text{ N/m}^2$

Table 6.3: Dynamic characteristics of squat & slender shear wall

Shear wall type	No. of Storeys	Fundamental Natural Period, $T(s)$	Fundamental Natural Frequency, $f (Hz)$	Stiffness proportional Beta (β) damping	
				2% of critical	5% of critical
Squat	5	1.11	0.90	0.00707	0.017690
Slender	10	2.23	0.45	0.01418	0.035461

Table 6.4: Geometrical details of openings

Case	1	2	3	4	5
Opening Dimensions (W × H)	1m × 1.5m	2m × 1.5m	2m × 2m	2m × 2.5m	2m × 3m
Percentage Openings (%)	5.35% ≈ 5%	10.71% ≈ 11%	14.28% ≈ 14%	17.86% ≈ 18%	21.43% ≈ 21%
Number of elements/storey	116	100	96	92	88

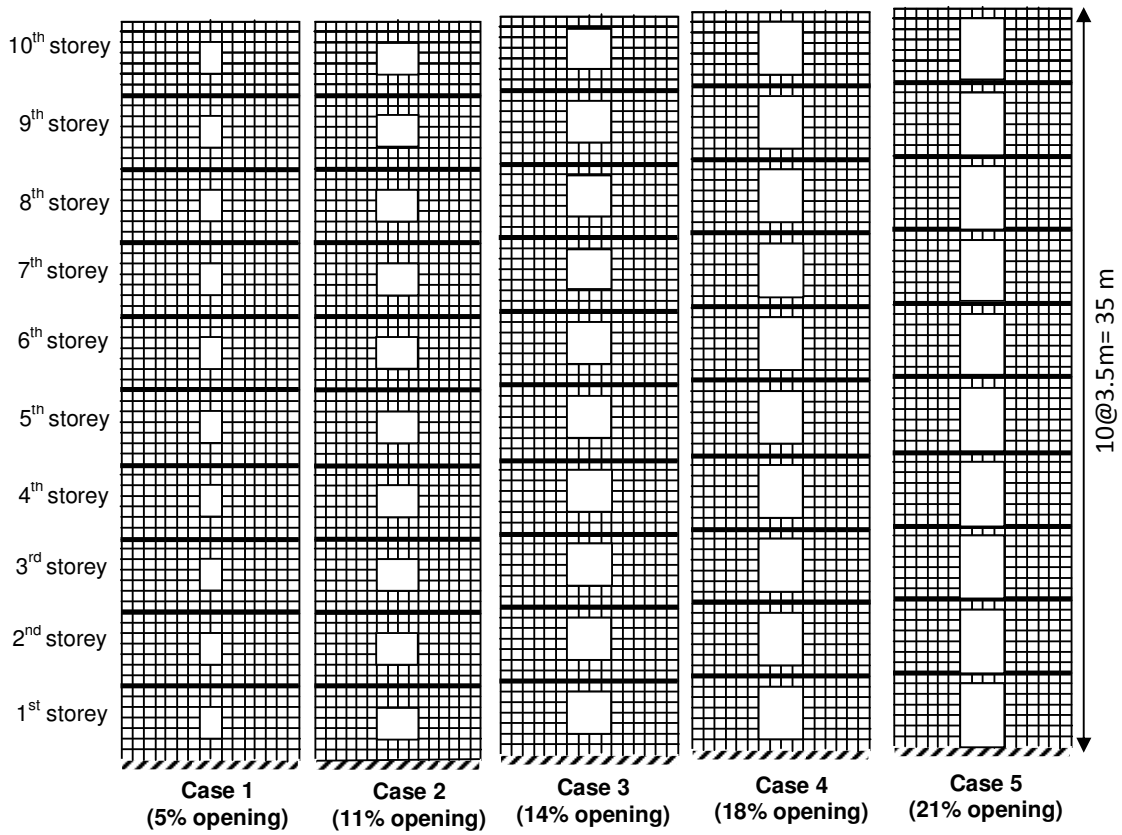


Fig. 6.4: Discretization of slender shear wall with various opening sizes

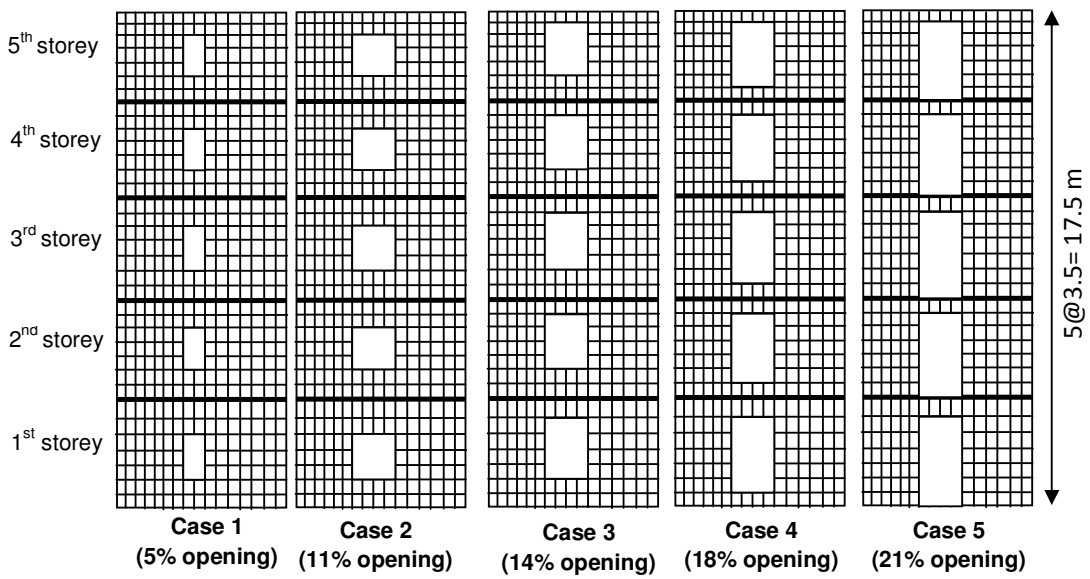
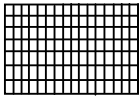
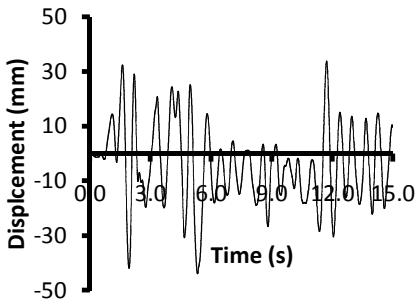
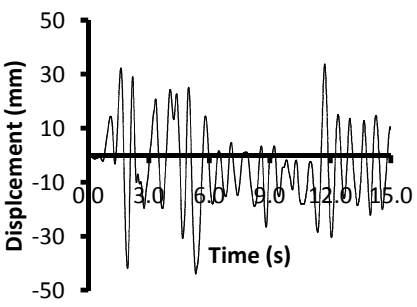
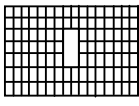
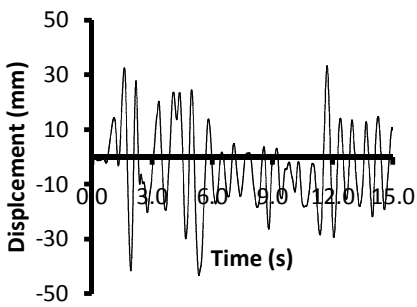
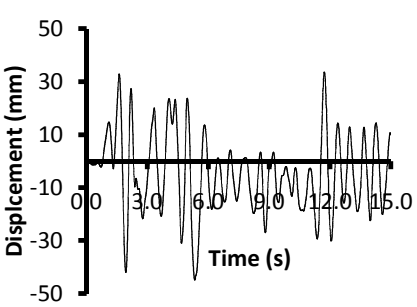
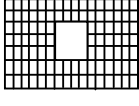
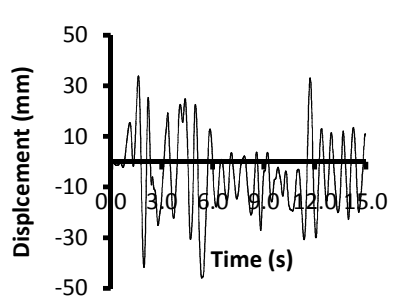
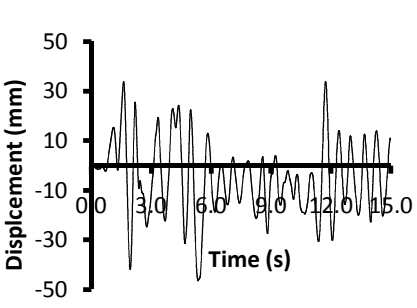
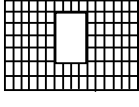
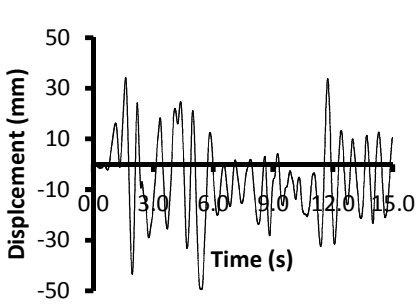
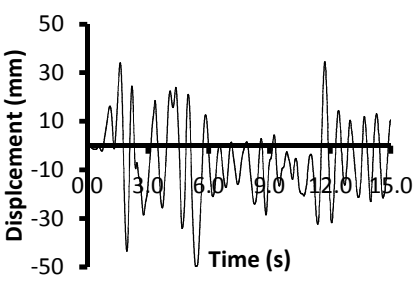
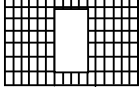
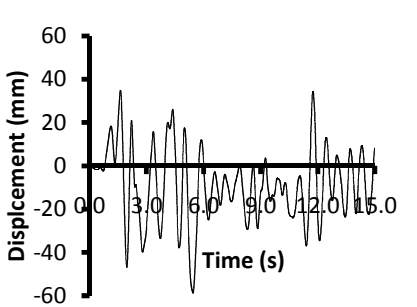
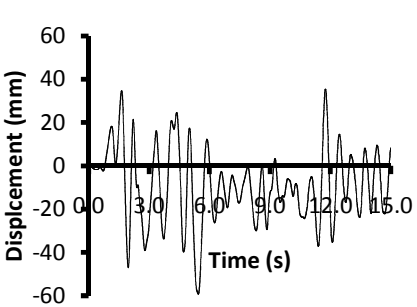


Fig. 6.5: Discretization of squat shear wall with various opening sizes

Opening size	Not strengthened	Strengthened
 <p data-bbox="292 451 479 525">Solid shear wall (No opening)</p>		
 <p data-bbox="308 787 462 861">5% opening (1m × 1.5m)</p>		
 <p data-bbox="308 1123 462 1197">11% opening (2m × 1.5m)</p>		
 <p data-bbox="308 1459 462 1533">14% opening (2m × 2m)</p>		
 <p data-bbox="308 1795 462 1869">18% opening (2m × 2.5m)</p>		

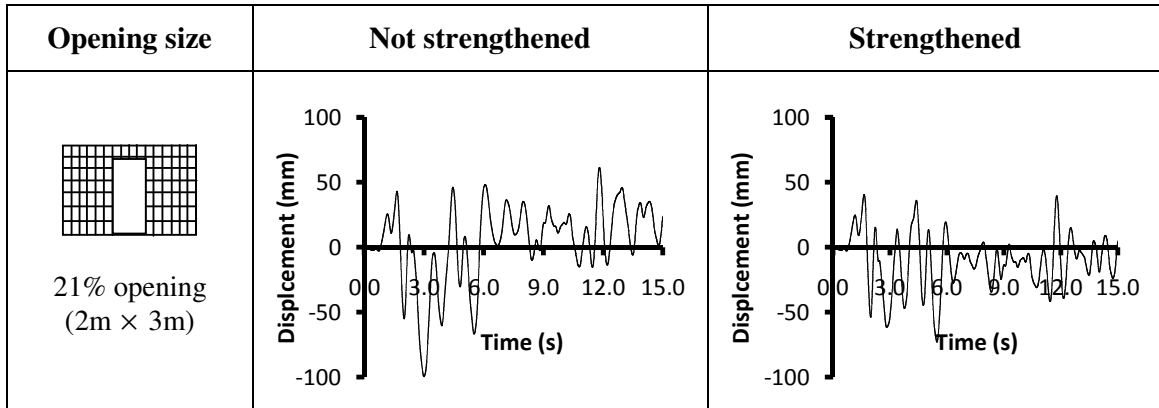
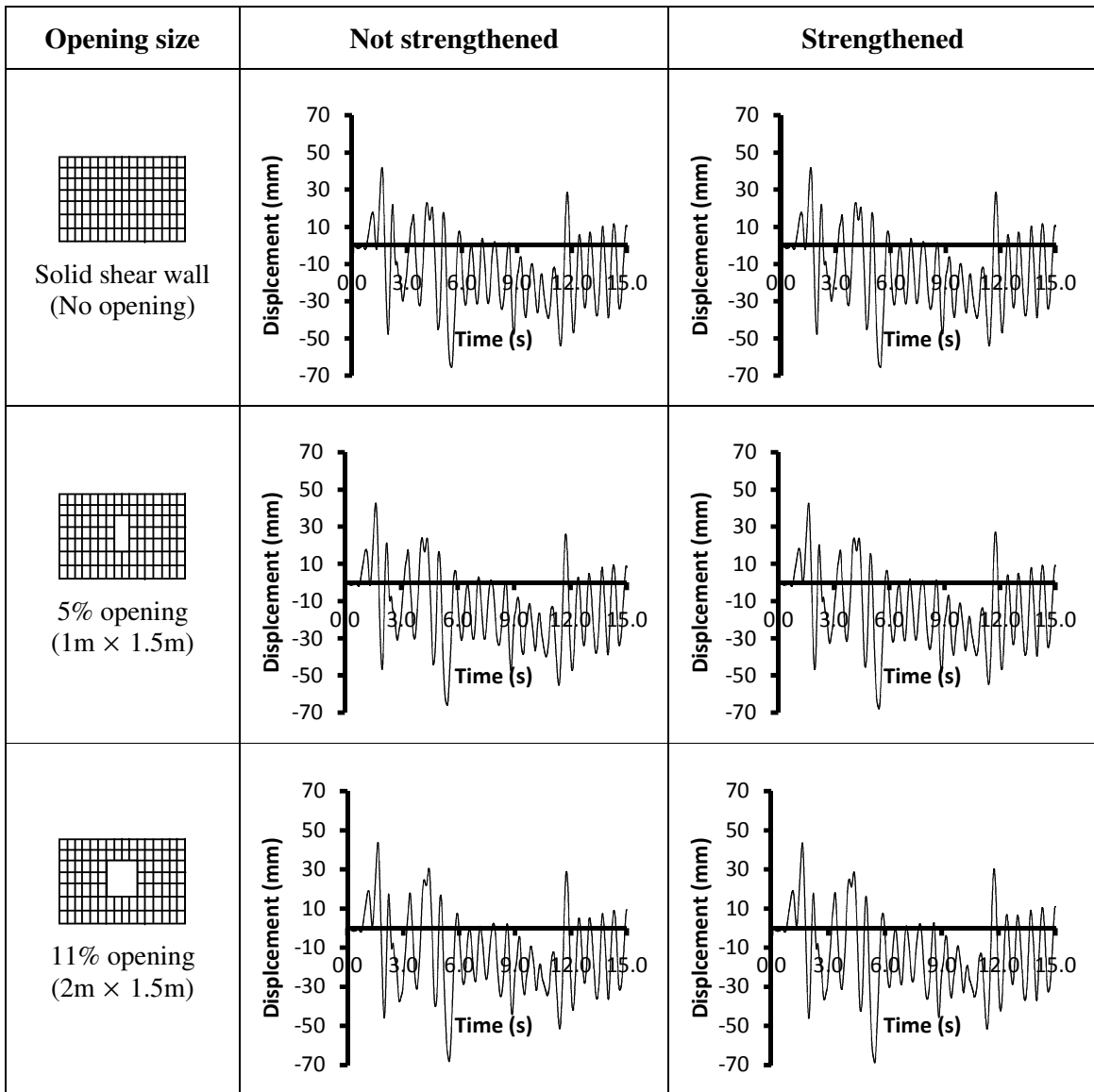


Fig 6.6: Displacement time history response of RC slender shear wall for different opening sizes for 5% damping



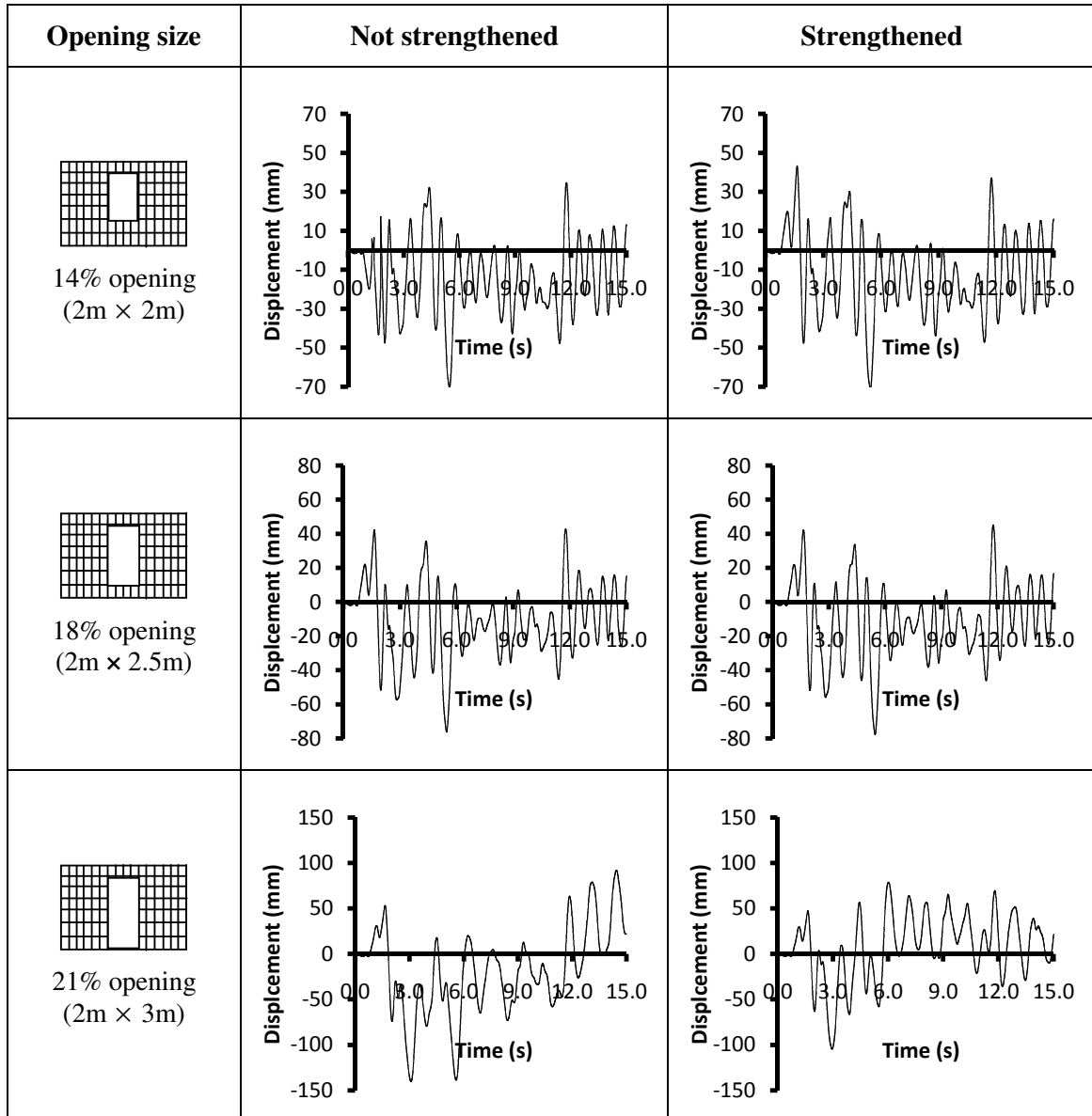


Fig 6.7: Displacement time history response of RC slender shear wall for different opening sizes for 2% damping

Slender shear wall:

Figs 6.6 and 6.7 depict the displacement time history responses of slender RC shear wall for 5% damping and 2% damping respectively subjected to the El Centro Earthquake. As already mentioned, the El Centro earthquake response of shear wall has been captured for first 15 seconds. Table 6.5 and Table 6.6 show the maximum displacement response of RC shear wall with and without strengthening for different opening sizes and for two different damping ratios 2% and 5%. As expected, the openings present in the shear wall

tend to weaken the shear wall and hence resulted in increase in the displacement with increase in opening size as shown in Table 6.5. In general, it is observed that the damping has significant impact in reducing the displacement response of RC shear wall. On decreasing the damping from 5% to 2%, the maximum displacement significantly increases. The detailed discussion on slender & squat shear walls subjected to earthquake ground motion is as follows.

Table 6.5: Max. displacement response and base shear demand - Slender shear wall with different opening sizes

Opening size	5% damping				2% damping			
	NS		ST		NS		ST	
	U_{max}	$V_{b d}$	U_{max}	$V_{b d}$	U_{max}	$V_{b d}$	U_{max}	$V_{b d}$
Nil	43.93	244.54	43.93	244.54	65.67	365.56	65.67	365.56
5%	43.36	241.37	44.81	249.44	66.16	368.29	68.08	378.98
11%	45.97	255.90	46.41	258.35	68.18	379.54	68.78	382.88
14%	49.43	275.16	49.86	277.55	70.62	393.12	71.43	397.63
18%	58.67	326.60	59.19	329.49	76.21	424.24	77.78	432.98
21%	99.41	553.38	72.91	405.87	140.40	781.56	104.50	581.72

For slender solid shear wall with 5% damping, the maximum displacement has been found to be 43.93 mm, and increased to 65.67 mm when the damping is decreased from 5% to 2%. The base shear demand of slender shear wall has been computed as 244.54 kN for 5% damping and 365.56 kN for 2% damping. Hence, there is an increase of around 50% in the maximum displacement and base shear demand when the damping is reduced from 5% to 2%.

For 5% opening in shear wall assuming 5% damping, the maximum displacement has been found to be 43.36 mm when not strengthened, but slightly increased to 44.81 mm upon strengthening, which indicates that there is not much difference in the responses with respect to solid shear wall in the maximum displacement response. The base shear demand of slender shear wall with 5% damping is 241.37 kN when not strengthened, but slightly increased to 249.44 kN when strengthened. However, for 2% damping, the maximum displacement has been found to be 66.16 mm when not strengthened, but

increased to 68.08 mm when strengthened. The base shear demand is 368.29 kN when not strengthened and 378.98 kN when strengthened. Hence, the increase in the base shear demand is only by 3.5% when strengthened around the openings. It may also be interpreted that such opening size may not alter the structural behavior when sufficient damping is present in the shear wall and the influence of strengthening has also not been found to be significant.

When the shear wall is provided with 11% opening assuming 5% damping, the maximum displacement has been found to be 45.97 mm when not strengthened, but slightly increased to 46.41 mm upon strengthening. The base shear demand is 255.90 kN when not strengthened, but went up to slightly 258.35 kN when strengthened. The base shear demand is certainly increasing with the increase in the opening size which is about 4.5% higher with respect to solid shear wall. However, for 2% damping, the maximum displacement has been found to be 68.18 mm when not strengthened, but almost remains unchanged when strengthened. The base shear demand is 379.54 kN when not strengthened and increased to 382.88 kN when strengthened which results in 4% increase in base shear demand with respect to solid shear wall. For 11% opening also, there is not much influence due to strengthening around the openings.

For 14% opening, the maximum displacement has been found to be 49.43 mm when not strengthened, but slightly increased to 49.86 mm upon strengthening for 5% damping case. The base shear demand of slender shear wall with 5% damping is 275.16 kN when not strengthened, but went slightly up to 277.55 kN when strengthened. which results in approximately 12% increase in the base shear demand with respect to solid shear wall. However, for 2% damping, the maximum displacement has been found to be around 70 mm irrespective of strengthening.. The base shear demand is 393.12 kN when not strengthened and 397.63 kN when strengthened thus resulting in the increase of 8% when strengthened. Influence of strengthening on the maximum displacement response has been found to be negligible for both 5% as well as 2% damping.

When the shear wall is provided with 18% opening with 5% damping the maximum displacement has been found to be 58.67 mm when not strengthened, but slightly increased to 59.19 mm upon strengthening, which results in an increase in the maximum displacement of 37% with respect to solid shear wall. The base shear demand of slender

shear wall with 5% damping is 326.60 kN when not strengthened, but went upto 329.49 kN when strengthened. But, with respect to solid shear wall, the base shear demand is increased by around 34%. However, the influence of strengthening is still not significant on maximum displacement response and base shear demand. However, for 2% damping, the maximum displacement has been found to be 76.21 mm when not strengthened, but increased to 77.78 mm when strengthened. The base shear demand is 424.24 kN when not strengthened and 432.98 kN when strengthened. The increase in the maximum displacement response and base shear demand is around 16% with respect to solid wall. From the above discussion, it may be observed that shear wall with 18% opening has resulted in reasonably accepted maximum displacement and base shear demand with respect to solid shear wall.

For 21% opening with 5% damping, the maximum displacement has been found to be 99.41 mm when not strengthened, but decreased significantly to 72.91 mm upon strengthening. In the similar lines, the base shear demand of slender shear wall with 5% damping is 553.38 kN when not strengthened, but went down to 405.87 kN when strengthened. With respect to solid shear wall, the increase in the maximum displacement response and the base shear demand for not strengthened and strengthened is 126% and 66% respectively. Hence, it may be concluded that the strengthening results in the significant reduction in the maximum displacement as well as the base shear demand. In spite of this, the slender shear wall with opening 21% is not recommended from displacement and base shear point of view because of more than 50% increase with solid shear wall. For 2% damping, the maximum displacement has been found to be 140.4 mm when not strengthened, but decreased to 104.5 mm when strengthened. The base shear demand is 781.56 kN when not strengthened and 581.72 kN when strengthened. The base shear demand is increased by around 2.2 times when strengthened and 1.4 times when not strengthened.

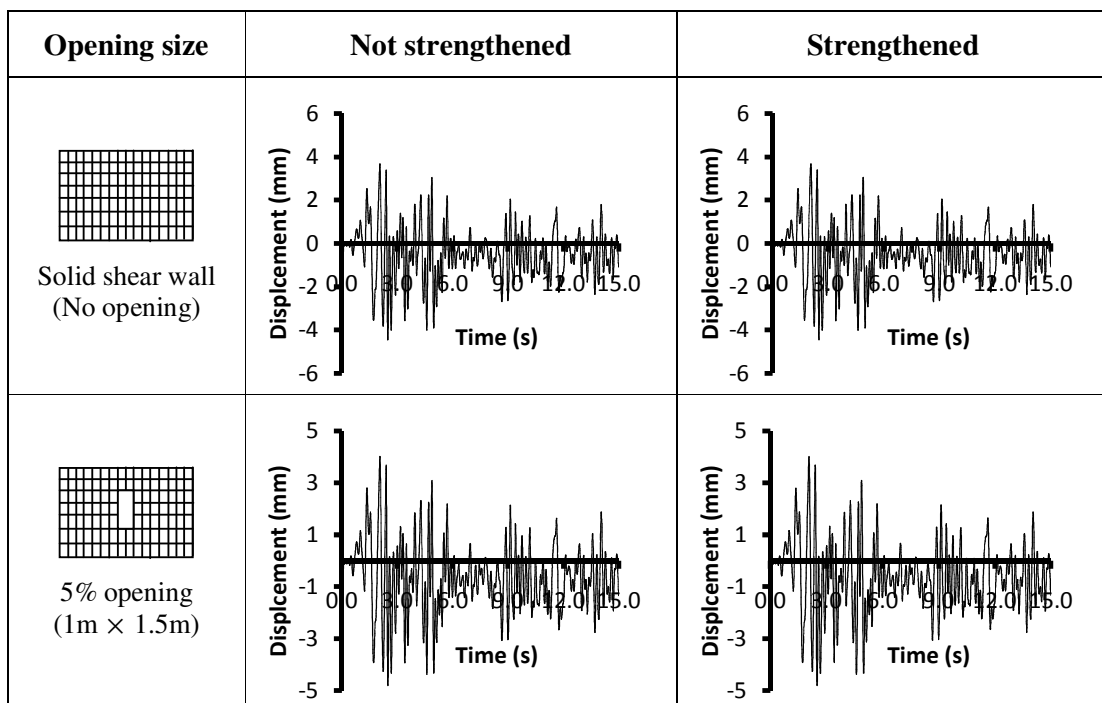
In general, upto 18% opening, the performance of shear wall has been found to be satisfactory for both 5% as well as 2% damping. However, for shear wall with 21% opening, the response has not been found to be satisfactory especially for 2% damping without strengthening.

Squat shear wall:

Figs. 6.8 and 6.9 show the time history displacement response of squat RC shear wall with different opening sizes. Table 6.6 shows the maximum displacement response and base shear demand of RC squat shear wall for different opening sizes and for two different damping ratios. The maximum displacements of squat shear walls are significantly less than that of slender walls.

Table 6.6: Max. displacement response and base shear demand- Squat shear wall with different opening sizes

Opening size	5% damping				2% damping			
	NS		ST		NS		ST	
	U _{max}	V _{b d}	U _{max}	V _{b d}	U _{max}	V _{b d}	U _{max}	V _{b d}
Nil	4.44	49.64	4.44	49.64	8.81	98.42	8.81	98.42
5%	4.80	53.57	4.80	53.61	9.14	102.11	9.10	101.66
11%	5.31	59.35	5.32	59.46	9.24	103.27	9.23	103.08
14%	6.18	68.99	6.16	68.79	9.91	110.73	9.98	111.54
18%	8.44	94.28	8.50	94.91	57.32	640.43	13.66	152.62
21%	29.09	325.02	16.80	187.70	92.86	1037.51	55.28	617.64



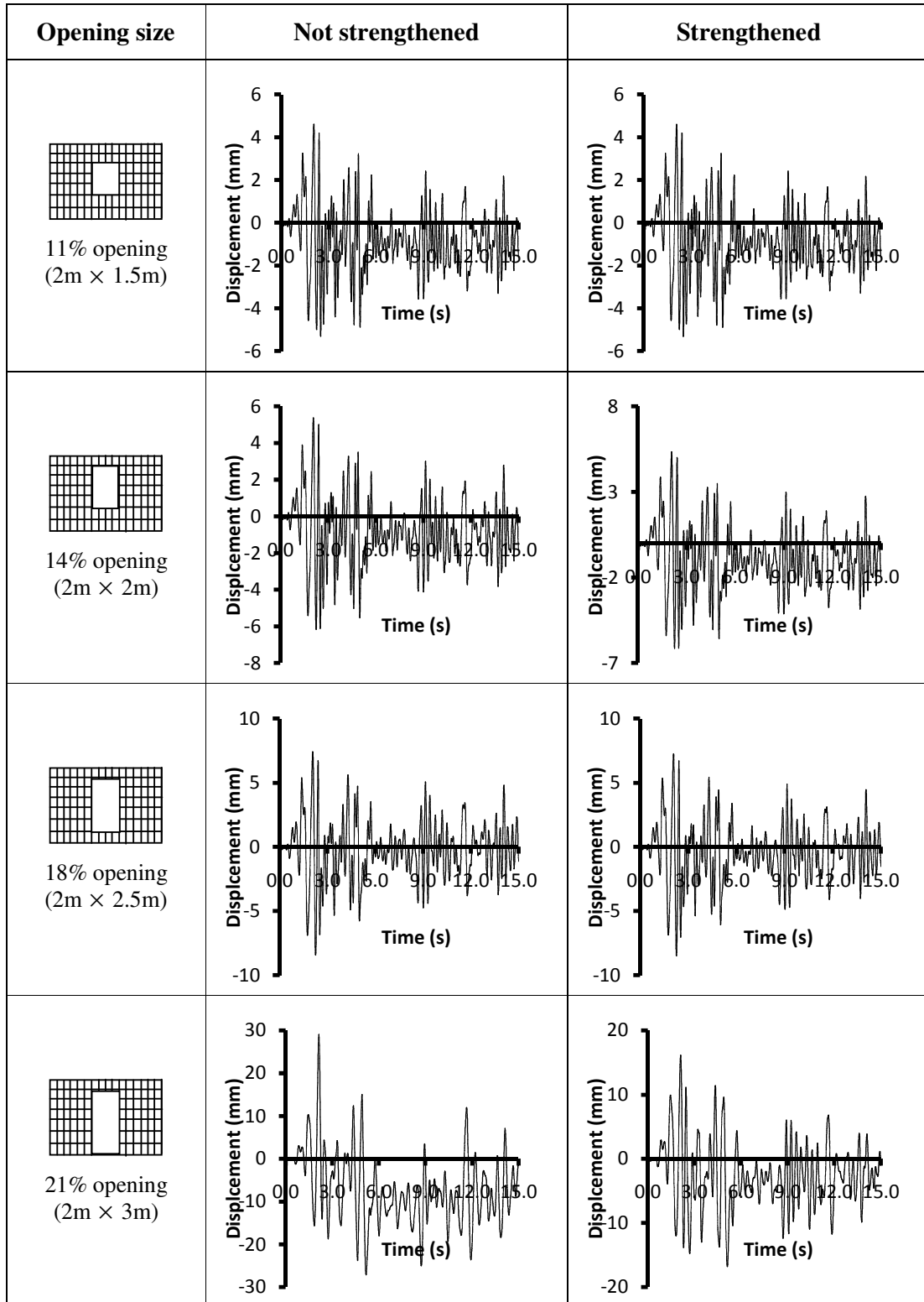
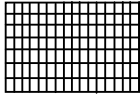
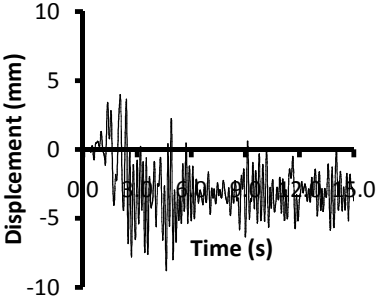
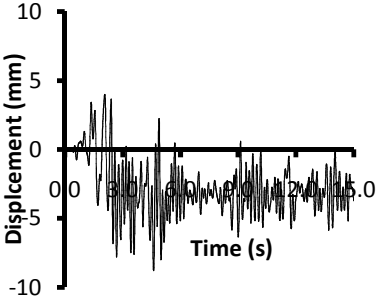
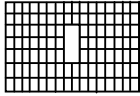
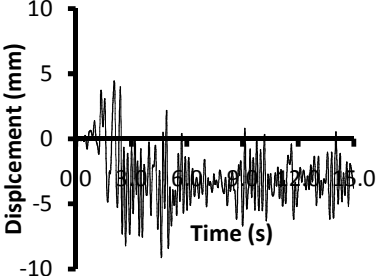
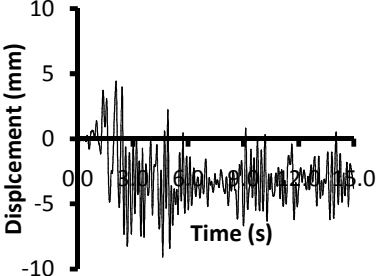
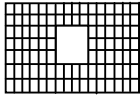
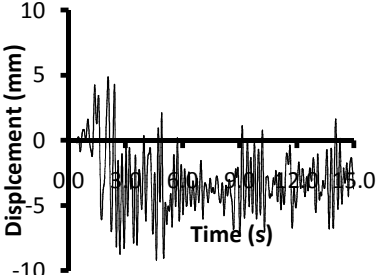
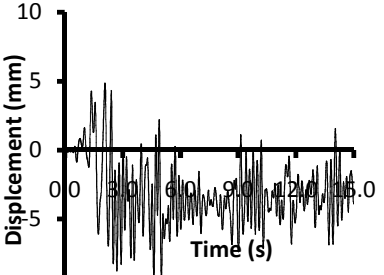
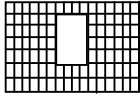
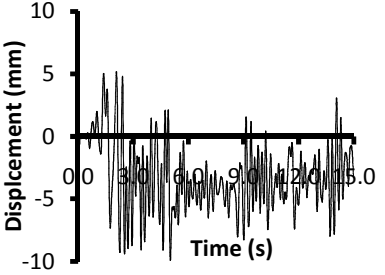
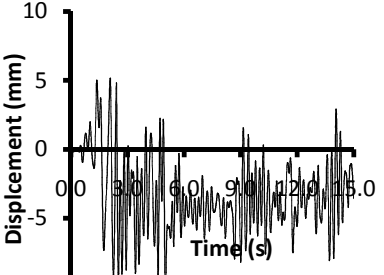
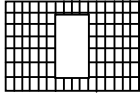
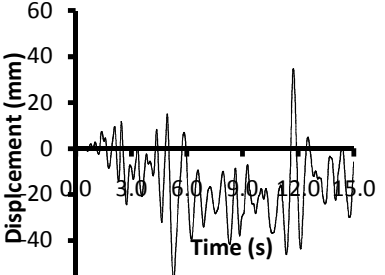
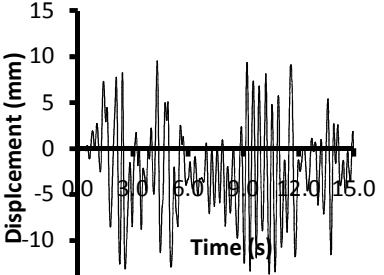


Fig. 6.8: Displacement time history response of RC squat shear wall for different opening sizes for 5% damping

Opening size	Not strengthened	Strengthened
 <p data-bbox="313 443 500 506">Solid shear wall (No opening)</p>		
 <p data-bbox="329 768 483 831">5% opening (1m × 1.5m)</p>		
 <p data-bbox="329 1094 483 1157">11% opening (2m × 1.5m)</p>		
 <p data-bbox="329 1430 483 1493">14% opening (2m × 2m)</p>		
 <p data-bbox="329 1766 483 1829">18% opening (2m × 2.5m)</p>		

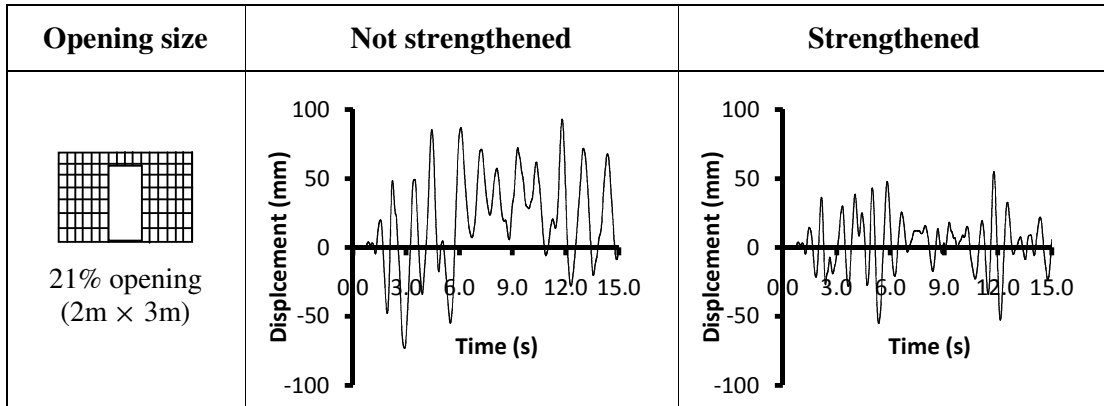


Fig. 6.9: Displacement time history response of RC squat shear wall for different opening sizes for 2% damping

For squat solid shear wall with 5% damping, the maximum displacement has been found to be 4.4 mm and increased to 8.8 mm for 2% damping. The base shear demand of slender shear wall has been computed as 49.64 kN for 5% damping and 98.42 kN for 2% damping. Hence, there is an increase in the maximum displacement response and base shear demand by about 100% when the damping is reduced from 5% to 2%.

When the squat shear wall is provided with 5% opening assuming 5% damping, the maximum displacement has been found to be 4.8 mm when not strengthened, but increased to 9.14 mm upon strengthening. However, there is not much difference in the responses with respect to solid shear wall in the maximum displacement response when the shear wall is penetrated with opening of size 5%. The influence of strengthening has also not been significant. The base shear demand of squat shear wall with 5% damping is approximately 53 kN for both strengthened and not strengthened. However, for with 2% damping, the maximum displacement has been found to be approximately 9 mm irrespective of strengthening. The base shear demand is 102 kN for both strengthened and not-strengthened. Hence, it may also be interpreted that such opening size may not alter the structural behavior when sufficient damping is present in the shear wall.

For squat shear wall with 11% opening assuming 5% damping, the maximum displacement has been found to be 5.31 mm irrespective of strengthening. The base shear demand shear wall with 5% damping is approximately 59 kN for both not strengthened, and strengthened. However, for squat shear wall with 2% damping, the maximum displacement has been found to be 9.2 mm for strengthened and not-strengthened. The base shear demand is approximately 103 kN for both not strengthened and strengthened.

When the squat shear wall is provided with 14% opening assuming 5% damping, the maximum displacement has been found to be 6.18 mm when not strengthened, but slightly decreased to 6.16 mm upon strengthening. The base shear demand of slender shear wall with 5% damping is approximately 68 kN for both not strengthened and strengthened. The base shear demand is increased by around 39% with respect to solid shear wall. Again, not much influence of strengthening has been found. However, for squat shear wall with 2% damping with or without strengthening, the maximum displacement has been found to be approximately 9.9 mm. The base shear demand is approximately 110 kN for both not strengthened and strengthened. However, the base shear demand is slightly increased by 12% for the slender shear wall. Nevertheless, the displacement time history responses of shear walls up to 14% opening have not been found to be different for both strengthened and not-strengthened.

For squat shear wall with 18% opening assuming 5% damping, the maximum displacement has been found to be 8.4 mm irrespective of strengthening and there is an increase in the maximum displacement of 37% with respect to solid shear wall. The base shear demand of slender shear wall with 5% damping is 94 kN for both not strengthened and strengthened. The base shear demand is increased significantly by around 92% with respect to solid shear wall. However, for squat shear wall with 2% damping, the maximum displacement has been found to be 57 mm when not strengthened, but decreased to 13.66 mm when strengthened. The base shear demand is approximately 640 kN when not strengthened and 152 kN when strengthened. When not strengthened, though the maximum displacement response and base shear demand is increased by around 6 times with respect to solid wall, but increased only by 55% upon strengthening. Hence, 2% damping is highly undesirable for squat shear wall with opening size 18% without strengthening the shear wall around the openings. When the shear wall is provided with 18% opening, there is a little bit of flexible behavior when the damping is small (2%), characterized by less number of cyclic loops (Fig. 6.9).

When the squat shear wall is provided with 21% opening with 5% damping, the maximum displacement has been found to be 29.09 mm when not strengthened, but decreased to 16.8 mm upon strengthening. Hence, there is the increase in the maximum displacement by around 6 times with respect to solid shear wall when not strengthened around the openings. However, the increase in the maximum displacement of slender

shear wall with 21% opening is only 2 times when strengthened around the openings. The base shear demand of slender shear wall with 5% damping is approximately 325.02 kN when not strengthened, but went down to 187.70 kN when strengthened. The base shear demand is increased significantly by around 5 times with respect to solid shear wall without strengthening but only by 2.7 times with strengthening. The strengthening results in the significant reduction in the maximum displacement response as well as the base shear demand. Even with strengthening, the squat shear wall with opening size 21% is not recommended from displacement and base shear demand point of view. This is evident from the displacement time history response where the number of loops is found to be very less as compared to 18% opening (Fig. 6.9). For squat shear wall with 2% damping, the maximum displacement has been found to be 92.86 mm when not strengthened, but decreased to 55.28 mm when strengthened. The base shear demand is 1037.51 kN when not strengthened and decreased to 617.64 kN when strengthened. The maximum displacement response as well as base shear demand is increased by around 9.5 times when strengthened and 5.3 times when not strengthened.

As observed in the case of slender shear wall, the maximum displacement response of squat RC shear wall with opening size 5%, 11% and 14% has been found to be negligible even for 2% damping, and hence the strengthening has not much role to play on displacement time history response and base shear demand. However, for shear wall with 18% opening, though 5% damping has resulted in less displacement, the response of RC shear wall with 2% damping is 57 mm with a drastic increase of around 6 times over 5% damping. Nevertheless, even for 2% damping, the strengthening results in the significant reduction in the maximum displacement response by around 3 times. For shear wall with opening size 21%, the response of shear wall has not been found to be satisfactory for both 5% damping and 2% damping even with strengthening.

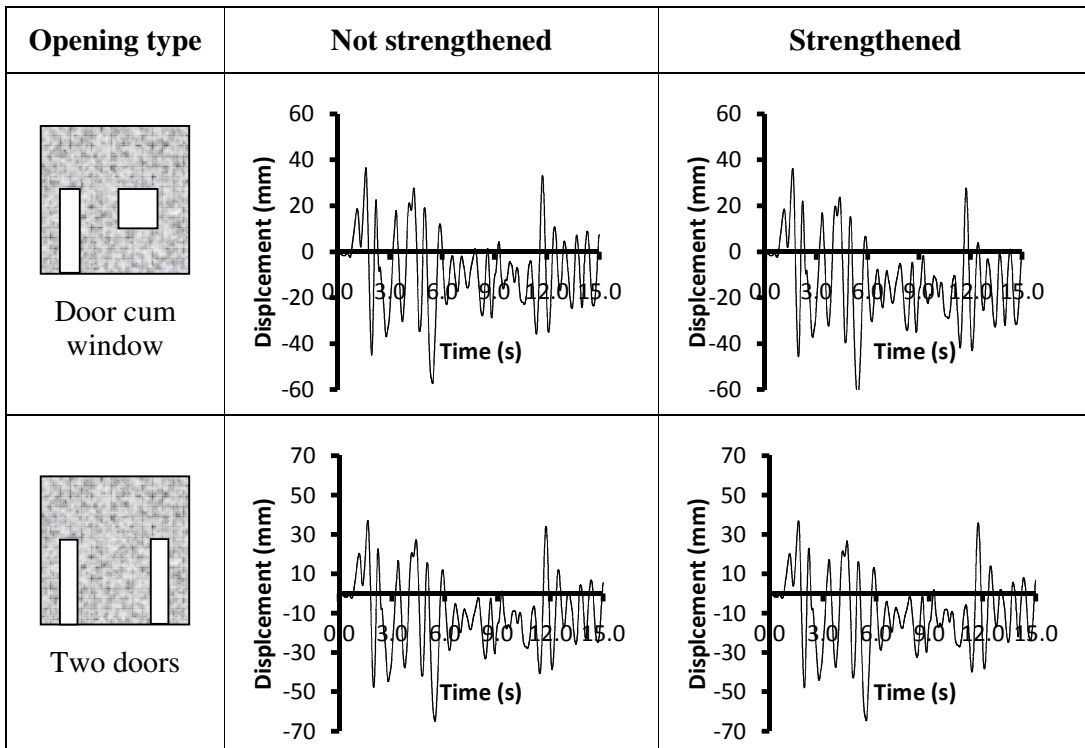
6.4 Influence of Door Window Openings on Displacement Time History Response of Shear Wall

In order to identify the safe regions where the openings can be provided in a shear wall, two representative problems of ten storey (35 m high, 8 m wide and 0.3 m thick) and five storey (17.5 m high, 8 m wide, 0.3 m thick), behaviorally slender and squat type, are chosen and analyzed for dynamic loading condition for 2% and 5% damping subjected to Fig. 6.2, using the finite element analysis. The opening location is varied

keeping all practical positions. The optimum opening size is identified from the previous section and is found to be 14% for slender as well as squat shear wall. The material properties used for the material modeling are as mentioned in Table 6.2. In total, there are six cases considered as the possible opening locations prevailed in practice, viz. (i) door cum window, (ii) two doors (iii) two windows (regular), (iv) three windows, (v) four windows and (vi) two windows (staggered). However, it is to be noted that these openings are repeated in each storey of shear wall.

Slender shear wall:

Figs. 6.10 and 6.11 show the influence of different doors and/or window openings on the displacement time history response of RC slender shear wall. Table 6.8 shows the maximum displacement response and the base shear demand of RC shear wall with and without strengthening around the openings. As elaborated in the previous section, it has been identified that 14% opening has been the safe opening size for both slender as well as squat shear wall. The previous section dealt with the identification of safe opening size by keeping the openings in the middle portion of the shear wall. When the openings are located in the central portion of the shear wall, it was observed that the performance of shear wall has been considered satisfactory.



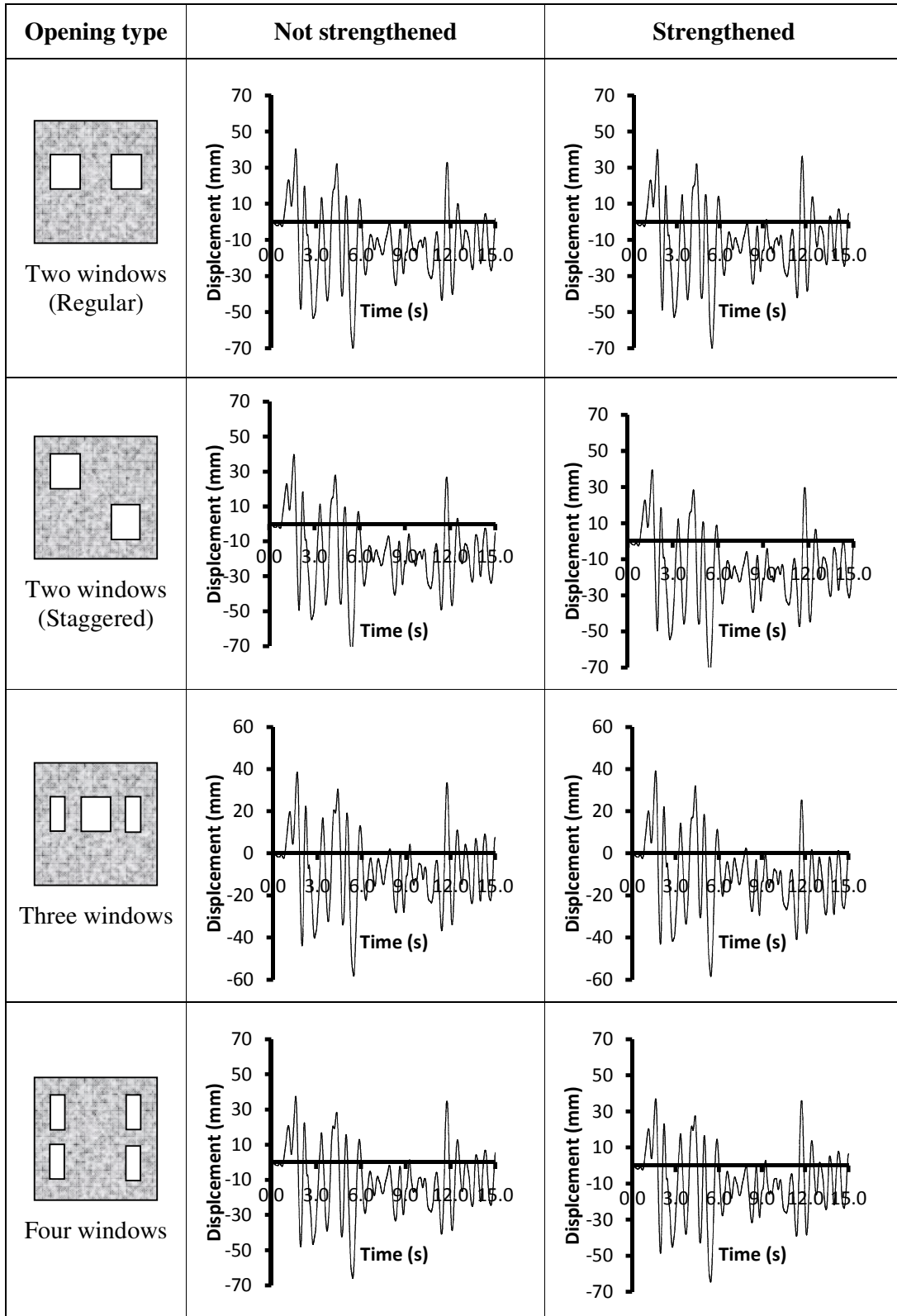
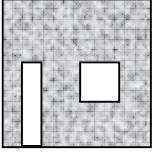
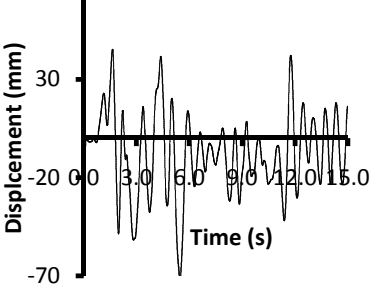
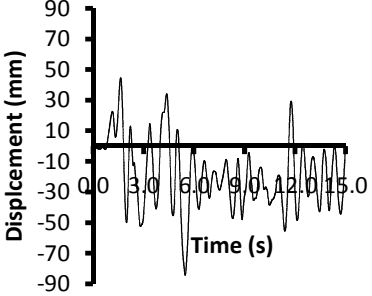
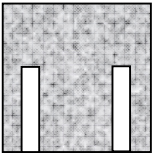
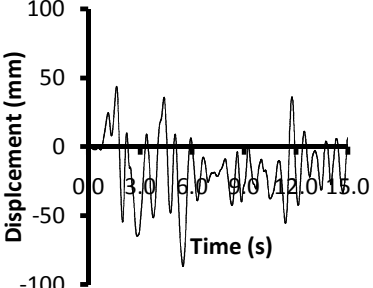
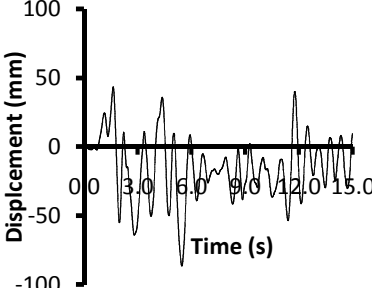
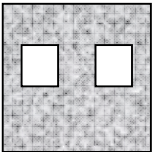
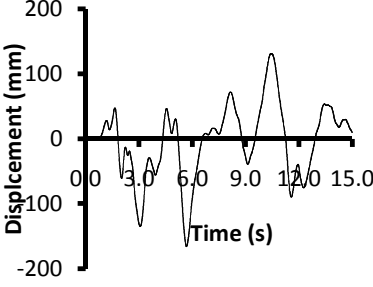
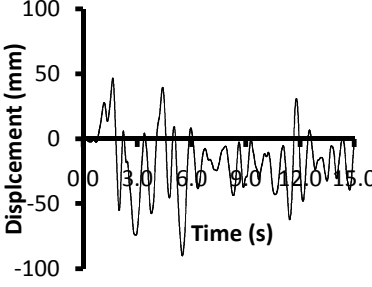
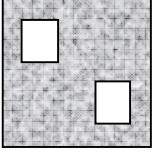
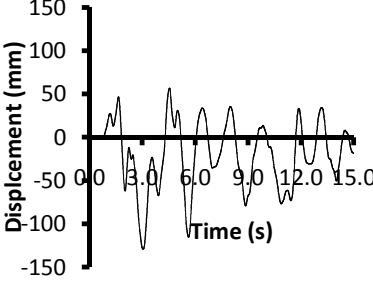
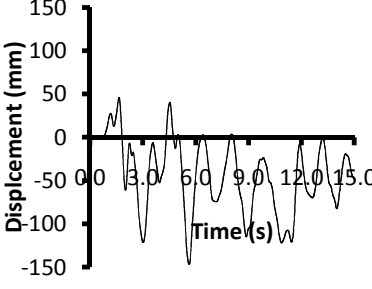
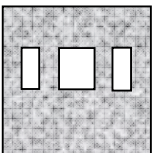
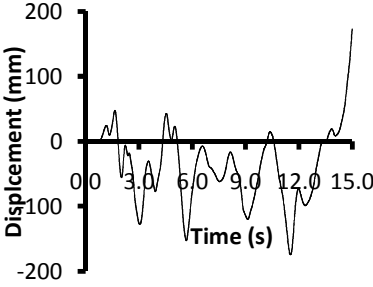
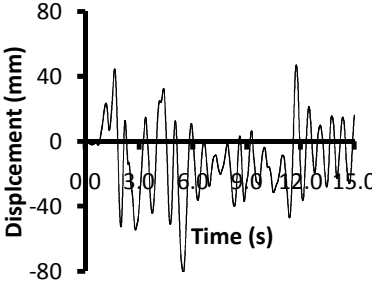


Fig. 6.10: Displacement time history response of RC slender shear wall for different door window opening combinations for 5% damping

Opening type	Not strengthened	Strengthened
 <p data-bbox="342 474 470 537">Door cum window</p>		
 <p data-bbox="342 831 470 863">Two doors</p>		
 <p data-bbox="321 1167 493 1199">Two windows</p>		
 <p data-bbox="321 1482 493 1545">Two windows (staggered)</p>		
 <p data-bbox="315 1818 509 1850">Three windows</p>		

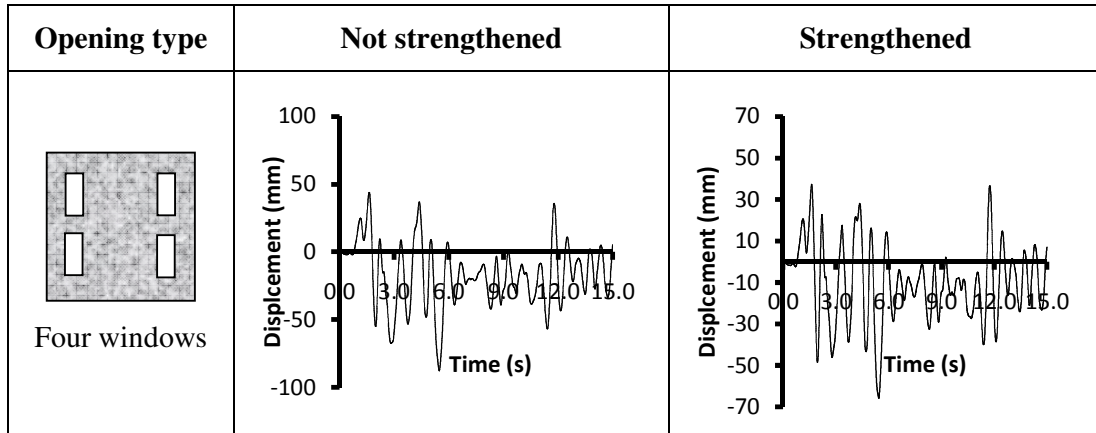


Fig. 6.11: Displacement time history response of RC slender shear wall for different door window opening combinations for 2% damping

When the slender shear wall having 5% damping is provided with door cum window opening placed in each storey, the maximum displacement and base shear demand of RC shear wall without strengthening are 57.33 mm and 319.14 kN respectively. There is an increase of around 32% in the maximum displacement response and base shear demand, respectively with respect to solid shear wall. When the shear wall is strengthened around the openings, the maximum displacement and base shear demand are 62.56 mm and 348.25 kN respectively. There is an increase in the maximum displacement and base shear demand of over 42% with respect to solid shear wall. The strengthening results in the increase in the maximum displacement response and the base shear demand. For slender shear wall with 2% damping, the maximum displacement and base shear demand of RC shear wall with door cum window opening are 72.12 mm and 401 kN respectively. There is an increase of around 10% in the maximum displacement response and base shear demand with respect to solid shear wall. When the shear wall is strengthened around the openings, the maximum displacement and base shear demand are 84.28 mm and 469 kN, respectively. There is an increase in the maximum displacement and base shear demand of over 30% with respect to solid shear wall. The strengthening results in the increase in the maximum displacement response and the base shear demand.

Table 6.7 Max. displacement response (U_{max}) and base shear demand ($V_{b,d}$) -Slender shear wall with different door window opening combinations

Opening type	5% damping				2% damping			
	NS		ST		NS		ST	
	U_{max}	$V_{b,d}$	U_{max}	$V_{b,d}$	U_{max}	$V_{b,d}$	U_{max}	$V_{b,d}$
Solid shear wall	43.93	244.54	43.93	244.54	65.67	365.56	65.67	365.56
Single Central opening	49.43	275.16	49.86	277.55	70.62	393.12	71.43	397.63
Door cum window	57.33	319.14	62.56	348.25	72.12	401.47	84.28	469.16
Two doors	64.94	361.50	64.63	359.77	86.88	483.63	86.49	481.46
Two windows (Regular)	70.29	391.28	70.23	390.95	165.30	920.17	89.93	500.61
Two windows (staggered)	75.24	418.84	74.41	414.22	129.10	718.66	146.70	816.63
Three windows	58.27	324.37	58.42	325.21	174.40	970.83	81.33	452.74
Four windows	66.06	367.73	64.53	359.22	87.79	488.70	65.70	365.73

For shear wall with 5% damping provided with two door openings placed in each storey, the maximum displacement and base shear demand of slender shear wall without strengthening are 64.94 mm and 360 kN, but remains almost unchanged upon strengthening. However, with respect to solid shear wall, there is an increase of around 49% in the maximum displacement as well as base shear demand. In the similar lines, for 2% damping, the maximum displacement and base shear demand of RC shear wall without strengthening are 86.88 mm and 483.63 kN, but remains almost unchanged upon strengthening. With respect to solid shear wall, there is an increase of around 32% in the maximum displacement and base shear demand.

When the slender shear wall having 5% damping is provided with two window openings located in each storey, the maximum displacement and base shear demand of RC shear wall without strengthening are 70.29 mm and 391.28 kN, but remains almost unchanged upon strengthening. However, with respect to solid shear wall, there is an increase of around 100% in the maximum displacement as well as in the base shear demand. However, for 2% damping, the maximum displacement and base shear demand of RC shear wall without strengthening are 165.3 mm and 920.17 kN, but reduced significantly to 89.93 mm and 500.61 kN upon strengthening. But, with respect to solid shear wall, there is an increase of around 150% in the maximum displacement as well as base shear

demand without strengthening and the increase is just over 37% in both maximum displacement as well as base shear demand when strengthened. The strengthening of shear wall around the openings is considered very essential in restricting the maximum displacement and base shear demand.

In the present case of two window opening, the aspect ratio of each opening is 0.5, with longer side of opening is in the direction parallel to the direction of earthquake ground motion and hence, for low damping such as 2%, the response has just gone manifolds than solid shear wall especially without strengthening around the openings. Adequate damping of at least 5% needs to be provided in the case of such opening combinations. Thus, on the basis of this study it can be deduced that the aspect ratio of the opening is very critical in achieving the better displacement response as well as base shear demand.

When each storey of the shear wall is provided with two staggered windows located diagonally assuming 5% damping, the maximum displacement and base shear demand of RC shear wall without strengthening are 75.24 mm and 418.84 kN, but almost remains unchanged upon strengthening. However, with respect to solid shear wall, there is an increase of around 70% in the maximum displacement and base shear demand. For 2% damping, the maximum displacement and base shear demand of RC shear wall without strengthening are 129.1 mm and 718.66 kN, but increased to 146.7 mm and 816.63 kN upon strengthening. But, with respect to solid shear wall, there is an increase of around 99% in the maximum displacement and base shear demand without strengthening. When strengthened, the increase is around 124% in both maximum displacement and base shear demand.

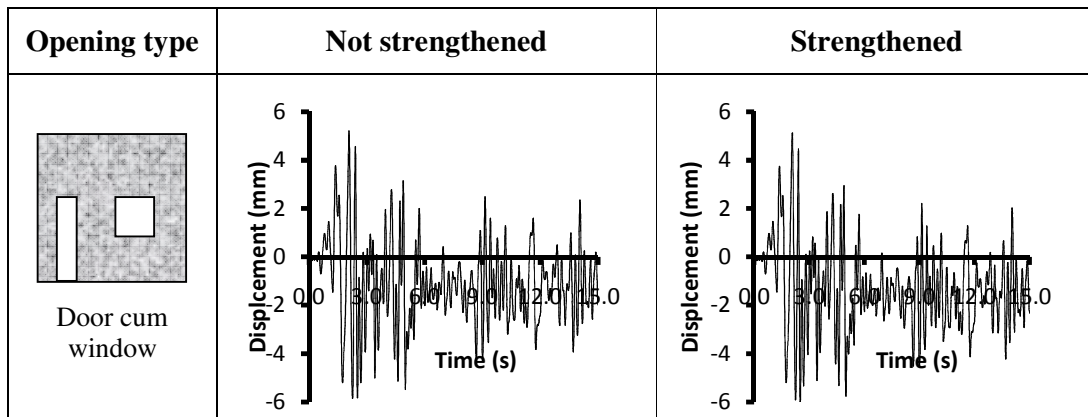
For shear wall provided with three window openings in each storey with 5% damping, the maximum displacement and base shear demand of RC shear wall without strengthening are 58.27 mm and 324.37 kN, but remains almost unchanged upon strengthening. But, with respect to solid shear wall, there is an increase of around 32% in the maximum displacement and base shear demand. However, for 2% damping, the maximum displacement and base shear demand of RC shear wall without strengthening are 174.4 mm and 970.83 kN, but reduced significantly to 81.33 mm and 452.74 kN upon strengthening. However, with respect to solid shear wall, there is an increase of around 167% in the maximum displacement and base shear demand without strengthening. When strengthened, the increase is just around 25% in both maximum

displacement and base shear demand. The strengthening of shear wall around the openings is considered very essential in restricting the maximum displacement and base shear when the damping is as low as 2%.

When the each storey of slender shear wall is provided with four window openings with 5% damping, the maximum displacement and base shear demand of RC shear wall without strengthening are 66.06 mm and 367.73 kN, but reduced slightly to 64.53 mm and 359.22 kN upon strengthening. However, with respect to solid shear wall, there is an increase of around 50% in the maximum displacement and base shear demand. For 2% damping, the maximum displacement and base shear demand of RC shear wall without strengthening are 87.79 mm and 488.70 kN, but reduced significantly to 65.7 mm and 365.7 kN upon strengthening. With respect to solid shear wall, there is an increase of around 35% in the maximum displacement and base shear demand without strengthening. When strengthened, the increase is just practically nil in both maximum displacement and base shear demand. The response of shear wall with four window opening has been considered satisfactory even for 2% damping.

Squat shear wall:

Figs. 6.12 and 6.13 show the displacement time history response of RC squat shear walls with various door window opening combinations. When the single central opening is provided in shear wall, the maximum displacement response as well as base shear demand has not been found to be varying very much with respect to solid shear wall, especially for 2% damping. In this section, the performance of shear wall with various door window opening combinations is assessed with respect to solid shear wall.



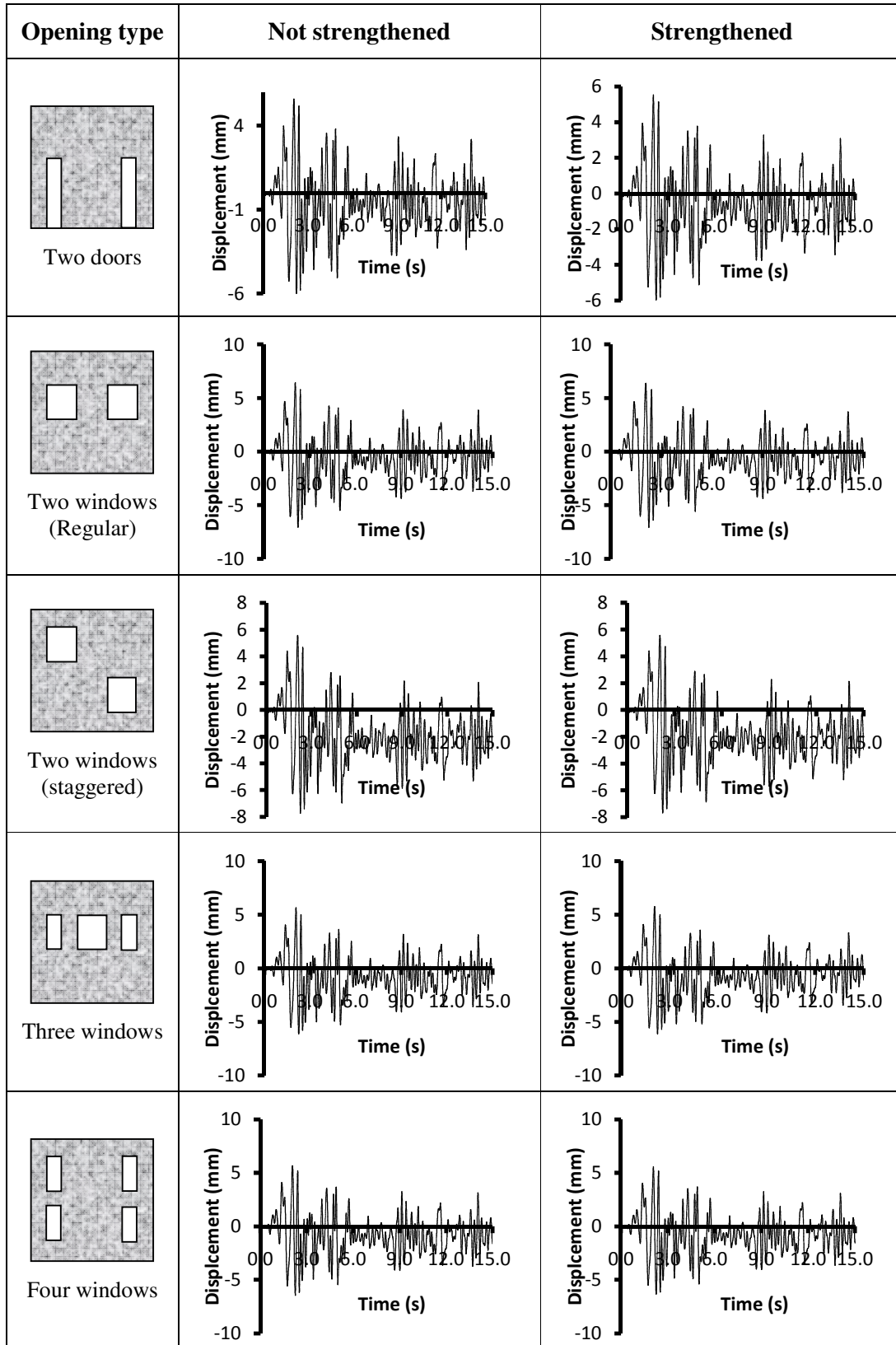
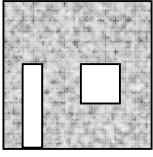
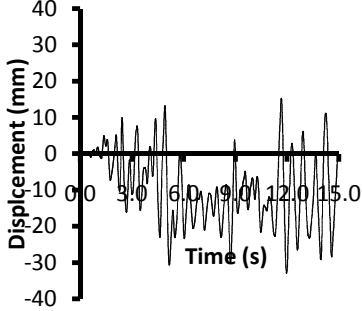
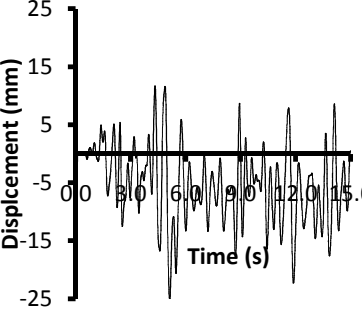
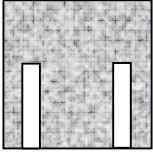
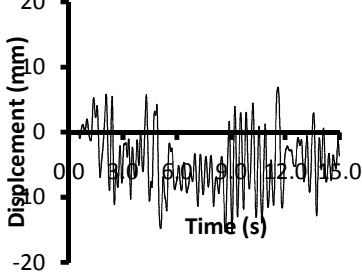
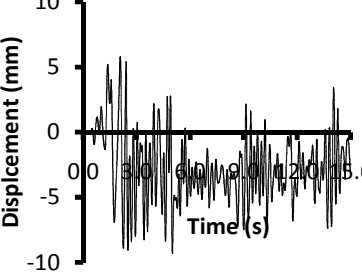
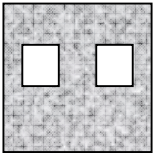
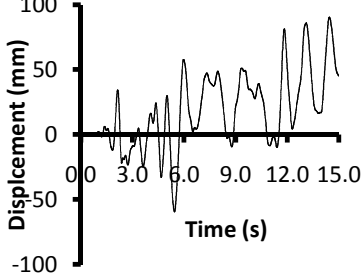
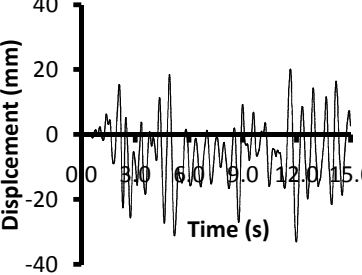
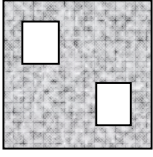
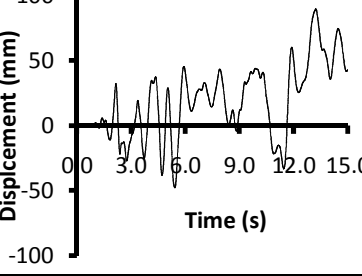
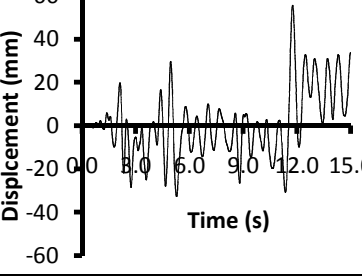
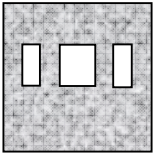
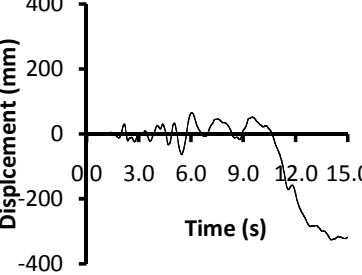
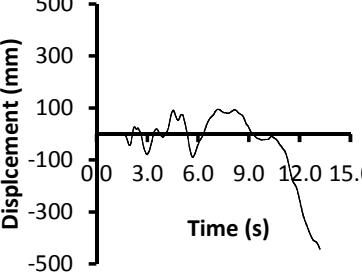


Fig. 6.12: Displacement time history response of RC squat shear wall for different door window opening combinations for 5% damping

Opening type	Not strengthened	Strengthened
 <p>Door cum window</p>		
 <p>Two doors</p>		
 <p>Two windows</p>		
 <p>Two windows (staggered)</p>		
 <p>Three windows</p>		

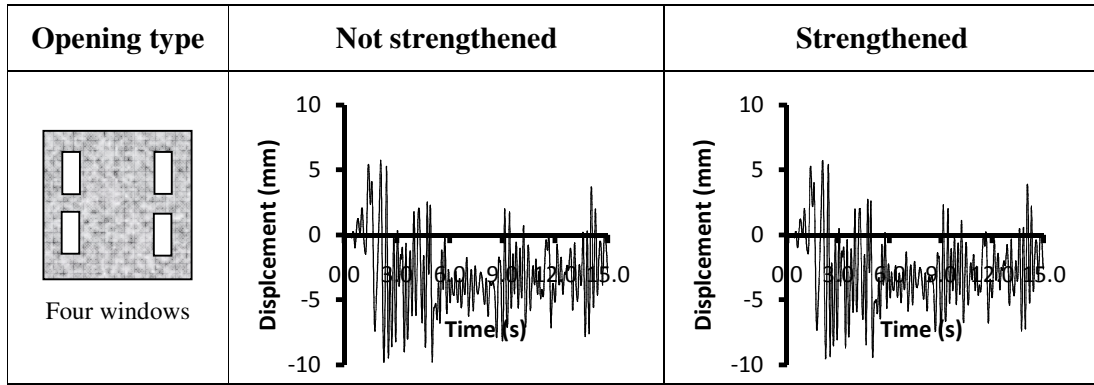


Fig. 6.13: Displacement time history response of RC squat shear wall for different door window opening combinations for 2% damping

When each storey of squat shear wall is provided with door cum window opening assuming 5% damping without strengthening, the maximum displacement and base shear demand of RC shear wall without strengthening are 5.85 mm and 65.34 kN, respectively. Not much change is observed in the displacement response and base shear demand due to strengthening and there is an increase of around 32% in the maximum displacement response as well as base shear demand with respect to solid shear wall. For same shear wall with 2% damping without strengthening, the maximum displacement and base shear demand of RC shear wall with door cum window opening are 32.91 mm and 367.70 kN, respectively and there is an increase of around 2.74 times in the maximum displacement response and base shear demand with respect to solid shear wall. When the shear wall is strengthened around the openings, the maximum displacement and base shear demand are 25.11 mm and 280.55 kN respectively and an increase in the maximum displacement and base shear demand of over 1.8 times with respect to solid shear wall. The strengthening results in the reduction in the maximum displacement response and the base shear demand. Due to non-symmetrical openings, the displacements are very severe for 2% damping, characterized by a couple of little bit of one sided cyclic displacements.

Table 6.8: Max. displacement response and base shear demand- Squat shear wall with different door window opening combinations

Opening type	5% damping				2% damping			
	NS		ST		NS		ST	
	U_{max}	$V_{b d}$	U_{max}	$V_{b d}$	U_{max}	$V_{b d}$	U_{max}	$V_{b d}$
Solid shear wall	4.44	49.64	4.44	49.64	8.81	98.42	8.81	98.42

Opening type	5% damping				2% damping			
	NS		ST		NS		ST	
	U_{max}	V_{bd}	U_{max}	V_{bd}	U_{max}	V_{bd}	U_{max}	V_{bd}
Single Central opening	6.18	68.99	6.16	68.79	9.91	110.73	9.98	111.54
Door cum window	5.85	65.34	6.00	66.98	32.91	367.70	25.11	280.55
Two doors	6.00	67.03	5.97	66.74	15.54	173.63	9.34	104.40
Two windows (Regular)	7.07	79.03	7.08	79.10	90.42	1010.25	33.00	368.70
Two windows (staggered)	7.72	86.30	7.69	85.87	89.76	1002.88	55.57	620.88
Three windows	6.12	68.42	6.15	68.71	325.50	3636.00	Collapse	Collapse
Four windows	6.44	71.90	6.33	70.70	9.79	109.38	9.49	106.06

For squat shear wall having 5% damping provided with two symmetrically placed door opening in each storey, the maximum displacement and base shear demand of RC shear wall without strengthening are 5.9 mm and 67.03 kN, but remains almost unchanged upon strengthening. For 2% damping, the maximum displacement and base shear demand of RC shear wall without strengthening are 15.54 mm and 173.63 kN, but changed to 9.344 mm and 104.40 kN upon strengthening. Thus, even with strengthening, with respect to solid shear wall, there is an increase of only around 6% in the maximum displacement and base shear demand. Nevertheless, the performance has been satisfactory in terms of maximum displacement and the base shear demand. The positive things above the squat shear wall with two door openings are the aspect ratio and symmetry of openings. Though aspect ratio is not unity, the longer side of the opening is in the perpendicular direction of the loading. The fact that the openings are located symmetrically adds to those benefits. Because of the aspect ratio of openings, the vertical bars are provided on the sides of the openings and it controls the deformation to the great extent. Stiff behavior is reflected in the shape of the time history with more frequent vibrations [Fig. 6.13].

When the squat shear wall is provided with two window openings in each storey assuming 5% damping, the maximum displacement and base shear demand of RC shear wall without strengthening are 7.07 mm and 79.03 kN, but remains almost unchanged upon strengthening. But, with respect to solid shear wall, there is an

increase of around 38% in the maximum displacement and the base shear demand. For 2% damping, the maximum displacement and base shear demand of squat shear wall without strengthening are 90 mm and 1010.25 kN, but reduced significantly to 33 mm and 368.70 kN upon strengthening. However, with respect to solid shear wall, there is an increase of around 9 times in the maximum displacement and base shear demand without strengthening. However, when strengthened, the increase is just around 3 times in both maximum displacement and base shear demand. The strengthening of shear wall around the openings is considered very essential in restricting the maximum displacement and base shear demand. The aspect ratio of the opening is found to be very critical in achieving the better displacement response and base shear demand. In the present case of two window opening, the aspect ratio of each opening is 0.5, and longer side of opening is in the direction parallel to the direction of earthquake ground motion. Hence, for low damping such as 2%, the response has just gone manifolds than solid shear wall especially without strengthening around the openings. The increase in the displacements is very high after 10 seconds as evident from the time history response (Fig. 6.13). Adequate damping of at least 5% needs to be provided in the case of such opening combinations.

For shear wall provided with two staggered window type opening placed diagonally in each storey assuming 5% damping, the maximum displacement and base shear demand of RC shear wall without strengthening are 7.72 mm and 86.30 kN respectively, but almost remains unchanged upon strengthening. With respect to solid shear wall, there is an increase of around 75% in the maximum displacement and base shear demand. Nevertheless, the displacements are still not alarming to make the shear wall unserviceable. Nevertheless for 2% damping, the maximum displacement and base shear demand of RC shear wall without strengthening are 89.76 mm and 1002.88 kN, but reduced significantly to 55.57 mm and 620.88 kN upon strengthening. But, with respect to solid shear wall, there is an increase of around 9.2 times in the maximum displacement and base shear demand without strengthening. When strengthened, the increase is around 5.3 times in both maximum displacement and base shear demand. The strengthening results in the significant reduction in the maximum displacement response and base shear demand. However, the performance of staggered openings has not been considered very satisfactory especially for 2% damping even with strengthening. This is signified by the fact that the number of cyclic loops appearing in

the displacement time history response (Fig. 6.13) is very less in the case of staggered openings as compared to solid shear wall. The aspect ratio of opening is such that the longer dimension is in the direction of excitation and hence there is a high displacement. Moreover, the openings are positioned towards the extremities of the walls and are located only at 1m from the edge of the shear wall. Since edges are vulnerable to severe ground shaking, it is essential to avoid the openings at the edges.

For shear wall provided with three symmetrically window openings in each storey assuming 5% damping, the maximum displacement and base shear demand of RC shear wall without strengthening are 6.12 mm and 68.42 kN, respectively, but remains almost unchanged upon strengthening. However, with respect to solid shear wall, there is an increase of around 39% in the maximum displacement and base shear demand. However, for squat shear wall with 2% damping, when the openings are provided in the form of three windows, the maximum displacement and base shear demand of RC shear wall without strengthening are 325 mm and 3636 kN, respectively, but collapsed before sustaining for 15 seconds upon strengthening. The brittle failure is partly due to the storey mechanism attributed to the presence of three openings at the same level, creating skewed distribution of stiffness at the different levels. But, with respect to solid shear wall, there is an increase of around 36 times in the maximum displacement and base shear demand without strengthening. When there are more openings situated at the same level, it is essential to rely on the damping mechanism than strengthening. The damping needs to be higher in order to safely dissipate energy without much degradation in strength and stiffness. The large displacement is characterized by the stray peak around 12 seconds and thus resulting in one sided cyclic displacements (Fig. 6.13). It essentially means that shear wall is too flexible to resist any deformation.

When the squat shear wall is provided with four symmetrically placed window openings assuming 5% damping, the maximum displacement and base shear demand of RC shear wall without strengthening are 6.44 mm and 71.90 kN respectively. But, with respect to solid shear wall, there is an increase of around 45% in the maximum displacement and base shear demand. The strengthening of the shear wall around the openings is not impacting the response significantly. However, the maximum displacement response of squat RC shear wall with four window opening is not very large and mostly the response is observed to be linear. The linear response is

characterized by very frequent spikes with the stiff response (Fig. 6.3). For 2% damping, when the openings are provided in the form of four window openings, the maximum displacement and base shear demand of RC shear wall without strengthening are 9.79 mm and 109.38 kN, respectively, but almost remains unchanged upon strengthening. With respect to solid shear wall, there is an increase of around only 8% in the maximum displacement and base shear demand. The response of shear wall with four window opening has been considered satisfactory even for 2% damping. The response of RC shear wall with four window opening has been characterized by the stiff behavior of the shear wall with frequent spikes (Fig. 6.13). This is attributed to the fact that the aspect ratio of the opening is square and the openings are not concentrated at one particular level, thus avoiding the story mechanism. Moreover, the openings are symmetrically located. The performance of shear wall with four window opening has been considered to be superior in terms of maximum displacement and base shear point of view.

6.5 Summary

The following conclusions have been made on the basis of time history dynamic responses of slender and squat RC shear walls in the presence of openings of different sizes and at different locations.

- The displacements are found to be less for squat shear walls than for slender shear walls. The stiff behavior is observed in the case of squat shear walls and flexible behavior is observed in the case of slender shear walls. The displacement time history has more peaks in the case of squat shear wall than that of slender shear wall. The strengthening results in the reduced displacement response for both slender and squat shear walls.
- The presence of damping has significant effect on the displacement time history responses of both slender and squat shear walls. The displacements have been significantly reduced when the damping is increased from 2% to 5%.
- The slender shear wall with 21% opening has been considered highly undesirable for both 5% damping and 2% damping without strengthening. This is characterized by the heavy one-sided displacement response history. However, it is to be noted that the 5% damped displacement response has been considered satisfactory with the help of strengthening around the openings. But with 2%

damping, the slender shear wall with 21% opening has suffered from very high displacement even with strengthening.

- Similarly, the squat shear wall with 21% opening has resulted in huge displacement with respect to solid shear wall, especially for 2% damping. Though strengthening results in reduction in the maximum displacement response, the magnitude of the displacement still remains very high with respect to solid shear wall.
- However, upto 18% opening, slender shear wall shows very stable displacement time history response characterized by vibrations of high frequency for both 5% and 2% damping. However, for squat shear wall, the displacements are relatively high with respect to solid squat shear wall especially for 2% damping without strengthening around the opening. Hence, 18% opening has not been considered very safe opening size for squat shear wall.
- The opening locations strongly affect the performance of shear wall. The single central opening results in less displacement response and base shear demand for both slender as well as squat shear wall. The shear wall provided with door cum window opening/two door opening results in satisfactory time history response for both 5% and 2% damping.
- For 2% damping, the performance of shear wall provided with three window openings have not been considered satisfactory for both slender as well as squat shear wall. However, for 5% damping, not much change is observed in the behavior of shear wall in the presence of openings of different opening locations.
- In the presence of three window openings with 2% damping, both slender and squat shear walls suffer from huge one-sided cyclic displacement even with strengthening. The three windows located at the same level created the kind of storey mechanism and hence results in flexible behavior.
- Similarly, the response of shear wall provided with diagonally placed openings has not been considered satisfactory, especially for 2% damping characterized by with heavy increase in the maximum displacement and base shear demand.
- The shear walls with four window openings have been considered very safe from the displacement and base shear point of view even without strengthening and hence can be considered to be safe opening location.

References:

- 1) Lefas, I.D., Kotsovos, M.D., and Ambraseys, N.N. (1990). "Behavior of reinforced concrete structural walls: Strength, deformation characteristics, and failure mechanism." *ACI Structural Journal*, 87(1), 23-31.
- 2) IS 1893 (2002). *Criteria for earthquake resistant design of structures*, BIS, New Delhi
- 3) IS 13920 (1993). *Code of practice for ductile detailing of reinforced concrete structures subjected to Seismic Forces*, BIS, New Delhi.

Summary and Conclusions

7.1 Summary

The main objective of this study has been to investigate the effectiveness and applicability of size of openings and their locations on the static and dynamic response of the shear wall with different damping characteristics. To achieve this objective, an analytical finite element model to predict the static and dynamic behavior of Reinforced Concrete (RC) shear wall was developed.

Since the behavior of RC shear walls is highly complex under the influence of severe lateral loads arising due to wind and earthquake, the response of shear wall no longer remains elastic and therefore, finite element method was needed to predict the behavior of shear wall in both linear and non-linear regimes under static and dynamic loading conditions. Though the non-linear static analysis (pushover analysis) of shear wall is performed to obtain the lateral force-displacement characteristics, it does not represent true dynamic characteristics of shear wall subjected to seismic loading, nor does it capture the effect of higher modes on its structural response.

The finite element program developed in FORTRAN was capable of capturing the non-linearity due to material characteristics (material non-linearity) that incorporates macro material model for concrete and steel. The non-linearity considered in the present study includes concrete cracking, yielding of steel & concrete and tension stiffening caused by bond slip between steel and concrete, aggregate interlock and the dowel action of reinforcement steel. Also, for the dynamic analysis, finite element model based on implicit solution algorithm was employed to study the nonlinear dynamic response of RC shear walls. It is well documented in literature that the nine-noded Lagrangian degenerated shell element with assumed strain approach does not suffer from spurious energy modes and locking and performs well in thin as well as thick situations with reasonable accuracy for static and dynamic analyses. The sensitivity analysis carried

out in this study revealed that the degenerated shell element in conjunction with assumed strain approach is not much sensitive to the finite element mesh size and the same has been used in the present study. The layered concept of the degenerated shell element has given the much-needed flexibility to allow different materials to be modeled through the thickness direction of the element. Moreover, the layered approach enabled to model the reinforcing steel in horizontal and vertical directions by defining appropriate properties pertaining to orientation of reinforcing steel. For the modeling of concrete in compression, the yield/failure surface has been predicted using Willam-Warnke five-parameter model with isotropic hardening and associated flow rule. The cracking in the concrete has been modeled using the smeared crack approach. The tension stiffening, incorporated in the material modeling has been found out to be essential in representing the realistic behavior of reinforced concrete. In order to perform the time-history analysis of shear wall, different methods have evolved over the years. It is well known fact that the non-linear implicit direct integration time history analysis is more accurate and predicts the results closer to the experimental results. In the present study the Newmark- β method (Trapezoidal rule) of direct implicit time integration has been used to perform the time-history analysis of shear wall. This method has been chosen since the computational time step is limited only from accuracy point of view and not from stability point of view. The consistent mass matrix approach has been adopted in the present study and the shape functions for determining the consistent mass matrix are considered the same as used for stiffness matrix. A study of literature shows that the exact formulation of damping is not mandatory for nonlinear dynamic analysis. Rayleigh damping, considered as simple and efficient way of modeling the damping, has been adopted in the present study. The input data preparation for the finite element analysis of structures is very cumbersome especially for the multi-storeyed shear wall with openings. To overcome this, a small program was developed in FORTRAN to generate the element nodal connectivity and co-ordinates of shear wall. This program was found very useful since it was a general program capable of generating the huge data file for shear wall with different size of the opening located at different positions.

In order to validate the program for both static and dynamic response of shear walls, three shear wall problems were selected. For the validation of program under static loading, the squat shear wall with top and bottom beams was considered. The displacement at the middle of the top slab was evaluated under monotonically increased lateral loading applied at the middle of the top beam. The load-displacement response as well as crack & yield patterns of shear wall have been found to be in close agreement with the experimental results published in literature.

For the dynamic response of shear walls, the flanged shear walls and rectangular shear walls were considered under simulated earthquake ground motion applied at the base of shear wall. The flanged shear wall is squat in nature whereas the rectangular shear wall is of slender type. The time history responses have been plotted at the top level of shear wall. It was found that the maximum displacement response as well as the profile of time history response was found to be satisfactory.

The focus of the present study is to investigate the influence of openings on the structural response of slender (10-storeyed) and squat (5-storeyed) RC shear walls under non-linear static and dynamic loading conditions. In order to determine the load carrying capacity and ductility, the non-linear static analysis of shear wall was carried out considering material non-linearity. Since the ductility is the important parameter in the earthquake resistant design, the present analyses focused on the comparison of ductile response of shear wall in the presence of openings. In this study, the ductility was evaluated in terms of displacement ductility index. The displacement ductility index was calculated as the ratio of yield to ultimate displacement. Since the well defined yield point was not easy to identify, the method based on the secant stiffness approach was adopted in the present study. In order to determine the displacement response of shear wall under dynamic ground motions, the shear walls were subjected to El Centro earthquake applied at the base of the shear wall. The displacement time history response, measured at the top of shear wall, was plotted for the period of first 15 seconds. The stiffness proportional Rayleigh damping was employed in the present study. The maximum displacement response and base shear demand were computed for shear wall with various opening sizes and locations.

On the basis of non-linear static and dynamic loading conditions, the following observations have been made on aspect ratio, opening size and opening locations.

Effect of aspect ratio of shear wall:

The aspect ratio of shear wall plays a crucial role on its structural response. For a given cross-section, the aspect ratio of shear wall significantly affects the load carrying capacity as well as the displacement response. The lateral load on the shear wall was linearly varied from maximum at top to zero at bottom representing the triangular distribution of loading. In general, the load carrying capacity of squat shear wall was found high as compared to slender shear wall. Nevertheless, the ultimate displacement of squat shear wall was found to be far less than that of slender shear wall. It was observed that the slender shear wall failed in ductile mode characterized by sufficient in-elastic deformation before failure. On the other hand, the squat shear wall failed by the shear mode and thus resulted in smaller ultimate displacement. Hence, it is concluded that the deformability of the slender shear wall was considered to be superior to the squat shear wall. Also, the displacement time history response demonstrated more peaks in the case of squat shear wall than that of slender shear wall which indicated that behavior of squat shear wall to be stiff compared to slender shear wall.

Effect of opening size:

Shear walls require openings to satisfy the functional requirement of the multi-storeyed building. However, the presence of openings in shear walls weakens the shear wall as envisaged by many researchers. A study of literature revealed that shear walls be penetrated only with smaller openings in order to get the desired structural response, but there is no clarity on the optimum size of openings in shear walls from strength, displacement and ductility point of view. Even though certain codes put limitation of 15% as the limiting opening percentage in the shear wall only from the perspective of analysis, but there are no common consensus on the limiting percentage of openings in shear walls. The present investigation deals with the identification of safe opening percentages to be allowed in slender and squat shear walls from strength and displacement point of view.

In order to examine the effect of openings on the response of shear wall, the whole study was made in two phases. In the first phase of the study the slender and squat shear walls were analyzed for monotonically increasing lateral load till the failure of shear wall while in the second phase the displacement time history analysis of shear walls subjected to El Centro earthquake ground motion were carried out. The shear walls considered for the parametric study had the uniform thickness & width and contained minimum steel as recommended by Indian code. The openings were located centrally in each storey and the size of the opening considered for each storey were 2%, 5%, 11%, 14%, 18% and 21%. In order to examine the influence of strengthening around the openings, all the shear walls with openings were analyzed with- and with-out strengthening and results were compared with the shear wall with no opening (solid). The strengthening of shear wall around the openings was as per Indian code of practice.

The load carrying capacity of shear wall was found to be reduced with the increase in the opening size. The reduction in the load carrying capacity with respect to solid shear wall was found to be severe for larger opening size without strengthening. However, the strengthening resulted in the better response of shear wall. Moreover, the displacement time history responses of slender and squat shear wall with larger opening sizes were found to be highly unstable characterized by one-sided cyclic displacements. The influence of damping was found to be very significant in restricting the maximum displacement response and base shear demand especially for large openings (21% opening). Invariably, the 5% damping has resulted in superior performance of shear wall in the presence of openings. Hence, damping (energy dissipating capacity) is very essential from the point of view of serviceability as well.

After studying the responses, it was found that the opening percentages need to be limited to 14% from load and displacement point of view. Hence, 14% opening was considered to be safe in both slender as well as squat shear walls as performance was not overly dependent on strengthening and damping.

Effect of opening location:

The functional requirement generally necessitates the need for providing multiple openings at different locations of shear walls. The openings were provided in the form of doors and windows and were positioned at different locations. The total opening size

adopted was 14% as identified in the previous section. The present investigation accomplished the identification of the safe door and window opening locations for slender and squat shear walls under static and dynamic loading conditions.

For static loading, it was observed that the opening locations strongly affect the performance of shear wall in terms of load carrying capacity and ultimate displacement. When the opening is provided in the form of single window located centrally in each storey, the reduction in the load carrying capacity of shear wall was not significantly reduced with respect to solid shear wall. Also, the influence of strengthening for this opening location was found to be insignificant. Moreover, the ultimate displacement was found to be higher with respect to solid shear wall which indicated the deformable behavior of shear wall. The shear wall in the presence of four window openings also resulted in the better structural response. On the other hand, the presence of openings in the form of two windows and three windows resulted in the severe degradation in strength especially without strengthening.

In the similar lines, the dynamic response analysis of shear wall in the presence of single window opening located centrally resulted in the stable displacement time history. The response of shear wall in the presence of two windows and three windows was found to be severely affected especially for 2% damping. The severity was found to be more in the case of squat shear walls than for slender shear walls. However, for 5% damping, the displacement response was found to be reasonably safer characterized by stable time history response. Hence, it was observed that the influence of damping was found to be significant on the displacement response.

7.2 Conclusions

On the basis of exhaustive numerical studies carried out to identify the limiting opening size and desirable locations of the openings at different floors of the multistoried shear wall, the following conclusions have been drawn.

- For openings up to 14%, the load carrying capacity and ultimate displacement response were not found to be severely affected by openings. However, for openings beyond 14%, the load carrying capacity of slender as well as squat shear wall gets affected due to the presence of openings.

- In general, strengthening of shear wall around openings was found beneficial in improving the load carrying capacity and ductility of the shear wall. However, for shear wall up to 14% opening, the responses of both slender as well as squat shear walls were not overly dependent on the strengthening around the openings. On the other hand, beyond 14% opening, the performance of shear wall was found to be strongly influenced due to strengthening around the openings.
- The shear wall with 18% opening was not considered very safe in case of squat shear wall. However, slender shear wall exhibited better performance than squat shear wall for the same opening size.
- The squat shear wall with 21% opening suffered from severe degradation in the load carrying capacity of more than 50% and hence such large openings are to be strictly avoided. The performance of slender shear wall in the presence of 21% opening was slightly better than that of squat shear wall. In spite of improved performance of slender shear wall over squat shear wall, 21% opening is not considered safe. Hence the shear wall with 14% opening is identified as safe opening size.
- The opening orientation in shear wall significantly affected the performance of shear wall. In case of rectangular openings, it is beneficial to provide the shorter side of the opening parallel to the loading direction in order to minimize the degradation in the load carrying capacity and ductility.
- The shear wall with door cum window opening as well as with two door opening resulted in satisfactory time history displacement response for both 5% and 2% damping. Moreover, for both opening combinations the reduction in the load carrying capacity was found to be less as compared to solid shear wall.
- For shear walls with two/three windows aligned horizontally at the same level, the load carrying capacity and ultimate displacement were found to be severely affected and resulted in the kind of storey mechanism. Moreover, the maximum displacement response was found to be very high under severe dynamic ground motion. It is suggested to avoid such openings to avoid detrimental effect on shear wall. The degradation was more severe for squat shear walls than for slender shear walls especially for 2% damping. Even the strengthening was not found to be positively influencing the behavior of shear wall.

- The aspect ratio of opening plays the crucial role on the structural response of shear wall. The degradation in the strength and displacement was found to be minimal for shear wall with four windows placed symmetrically. The strengthening around the openings as well as damping was not impacting the behavior of the shear wall significantly.

7.3 Further Scope of the Work

While conducting the study, it was found that certain aspects of the investigation needs further examination and are presented as under.

- Even though the optimum size and location of openings on the shear wall are determined in the present study analytically, it may be better to investigate experimentally especially for dynamic loading conditions. Moreover, the influence of opening shapes on the structural response can also be investigated. Since only 10 storeyed shear walls have been considered in the present study, there is a need to investigate further for taller and slender shear walls.
- The core wall around the lift has become popular these days and hence there is a need to investigate the performance of the lift/core wall in the presence of openings.
- Since shear walls in high-rise buildings are also used as the fire-resistant wall, it is essential to investigate the post-fire seismic behavior of RC shear walls.
- The present study uses the assumed strain based degenerated shell element in conjunction with fixed smeared approach to model the RC shear wall. However, there are many recent advances in the element technology and crack simulating approach of RC structures. Hence, there is a need to capture the analytical response of shear wall by adopting state-of-the art analytical procedures.
- The strain hardening has been modeled in the present study to capture the post-cracking behavior of shear wall. In order to capture the realistic behavior of RC structures, there is a need to incorporate the softening behavior of Reinforced Concrete due to un-loading.

Appendix-1: Evaluation of Constants - Willam Warnke Five Parameter Model

A1 Determination of model parameters

These two meridians must intersect the hydrostatic axis at the same point $\sigma_m / f'_c = \bar{\xi}_0$ (corresponding to hydrostatic tension), the number of parameters need to be determined is reduced to five. The five parameters (a_0 or b_0 , a_1 , a_2 , b_1 , b_2) are to be determined from a set of experimental data (Fig. A.1), with which the failure surface can be constructed using second-order parabolic expressions. The five parameters in the present failure criterion are now determined such that the following five stress states are inbuilt in the criterion. This includes three simple tests and two arbitrary strength points in the high compression regime.

- The uni-axial compressive strength f'_c ($\theta = 60^\circ$), $f'_c > 0$.
- The uni-axial tensile strength f'_t ($\theta = 0^\circ$) with the strength ratio $\bar{f}'_t = f'_t / f'_c$.
- The equal biaxial compressive strength f'_{bc} ($\theta = 0^\circ$, $f'_{bc} > 0$) with the strength ratio $\bar{f}'_{bc} = f'_{bc} / f'_c$.
- The high compressive stress point $(\sigma_m / f'_c, \tau_m / f'_c) = (\xi_1, \bar{\rho}_1)$ on the tensile meridian ($\theta = 0^\circ$, $\bar{\xi}_1 > 0$).
- The high compressive stress point $(\sigma_m / f'_c, \tau_m / f'_c) = (\xi_2, \bar{\rho}_2)$ on the compressive meridian ($\theta = 60^\circ$, $\bar{\xi}_2 > 0$).

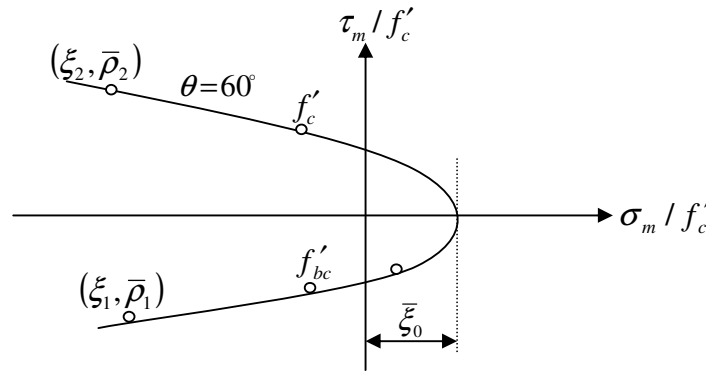


Fig. A.1: Experimental failure stress states for the determination of parameters in the five-parameter model

In addition to the above points, the two parabolas must pass through a common apex at the hydrostatic axis; this imposes the condition

$$\rho_t(\bar{\xi}_o) = \rho_c(\bar{\xi}_o) = 0 \text{ for } \bar{\xi}_o = \frac{\sigma_{mo}}{f'_c} > 0 \quad [\text{A.1}]$$

It has been mentioned in the literature that the five parameter failure model is very effective for compressive state of stress. Based on Kupfer's tests and other tri-axial tests, the test points to determine the material constants (five parameter model) are given in Table A1.

A2 Determination of six parameters

The various tests which are conducted to determine the six parameters are depicted in Table A1. The first three strength values are reserved for determination of parameters in the tensile meridian and other three strength values are reserved for compressive meridian.

Table A1: Calculation of parameters for five parameter model

Test	σ_m / f'_c	τ_m / f'_c	θ	$\rho(\sigma_m, \theta)$
$\sigma_1 = f'_t$	$\frac{1}{3} \bar{f}'_t$	$\sqrt{\frac{2}{15}} \bar{f}'_t$	0°	$\rho_t = \sqrt{\frac{2}{3}} f'_t$
$\sigma_2 = \sigma_3 = f'_{bc}$	$\frac{2}{3} \bar{f}'_{bc}$	$\sqrt{\frac{2}{15}} \bar{f}'_{bc}$	0°	$\rho_t = \sqrt{\frac{2}{3}} f'_{bc}$
$(-\bar{\xi}_1, \bar{\rho}_1)$	$-\bar{\xi}_1$	$\bar{\rho}_1$	0°	$\rho_t = \sqrt{5} \bar{\rho}_1 f'_c$
$\sigma_3 = f'_c$	$-\frac{1}{3}$	$\sqrt{\frac{2}{15}}$	60°	$\rho_c = \sqrt{\frac{2}{3}} f'_c$
$(-\bar{\xi}_2, \bar{\rho}_2)$	$-\bar{\xi}_2$	$\bar{\rho}_2$	60°	$\rho_c = \sqrt{5} \bar{\rho}_2 f'_c$
Eq.3.41	$\bar{\xi}_o$	0	$0^\circ, 60^\circ$	$\rho_t = \rho_c = 0$

Substituting the three strength values corresponding to tensile meridian

$$\left. \begin{aligned} \sqrt{\frac{2}{15}} \bar{f}'_t &= a_0 + a_1 \left(\frac{1}{3} \bar{f}'_t \right)^2 \\ \sqrt{\frac{2}{15}} \bar{f}'_{bc} &= a_0 + a_1 \left(\frac{2}{3} \bar{f}'_{bc} \right) + a_2 \left(\frac{2}{3} \bar{f}'_{bc} \right)^2 \\ \bar{\rho}'_1 &= a_0 + a_1 \left(\bar{\xi}_1 \right) + a_2 \left(\bar{\xi}_1 \right)^2 \end{aligned} \right\} \quad [\text{A.2}]$$

Solving these equations, the three parameters are found to possess the value as follows:

$$\begin{aligned}
 a_0 &= \frac{2}{3} \bar{f}'_{bc} a_1 - \frac{4}{9} \bar{f}'_{bc} a_2 + \sqrt{\frac{2}{15} \bar{f}'_{bc}} \\
 a_1 &= \frac{1}{3} (2\bar{f}'_{bc} - \bar{f}'_t) a_2 + \sqrt{\frac{6}{5} \frac{\bar{f}'_t - \bar{f}'_{bc}}{2\bar{f}'_{bc} + \bar{f}'_t}} \\
 a_2 &= \frac{\sqrt{\frac{6}{5} \bar{\xi}_1 (\bar{f}'_t - \bar{f}'_{bc})} - \sqrt{\frac{6}{5} \bar{f}'_t \bar{f}'_{bc}} + \bar{\rho}_1 (2\bar{f}'_{bc} + \bar{f}'_t)}{(2\bar{f}'_{bc} + \bar{f}'_t) \left(\bar{\xi}_1^2 - \frac{2}{3} \bar{f}'_{bc} \bar{\xi}_1 + \frac{1}{3} \bar{f}'_t \bar{\xi}_1 - \frac{2}{9} \bar{f}'_t \bar{f}'_{bc} \right)}
 \end{aligned} \tag{A.3}$$

The apex of the failure surface is determined by using the condition 6, $\rho(\bar{\xi}_0 = 0)$.

$$a_0 + a_1 \bar{\xi}_0 + a_2 \bar{\xi}_0^2 = 0; \rightarrow \bar{\xi}_0 = \frac{-a_1 - \sqrt{a_1^2 - 4a_0 a_2}}{2a_2} \tag{A.4}$$

Substituting the three strength values corresponding to compressive meridian, the remaining three parameters can be determined as follows:

$$\begin{aligned}
 b_0 &= -\bar{\xi}_0 b_1 - \bar{\xi}_0^2 b_2 \\
 b_1 &= \left(\bar{\xi}_2 + \frac{1}{3} \right) b_2 + \frac{\sqrt{6/5} - 3\bar{\rho}_2}{3\bar{\xi}_2 - 1} \\
 b_2 &= \frac{\bar{\rho}_2 \left(\bar{\xi}_0 + \frac{1}{3} \right) - \sqrt{2/15} (\bar{\xi}_0 + \bar{\xi}_2)}{(\bar{\xi}_2 + \bar{\xi}_0) \left(\bar{\xi}_2 - \frac{1}{3} \right) \left(\bar{\xi}_0 + \frac{1}{3} \right)}
 \end{aligned} \tag{A.5}$$

The experimental strength values used to determine the parameters of the model are

$$f'_t = 0.15; f'_{bc} = 1.8; \bar{\xi}_1 = \bar{\xi}_2 = 3.67; \bar{\rho}_1 = 1.5; \bar{\rho}_2 = 1.94.$$

Appendix-2: Finite Element Software

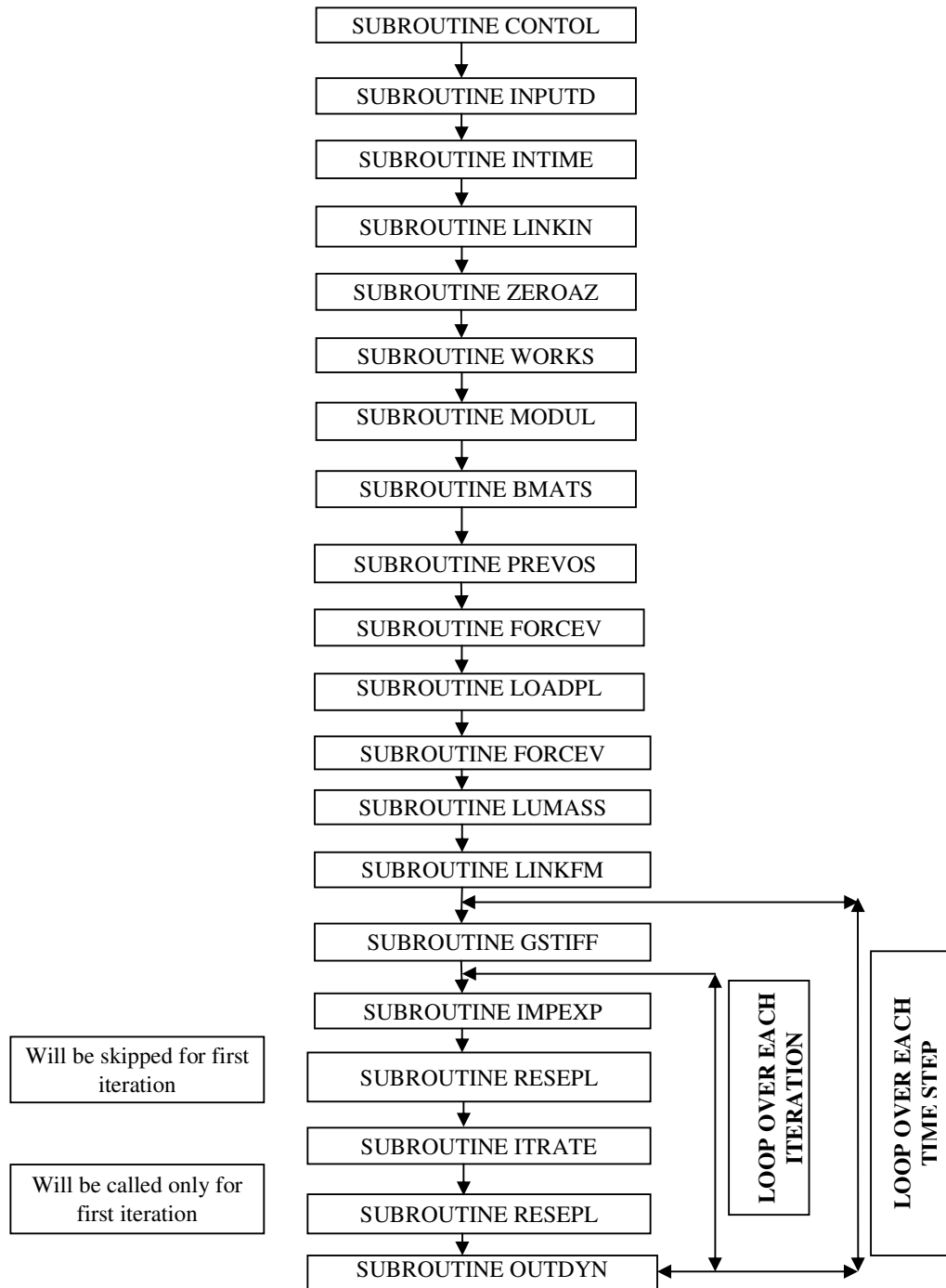


Fig. A.2: Sequence of finite element programming

CONTOL: In this subroutine, the variables required for dynamic dimensioning are read and a check is made on the maximum available dimensions. The maximum dimension of the variables, viz NELEM, NPOIN AND NMATS is specified in this subroutine. In case the variables specified in the program exceeds as mentioned in this subroutine, the program will be terminated.

INPUTD: This subroutine reads and writes most of the control parameters viz. nodal point coordinates (COORD), thickness of elements (MEATK), nature of elements (INTGR), element connectivities (LNODS), boundary conditions (IFPRE), material properties (NPROP), number of concrete layers (NCLAY), number of steel layers (NSLAY), maximum concrete layers (MACON), maximum steel layers (MASTE) etc. However, the dynamic parameters will be dealt separately in INTIME subroutine.

INTIME: This subroutine reads and writes all time integration data required for dynamic analysis. It reads and writes the information such as number of time steps specified for dynamic analysis (NSTEP), number of points at which the displacements (NOUTD) and stresses (NOUTS) are to be output, number of acceleration points (NACCE), nature of dynamic loading (IFUNC), direction of excitation (IFIXD), number of steps after which the stiffness matrix is to be updated (KSTEP), the type of algorithm (IPRED), maximum tolerance limit specified for convergence (TOLER) Also reads and writes initial displacement and velocities, time acceleration.

LINKIN: This subroutine calculates the number of variables (NEVAB) associated with a finite element and also the total number of unknowns (NEQNS) in the entire structure. The equations numbers are assigned based on the constrained degrees of freedom (IFPRE). This subroutine links the rest of the program with the skyline solver. It also calculates the column height (MHIGH) for all elements and stores the addresses of the diagonal elements (MAXA). Here, the check is made to ensure the number of equations to be solved is less than the maximum dimension specified. Otherwise, the program will be terminated. Calculates column height above the diagonal in global matrix. Assigns location for diagonal elements in global matrix.

ZEROAZ: Its function is to initialize to zero various vectors and matrices at the solution of the process. The strains (EPSTN) and (GRTST), stresses (STRAG), directions of steel reinforcement (DIREC), displacements (DISP), accelerations (ACCE), velocities (VELO), forces (FORCES) are set to zero.

WORKS: In this subroutine, the thickness of the nodes (THICK) in a particular element is calculated and stored with the help of top and bottom coordinates of the node. Also establishes the local orthogonal system of axes at each nodal point. Calculates the direction cosines (DICOS) and the vectors V_1 , V_2 and V_{3k} (normal vector) at each node.

MODUL: Calculates the elasticity matrix (NSTAT = 1) and material constitutive matrix (DMATX) depending upon the state of stress in the local axes system using the transformation matrix. This subroutine is very importance as change in the stiffness of any element gets modified due to the variation in DMATX. The size of DMATX is 5×5 as there are five degrees of freedom in the degenerated shell element. For Concrete yielding (NSTAT = 4), DMATX is calculated the same as for NSTAT = 1.

BMATS: Calculates the strain displacement matrix at sampling points. The element shape functions and its derivatives are calculated in this subroutine. The sampling points and weighting factors are selected based on integration rule (NGAUS). Evaluates the membrane strain displacement matrix and transverse shear strain displacement matrix at the element middle surface. Here, the strain displacement matrix (BMATX) is replaced by the substitute transverse shear strain and membrane strain matrices. The BMATX and DVOLU are stored in Tape 8 for further usage.

PREVOS: It reads and stores the initial loads (RLOAD) and stresses (STRIN). This is indicated by the parameter (NPREV). If NPREV = 0, there are no initial loads and stresses. These initial stresses and loads are stored in Tape 2 for further usage.

FORECEV: This subroutine calculates the nodal loads due to pressure and gravity. The pressure load can be applied on the top and bottom faces respectively. The gravity can be defined in any one of three directions.

LOADPL: This subroutine generates applied force vector.

Gravity forces are equivalent to a body force/unit volume acting within the solid in the direction of the gravity axis. The gravity axis need not be coincident with either of the coordinate axes and consequently gravity force components may act in x-, y-, and z- directions. If g is the gravitational acceleration and ρ_m is the material mass density, then the gravity force acting on an element volume dV is

$$dG = \rho g_m dV$$

The components acting in the x and y directions respectively are

$$dG_x = \rho_m g dV \sin \theta; \quad dG_y = -\rho_m g dV \cos \theta$$

Using principle of virtual work, the equivalent nodal forces P_{xi} and P_{yi} are given by

$$P_{xi} u^* = \int_{V_e} N_i u^* \rho_m g \sin \theta dV; \quad P_{yi} v^* = -\int_{V_e} N_i v^* \rho_m g \cos \theta dV$$

In the above equations, u^* and v^* are virtual displacements, N_i are the shape functions and integration is taken over the entire volume of the element. The expression used to calculate the equivalent nodal forces due to gravitational acceleration g acting on a material of mass density ρ_m is

$$\begin{bmatrix} P_{xi} \\ P_{yi} \end{bmatrix} = \int_{V_e} N_i \rho_m g \begin{bmatrix} \sin \theta \\ -\cos \theta \end{bmatrix} dV$$

Using Numerical Gaussian integration, the above equation is practically replaced by

$$\begin{bmatrix} P_{xi} \\ P_{yi} \end{bmatrix} = \sum_{m=1}^3 \sum_{n=1}^3 \rho_m g t \begin{bmatrix} \sin \theta \\ -\cos \theta \end{bmatrix} N_i(\xi_n, \eta_m) W_n W_m |J|$$

In the above equation, t is the element thickness, J is the Jacobian matrix. In the similar fashion, other loads can also be deduced.

LUMASS: This subroutine generates the lumped mass vector.

LINKFM: Calculates the data required for the storage of data.

GSTIFF: This subroutine calculates the global stiffness matrix in compacted form.

IMPEXP: This subroutine generates the partial effective load vector for direct time integration. Performs direct time integration using either (i) Implicit (ii) Explicit and Combined Implicit-Explicit schemes.

RESEPL: This subroutine evaluates the internal force vector for elasto-plastic materials.

ITRATE: This subroutine generates the total effective load vector and solves for the incremental displacements. It also checks for convergence.

OUTDYN: This subroutine writes out most of the output on the various tapes for post processing. It outputs displacement and stresses every NOUTP steps. Displacement and stress histories of specified nodal and integration points are also captured in this routine. The complete state of displacements, stresses are written in separate tapes.

Conferences

- 1) Muthukumar, G and Kumar, Manoj, (2009). “Finite Element Analysis of Shear Walled Structures”, *Int. Conf. on Advances in Concrete, Structural and Geo-technical Engineering (ACSGE-2009), BITS, Pilani.*
- 2) Muthukumar, G. and Kumar, Manoj, (2009). “Effect of Openings on Structural Response of Shear wall”, *Int. Conf. on Advances in Concrete, Structural and Geo-technical engineering (ACSGE-2009), BITS, Pilani.*
- 3) Muthukumar, G and Manoj Kumar, (2011) “Finite Element Dynamic Analysis of Shear Wall”. *2nd International Conference on Advances in Mechanical, Manufacturing and Building Sciences, ICAMB -2012, VIT University, Vellore.*
- 4) Muthukumar, G and Manoj Kumar (2013) “Effect of Opening Size on the Structural Response of Rectangular Slender Shear Wall without Boundary Elements.” *Proceedings of the National Conference on Recent Advances in Civil Engineering (RACE)-2013, NIT Patna.*
- 5) Muthukumar, G and Manoj Kumar (2013) “Influence of Openings on the Dynamic Structural Response of Rectangular Slender Shear Wall for different Damping Ratios.” *International Conference on Structural Engineering & Mechanics (ICSEM)-2013, NIT Rourkela.*
- 6) Muthukumar, G and Manoj Kumar (2014) “Influence of openings on the structural response of shear wall”, *Structural Engineering Convention (SEC), 9th Biennial Event, Under the Auspices of Indian Association for Structural Engineering, IIT Delhi.*
- 7) Muthukumar, G and Manoj Kumar (2014) “Influence of opening size on the displacement response of squat shear wall.” *5th International Congress on Computational Mechanics and Simulation, Chennai.*

Journals

- 1) Muthukumar, G and Manoj Kumar (2013) “Nonlinear finite element dynamic analysis of squat shear wall with openings” *International Journal of Advanced Structural Engineering, Springer Open*, Vol. 5, Issue 27, PP. 1-20.
- 2) Muthukumar, G and Manoj Kumar (2014) “Analytical Modeling of Damping”, *The Indian Concrete Journal*, Vol. 88, Issue 9, pp. 64-72.
- 3) Muthukumar, G and Manoj Kumar “Failure Criteria of Concrete - A Review”, *Computers & Concrete*, Techno-press Publications, Vol. 14, Issue 5, pp. 503-526.
- 4) Muthukumar, G and Manoj Kumar (2014) “Influence of opening locations on the structural response of shear wall.” *Journal of Nonlinear Dynamics*, Hindawi Publishing Corporation, pp. 18.
- 5) Muthukumar, G and Manoj Kumar (2014) “Influence of opening location on the static and dynamic structural response of slender and squat shear walls.” *Advances in Structural Engineering*, Multi-Science Publishing Company Ltd
(Under review)

Brief biography of the Candidate

G. Muthukumar is a Lecturer in Department of Civil Engineering at Birla Institute of Technology & Science (BITS) Pilani, Rajasthan. He completed his B.Tech (Hons.) from SASTRA University, Thanjavur in the year 2005 and M.E. in Civil Engineering with specialization in Structural Engineering from BITS Pilani in the year 2007. His research interest lies in the earthquake response of RC structures and repair and rehabilitation of structures. He has 7 conference publications and 4 journal publications to his credit.

Brief biography of the Supervisor

Dr. Manoj Kumar is as an Associate Professor of Department of Civil Engineering at the Birla Institute of Technology & Science (BITS) Pilani, Rajasthan. He has completed his B.E., M.E., and Ph.D from IIT Roorkee. His research interests lie in Post-peak Behavior of Reinforced Concrete and Composite Bridges, Non-linear Finite Element Analysis of Reinforced Concrete plated and shell Structures and Seismic Analysis of Shear Walled Structures. He has 7 journal publications and 15 conference publications.